INVESTIGATIONS ON LOW LOSS DIELECTRIC CERAMIC MATERIALS FOR WIRELESS COMMUNICATION

THESIS SUBMITTED TO THE UNIVERSITY OF KERALA
IN FULFILMENT OF THE
REQUIREMENTS FOR THE DEGREE OF
DOCTOR OF PHILOSOPHY
IN PHYSICS
UNDER THE FACULTY OF SCIENCE

BY

K. P. SURENDRAN

UNDER THE SUPERVISION OF

Dr. M. T. SEBASTIAN

CERAMIC TECHNOLOGY DIVISION
REGIONAL RESEARCH LABORATORY (CSIR)
TRIVANDRUM – 695 019
KERALA, INDIA

AUGUST 2004

DECLARATION

I hereby declare that the matter embodied in the thesis entitled "INVESTIGATIONS ON LOW LOSS DIELECTRIC CERAMIC MATERIALS FOR WIRELESS COMMUNICATION" is a result of the investigations carried out by me at Ceramic Technology Division under the supervision of Dr. M. T. Sebastian, Scientist, Regional Research Laboratory (CSIR), Trivandrum, and the same has not been submitted elsewhere for any other degree.

Trivandrum

Dated: 21st Aug. 2004 **K. P. Surendran**

CERTIFICATE

This is to certify that this thesis entitled "INVESTIGATIONS ON LOW LOSS DIELECTRIC CERAMIC MATERIALS FOR WIRELESS COMMUNICATION" is an authentic record of the investigations carried out by Mr. K. P. Surendran, at the Ceramic Technology Division, Regional Research Laboratory (CSIR), Trivandrum, under my supervision. This thesis or any part thereof has not been submitted elsewhere for any other degree.

Trivandrum

Dated : 21st Aug. 2004 **M. T. Sebastian**

CONTENTS

PREFACE

Dielectric Resonators (DR) are low dielectric loss ceramic pucks that can act as frequency determining components in microwave filters and oscillators used in wireless communication industry. DRs should have high dielectric constant (e_r) in the range 20 to 100 for better miniaturization, high Q factor (Q>2000) for better frequency selectivity and nearly zero temperature coefficient of resonant frequency (t_f) for frequency stability with temperature. Though several temperature-stable DRs are available at present, investigation is still going on to find new materials having better dielectric resonator properties and to improve the properties of the already available materials.

This thesis entitled "INVESTIGATIONS ON LOW LOSS DIELECTRIC CERAMIC MATERIALS FOR WIRELESS COMMUNICATION" which is divided into nine chapters, is the outcome of a detailed investigation carried out on the synthesis, characterization and microwave dielectric properties of three different groups of low loss ceramics (a) ordered complex perovskites $Ba(Mg_{1/3}Ta_{2/3})O_3$ [BMT], (b) orthorhombic ceramics $RETiAO_6$ [RE=Rare Earths, A=Ta, Nb] with aeschynite and euxenite mineral structure and (c) aluminate spinels based on MAl_2O_4 [M=Mg, Zn].

Chapter 1 is a general introduction about the material, scientific and technological aspects of low loss materials. The different experimental techniques used to characterize the dielectric properties of low loss materials are also discussed. The practical applications of DRs such as filters, oscillators, antennas etc. are briefly discussed.

The chapter 2 presents details of preparation of dielectric resonators by conventional solid state ceramic and other routes. A brief description of the instrumentation used for studying the structural, microstructural and dielectric characteristics of low loss materials studied in the purview of this thesis is also presented.

The chapter 3 describes the preparation, characterization and properties of stoichiometric and non-stoichiometric $Ba(Mg_{1/3}Ta_{2/3})O_3$ [BMT] ceramics. The effect of nonstoichiometry on the densification, structural ordering and microwave dielectric properties of BMT is discussed. It is found that a slight deficiency of Mg or Ba increase the density and order parameter which in turn improved the microwave dielectric properties. However excess of Mg or Ba deteriorate the properties considerably.

The fourth chapter describes the effect of different dopants on the properties of BMT. It is found that dopants such as Sb_2O_5, MnO, ZrO_2, WO_3 and ZnO improve the microwave dielectric properties of BMT. A correlation between the microwave dielectric properties of BMT and ionic radii of the dopant has been established.

The liquid phase sintering aspects of BMT with addition of low melting glass fluxes is discussed in the fifth chapter. The effect of these glass additives on the sintering temperature, suppression additional phases, densification, cation ordering and microwave dielectric properties of BMT is discussed. It is found that glasses such as B_2O_3, $ZnO\text{-}B_2O_3$, $5ZnO\text{-}2B_2O_3$ and $ZnO\text{-}B_2O_3\text{-}SiO_2$ improve the Q factor t_f and reduce the sintering temperature.

The sixth chapter deals with an investigation carried out on the effects of substitution on the chemistry and physics of BMT. In this study solid solution phases such as $Ba[Mg_{1/3}Ta_{(1-x)2/3}\ Ti_{x/3}W_{x/3}]O_3$, $Ba(Mg_{1/3}Ta_{2/3})_{1-x}Ti_xO_3$ and $Ba(Mg_{1-x}Zn_x)_{1/3}Ta_{2/3})O_3$ were investigated. The effect of solid solution formation on the phase transition from 1:2 ordered to disordered structure, and on the microwave dielectric properties is also discussed in this chapter.

The tailoring of the microwave dielectric properties by making solid solution phases between positive (aeschynites) and negative (euxenites) t_f materials in an effort to develope a possible zero t_f material is discussed in seventh chapter. This has been successfully achieved in 5 different systems such as $Pr_{1-x}Gd_xTiNbO_6$, $Nd_{1-x}Dy_xTiNbO_6$, $Sm_{1-x}Y_xTiNbO_6$, $GdTiNb_{1-x}Ta_xO_6$ and $Sm_{1-x}Y_xTiTaO_6$ dielectric ceramics. The range of solid solution formation and the effect of morphotropic phase transition from aeschynite to euxenite on the density, phase evolution and microwave dielectric properties of the solid solution phases are also discussed in this chapter.

The eighth chapter probes the dielectric loss phenomena of $ZnAl_2O_4$ and $MgAl_2O_4$ spinels. The dielectric properties of these spinels were tailored by preparing isomolar mixtures with TiO_2 in an effort to tune their t_f close to zero. The dielectric, thermal and mechanical properties of two new ideal microwave substrate material in the system $MAl_2O_4\text{-}TiO_2$ [M=Zn, Mg] which are even advantageous over alumina, have been developed.

The ninth chapter gives the conclusion of the thesis and scope for future work.

ACKNOWLEDGEMENT

It is with great pleasure and privilege that I place on record my deepest sense of gratitude to Dr. M. T. Sebastian, my supervisor for suggesting the research problem and for his efficient guidance, creative discussions and constant encouragement for the successful completion of this research thesis.

I am grateful to Prof. T. K. Chandrasekhar, Director, Regional Research Laboratory (RRL), Trivandrum for kindly providing the facilities for this work.

My sincere gratitude is also due to Dr. G. Vijay Nair, Dr. K. G. Satyanarayana, Prof. Javed Iqbal and Dr. B. C. Pai (Former Directors, RRL, TVM) for their encouragement during the period of my research.

The invaluable support given by Dr. Manoj Raama Varma is greatly acknowledged. I am always grateful to my friends in the lab, Dr. Santha, Dr. I. N. Jawahar, Mr. P. V. Bijumon, Mr. G. Subodh, Mr. Rajath Varma, Mr. Krishnakumar, Ms. P. S. Anjana, Ms. Rejini and Mr. L. A. Khalam for their immense help and for keeping my cool all along my research tenure.

This work would not have been complete without remembering the favours I got from CUSAT. I am thankful to Prof. P. Mohanan and my friends in MERL, for their kind helps in microwave dielectric measurements. The help provided by Prof. Jacob Philip in the thermoelectric characterisation of ceramics is also thankfully remembered

Dr. Ratheesh (Scientist, C-MET, Trissur) and Dr. Sreemoolanadhan (Scientist, VSSC) who provided a lot of favour to me and I am thankful to them. I am grateful to Dr. Peter Koshy and Mr. Prabhakar Rao for extending the SEM facility for this work.

I wish to express my sincere thanks to Dr. K. G. K. Warrier, Mr. P. Mukundan, and present and former members of the Ceramic Technology Division for their help and support.

I express my sincere thanks to Dr. U. Shyama Prasad, Mr. P. Gurusamy and Mr. K. V. Oonnikrishnan Nair for their help to record XRD patterns of the ceramics.

I am thankful to Prof. R. L. Moreira, Dr. C. W. A. Paschoal and Dr. Anderson Dias, UFMG, Brazil, for having kindly associated with the Laser Raman Analysis of dielectrics discussed in this thesis.

The help provided by Dr. Mohan Jacob, James Cook University, Australian for having done the microwave characterisation of the ceramic samples at the cryogenic temperatures, is acknowledged.

I am also thankful to Dr. Anna Axelson and Prof. N. McN Alford, South Bank University, London, for their help in Microstructural Analysis of the ceramics samples.

I with to thank Prof. Jacob Koshy, Dr. Jose James, Dr. Jose Kurian, Dr. R. Jose, Dr. Asha Mary John, Mr. Senthil Kumar and Mr. M. Sankar for their help given during the course of this work.

I am thankful to DRDO and DST, Govt of India, New Delhi for financial assistance for the successful completion of this work.

I am indebted to my parents who stood with me in my thick and thin, family members, friends, well wishers and above all, the Almighty for the physical, mental and spiritual support.

K. P. Surendran

CHAPTER 1

DIELECTRIC RESONATORS

Chapter 1 gives a general introduction about the material, scientific and technological aspects of low loss materials. Three important parameters, ε_r, Q and τ_f, used for the DR characterization are described. The relationship of the above parameters with the fundamental material characteristics is also discussed. The different experimental techniques used to characterize the dielectric properties of low loss materials are also discussed. The practical applications of DRs such as filters, oscillators, antennas etc. are briefly discussed.

1. 1 DIELECTRIC RESONATORS

1.1.1 Introduction

The past few decades have witnessed a tremendous demand for microwave low loss components consequent to the recent explosive growth of telecommunications industry. The combined U.S. and Japanese microwave filter market is conservatively estimated at £500 - £600 million which is extensively used in satellite and personal communication. The mobile phone industry experienced better sales in the year 2003 than expected, as worldwide mobile phone unit sales totalled 520 million units, a 20.5 percent increase from 2002 figures according to Gartner Inc.[1].

Frequencies above about 30 MHz can pass through the ionosphere and so are available for communicating with satellites and other extra-terrestrial sources. Frequencies from 1-30 GHz are usually called "microwaves". The frequency range 2-24 GHz are useful for geostationary satellite communications.

For the microwave circuit to work, part of it needs to vibrate, or 'resonate' at the specific working frequency. The frequency determining component (resonator) used in such a high frequency device should satisfy certain criteria. It should have high dielectric constant, high quality factor, and high frequency stability with temperature. The quality factor (which is the inverse of the loss tangent, tanδ) should be high enough (usually >2000). Higher the Q factor, lower the insertion loss and steeper the cut-off frequency. Moreover the high quality factor enables the allocation of more number of channels within a given frequency range. High dielectric constant is mandatory since it is the key factor for miniaturization. Moreover the resonant frequency of the dielectric ceramic should be constant against ambient temperature variation in the microwave circuitry (*i.e.* the temperature coefficient of resonant frequency τ_f should be close to zero)[2].

The quartz resonators are unattractive at microwave frequencies due to the small signal to noise ratio with frequency multiplication. Another option is metallic cavity resonators, which were used in microwave components are bulky and non-integrable for Microwave Integrated Circuits (MIC). Later on microstrip resonators were emerged which had poor thermal stability and high dielectric loss. Thus miniaturisation was possible in communication circuits by compromising on the quality factor and temperature stability. The dielectric resonators (DRs) are unmetallised polycrystalline

ceramics which have almost all the necessary requirements mentioned above. Microwave dielectric resonators are present in almost all telecommunication systems and are also an integral part of the personal (cellular) telephone network. They generally act as filters and waveguides for microwave radiation over a large range of frequencies. The principle of their operation is the ability of the dielectric/air interface to reflect electromagnetic (EM) radiation, and thus the material can sustain a standing electromagnetic wave within its body. Clearly, the smaller the resonating body, the higher the frequency. However, the physics of the standing wave in a dielectric is complex due to the fact that EM radiation has both magnetic and electric components[3].

1. 1. 2 History of Dielectric Resonators

The temperature compensating ceramic capacitors were developed as early as in 1930s and were widely used for stabilization of an electronic circuit such as LC resonance circuit and CR timing circuit etc. Fortunately, temperature compensating ceramic capacitor showed relatively high Q value (approximately 2000-10000) compared with LC resonators (usually 200-1000). By this reason a special attention to improve the Q value of ceramic capacitor was not considered until at the end of 1960s when the application of dielectric ceramics to microwave started. Eventhough single crystals have higher Q than their equivalent polycrystalline materials, they are unsuitable for most applications due to their high cost and tedious growth processes. Besides, some high dielectric constant multicomponent materials are difficult to grow as single crystals.

It was Lord Rayleigh[4] who in 1897 showed that an infinitely long cylinder of a dielectric material can serve as a guide for electromagnetic waves at certain frequencies. This means that the dielectric has the effect of causing the electromagnetic wave to be confined to the cylinder itself and the immediately surrounding region of space. In 1939 Richtmeyer theoretically predicted [5] that a suitably shaped dielectric material could behave as an electromagnetic resonator. He argued that if a long cylinder were bent into a ring and the ends joined together, it would guide the waves round and round indefinitely so that they would be confined to a finite region of space. Such an object would act as an electrical resonator, the resonant frequencies being determined by the fact that the field must have the same phase at the two ends which are joined together to make the ring.

During the second quarter of the last century, a lot of work has been done[6, 7, 8] on the resonance properties of symmetrical structures like sphere, hemisphere, toroidal ring rectangular blocks etc. However the first reported work on the adaptability of a high dielectric constant dielectric rod to generate standing wave resonance phenomena is proposed by Schlicke[9] . He proposed that in a circular cylindrical bodies of high dielectric constant such as polytitanates, in which for a wave coming from electrically dense high dielectric constant material to the electrically thin air, the air dielectric interface offers an infinite impedance, insisting the wave to be confined within the dielectric cylinder.

The theoretical aspects of dielectric rod resonators has aroused a lot of academic interest as the solution of Maxwell's equation for a cylindrical system is straightforward both for the case of isotropic and anisotropic media[10,11]. In 1960, Okaya [12] found that a piece of rutile (TiO_2) acted as a resonator and later in 1962 Okaya and Barash[13] analyzed the different modes of a dielectric resonator. A significant breakthrough came in the year 1968 when Cohen [14] for the first time experimentally determined the microwave dielectric properties of a rutile resonator with dielectric constant ε_r=104, quality factor Q=10,000 and coefficient of temperature variation of the resonant frequency τ_f=+450 ppm/^oC. It is evident that the τ_f of rutile resonator is unusually high for practical applications[15]. Until 1970's the search for new temperature stable dielectrics were not fruitful. Two concepts to solve the above mentioned temperature drift problem of resonant frequency were practically thought out (i) to develop the temperature stable dielectric material and (ii) is to make a composite material in which constituents compensate their temperature drift of performance to each other. Historically, first temperature stable, low loss resonator was developed in 1971 by Masse et al[16]. who found that barium tetra-titanate ($BaTi_4O_9$) has excellent thermal stability and microwave dielectric characteristics. Since then the search for temperature stable high dielectric constant materials with low dielectric loss has been one of the most challenging problems in Materials Science.

Technological improvements in DRs have contributed to considerable advancements in wireless communications[17, 18, 19, 20, 21, 22, 23, 24]. Ceramic dielectric resonators have advantage of being more miniaturized as compared to traditional

microwave cavities, while having a significantly higher quality factor than transmission lines and microstrips. DRs are advantageous in terms of compactness, light weight, stability and relatively low cost of production as compared to the conventional bulky metallic cavity resonators. In addition temperature variation of the resonant frequency of dielectric resonators can be engineered to a desired value to meet circuit designer's requirements.

1. 2 PHYSICS OF DIELECTRIC RESONATORS

1. 2. 1 Polarization Mechanisms in Dielectrics

Under the influence of an electric field on a dielectric material four types polarization mechanisms can occur, i.e. interfacial, dipolar, ionic and electronic. Piling up of mobile charge carriers at physical barrier such as grain boundary causes for interfacial polarization or space charge polarization. At low frequencies the mechanism gives rise to high dielectric constant and in some cases may extend up to 10^3 Hz.

In zero field the permanent dipoles will be randomly oriented and the system has no net polarization, but an electric field will tend to align the dipoles and the materials will acquire a net moment. This is called orientational polarization[25]. In other words, the perturbation of thermal motion of the ionic or molecular dipoles, producing a net dipolar orientation in the direction of the applied field. Two mechanisms can be operative in this case. (a) In linear dielectrics (non-ferroelectrics) dipolar polarization results from the motion of the charged ions between the interstitial positions in ionic structures parallel to the applied field direction. The mechanism is active in the 10^3-10^6 Hz range. (b) Molecules having permanent dipole moment may be rotated about an equilibrium position against an elastic restoring position. Its frequency of relaxation is very high of the order of ~10^{11}Hz. The dipolar polarization contributes to the dielectric constant in the sub-infrared range of frequencies.

The displacement of positive and negative ions with respect to each other gives rise to ionic polarisation. The mechanism contributes to the dielectric constant at infrared frequency range (~10^{12}-10^{13} Hz).

When an electric field is applied the valence electron cloud shifts with respect to the nucleus the atom acquires a dipole moment. This occurs at high frequencies of about

10^{15} GHz. At microwave frequencies the mechanisms due to ionic and electronic polarisation contribute to the dielectric properties.

1. 2. 2 Resonance

The quality factor of a dielectric resonator can be visualized using a parallel *LCR* resonant circuit. All the three components, capacitor (*C*), inductor (*L*) and ohmic resistance (*R*) in the circuit have a common voltage $v(t) = |V| \cos ?t$. The corresponding electric energy stored in capacitor is given by [26]

$$W_e(t) = \frac{1}{2} C[v(t)]^2 = \frac{1}{2} C|V|^2 \cos^2(?t) \tag{1.1}$$

And the magnetic energy stored in the inductor is

$$W_m(t) = \frac{1}{2} L\,[i(t)]^2 = \frac{|V|^2}{2w^2 L} \sin^2(wt) \tag{1.2}$$

The stored electric energy is thus proportional to $\cos^2$ function and the stored magnetic energy is proportional to $\sin^2$ function of time. As functions of time the stored energies $W_e(t)$ and $W_m(t)$ fluctuate between zero and their maximum values $W_{e,max}$ and $W_{m,max}$. The average values W_e and W_m are equal to one half of the corresponding maximum values. The frequency must take a special value which is equal to the applied frequency. Under this situation, the impedance is equal to ohmic resistance of the circuit and this condition is called the resonance. This happens when

$$? = ?_{res} = \frac{1}{\sqrt{LC}} \tag{.13}$$

Since the average energy values are equal to one half of their peak values, the maximum stored energy can be of the following form, $W_{max} = 2W_e = 2W_m = W_e + W_m$ where are the average electric and magnetic energies stored in the volume *v* defined by[27]

$$W_e = \frac{1}{2}\int_v e\,|E|^2\,dv \text{ and } W_e = \frac{1}{2}\int_v m\,|H|^2\,dv \tag{1.4}$$

In terms of the average stored energies, the definition of Q becomes

$$Q = \left[\frac{w(W_e + W_m)}{P_d}\right]_{w=w_{res}} \tag{1.5}$$

If the operation frequency is not equal to the resonant frequency, the peak of the stored electric energy is not equal to the peak of the stored magnetic energy. Therefore the definition of Q is not unique at any other frequency than $?_{res}$.

A microwave resonator has infinitely many resonant modes, each of them corresponding to a particular resonant frequency, at which the electric stored energy is equal to the magnetic one. As shown in the Fig. 1.1, the resonator can be coupled to a microstripline circuit to excite TE or TM modes[28]. One single resonant cavity has many different Q factors each of them describing one of the resonant modes only.

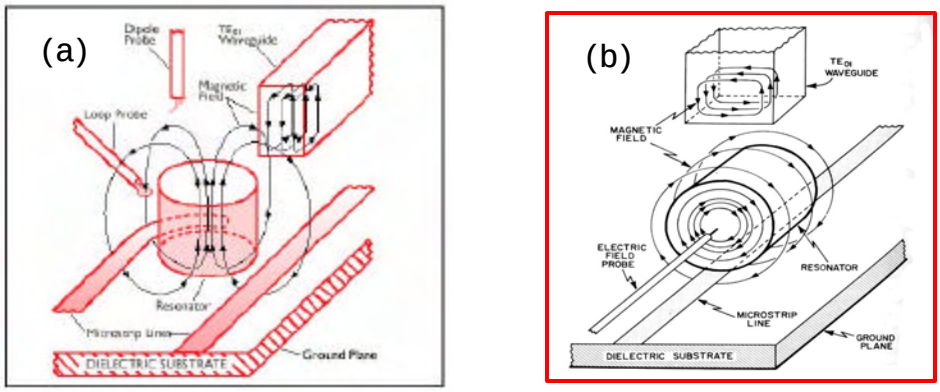

Fig. 1. 1 Dielectric Resonator coupled to (a) TE_{01d} mode and (b)TM_{01d} mode

A dielectric resonator should have maximum confinement of energy within the resonator when used at a particular resonant frequency. The resonance occurs by total multiple internal reflections of microwaves at the boundary or dielectric-air interface. If

the transverse dimensions of the dielectric are comparable to the wave length of the microwave, then certain field distributions or modes will satisfy Maxwell's equations and boundary conditions[29]. It was found that through multiple total internal reflections, a piece of dielectric with high dielectric constant can confine microwave energy at a few discrete frequencies, provided that the energy is fed in the appropriate direction. The reflection coefficient approaches unity when the dielectric constant approaches infinity. In the microwave frequency range free space wavelength (λ_o) is in centimetres and hence the wavelength (λ_g) inside the dielectric will be in millimeters only when the value of the dielectric constant ε is in the range 20-100. Hence the dimensions of the dielectric sample must be of the same order (in millimeters) for the resonance to occur. Still larger values of the dielectric constant gives better confinement of energy, reduced radiation loss and further miniaturization but will result in higher dielectric losses because of the inherent material properties. A high dielectric constant material can confine most of the standing electromagnetic wave within its volume due to reflections at the air dielectric interface. The frequency of the standing wave depends on the dimensions and dielectric constant of the dielectric. The electromagnetic fields outside the dielectric sample decay rapidly. One can prevent radiation losses by placing the DR in a small metallic enclosure. Since only a small radiation field sees the metallic surface, the resulting conduction loss will be too small and can be neglected[30].

1. 2. 3 TE_{01d} Mode Characteristics

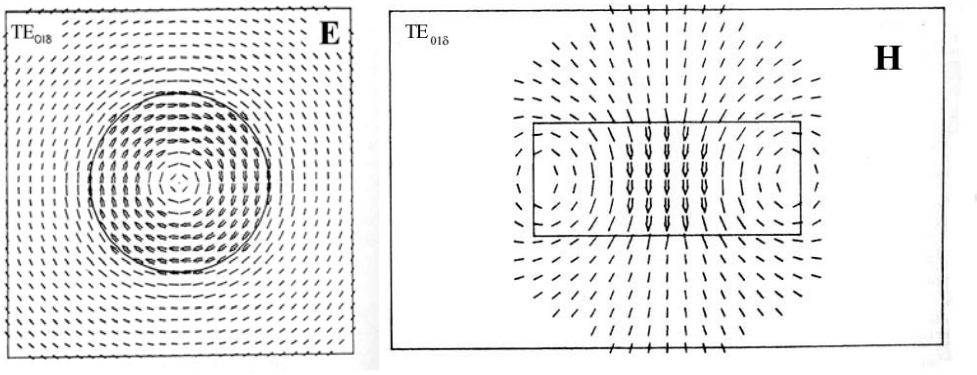

Fig. 1.2 Electric field distribution of TE_{01d} mode in equatorial plane (left) ; Magnetic filed distribution of TE_{01d} in the meridian plane (right).

The resonant fields of a cylindrical resonator can be divided into constituent modes with azimuthal variation represented either by cos*nf* or sin*nf* (n = 0, 1, 2, 3..). For n = 0 (axial symmetric case) the set of modes can be divided into TE_{nml} and TM_{nml} modes. The subscript n (azimuthal mode number) refers to the number of circumferential variations in the f direction. The second subscript m (radial mode number) and the third subscript *l* (axial mode number) refer to the field extrema within the dielectric resonator in the radial (*r*) and axial direction (*z*). Due to the evanescent field effects in a dielectric resonator it is customary to replace *l* with δ with $0 < \delta < 1$ to indicate the fraction of the half cycle variation in the axial direction[31].

The most commonly used mode of resonance for a cylindrical resonator is the TE_{01d} mode. It is a transverse electrical mode having azimuthal symmetry ?/?f = 0, and less than a half cycle variation in field in the z-direction. Fig. 1.2 shows the typical field distributions for TE_{01d} mode of a cylindrical dielectric resonator. The magnitude of the electrical field component is zero at the centre of the resonator and has a maximum value at around $x = 2r/3$ where *r* is the radius of the disk. Outside the resonator, the field decays exponentially. The field variation as a function of radial distance remains the same in different planes parallel to the equatorial plane [32].

1. 2. 4 DR Equivalent Circuit

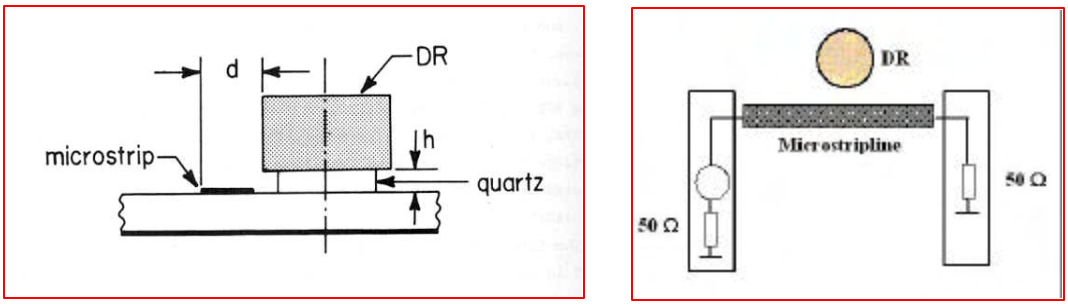

Fig. 1. 3 DR as circuit element coupled to a microstripline (left) and its equivalent circuit (right)

For solid-state microstrip circuits DR is usually placed near a microstrip line. In this it is proper to use an equivalent circuit consisting of an equivalent parallel resonance

circuit and an ideal transformer, which models the coupling between DR and the microstripline (having the transformation ratio n)

The elements of this equivalent circuit may be evaluated from the experimental data of the band rejection filter consisting of a DR coupled to a microstripline. There are four unknown values: three for the DR and one for the coupling between it and the microstripline. From the experimental data it is not possible to calculate the factor n.

The Fig 1.3 shows a schematic representation of a DR coupled to a microstripline. This coupling is a result of field interaction due to the microstripline and DR. For $TE_{01\delta}$ resonance mode, the components of the electromagnetic field is similar to a magnetic dipole[33]. Then the coupling between DR and microstripline is caused by magnetic field. There fore the equivalent circuit may be drawn as in Fig. 1.3 where the mutual inductance M depends on the coupling coefficient.

The parallel equivalent impedance in series with the microstripline may be written as

$$Z = \left[\frac{n^2}{R_o} + j(2\pi f_o n^2 C_o - \frac{n^2}{2\pi f_o L_o} \right]^{-1} \tag{1.6}$$

where f_o is the resonance frequency and n is given by

$$n = \sqrt{\frac{Q_l R_o}{Q_u (Z_g + Z_l)}} \tag{1.7}$$

where Q_l and Q_u are the loaded and unloaded quality factors of the DR respectively. Using Eqn. 1.7, the expressions for ohmic resistive, capacitative and inductive parts of the DR equivalent circuit may be obtained as

$$\frac{R_o}{n^2} = \frac{Q_u (Z_g + Z_l)}{Q_l} \tag{1.8}$$

$$n^2 C_o = \frac{1}{2\pi f_o} \frac{Q_l}{(Z_g + Z_l)} \tag{1.9}$$

$$\frac{L_o}{n^2} = \frac{1}{2\pi f_o} \frac{(Z_g + Z_l)}{Q_l} \tag{1.10}$$

Therefore if Q and Q_l are known, then from 1 and 2 the circuit consisting of a DR coupled to a microstrip is completely characterized. The loaded quality factor Q_l is expressed [34] as

$$Q_l = \frac{2\pi f_o (Z_g + Z_l) W_m}{E^2} \tag{1.11}$$

where W_m is the stored magnetic energy in the DR and E is the voltage induced into the microstripline which is computed using

$$E = \int_l \dot{E} \quad d\dot{l} \tag{1.12}$$

The unloaded quality factor depends on the elements of the equivalent circuit

$$Q_u = \frac{R_o}{2\pi f_o L_o} = 2\pi f_o C_o R_o \tag{1.13}$$

1. 2. 5 Types of Dielectric Resonators

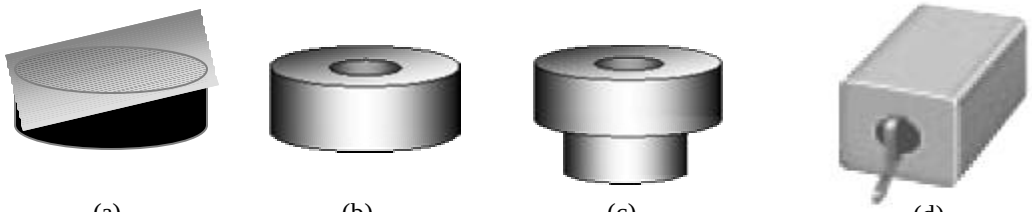

(a) (b) (c) (d)

Fig. 1. 4 Pictures of DRs with various shapes: (a) Disk (b) Coaxial Cylinder (c) Supported Coaxial Cylinder and (d) TEM Mode Dielectric Resonator

The disk shaped dielectric material is the simplest form of a dielectric resonator. The usual geometries of DRs are discs, rings and parallelpipeds. By inserting a metal or ferrite screws into the central hole of a ring resonator, the resonant frequency of modes can be tuned. Similar techniques are used to suppress the modes adjacent to the desired mode, to avoid interference and to reduce the dielectric loss. The mode spectrum and resonant frequencies of DRs greatly depend on the aspect ratio (diameter D/length L). The dimensions of the specimen are important to achieve wide separation of modes. The proper aspect ratios are 1.0 to 1.3 and 1.9 to 2.3. In practice the specimen diameters in the range 7 to 25 mm have been found most suitable.

1. 3 MATERIALS REQUIREMENTS

The important characteristics required for a dielectric resonator material for practical applications are

1. 3. 1. High dielectric constant

From the classical dispersion equation, at frequencies very much less than the oscillation frequency of dipole, i. e, when $w << w_i$, it can be shown that e_r is independent of frequencies in the microwave range. Hence we can write

$$e' = e_\infty + \sum 4p r_i \qquad (1.14)$$

where e_∞ is the dielectric constant caused by electronic polarisability at very high frequencies and $4p r_i$ is the strength of oscillation. It can be understood that e_r is a constant in the microwave region since it is independent of frequency. Using Far-Infrared spectroscopy the reflectance as well as transmittance can be recorded. From the reflection band, e_r is calculated using Krammer- Kronig Analysis[35] and classical dispersion theory. The method gives an indirect estimation of the dielectric constant. In the microwave frequency region e_r is measured from the resonance spectra using the resonance method.

High dielectric constant facilitates miniaturization of the devices and the miniaturization is proportional to $1/(e)^{1/2}$. According to classical dispersion theory the crystal is approximated as a system of damped oscillators having an appropriate frequency and dipole moment. The real and imaginary parts of the complex dielectric constant *(e', e")* as functions of ω (where $w = 2pn$) are given by

$$e'(w) = e_\infty + \sum_j \frac{4p r_j (w_j^2 - w^2) w_j^2}{(w_j - w^2)^2 + (g_j w)^2} \tag{1.15}$$

where $4\pi\rho_j$ is the oscillator strength, ω_j is the resonant angular frequency of frequency of the j^{th} oscillator, ε_∞ is the dielectric constant caused by electronic polarization at higher frequencies and g_j is the damping constant which is given by the width of the peak. The summation is over the j resonances in the spectrum. Each resonance is characterized by its dispersion parameters. For $w_j >> w$,

$$e'(w) = e_\infty + \sum_j 4p r_j \tag{1.16}$$

From the above equation it is clear that the dielectric constant is independent of frequency in the microwave frequency region.

1. 3. 2 High Quality Factor (Low Dielectric Loss)

Any type of defects such as grain boundaries, stacking faults, chemical or structural disorder, point defects, planar defects, line defects, inclusions, secondary phases, twinning, porosity etc contribute losses. For an ideal crystal quality factor is approximately equal to the reciprocal of the dielectric loss (tanδ). In the microwave region the loss is mainly due to the interaction of the applied field with phonons. The microwave energy is transferred to transverse optical phonons. These optical phonons can then generate thermal phonons. This leads to damping of the optical lattice vibrations and therefore causes dielectric loss. Hence there is a linear increase of loss with frequency

and is a characteristic phonon effect. In general the losses are lower for centro-symmetric crystals than the non centro-symmetric crystals. Normally a quality factor greater than 2000 is required for practical applications

The figure of merit for assessing the performance or quality of a resonator is Q factor. It is a measure of energy loss or dissipation per cycle as compared to the energy stored in the fields inside the resonator. Q factor is defined by[36]

$$Q = \frac{Maximum\ \ Energy\ \ Stored\ \ per\ \ cycle}{Average\ \ Energy\ \ Dissipated\ \ per\ \ cycle} \tag{1.17}$$

$$Q = \frac{2p\,W_0}{PT} = \frac{w_0 W_0}{P} \tag{1.18}$$

where W_0 is the stored energy, P is power dissipation, $?_o$ is resonant radian frequency and period $T = \frac{2p}{w_0}$. To a very good approximation, it can be shown that

$$Q = \frac{w_o}{\Delta w} = \frac{f_r}{\Delta f} \tag{1.19}$$

When a resonant circuit or cavity is used as a load in a microwave circuit, several different Q factors can be defined. First Q accounts for internal losses. It is the unloaded Q factor Q_0. Next external quality factor (Q_e), accounts for external losses. When the resonator is used in actual circuit there arises the loaded Q factor, Q_L which is the overall Q factor and includes both internal and external losses. The dielectric Q factor Q_d for homogeneous dielectric material is given by

$$Q_d = \frac{1}{\tan d} \tag{1.20}$$

For a dielectric loaded cavity where cavity containing an aperture

$$\frac{1}{Q_0} = \frac{1}{Q_c} + \frac{1}{Q_d} + \frac{1}{Q_r} \tag{1.21}$$

where Q_c is the conduction Q factor, Q_d is the dielectric Q factor and Q_r the radiation Q factor. When the resonator is connected to load

$$\frac{1}{Q_L} = \frac{1}{Q_e} + \frac{1}{Q_o} \tag{1.22}$$

where Q_L is the loaded Q factor, Q_e the external Q factor and Q_0 the unloaded Q factor.

1. 3. 3 Small Temperature Coefficient of Resonant Frequency (t_f)

The coefficient of temperature variation of the resonant frequency (τ_f) determines the frequency stability. It is defined as

$$\tau_f = \frac{1}{f_r} \times \frac{\Delta f}{\Delta T} \tag{1.23}$$

where f_r is the resonant frequency at room temperature, Δf is the variation of resonant frequency from room temperature for a change in temperature ΔT. The τ_f depends on the temperature variation of ε_r and coefficient of linear thermal expansion according to the expression

$$t_f = -a_L - \frac{t_e}{2} \tag{1.24}$$

The value of τ_f should be near to zero for practical applications. However often the device engineer requires a small positive or negative τ_f to compensate for the temperature variation of the resonant frequency due to the circuit.

1. 4 DETERMINATION OF MICROWAVE DIELECTRIC PROPERTIES

The ideal technique for the determination of the microwave dielectric properties of low loss materials are exact resonance methods which will be discussed in detail in Chapter 2. Apart from this technique, there has been alternate methods to characterise DRs such as Cavity Perturbation, Surface Resistance method and Whispering Gallery Mode Techniques which will be discussed in the following sections.

1. 4. 1 Cavity Perturbation

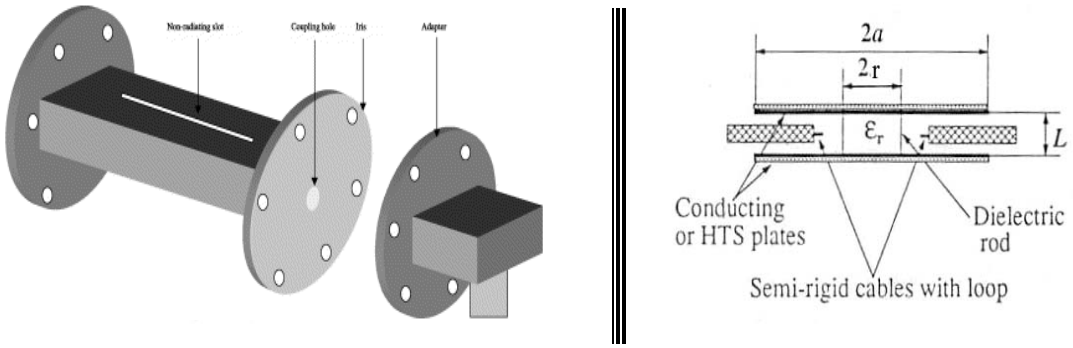

Fig. 1.5 Microwave Resonant Cavity (left) Post Resonator setup with end shorting plates coated with superconductor (right)

The Hakki-Coleman post resonator setup (See Fig. 1.5) is used for the microwave characterization of DR using surface resistance technique. The cavity perturbation method is performed by inserting a small appropriately shaped sample into the cavity and determining the dielectric properties of the sample from the resultant change in the resonant frequency and quality factor[37]. The basic assumption of the cavity perturbation is that the change in the overall geometrical configuration of the electromagnetic fields upon introduction of the sample be small[38].

Consider a cavity partially filled with dielectric. Then the loaded quality factor is given by

$$Q_d = \omega \frac{W}{P_d} = \frac{1}{\tan d} \frac{W_d + W_a}{W_d} \tag{1.25}$$

where $W = 2(W_d + W_a)$ and $P_d = 2wW_d \tan\delta$, where W_d and W_a are the electric energy stored in the dielectric and in the air respectively, and P_d is the average power dissipated in the dielectric. Then applying a formula for cavity perturbation[39]

$$\frac{\Delta f_r}{f_r} = -\frac{\Delta \varepsilon_r}{2\varepsilon_r}\left(\frac{W_d + W_a}{W_d}\right) \tag{1.26}$$

where Δf_r and $\Delta \varepsilon_r$ are the frequency shift and change of dielectric constant respectively. On substituting Eqn. 1.25 in Eqn. 1.24, we get

$$Q_d = \frac{1}{\tan\delta}\,\frac{f_r}{(-\Delta f_r / \Delta \varepsilon_r)2\varepsilon_r} \tag{1.27}$$

Knowing the quality factor of the cavity Q_c, the unloaded quality factor of the specimen can be determined using the relation[40]

$$\frac{1}{Q_u} = \frac{1}{Q_c} + \frac{1}{Q_d} \tag{1.28}$$

1. 4. 2 Surface Resistance Method

For the TE_{011} mode in a cylindrical rod, the electromagnetic waves decay almost exponentially along radial direction away from the surface resistance of the DR [41]

$$R_s = A_s\left[\frac{1}{Q_u} - \left(\frac{R_m}{A_m} + P_d \tan\delta\right)\right] \tag{1.29}$$

where A_s, A_m are geometrical factors of superconducting and metallic part respectively, P_d is the electrical energy filling factor of the dielectric resonator, R_m is the surface resistance of the metal with which the cavity is made of and Q_u is the unloaded quality

factor the resonator. If Q_L is the loaded quality factor, then the unloaded quality factor is given by

$$Q_u = Q_L(1 + ß_1 + ß_2) \tag{1.30}$$

where $ß_1$ and $ß_2$ are coupling coefficients of the resonator. The definition of the coupling coefficients is based on energy leakage through the input and output port respectively

$$ß_1 = \frac{P_{ext}}{P_{DR}} = \frac{Q_u}{Q_{ext}} \tag{1.31}$$

With low coupling constants, $ß_1 = ß_2 = 0$, the unloaded quality factor can be calculated using the equation

$$Q_u = \frac{Q_L}{1-|S_{21}|_{max}} \tag{1.32}$$

Where $|S_{21}|_{max}$ is the magnitude of the transmission coefficient at the resonant frequency.

1. 4. 3 Whispering Gallery Mode Resonators

The accuracy of microwave quality factor of low loss dielectrics measured in stripline or Courtney methods are limited due to conductor and radiation losses. The quality factor of WGM resonators are limited only by the intrinsic loss of the dielectric material. In WGM resonators, most of the electromagnetic energy is confined to the dielectric near the perimeter of the air-dielectric interface which in turn reduces the radiation and conductor loss[42, 43]. They also offer good suppression of spurious modes that leak out of the resonator and can be absorbed without perturbing the desired ones. The resonant frequencies were calculated from the dimensions and dielectric constant, determined by the end-shorted method assuming $e_{??} = e_{\perp}$ where $e_{??}$ is the dielectric constant parallel to the anisotropic axis and $e_{\perp}$, the one perpendicular to it. The energy filling factors for E and H modes are given by[44]

$$P_{e_\perp} = 2\,\frac{\partial f_r}{\partial e_\perp}\,\frac{e_\perp}{f_r} \tag{1.33}$$

$$P_{e_{II}} = 2\,\frac{\partial f_r}{\partial e_{II}}\,\frac{e_{II}}{f_r} \tag{1.34}$$

The dielectric loss tangent for the isotropic dielectric can be determined using the equations

$$Q_{(E)}^{-1} = \tan\delta\,(P_{e_\perp} + P_{e_{II}}) + R_s/G_{(E)} \tag{1.35}$$

$$Q_{(H)}^{-1} = \tan\delta\,(P_{e_\perp} + P_{e_{II}}) + R_s/G_{(H)} \tag{1.36}$$

where R_s is the surface resistance of the cavity enclosing the DR. For WGMs the geometric factor G is significantly large that the effect of cavity can be ignored when compared to the loss tangent. The energy filling factors of DR for all these modes are close to unity. The modes which have high electric energy filling factor (WGM modes) will have the highest quality factor.

1. 5 APPLICATIONS OF DIELECTRIC RESONATORS

Dielectric Resonators (DRs) can create, filter and select frequencies in oscillators, amplifiers and tuners. DRs are important components in microwave filters, oscillators, duplexers, multiplexers, combiners, radar detectors, collision avoidance systems, automatic door opening systems, telemetry, cellular radio, cordless phones or personnel communication systems, global positioning systems, satellite or military communication systems.

1. 5. 1 Dielectric Resonator Oscillators (DRO)

Oscillators represent the basic microwave energy source for all microwave systems such as radar, communications and navigation. A typical oscillator essentially consists of an active device and a passive frequency-determining resonant element such

as a dielectric resonator for fixed frequency oscillators or a varactor for a tunable oscillator. The performance of modern radar and communication systems is determined by the spectral purity of the local oscillators in the transmitters and receivers. Hence high Q ceramics having low value of residual noise are required. DR can confine most of the electromagnetic energy within itself and is suitable for oscillator applications[45]. The schematic diagram of an oscillator using DR is shown in Fig. 1. 6.

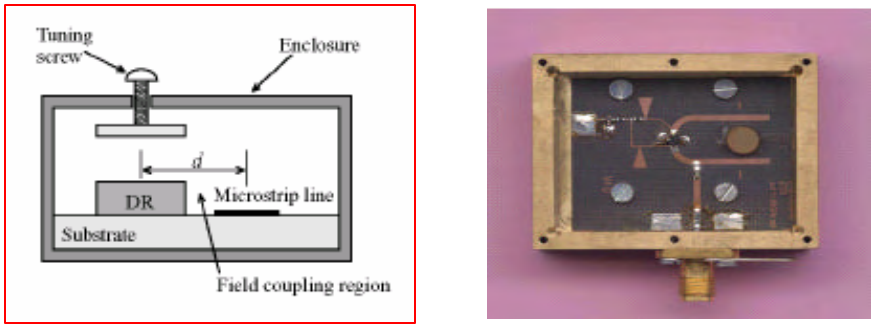

Fig. 1. 6 Schematic diagram of an oscillator using DR with mechanical tuning (left); Picture of a fixed frequency DRO

1. 5. 2 Dielectric Resonator Filters (DRF)

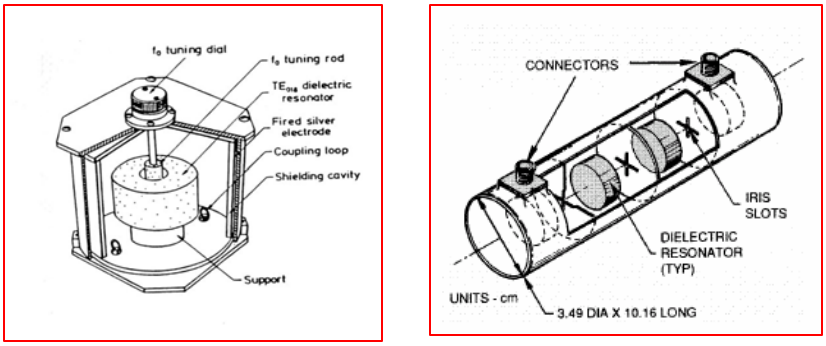

Fig. 1. 7 Schematic diagram of a typical filter using DR (left); Dual mode DR filter configuration

The high-unloaded Q factor of dielectric resonators makes it possible to produce filters with very narrow bandwidth and very low insertion loss. A variety of filter configurations are developed. The major disadvantage of DR band pass filters is that the necessary encapsulation in a metal case to minimize radiation loss makes them bulky, especially for medium and low frequencies. Therefore several miniaturization techniques

such as multimode reuse of space, supplementary energy resonators, low stored energy filter using transversal filter and mirror image techniques are developed. The schematic diagram of a filter using DR is shown in Fig. 1. 4

1. 5. 3 Dielectric Resonator Antennas (DRA)

The dielectric resonator antenna is a radiating device that has proved beneficial in the millimeter wave region since it is nonmetallic and will not suffer substantially from increasing ohmic losses at these frequencies.

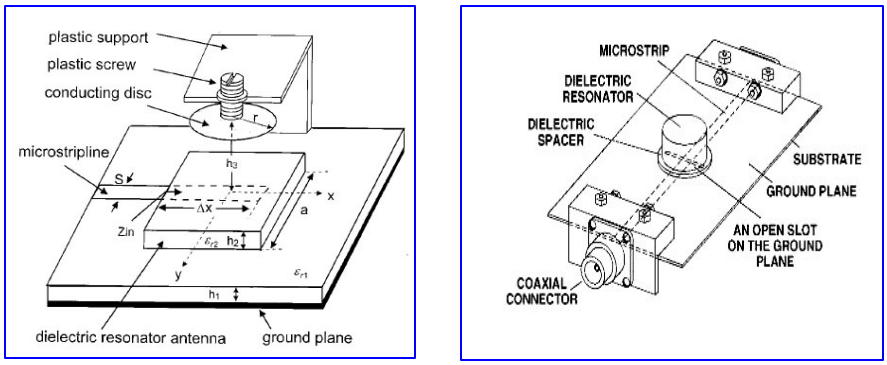

Fig. 1. 8 (a) Geometry of a DRA with adjustable frequency and (b) fixed frequency

The DR antenna element has the potential to provide significant advantages in terms of size reduction, improved bandwidth, higher power handling capability, and increased efficiency as compared with the microstrip antennas (See accompanying figures). DR antennas made from new ceramic materials with high dielectric constants and low loss are inherently smaller in size and they have greater operating bandwidths than microstrip antennas. DRAs are found to be advantageous in terms of small size, mechanical simplicity, high radiation efficiency, relatively large bandwidth, simple coupling schemes to nearly all commonly used transmission lines, and can obtain different radiation characteristics using different modes. The radiation Q factor of a DRA depends on its excitation modes as well as the dielectric constant of the ceramic material. DRs of relatively low e_r are mostly used in DR applications. On the other hand, high e_r DRs results in low profile DRAs with low resonant frequency is obtained.

1. 6 REFERENCES

1. Press Release, *Gartner Symp*., IT Expo 2004, San Diego, California (2004)

2. W. Wersing, *Cur. Opin. Sol. St. Mater. Sci*., **1**, 715–31 (1996).

3. J. C. Burfoot and G. W. Taylor, *Polar Dielectrics and Their Applications.* Macmillan Press, London (1979).

4. Rayleigh, *Phil. Mag*., **43**, 123-28 (1892).

5. R. D. Richtmeyer, *J. Appl. Phys.*, **10** 391-98 (1939).

6. F. Borgnis, *Ann. Physik*., **35**, 359-61 (1939).

7. W. L. Barrow and W. W. Maher, *Proc. Inst. Radio Engrs.*, **28**, 189-95 (1940).

8. Carrson, Mead and Schelkunoff, *Bell Systems Tech. J*., **15**, 310-14 (1936).

9. H. M. Schlicke, *J. Appl. Phys*., **24**, 187-193 (1953).

10. P. R. Longarker and C.S. Roberts, *IEEE Trans. Microw. Thoer. Tech*., **MTT-11**, 543-46 (1963).

11. J. A. Amstrong, N. Blombergen, J. Ducuing and P. S. Pershan, *Phys. Rev*., **127**, 1918-39 (1962).

12. A. Okaya, *Proc. IRE*., **48,** 1921-24 (1960).

13. A. Okaya and L. F. Barash, *Proc. IRE*, **50,** 2081-92 (1962).

14. S. B. Cohn, *IEEE Trans. Microwave Theory Tech*., **MTT-16,** 218-27,(1968)

15. H. J. Shaw, D. K. Winslow, A. Kerp and R. A. Wilson, *Appl. Phys. Lett*., **4**, 28-30 (1964).

16. D. J. Masse, R. A. Purcel, D. W. Ready, E. A. Maguire and C. D. Hartwig, *Proc. IEE*, **59,** 1628-29 (1971).

17. Y. Konishi, *Tech. Report of NHK-Nippon Hohsoh Kyoukai*, 111–117 (1971).

18. K. Plourde, *IEEE MTT-S Digest*, **25**, 202–205 (1973).

19. S. Nomura, K. Toyama, and K. Tanaka, *Jpn. J. Appl. Phys*., **21**, L624–26 (1982).

20. S. Kawashima, M. Nishida, I. Ueda, and H. Ouchi, *J. Am. Ceram. Soc*., **66**, 421–23 (1983).

21. K. Wakino, K. Minai, and H. Tamura, *J. Am. Ceram. Soc*., **67**, 278–81 (1984).

22. H. Tamura, T. Konoike, and K. Wakino, *J. Am. Ceram. Soc*., **67**, C59–61 (1984).

23. G. Wolfram and H.E. Goebel, *Mat. Res. Bull.*, **16**, 1455–63 (1981).

24. D. Kolar, Z. Stadler, S. Gaberscek, and D. Suvorov, *Ber. Dt. Keram. Ges*., **55**, 346–48 (1878).

25. A. J. Moulson and J. M. Herbert, *Electroceramics, Materials, Properties, Applications*. Chapman Hall, 1990.

26. P. J. Harrop, *Dielectrics*, Butterworth, London, 1972

27. M. Sucher and J. Fox, *Measurement of Q in Handbook of Microwave Measuremens*, 3rd Edn., Polytechnic Press, Brooklyn (1963).

28. D. Kajfez and P. Guillon, *Dielectric Resonators*, Noble Publishing Corp., Atlanta (1998).

29. D. Kajfez, *Q Factor*, Vector Fields , Oxford (1994).

30. L. A. Trinogga. G. Kaizhou and I. C. Hunter, *Practical Microstrip Circuit Design*, Ellis Horwood, Boston (1991).

31. P. Vincent, *Appl. Phys*., **A-31**, 51-54 (1983).

32. S. K. Kaul, *Millimeterwaves and Optical Dielectric Integrated Circuits*, Wiley, New York (1997).

33. P. Guillion, B. Byzery and M. Chaubet, *IEEE Trans. Micro. Theor. Tech*., **MTT-33**, 222-26 (1985)

34. Y. Konishi, *Proc. IEE*, **79**, 726-40 (1991).

35. V. L. Gurevich, and A. K. Tagantsev, *Adv. Phys*., **40**, 719–67 (1991).

36. I. J. Bahl and P. Bhartia, *Microwave Solid State Circuit Design*, New York: Wiley, 1988.

37. H. A. Bethe and J. Schwinger, *NDRC Rep*., **D1,** 117-17 (1943).

38. S-H. Chao, *IEEE Trans. Microwave Theory Tech*., **MTT-33**, 519-26 (1985).

39. R. F. Harrington, *Time Harmonic Electromagnetic Fields*, p. 321-26, McGraw Hill, New York (1961).

40. Y. Kobayashi, T. Aoki and Y. Kabe, *IEEE Trans. Microwave Theory Tech*., **MTT-33**, 1361-65 (1985).

41. J. Mazierska, *J. Supercond*., **10**, 73-84 (1997).

42. L. Rayleigh, *Phil. Mag*., **20**, 1001-04 (1910).

43. J. R. Wait, *Radio Sci.*, **2**, 1005-17 (1967).

44. J. Krupka, D. Cros, M. Aubourg and P. Guillon, *IEEE Trans. Microwave Theory Tech*., **42**, 56-61 (1994).

45. J-S. Sun and Y-L Huang, *Microwave J.*, 93-103 (1999).

CHAPTER 2

SYNTHESIS AND CHARACTERIZATION

Chapter 2 presents a detailed account of the most commonly used preparation method (solid state mixed oxide route) for the synthesis of low loss dielectric ceramics. A qualitative discussion on the microwave characterisation tools to determine the dielectric constant, quality factor and temperature coefficient of resonant frequency, of the dielectric resonators are given. A brief description of the instrumentation used for studying the structural, microstructural and dielectric characteristics of low loss materials studied in the purview of this thesis is also presented.

2. 1 CERAMIC FABRICATION TECHNOLOGY

2. 1. 1 Introduction

Ceramic fabrication is the combination of various process technologies to produce monolithic or composite ceramic components within a given shape, size and microstructure property bounds for a given composition[1]. The ceramics are in general compounds of the electropositive and electronegative elements of the periodic table. They are polycrystalline materials, which contain fine crystalline grains, grain boundaries, impurities segregated in the grain boundaries as well as the grains, pores in the grains, grain boundaries and imperfections.

Most of the synthesis methods of organic and metallic counterparts are generally not suitable for ceramics, due to the brittleness and to the refractory nature of ceramic materials. With exception of glass technology, ceramic forming techniques are generally based on powder processing with powder synthesis, forming and sintering. The synthesis of specific powders and the better control of chemical and of physical characteristics of ceramic powders allow obtaining improved and/or reproducible properties

It is then necessary to understand the fundamental mechanisms, which take place during the different steps of the process to obtain reliable and desirable properties of the final parts. Several methods[2] can be used for the preparation of ceramic powders. The methods can be divided into three categories: (a) mechanical methods and (b) solid state reaction methods and (c) chemical methods.

In the mechanical methods, small particles are produced from larger ones by mechanical forces, a process referred to as comminution. The process of comminution involves operations such as crushing, grinding and milling. Powders of traditional ceramics are generally prepared by mechanical methods from naturally occurring raw materials.

2. 1. 2 Solid State Synthesis of Ceramics

The solid state oxide route is considered to be one of the oldest and easiest materials synthesizing techniques for the synthesis of complex oxide materials.

Metal oxides containing more than one type of cation are of interest from both an academic and commercial point of view. This is because complex metal oxides exhibit a number of features that are not found in simple oxides. For example, mixed metal oxides can stabilize both high and mixed volume states of transition metal elements[3]. Additionally mixed oxides can provide new structural arrangements such as those found in perovskites, spinels or pyrochlores[4].

The conventional ceramic approach involves basically three steps (a) intimate mixing of the stoichiometric oxides, (b) high temperature firing and (c) intermediate grinding.

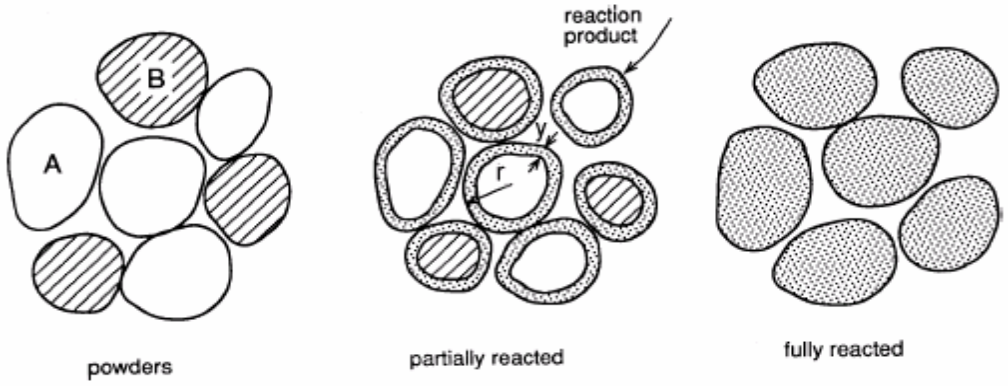

Fig. 2. 1 Reaction between two kinds of particles to form a product at the points of contact

On heating at high temperatures, a new material is formed (see Fig. 2.1) to reduce the free energy, at the points of contact through solid state diffusion. This new product layer (of a few ?) eventually acts as a potential barrier between two grains and thus impeding further grain to grain material transport. This demands the need of new points of contacts to be introduced which is usually achieved though grinding or ball milling. This frequent grinding coupled with multiple calcination maximizes the product to reactant ratio.

The reactant particles are schematically illustrated to emphasize the fact that no matter what the particle size is, each reactant particle contains only one type of cation. The severe reaction conditions are necessary to obtain single phase product because of the diffusional limitations of the solid state reactions. Initial reaction is rapid but further

reaction goes slower and slower as the product layer builds up and the diffusion paths become longer. A fine powder of approximately 10 μm (or 100,000 ?) particle size still represents diffusion distances of the order of 10,000 unit cell dimensions[5]. The use solution synthesis improves the reactivity of the component oxides or salts because these methods can give initial crystallites of the order of only several hundred ? in diameter. This means that diffusion must occur across 10 to 50 unit cell dimensions in chemical synthesis techniques. The main disadvantage of solid state synthesis is obviously the high temperature needed to form the product which leads to agglomerated particles with poor surface area[6].

The solid-state reaction method, which is employed in the present work, involves the following steps:

2. 1. 2. 1 Weighing of Raw Materials

The first step in the solid-state reaction method is to weigh the different powders which act as reactants according to the stoichiometry. The presence of impurities in the raw materials can affect reactivity as well as dielectric properties of the fired ceramics. The raw material purity of greater than 99.9 % is essential for obtaining phase pure compounds. Electronic Balance is used to obtain accuracy up to four decimal places.

2. 1. 2. 2 Stoichiometric Mixing

The raw materials need to be intimately mixed to increase the points of contacts between reactant oxides, which in turn act as ‘product layer formation centres’. Hence the raw materials constituting the batch must be intimately mixed. The mixing and milling eliminates agglomerates and reduces particle size. If agglomerates are present they densify more rapidly resulting in pores. During the mixing process agglomerates are broken and defects are introduced into the grains that enhance diffusion mechanism. Therefore the mixture of powders is ground well and thoroughly mixed using distilled water or acetone. Ball mills are used for the mixing purpose. Zirconia balls are used in the present investigation.

2. 1. 2. 2. 1 Ball Milling

In the milling process, the particles experience mechanical stresses at their contact points due to compression, impact or shear with the milling medium or with other particles [7]. The mechanical stress leads to elastic and inelastic deformation. If the stresses exceed ultimate strength of the particle, it will fracture the particles. The mechanical energy supplied to the particle is used not only to create new surfaces but also to produce other physical changes in the particle[8].

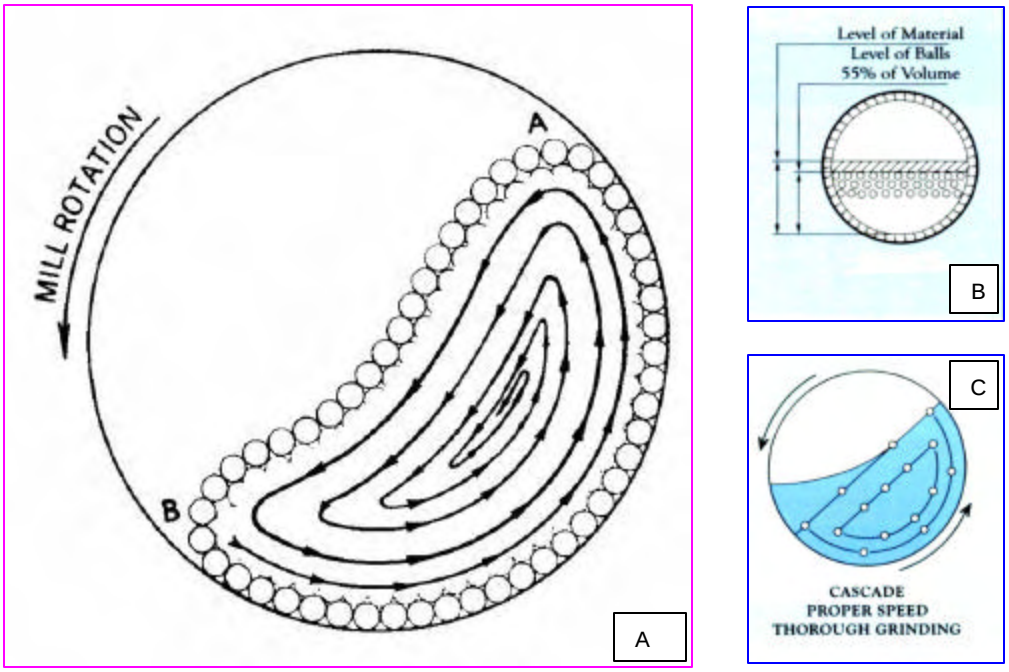

Fig. 2. 2 (A) Size reduction process in tumbling ball milling (B) Optimum ball-to-powder ratio and (C) Optimum speed in ideal milling conditions.

Tumbling ball mills usually refer to simply as ball mills consisted of a slowly rotating horizontal jar that is partially filled with grinding media and particle to be ground. In a tumbling ball-mill the rate of grinding depends on a number of factors including mill parameters (diameter, speed, amount of milling media), properties of the milling media (size, hardness, shape) and the properties of the particles to be ground.. The rate of grinding increases inversely as the radius of the balls. The rate of grinding depends upon the radii of the mill bottle and density of the milling media and initial particle size of the powder [9]

$$\text{Rate of grinding} \approx \frac{AR^{1/2}\, r\, d}{r} \qquad (2.1)$$

where A = numerical constant that is specific to the mill being used, R = radius of the mill, r = density of the balls, d = particle size of the powder and r = radius of the balls. According to the above equation, the rate decreases with decreasing particle size, but after a finite time a practical grinding limit is reached.

For wet milling, a useful guide is for the balls and slurry together should occupy 50 % of the mill volume with the solid content of the slurry equal to 20-40% (see Fig. 2.2). For dry milling, for a quantity of balls filling about 50 % of the mill volume, the permissible charge content is 25 %. Wet milling has the advantage of higher energy utilisation (by 10-20 %) over dry milling.

The shape of the milling media (balls) is an important factor in ball milling as it determines the product size distribution. Using spherical ball the size distribution is broad since two balls have only one point of contact between them. On the other hand using cylindrical balls with 'dome ends' the particle size distribution is more uniform with narrow distribution curves[10]. This is due to the fact that cylindrical balls offer a line of contact between them. We used a very dense (density = 6.1 g/cm^3), hard (hardness = 9 in Moh's scale) Zirconox (which is Ceria stabilised Zirconia) balls for ball milling.

2. 1. 2. 3 Calcination

Chemical reactions between solid starting materials, usually in the form of mixed powders, are common for the production of powders of complex oxides such as titanates, ferrites and silicates. The reactants normally consist of simple oxides, carbonates, nitrates, sulfates, oxalates or acetates. An example is the reaction between barium carbonate and titania to produce barium titanate:

Calcination is the intermediate heat treatment at a lower temperature prior to sintering. Calcination involves chemical decomposition reactions, in which a solid

reactant is heated to produce a new solid plus a gas which are commonly used for the production of powders of simple oxides from carbonates, hydroxides, nitrates, sulfates, acetates, oxalates, alkoxides and other metal salts.

The kinetics of solid state reactions occurring during calcination may be controlled by any one of three processes: (i) the reaction at the interface between the reactant and the solid product, (ii) heat transfer to the reaction surface or (iii) gas diffusion or permeation from the reaction surface through the porous product layer. The calcination conditions such as temperature, duration of heating and atmosphere are important factors controlling shrinkage during sintering. Though the final phases of interest may not be completely formed, the calcination yields a consistent product.

Cost effectiveness and simplicity of synthesis are the major advantages of this solid state reaction procedure.

2. 1. 2. 4 Grinding

Grinding can be accomplished by any suitable means. It prepares the reacted material for ceramic forming. The grinding also helps to homogenise the compositional variations that may still exist or that may arise during calcination. Generally, grinding to somewhere around 1 to 10 μm is advisable. If the grind is coarser the ceramic can have larger intergranular voids and lower fired density. If grinding is too fine, the colloidal properties may interfere with subsequent forming operations[11]. Generally for grinding purpose ball mill or mortar with pestle is used. In large scale operation a grinding medium is chosen that suffers very little wear.

2. 1. 2. 5 Addition of Polymeric Binder

The principal functions of a ceramic binder is to impart sufficient strength and appropriate elastic properties for handling and shaping during the post forming stage. In modern ceramics technology, in die pressing, a narrow range of water-soluble organic binders, such as poly vinyl alcohol is most often applied to improve the rheological properties of the powder compact [12]. The polymeric dispersions and organic binders provide the pressed ceramic powders with optimal properties from the point of view of

thickening abilities and mechanical strength of the pressed samples[13]. The commonly used polymers ceramic binding purpose are poly vinyl alcohol (PVA), poly ethylene glycol (PEG), carboxymethylcellulose etc. most of which are water thinnable polymeric dispersions. The binder concentration for each process is about 3 % in dry process, 3-17 % in wet processing and 7-20 % in plastic forming [14]. The recent research trends suggest that the PVA and PEG are ideal binder additives for fabrication of microwave dielectric ceramics [15]. The PVA burn out on heating to about 400^{o}C

2. 1. 2. 6 Uniaxial Pressing

Calcined product undergoes a limited amount of sintering and hence it is again thoroughly ground. The fine powder is then compacted into cylindrical specimen by uniaxial dry-pressing. Compaction is done slowly to facilitate the escape of the entrapped air.

Uniaxial pressing involves the compaction of powder into a rigid die by applying pressure in a single axial direction through a rigid punch or piston. The pressure gradient in powder compact as function of the distance from the upper punch is given by the formula

$$P_x = P_a \exp\left[-4\mu K\frac{L}{D}\right] \qquad (2.2)$$

where μ is the coefficient of friction, P_a is the applied pressure, L is the length and D is the diameter of the powder compact. It is evident that the pressure distribution of a powder compact is more uniform when the length to diameter ratio is smaller[16].

In the microwave dielectric measurements we prepare samples with D/L ratio = 2.0 and hence the pressure distribution is more or less uniform in the powder compacts. Pressures of 50-150 MPa is ideal in ceramic forming.

Friction between the powder and die wall decreases the pressure available for compaction with increasing distance from the pressing punch. Since compact density is directly related to forming pressure, a forming pressure gradient becomes a density

gradient in the compact. Friction is influenced by the die material and its surface finish, nature of the powder and the organic additives used. Internal lubricants such as Stearic Acid dissolved in Propan 2-ole, can aid processing.

2. 1. 2. 7 Solid State Sintering

Sintering is the heat treatment of powder compacts at elevated temperatures, where diffusional mass transport is appreciable which results in a dense polycrystalline solid[17]. The driving force for sintering is a decrease in the surface free energy of powdered compacts, by replacing solid-vapour interfaces (of surface energy Γ_{SV}) with solid-solid (Γ_{SS}) interfaces, where $\Gamma_{SS} < \Gamma_{SV}$. Thermodynamically, then, sintering is an irreversible process in which a free energy decrease is brought about by a decrease in surface area.

The principal goal of sintering is the reduction of compact porosity. The development of microstructure and densification during sintering is a direct consequence of mass transport through several possible paths and one of these paths is usually predominant at any given stage of sintering[18]. They are (i) evaporation/condensation (ii) solution/ precipitation (ii) lattice diffusion and (iv) surface diffusion or grain boundary diffusion.

The sintering phenomena are of two types: Solid-state sintering, where all densification is achieved through changes in particle shape, without particle rearrangement or the presence of liquid and liquid-phase sintering, where some liquid that is present at sintering temperatures aids compaction.

The change of system energy dE due to sintering is composed of the increase due to the creation of new grain boundary areas, d$A_{SS} > 0$, and due to the annihilation of vapour-solid interfaces, d$A_{SV} < 0$. The necessary thermodynamic condition for the sintering to proceed is [19]

$$dE = \Gamma_{SS}\, dA_{SS} + \Gamma_{SV}\, dA_{SV} < 0 \qquad (2.3)$$

The sintering process will stop when dE = 0, i.e.

$$\Gamma_{SS}\, dA_{SS} + \Gamma_{SV}\, dA_{SV} = 0 \quad \text{i.e.} \tag{2.4}$$

$$\Gamma_{SS} / \Gamma_{SV} = - dA_{SV} / dA_{SS} \tag{2.5}$$

2. 1. 2. 7. 1 Stages of Sintering

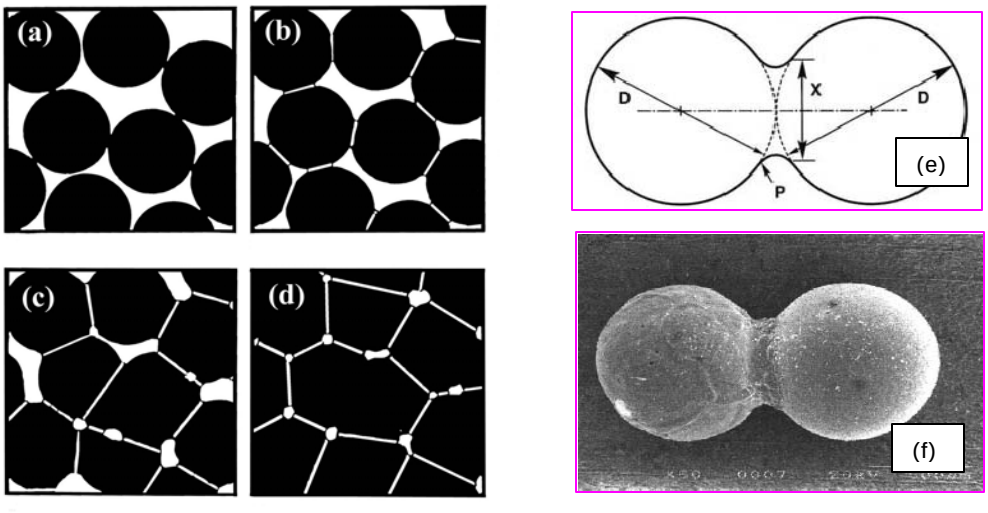

Fig. 2.3 (a) & (b) Initial stage, (c) Intermediate stage and (d) Final stage of sintering. (e) Neck formation during first stage and (f) SEM picture of neck formation in sintered alumina

(a). Initial stage of sintering, involving

- (i) Local point of contact formation or "fusion", without shrinkage of compact. This is accompanied by smoothing of the free surface of particles.
- (ii) Neck formation at the contact point, with the resulting concave curvature δ_n (where $\delta_n = 1/r_n$) at the neck, in contrast to the convex curvature on the particle surface of radius r, where $r >> r_n$.

The processes (i) and (ii) result in densification of the sintering component by ~10%. That is, if the relative green density after forming of the particle compact was 60%, the density after initial stage would be about 70% of the theoretical density (TD). However, the 10% densification in the initial stage is reached very quickly (seconds or

minutes) after exposing powder to high temperature, because of the large surface area and the high driving force for sintering[20].

(b). Intermediate stage of sintering, involving:

- (c) Neck growth,
- (d) Pores forming arrays of interconnected cylindrical channels.
- (e) Particle centres approaching one another, resulting in the compact shrinkage

The shrinkage in the intermediate stage can result in additional densification by as much as 25%, or to a total of about 95% of the TD (theoretical density)[21]. However, shrinkage does not necessarily have to take place during the intermediate stage of sintering.

(c). Final stage of sintering, involving:

- (f) Isolation of pores, i.e. relative density exceeding ~93%
- (g) Elimination of porosity
- (h) Grain growth

The final sintering stage begins at about 93-95% of theoretical density, when porosity is already isolated [22]. Ideally, at the end of this stage all porosity is eliminated. The complete elimination of porosity in the final stage of sintering can only happen when all pores are connected to fast, short diffusion paths along grain boundaries (or, equivalently, if the grain boundaries remain attached to the pores).

2. 1. 2. 8 Liquid Phase Sintering

When a wetting liquid is present during the process of sintering, bulk viscous flow can result in volume shrinkage. However, commercial ceramics tend to have a small amount of reactive liquid that accelerates the densification rather than facilitate viscous flow. A simple type is a eutectic liquid in which the primary phase is partially soluble is often used in perovskite systems. When the liquid coats each grain, the material can often be sintered to a higher density at a lower temperature with less of a

tendency for exaggerated grain growth. Less than 1 volume % of the liquid phase is sufficient to coat the grains if the liquid is distributed uniformly and the grain size is about 1μm. The wetting liquid concentrates at the particle contacts and forms a meniscus; this exerts an effective compressive pressure on the compact. There is a rapid rearrangement of particles into a higher density configuration.

2. 2 MICROWAVE CHARACTERISATION OF DIELECTRIC RESONATORS

2. 2.1 Introduction

Generally the methods for the measurement of dielectric and magnetic properties of materials at microwave frequencies can be subdivided into 5. They are (i) perturbation methods, (ii) optical methods, (iii) transmission line methods, (iv) reflection methods and (v) exact resonance methods. The choice of method or combination of methods will depend on the value of ε_r and loss factor, the amount of material available, the accuracy required, and whether the technique is required for research or routine measurements.

Perturbation Technique: The perturbation methods are highly suitable for materials of small size since the material should not alter the field configuration considerably. These techniques are suitable for dielectric constants less than 10, although this range can be extended by an exact solution of the resonator containing the specimen[23]. Hence this technique is not commonly used for DR characterisation.

Optical Methods: Optical methods are applicable for below wavelength of one centimetre. Since this method requires large amount of material it is not suitable for DRs[24].

Transmission line techniques: This technique has a serious disadvantage of the very small waveguide size used below 4 mm, which gives rise to practical difficulties[25]. More over imperfections in the sample dimensions produce errors in the measurement. It was reported that the accuracy of transmission mode measurements of the dielectric properties is more in weak coupling conditions[26].

Reflection methods: In reflection methods, waves reflected from the dielectric are studied. When the dielectric constant becomes large, there occurs considerable error in the measurement of complex voltage reflection coefficient[27].

Resonance methods: Exact resonance method is the most accurate method as compared to the above-mentioned methods for the measurement of DRs. In this method, the exact resonant frequency of the resonator is measured using different techniques[28]. From the resonant characteristics, parameters like ε_r, Q etc are determined. Special techniques of exact resonance methods are used in the present study, which are described in detail in the following sections.

2. 2. 2 Measurement of Dielectric Constant (e_r)

In this method developed by Hakki and Coleman[29] a circular disc of material to be measured is inserted between two mathematically infinite conducting plates, as shown in Fig 2.4. The apparatus used by them is shown in Fig. 2.4 (right). If the dielectric material is isotropic then the characteristic equation for this resonant structure operating in the TE_{0nl} mode is written as

$$a\frac{J_0(a)}{J_1(a)} = -b\frac{K_0(b)}{K_1(b)} \qquad (2.6)$$

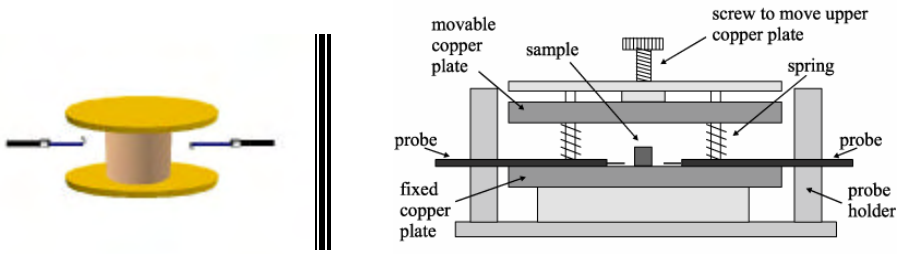

Fig. 2. 4 A dielectric rod kept end shorted between two mathematically infinite conducting plates

where $J_0(\alpha)$ and $J_1(\alpha)$ are Bessel functions of the first kind of orders zero and one respectively. The $K_0(b)$ and $K_1(b)$ are the modified Bessel functions of the second kind

of order zero and one respectively. The parameter a and b depend on the geometry, the resonant wavelength inside and outside the DR respectively and dielectric properties. Thus

$$a = \frac{pD}{l_o}\left[e_r - \left(\frac{l l_o}{2L}\right)^2\right]^{1/2} \tag{2.7}$$

$$ß = \frac{pD}{l_o}\left[\left(\frac{l l_o}{2L}\right)^2 - 1\right]^{1/2} \tag{2.8}$$

where

l = the longitudinal variations of the field along the axis

L= Length of the DR

D= Diameter of the DR

l_0 = free space resonant wave length

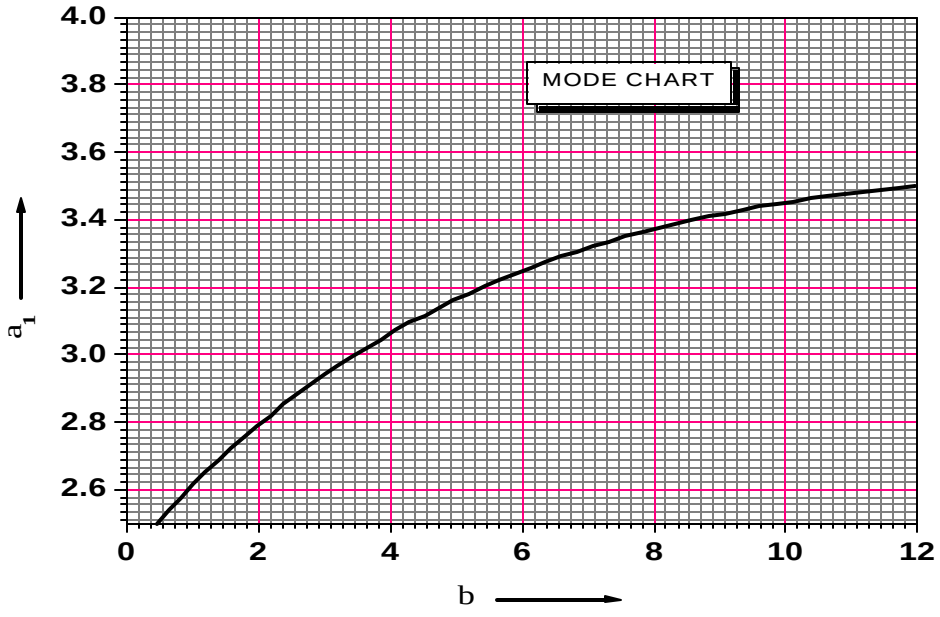

Fig. 2.5 Mode charts of Hakki and Coleman giving a_1 as functions of b.

The characteristic equation is a transcendental equation and hence a graphical solution is necessary. Corresponding to each value of b there are infinite number of (a_n) that solves the characteristic equation. Hakki and Coleman obtained a mode chart showing the variation of a values as a function of b and are shown in Fig. 2. 5.

The dielectric constant of the resonator can be calculated using the mode chart parameters (a_1 and b_1), the resonant frequency (f_r) and the dimensions of the dielectric puck using the equation

$$e_r = 1 + \left[\frac{c}{pDf_r}\right]^2 \left(a_1^2 + b_1^2\right) \tag{2.9}$$

The horizontally oriented E-field probes for coupling microwaves to the DRs, was proposed by Courtney[30] which enabled to span a wide range of frequencies, since there is no cut-off frequency for coaxial lines. The TE_{011} mode is used for the measurements since this mode propagates inside the sample but is evanescent out side it. Therefore a large amount of electrical energy can be stored in the high Q dielectric resonators[31]. However, in the open space post resonators setup, a part of electrical energy is radiated out as evanescent field and hence the axial mode number is usually expressed as d since it is less than 1 (i.e. TE_{01d}). In the end shorted condition the E field becomes zero close to the metal wall and electric energy vanishes in the air gap[32].

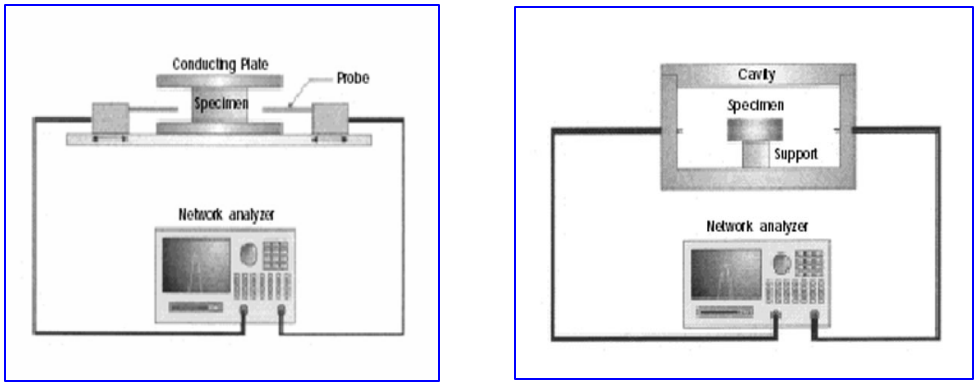

Fig. 2.6 Dielectric resonator in (a) Hakki-Coleman and (b) Krupka configurations for measuring e_r and Q factor

In the experimental setup, a Vector Network Analyser, HP 8510 C is used for taking measurements at microwave frequencies. The HP 9000, 300 series instrumentation computer, interfaced with network analyser makes the measurement quicker and accurate. The specimen is placed approximately symmetrical with the two probes. The resonant modes are visualised by giving a wide frequency range by adjusting the Network Analyser. To select the TE_{011} resonance from the several modes having non zero E_z components the upper metal plate is slightly tilted to introduce an air gap. As the plate is tilted the entire TM modes move rapidly to the higher frequencies while the $TE_{01\delta}$ mode remains almost stationary. It is well known that in exact resonance technique, $TE_{01\delta}$ is least perturbed by the surroundings. After identifying the $TE_{01\delta}$ resonant frequency or central frequency (f_o), the span around f_o is reduced as much as possible to get maximum resolution. The 3 dB bandwidth of the curve decreases and a stage of saturation is reached when the width will remain the least possible. The coupling loops are fixed at this position and the centre frequency can be noted corresponding to the maxima as f_0. By knowing the diameter 'D' and length 'L' of the sample β is calculated using equation 2. 11. From the mode chart the value of α_1 corresponding to β_1 value is noted. The dielectric constant ε_r is calculated using Eqn. 2.9.

2. 2. 3 Measurement of Unloaded Quality Factor (Q_u)

Accurate measurements of microwave properties of materials using dielectric resonators requires precise computations of the unloaded Q factor of the resonator. There are various methods which enables measurement the Q-factors of microwave resonators [33, 34, 35, 36]. However, not all of them take into account practical effects introduced by a real measurement system. The practical effects include noise, crosstalk, coupling losses, transmission line delay, and impedance mismatch. Inadequate accounting of these effects may lead to significant uncertainty in the Q-factor obtained

For a DR, the quality factor measured for the TE_{011} mode using the parallel plate rod resonator is very low since there occurs losses due to conducting plates, radiation etc. under end shorted condition. This can be mathematically written as

$$\frac{1}{Q_L} = \frac{1}{Q_D} + \frac{1}{Q_c} + \frac{1}{Q_r} + \frac{1}{Q_{EXT}} \tag{2.10}$$

where $\frac{1}{Q_L}$ is the total loss of the system, $\frac{1}{Q_D}$ is dielectric loss, $\frac{1}{Q_c}$ loss due to conductivity of the metallic plates, $\frac{1}{Q_r}$ is the loss due to radiation and $\frac{1}{Q_{EXT}}$ is the loss due to external coupling. First three terms on the right hand side of the Eqn. 2.10 comprise what is usually called the unloaded loss factor of the resonant cavity. That is

$$\frac{1}{Q_u} = \frac{1}{Q_D} + \frac{1}{Q_c} + \frac{1}{Q_r} \tag{2.11}$$

In the present study the unloaded quality factor (Q_u) of the DRs is measured using a transmission mode cavity proposed by Krupka et al[37]. The DR is placed inside a cylindrical cavity. The cavity is made of copper and the inner surfaces are silver coated. The sample can be mounted centrally on a cylindrical quartz support. Microwave is fed using loop coupling. The ability to tune the frequency is very useful for the accurate determination of the resonant mode and to allow it to measure samples various dimensions.

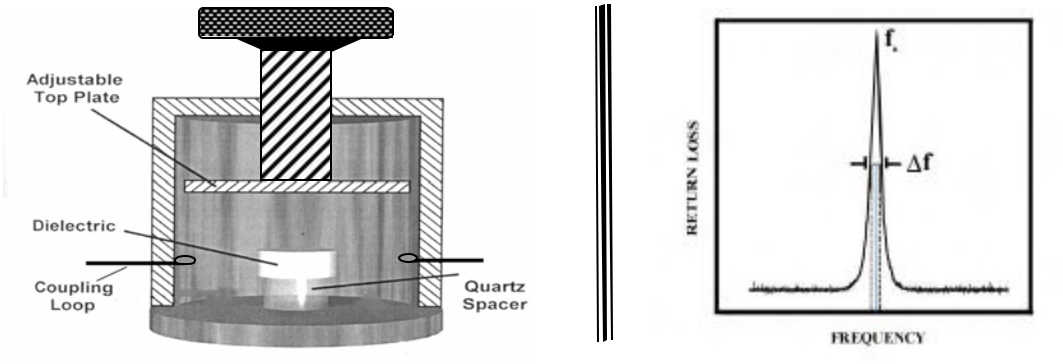

Fig 2. 7 The cavity set up for the measurement of Q factor (left); The method of calculating from resonant mode using Eqn. 2.15 (right).

In principle the cavity has infinite number of modes, when excited with microwave spectrum of frequencies. Samples with 12.5 to 20 mm diameter is the optimum for the measurements. Usually D/L ratio of 2-2.5 is maintained to get maximum mode separation to avoid interference from other modes. Also the electric field is symmetric with the geometry of the sample and the cavity, which helps to reduce the sources of loss due to cavity. As seen in Fig. 2.7, the sample is isolated using a quartz spacer, from the effects of losses due to the finite resistivity of the cavity end-plates.

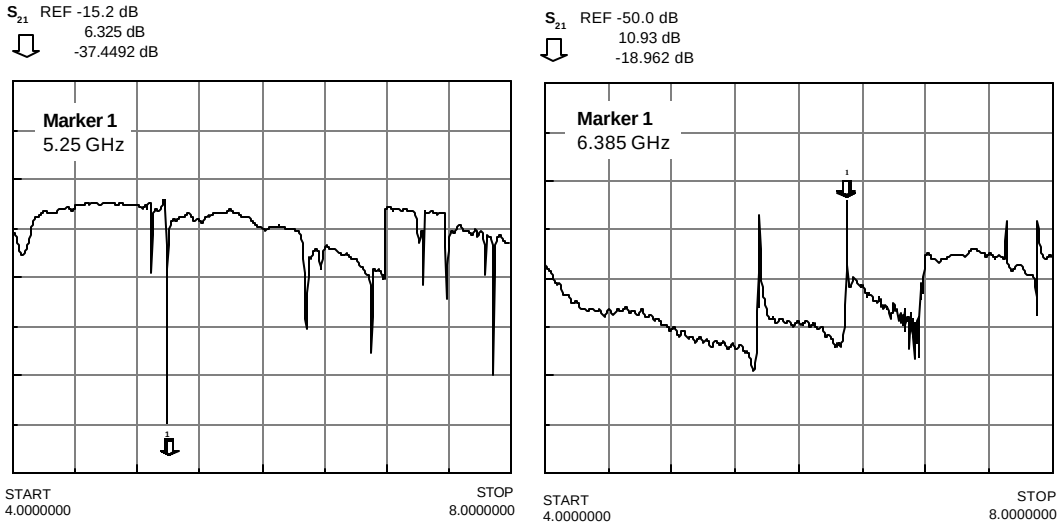

Fig. 2. 8 The microwave resonance spectrum of $Ba(Mg_{1/3}Ta_{2/3})O_3$ (e_r=24.5) in reflection (left) and transmission (right) configuration

In order to measure the Q factor the sample is mounted centrally at the cavity on the quartz support and the cavity is closed with the lid. Observe S_{21} versus frequency. For lossy samples coupling need to be increased to get the resonance. Measure $TE_{01\delta}$ mode frequency and the unloaded Q factor. One can assume that the unloaded Q factor is equal to loaded Q factor if coupling is weak. The coupling is assured symmetric. The Q factor can be calculated using the expression

$$Q = \frac{f_o}{\Delta f} \tag{2.15}$$

2. 2. 4 Measurement of Temperature Coefficient of Resonant Frequency (t_f)

For an ideal resonator the temperature coefficient of resonant frequency (τ_f) should be near to zero. Since resonators are used in communication systems temperature stability is an important factor and should be near to zero.

In order to measure τ_f, DR is kept end shorted between two copper plates. This is then kept on a hot plate and insulated in an isothermal enclosure. The E-field probe is kept near the DR in such a way to get resonance. The TE_{011} mode is identified as described in section 2. 2. 2. The set up is then slowly heated (~ 1^oC/minute) in the range 25 to 80^oC. The probe of the thermocouple is kept just inside the isothermal enclosure so that it does not disturb the resonant frequency. Shift of the resonant frequency as a result of heating in the reflection mode is noted using Network Analyser and HP 8350 B Sweep Oscillator. The variation of resonant frequency is plotted as function of temperature. The t_f is calculated from the slope of the curve using equation

$$t_f = \frac{1}{f}\frac{\Delta f}{\Delta T} \tag{2.16}$$

2. 2. 5 Error Calculations in Dielectric Property Measurements

The measurement of microwave dielectric properties were done with two decimal point accuracy. Usually three samples were prepared in a batch corresponding to a particular composition and the measurements were made at least twice per each specimen. The error in e_r is calculated using the root sum of squares (RSS) method. The accuracy of e_r measurement is restricted to the accuracy in measurement of resonant frequency and dimensions of the sample. The error in e_r measurement is less than $\pm$ 0.01. The possible errors in the measured value of dielectric constant include that associated with the samples height (L), radius (r) and resonant frequency (f_r) given by

$$? e_r = \left[\left(\frac{\partial e_r}{\partial L} \quad \Delta L \right)^2 + \left(\frac{\partial e_r}{\partial r} \quad \Delta r \right)^2 + \left(\frac{\partial e_r}{\partial f_r} \quad \Delta f_r \right)^2 \right]^{1/2} \tag{2.17}$$

If the independent sources of error corresponds to one standard deviation, then the error in e_r will also corresponds to one standard deviation[38]. The errors in unloaded quality factor (Q_u) and temperature coefficient of resonant frequency (t_f) were calculated using RSS method by taking partial derivative of these parameters with respect to independent variables.

2.3 MAJOR INSTRUMENTATIONS USED

2. 3. 1 X-Ray Diffractometer

An X-ray incident upon a sample will either be transmitted, in which case it will continue along its original direction, or it will be scattered by the electrons of the atoms in the material. All the atoms in the path of the X-ray beam scatter X-rays. In general, the scattered waves destructively interfere with each other, with the exception of special orientations at which Bragg's law is satisfied.

The phenomenon of diffraction occurs when penetrating radiation, such as X-rays, enters a crystalline substance and is scattered. The direction and intensity of the scattered (diffracted) beams depends on the orientation of the crystal lattice with respect to the incident beam[39]. Any face of a crystal lattice consists of parallel rows of atoms separated by a unique distance (d-spacing), which are capable of diffracting X-rays. In order for a beam to be 100 % diffracted, the distance it travels between rows of atoms at the angle of incidence must be equal to an integral multiple of the wavelength of the incident beam [40].

An X-ray diffractometer utilizes a powdered sample, a goniometer, and a fixed-position detector to measure the diffraction patterns of unknowns. The powdered sample provides (theoretically) all possible orientations of the crystal lattice, the goniometer provides a variety of angles of incidence, and the detector measures the intensity of the diffracted beam. The resulting analysis is described graphically as a set

of peaks with % intensity on the Y-axis and goniometer angle on the X-axis. The exact angle and intensity of a set of peaks is unique to the crystal structure being examined[41]. The X-Ray diffraction method is most useful for qualitative, rather than quantitative, analysis (although it can be used for both). The monochromator is used to ensure a specific wavelength reaches the detector, eliminating fluorescent radiation. The resulting trace consists of a recording of the intensity Vs. counter angle (2θ). The trace can then be used to identify the phases present in the sample. Diffraction data from many materials have been recorded in a computer searchable Powder Diffraction File (JCPDS File). Matching the observed data in the PDF allows the phases in the sample to be identified [42, 43].

2. 3. 2 Scanning Electron Microscope

In light microscopy, a specimen is viewed through a series of lenses that magnify the visible-light image. However, the scanning electron microscope (SEM) does not actually view a true image of the specimen, but rather produces an electronic map of the specimen that is displayed on a cathode ray tube. The SEM is a microscope that uses electrons instead of visible light to form an image. The scanning electron microscope has many advantages over traditional microscopes. The SEM has a large depth of field, which allows more of a specimen to be in focus at one time[44]. The SEM also has much higher resolution, so closely spaced specimens can be magnified at much higher levels. Because the SEM uses electromagnets rather than lenses, the researcher has much more control in the degree of magnification.

A beam of electrons is produced at the top of the microscope by an electron gun. The electron beam follows a vertical path through the microscope, which is held within a vacuum. The beam travels through electromagnetic fields and lenses, which focus the beam down toward the sample. Once the beam hits the sample, electrons and X-rays are ejected from the sample (see Fig. 2.9(a)). Detectors collect these X-rays, backscattered electrons, and secondary electrons and convert them into a signal that is sent to a screen similar to a television screen. This produces the final image [45]. All metals are conductive and require no preparation before being used. All non-metals

need to be made conductive by covering the sample with a thin layer of conductive material like gold [46].

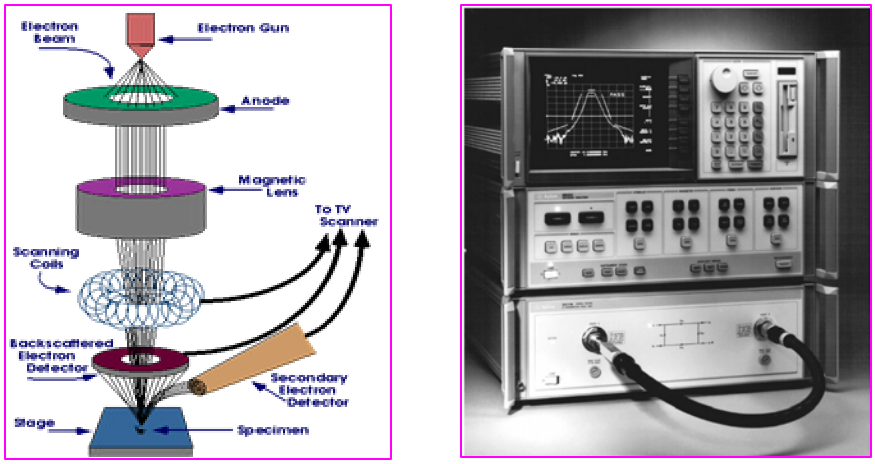

(a) **(b)**

Fig. 2.9 (a) Schematic Diagram of SEM (b) Picture of HP 8510 C Vector Network Analyzer

2. 3. 4 Network Analyzer

A basic network analyzer is designed to show graphically, a plot of the voltage gain or loss of a network versus frequency. The network analyzer measures the magnitude, phase, and group delay of two-port networks to characterize their linear behaviour. These sorts of plots are called Bode plots and are frequently shown in textbooks on circuit design and are produced by computer circuit analysis programs. A network analyzer consists of a swept frequency source that drives the network under test and two receivers. The first receiver is used to accurately measure the Reflection or input voltage to the network. The second receiver is called the Transmission channel and is used to measure the output of the network under test. The ratio of the output to the input level is displayed as dB and is the voltage gain or loss of the network. The source is swept over the frequency range of interest and a Bode response plot of the network results. Network analyzers fall into two categories. (a) Vector Network Analyzers which are capable of measuring complex (magnitude and phase) reflection and transmission and (b) Scalar Network Analyzers can measure only measure magnitude.

Vector Network Analyzers: This type of network analyzer consists of a sweep oscillator (almost always a synthesizer so that measurements will be repeatable), a test set which includes two ports, a control panel, an information display, and an RF cable. Each port of the test set includes dual directional couplers and a complex ratio measuring device. Other options include a means for bias voltage/current injection, and a computer controller to manipulate and store data. The "classic" vector network analyzer is the Agilent (HP) 8510 C, shown in Fig. 2.9 (b).

2. 3. 5 Thermal Characterisation Tools

Thermal analysis is defined as a group of methods by which the physical or chemical properties of a substance, a mixture and/or a reactant are measured as a function of temperature or time while the sample is subjected to a controlled temperature program. The program may involve heating or cooling (dynamic), or holding the temperature constant (isothermal), or any sequence of these. Thermal methods are multi-component techniques and include thermogravimetry (TGA), differential thermal analysis (DTA) and differential scanning calorimetry (DSC).

2. 4 REFERENCES

1. R. Rice, *Ceramic Fabrication Technology,* Marcel Dekker, Boston (2003).

2. D. Seagal, *Chemical Synthesis of Advanced Ceramic Materials*, Cambridge University Press, Cambridge, (1991)

3. R. E. Carter, *J. Chem. Phys.,* **34**, 2010–15 (1961).

4. J. M. Longo and H. S. Horowitz, *Solid State Synthesis of Complex Oxides in Preparation and Characterization of Materials,* Academic Press, London, (1981).

5. J. Beretka, *J. Am. Ceram. Soc.*, **67**, 9-12 (1984).

6. S. F. Hubert, *Br. Ceram. Soc. J.*, **6**, 11–20 (1967).

7. C. C. Harris, *Trans. AIME*, **238**, 17-30 (1967).

8. B. Beke, *Principles of Communition*, Akademi Kiado, Budapest (1964).

9. J. G. Austin, *Powder Technol*., **5**, 1-17 (1971).

10. H. E. Rose and R. M. E. Sullivan, *A Treatise on the Internal Mechanics of Ball, Tube and Rod mills*, Chemical Publishing, Boston (1958).

11. L. M. Sheppard, *Ceram. Ind*., **149**, 51-63 (1999).

12. G. Y. Onoda and L. L. Hench, *Ceramic Processing before Firing*, Wiley Interscience, New York (1973).

13. P. Winiewski, M. Szafran, G. Rokicki, *Key Engineering Materials, Euro Ceramics – VIII*, 264, 428-32 (2000).

14. A. E. McHale, *Processing Additives*, *Engineering Materials Handbook, Ceramics and Glasses,* Volume- 4, The Materials Information Society, SC (1991).

15. N. M. Alford, X. Wang, S. J. Penn, M. Poole and A. Jones, *Br. Ceram. Trans*., **99**, 212-14 (2000).

16. D. F. Castro, *Sintering Course*, Presented at Centro de Estudios e Investigaciones Técnicas de Gipuzkoa Centro de Estudios e Investigaciones Técnicas de Gipuzkoa, San Sebastián. (June 2000).

17. S-J. L. Kang, *Sintering, Densification, Grain Growth and Microstructure*,

Elsevier, Amsterdam (2002).

18. R. L. Coble, *J. Appl. Phys*., **32**, 789-92 (1961).

19. C. Herring, *J. Appl. Phys*., **21**, 301-03 (1950).

20. W. D. Kingery and M. Berg, *J. Appl. Phys*., **26**, 1205-12 (1955).

21. T. K. Gupta, *J. Am. Ceram. Soc*., **61**, 191-95 (1978).

22. W. D. Kingery, *J. Am. Ceram. Soc*., **37**, 42-45 (1954).

23. G. Birnbaum and J. Franeaue, *J. Appl. Phys*., **20**, 817-18 (1949).

24. J. Mussil and F. Zacek, *Microwave Measurement of Complex Permittivity by Free Space Methods And Applications*, Elsevier, New York, (1986).

25. K. Leong, *Precise Measurements of Surface Resistance of HTS Thin Films using A Novel Method of Q-Factor Computations for Sapphire Dielectric Resonators in the Transmission Mode*, Ph. D. thesis, James Cook University (2000).

26. K. Leong and J. Mazierska, *J. Supercond.*, **14**, 93-103 (2001).

27. D. Kajfez, *Q Factor*, Vector Fields, Massachusetts (1994).

28. K. Wakino, *Proc. of The Second Sendai Inter. Conference*, YAGI Symposium on Advanced Technology Bridging the Gap between Light and Microwaves, p. 187–196 (1990).

29. B. W. Hakki and P.D. Coleman, *IRE Trans. Microwave Theory Tech*, **MTT-8**, 402–10 (1960).

30. W. E. Courtney, *IEEE Trans. on Microwave Theory Tech.*, **MTT-18**, 476-85 (1970).

31. Y. Kobayashi, *IEEE Trans. Microwave Theory Tech*., **MTT-28**, 1077-85 (1980).

32. S. B. Cohn and K. C. Kelly, *IEEE Trans. Microwave Theory Tech*., **MTT-14,** 406 -10 (1966).

33. E. L. Ginzton, Microwave Measurements, McGraw Hill Book Co., Boston, (1957).

34. E. J. Vanzura, J. E. Rogers: *Proceedings of the IEEE Conference on* Instrumentation and Measurement Technology, May 14-16, Atlanta, (1991).

35. T. Miura, T. Takahashi, M. Kobayashi, *IEICE Transactions on Electronics*, **E7 7-C**, 900-07 (1994).

36. M. C. Sanchez, *IEE Proceedings*, **134**, Part. H, 243-46 (1987).

37. J. Krupka, K. Derzakowski, B. Riddle, and J. B. Jarvis, *Meas. Sci. Technol.*, **9**, 1751-58 (1998).

38. J. B. Jarvis, R.G. Gayer, J. H. Grosvenor Jr., M. D. Janezic, C. A. Jones, B. Riddle, C. M. Weil and J. Krupka, *IEEE Trans. Dielec. Electrical Insul*., **5**, 571-77 (1998).

39. D. M. Moore and R. C. Reynolds Jr., *X-Ray Diffraction and the Identification and Analysis of Clay Minerals*, Oxford University Press, New York, (1989).

40. C. Hammond, *The Basics of Crystallography and Diffraction*, 2nd Edn., OUP, London (2001).

41. G. E. Bacon, *X-ray and Neutron Diffraction*, Pergamon Press, Amsterdam (1966)

42. B. D. Cullity and S. R. Stock, *Elements of X-ray diffraction*, Prentice Hall, New Delhi, (2001).

43. D. L. Bish and J. E. Post, *Modern Powder Diffraction. Reviews in Mineralogy*, **20**, Mineralogical Association of America, Boston (1989).

44. L. Reimer, *Scanning Electron Microscopy, Physics of Image Formation and Microanalysis*, Springer Series in Optical Sciences, **45**, Springer, Berlin (1985).

45. Internet File : *http://www.mse.iastate.edu/microscopy/college.html*

46. Ian M. Watt, *The Principles and Practice of Electron Microscopy*- 2nd Edn., Cambridge University Press, Cambridge (1997).

CHAPTER 3

EFFECT OF STOICHIOMETRY ON THE PROPERTIES OF $Ba(Mg_{1/3}Ta_{2/3})O_3$ CERAMICS

This Chapter describes historical emergence of complex perovskites as ideal candidate materials for DR application. The synthesis and microwave dielectric properties of stoichiometric BMT using solid state (one step and two step processes) and chemical (precipitation and citrate gel) routes are presented in this chapter. The complex relationship between stoichiometry and microwave dielectric loss is investigated. This has been done by deliberately introducing Mg and Ba non-stoichiometry in $Ba(Mg_{1/3}Ta_{2/3})O_3$ dielectrics. The effect of this non-stoichiometry on the densification, structural ordering and microwave dielectric properties of BMT is discussed. It is found that a slight deficiency of Mg or Ba increase the density and order parameter which in turn improved the microwave dielectric properties. However excess of Mg or Ba deteriorate the dielectric properties considerably. Raman spectral analysis was employed to study the distortions of oxygen octahedra due to the cation movement (from *A*-site to *B*-site and vice-versa) resulting from nonstoichiometry.

3. 1 SIMPLE AND COMPLEX PEROVSKITES

3. 1. 1 Introduction

Perovskites are a large family of crystalline materials that derive their name from a specific mineral $CaTiO_3$. The parent material, perovskite, was first described in the 1830's by the geologist Gustav Rose, who named it after the famous Russian mineralogist Count Lev Aleksevich von Perovski[1].

3. 1. 2 ABX_3 Structure

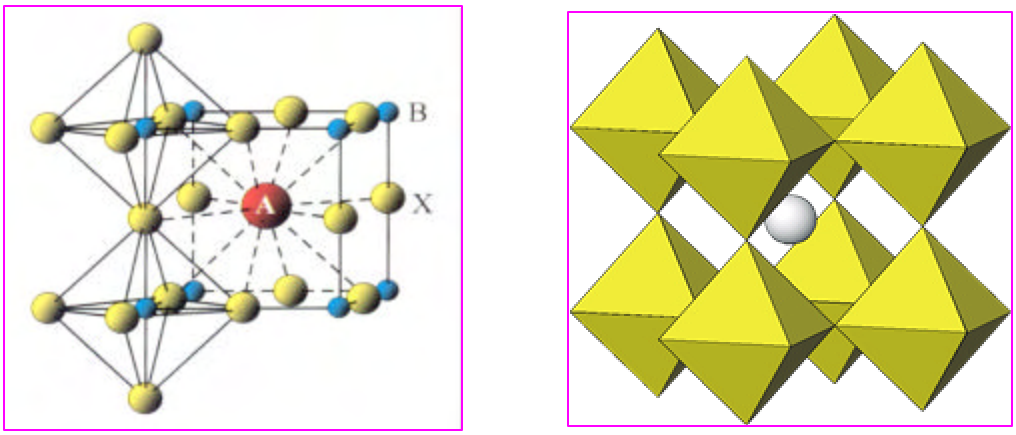

(a) (b)

Fig. 3.1 (a) Ideal Perovskite (ABX_3) structure showing 6-fold and 12-fold coordinations of B and A site cations respectively (b) Unit cell of ABX_3 perovskite showing eight BX_6 octahedron enclosing the A-site

The principle perovskite structure found in ferroelectric materials is a simple cubic structure containing three different ions of the form ABX_3. The A and B atoms represent +2 and +4 valent ions, respectively, while the X atom is the Oxygen^{-2} ion. The A atom is the largest of the atoms and consequently increases the overall size of the AO_3 (fcc) structure. In the unit cell, A atoms are located at position [0, 0, 0], the B atoms at [½, ½, ½] and three O atoms at [0, ½, ½]; [½, 0, ½]; [½, ½, 0]. The A atoms are coordinated with twelve O atoms and B atoms are coordinated by six O atoms (see Fig. 1.3(a)). In a simple ABO_3 phase with only one element at each site possible combinations of A and B site charges are $A^{+1}B^{+5}O_3$ [e.g. $LiNbO_3$], $A^{+2}B^{+4}O_3$ [e.g. $CaTiO_3$], $A^{+3}B^{+3}O_3$ [e.g. $LaAlO_3$] and $A^{0}B^{+6}O_3$ [e.g. ReO_3] while $A^{4+}B^{2+}O_3$ is rare for coulombic reasons [2].

Most of the perovskites are considered to be ionic compounds [3], and the ions comprising them can be regarded to a first approximation as spheres with ionic radii R (?). For a small cell drawn with origin on the B-site cation (see Fig. 3.1(a)) Goldschmidt[4] observed that if the A-site cations are equal in size to the anion, and thus precisely fit the 12-fold site, then the length of a line joining O-A-O would be equal to $2(R_O+2R_A)$ or $\sqrt{2}$ times the edge of the unit cell. The latter equals $2(R_O+2R_B)$, and in an ideal case, $R_A+R_O=\sqrt{2}(R_O+R_B)$. In real structures, because of differences in size of the A, B and O ions, this relationships must be modified to include a parameter known as the tolerance factor (*t*) given by

$$t = \frac{R_O + R_A}{\sqrt{2}\ (R_O + R_B)} \tag{3.1}$$

For $Ba(B'_{1/3}B''_{2/3})O_3$ type complex perovskites the above equation modifies to

$$t = \frac{R_O + R_{Ba}}{\sqrt{2}\ [R_O + (0.33R_{B'} + 0.67R_{B''})]} \tag{3.2}$$

For ideal perovskites, *t* is unity although diverse perovskite structures of lower symmetry can exist for values greater than 0.8. For cubic $SrTiO_3$ on the other hand *t* = 1.002. The tolerance factor may be treated as a guide as to whether a given assemblage of ions will adopt the perovskite structure at a particular temperature and pressure.

3. 1. 3 $A(B'_{1/3}B'_{2/3})O_3$ Structured Compounds

Interestingly, most of the perovskite compounds which are of greater technological interest are not simple systems, but rather $(A'A'')BO_3$ or $A(B'B'')O_3$ type alloys with two different kind of A and B atoms respectively [5]. In the early years of fifties itself, the search for newly structured complex perovskites has started. In 1954, it was Rustam Roy[6] who has made extensive research on a series of barium based complex perovskite compositions in which there are more than one ion in the B-site like $Ba(B'_{1/2}B''_{1/2})O_3$ and $Ba(B'_{1/3}B''_{2/3})O_3$. He could index their powder diffraction patterns based on a psuedocubic unit cell which was only partially successful. In 1961, Galasso et al. [7] studied the effect of different ions

such as Sr, Ca, Zn, Co, and Ni on the B' site in the complex perovskite composition $Ba_3B'^{II}Ta_2^{V}O_9$ using powder diffraction methods. This study was mainly carried out in $Ba_3SrTa_2O_9$, with a presumption that these compounds will crystallize in a cubic unit cell with a = 4.17 ?. In this structure there are three layers of BaO_3, one layer of B'^{2+} and two layers of B''^{5+} in the unit cell. But in addition to the standard cubic perovskite diffraction line positions, some weak (less than 1-5 % of the I_{012} line) additional lines (at $2\theta < 40^o$) were also present in the XRD pattern. These lines can be indexed as 001, 100, 101, 011, 111 and 200 respectively. All but three of the remaining lines could be indexed by assuming a small rhombohedral distortion of the basic perovskite cube. To account for the other lines it was necessary to assume a hexagonal cell with cell parameters a = 5.95 ? ; c =7.47 ?. This large cell, called the superstructure permits an ordered arrangement of the Sr and Ta ions in the octahedrally coordinated positions.

According to Galasso[8], oxides which contain twice as much of the higher valence state B" element as the lower valence state B; element may form a $Ba(Sr_{0.33}Ta_{0.67})O_3$ type structure. This structure can be described by a hexagonal a hexagonal unit cell whose c-axis is equivalent to the <111> direction in the original perovskite unit cell. There are two layers B" cations and a layer of B' cation in each unit cell. In $Ba(Sr_{0.33}Ta_{0.67})O_3$, one Ba atom is at [0, 0, 0], two more at [? , ? , z] ; [? , ? , $\bar{z}$] with z = **?** . One Sr atom at [x, $\bar{x}$, z]; [x, 2x, z]; [2$\bar{x}$, $\bar{x}$, z]; [$\bar{x}$, x, $\bar{z}$]; [$\bar{x}$, 2$\bar{x}$, $\bar{z}$]; [2x, x, $\bar{z}$] with x= $\frac{1}{6}$, z = $\frac{1}{3}$ and three O at [½, 0, 0]; [0, ½, 0]; [½, ½, 0] [9]. Of the $Ba(Sr_{0.33}Ta_{0.67})O_3$ type complex perovskites, $Ba(Mg_{1/3}Ta_{2/3})O_3$ seems to be one of the most explored compositions due to their exceptional dielectric properties.

3. 2 $Ba(Mg_{1/3}Ta_{2/3})O_3$ COMPLEX PEROVSKITES

3. 2. 1 Introduction

In 1963, Galasso and Pyle[10] established the conditions that can lead to the formation of structural order in $Ba(B'_{1/3}Ta_{2/3})O_3$ type complex perovskites. The duo observed that the larger difference in size and charge between B site cations in complex perovskites give rise to more ordered structure-a rule that is still considered to be a thumb rule in 1:2 complex perovskites. The same paper reported the unit cell properties of some new compounds like

$Ba(Mg_{1/3}Ta_{2/3})O_3$ [a = 5.782 ?, c = 7.067 ?] and $Ba(Zn_{1/3}Ta_{2/3})O_3$ [a = 5.782 ?, c = 7.097 ?] for the first time. The niobium counter parts of the above said compounds were also published[11] subsequently of which $Ba(Zn_{1/3}Nb_{2/3})O_3$ crystallizes only in cubic perovskite form.

3. 2. 2 Cation Ordering in $Ba(Mg_{1/3}Ta_{2/3})O_3$

In most of the substitutional solid solutions, the two kinds of atoms A and B are arranged more or less at random in the atomic sites of the lattice. In compositions of this kind, the only major effect of a change in temperature is to increase or decrease the amplitude of thermal vibrations. But there are some solid solutions in perovskite family, which have the random structure of cations only existing at elevated temperature. Consider a more specific case, in which the B site of simple perovskite $BaTiO_3$ has been partly occupied by two cations of comparable sizes, to form a structure $Ba(Mg_{1/3}Ta_{2/3})O_3$

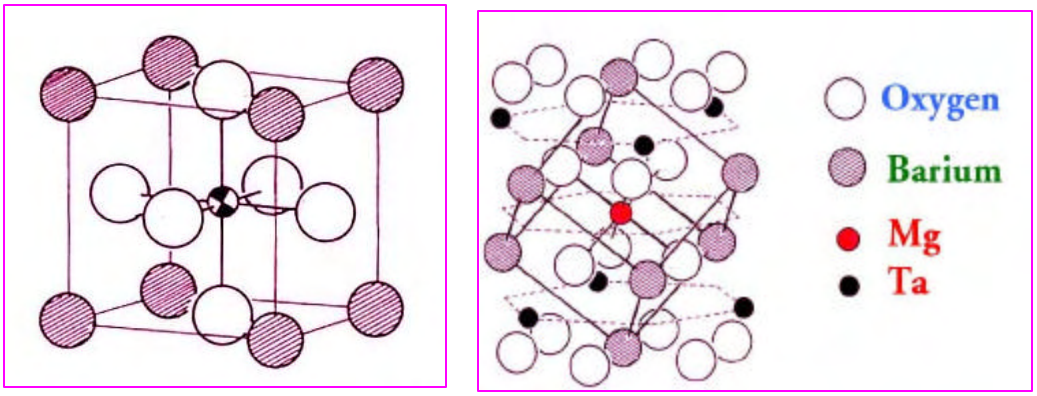

Fig. 3.2 (a) Crystal structure of $Ba(Mg_{1/3}Ta_{2/3})O_3$ (left) disordered and (right) ordered state

(see Fig. 3.2 (a)). As seen from Fig. 3.2 (b), when the periodic arrangement of Mg and Ta persist over a very large distance in the crystal, it is known a long range order (LRO). If the ordered structure is heated above the critical temperature, the periodic arrangement becomes more or less at random and then the compound is said to be disordered. The B-site cation ordering has a very prominent role in the physical properties of $Ba(Mg_{1/3}Ta_{2/3})O_3$ ceramics. Unfortunately, owing to the complexity of growing multi component crystals, only very few researchers have worked on the single crystals of $Ba(Mg_{1/3}Ta_{2/3})O_3$[12]. But the factors controlling ordering in single crystals have not been

worked out by these researchers[13]. In 1993, Vincent et al.[14] have shown that in $Ba_3MgTa_2O_9$ exhibit only partial ordering where as $Ba_3ZnTa_2O_9$ is fully ordered[15].

3. 2. 3 Calculation of Ordering Parameter

The long range cation ordering parameter (S) is defined as the occupational probability difference between two non equivalent states[16]. In 1:1 ordered complex perovskites, the long range ordering parameter gradually reduces to zero when the temperature increases. So the 1:1 order-disorder transition is a second order phase transition. On the other hand, the long range ordering parameter of 1:2 type ordering suddenly drop to zero at the transition temperature, which indicates that the transition is a first order one [17]. The conventional formula [18] for determining the ordering parameter is given by

$$S = \frac{I_{100}}{I_{110} + I_{012}} \times \frac{\left(1 + \cos^2 2q_1\right) \sin^2 q_2 \cos q_2}{\left(1 + \cos^2 2q_1\right) \sin^2 q_1 \cos q_1} \times \frac{\left(m_1 \left|F_{110}\right|^2 + m_2 \left|F_{102}\right|^2\right)}{m_2 \left|F_{100}\right|^2} \qquad (3.3)$$

where I_{hkl} = Measured X-ray diffraction intensity, $?_1$= Difference in Bragg angle between 110 fundamental and 011 ordered reflection, $?_2$ = Difference in Bragg angle between 012 fundamental and 001 ordered reflection, F_{hkl} = Structure factor for hexagonal ordered structure, m_i = multiplicity factor for each reflection (i = 1, 2, 3.. The cation ordering parameter of $Ba(Mg_{1/3}Ta_{2/3})O_3$ can be conveniently calculated by comparing the intensities of the strongest powder line profiles (110,102) with that of the superstructure line (100) as given below

$$S = \sqrt{\frac{(I_{(100)} / I_{(110),(102)})_{observed}}{(I_{(100)} / I_{(110),(102)})_{theoretical}}} \qquad (3.4)$$

Matsumoto et al[19] calculated the theoretical value of the ratio of the integral intensity of super structural reflection line (100) to that of (110,102) line, $(I_{100} / I_{110,102})_{theoreticd}$ as 8.3 % and using this value in 3.4, order parameter is calculated as [20]

$$S = \sqrt{\frac{28.13 \times I_{100}/I_{110,102}}{1.814 - I_{100}/I_{110,102}}} \quad (3.5)$$

This equation is used for calculation of the ordering parameter of $Ba(Mg_{1/3}Ta_{2/3})O_3$ in this thesis.

3. 2. 4 Milestones in the Research of $Ba(Mg_{1/3}Ta_{2/3})O_3$ Ceramics

Since the discovery of $Ba(Zn_{1/3}Nb_{2/3})O_3$-$Ba(Zn_{1/3}Ta_{2/3})O_3$ ceramics by Kawashima et al. [21], as a suitable candidate for applications in mobile and satellite communication systems, there has been intense research to develop low loss dielectric materials with complex perovskite structure. Kawashima et al. [21] found that one of the end member of the solid solution $Ba(Zn_{1/3}Ta_{2/3})O_3$ (BZT) has a dielectric constant of 30 and quality factor of 9,200 at 11-12 GHz with near to zero temperature coefficient of resonant frequency. It was Nomura et al. [22] who made a break through discovery that, a dense ceramic with an ordered perovskite structure, with chemical formula $Ba(Mg_{1/3}Ta_{2/3})O_3$ has high quality factor and temperature stability of the resonant frequency which can be used for microwave dielectric resonator applications. To enhance its sinterability, a small amount of Mn was doped to $Ba(Mg_{1/3}Ta_{2/3})O_3$ and microwave dielectric properties of this complex perovskite ceramic was determined as Q_u=16,800±300 at 10.5 GHz, ε_r= 25, τ_f= 2.7 ppm/^oC. Following this report a considerable amount of work has been carried out on the microwave dielectric properties of Ba based 1:2 complex perovskites such as $Ba(Zn_{1/3}Ta_{2/3})O_3$, $Ba(Mg_{1/3}Nb_{2/3})O_3$ and $Ba(Zn_{1/3}Nb_{2/3})O_3$. The emergence of $Ba(Mg_{1/3}Ta_{2/3})O_3$ as a high Q dielectric resonator for microwave communication applications has stimulated a new surge of interest among researchers working on the Materials Science aspects of low loss materials.

Nomura and Konishi[23] outlined the conditions for best dielectric properties of this dielectric. The duo have observed the formation of additional phases such as $BaTa_2O_6$ and $Ba_5Ta_4O_{15}$ which promoted extensive grain growth in $Ba(Mg_{1/3}Ta_{2/3})O_3$ specimen which is detrimental to its microwave dielectric properties. In a significant publication Sugiyama et al.[24] observed that the impingement of ordered domains resulted in the formation of sub-boundaries in the parent $Ba(Mg_{1/3}Ta_{2/3})O_3$ grain. These sub-boundaries are in a strained

condition which introduce dislocations at the interface resulting in dielectric loss. The first attempt to investigate the low loss property of $Ba(Mg_{1/3}Ta_{2/3})O_3$ was undertaken by Wakino and Tamura [25] who studied their low temperature dielectric properties and correlated them with the unharmonic terms in the crystals Hamiltonian.

The efforts to improve the dielectric properties of these ceramics were carried out by many researchers[26] in resonance with the innovations in the science of advanced material synthesis. The main hurdles in the synthesis of $Ba(Mg_{1/3}Ta_{2/3})O_3$ ceramics include (a) the high sintering temperature above 1600 ^oC where the volatisation of constituent MgO can occur; (b) formation of magnesium free additional phases like $BaTa_2O_6$, $Ba_5Ta_4O_{15}$ and $Ba_4Ta_2O_9$; (c) and thermal destabilization of cation order from 1:2 to 1:1 or disordered perovskite [27]. It is understood that the bulk material transport mechanisms of $Ba(Mg_{1/3}Ta_{2/3})O_3$ ceramic can be enhanced through a rapid heating procedure as suggested by Matsumoto and Hiuga[28]. They have succeeded in densifying the ceramic from a green density of 49 % to a final sintered density of above 91 % of its theoretical density (7.625 g/cm^3) with excellent microwave dielectric properties (ε_r = 25, τ_f = 4 ppm/^oC and Q = 20,000 at 10-22 GHz). Yet another modification in the synthesis of this ceramic was reported by Kageyama[29], who found that using hot isostatic pressing (HIP), the density and dielectric constant were improved but the unloaded quality factor was hardly affected. Alternate synthesizing techniques like solution synthesis have also been attempted [30, 31] but the dielectric properties are not appreciable for practical applications. Several authors[32, 33] used liquid phase sintering as a means for synthesizing $Ba(Mg_{1/3}Ta_{2/3})O_3$ microwave dielectric at low temperature with higher density. The additives such as [34]MnO, [35]SnO_2, [36]NiO, [37]WO_3, [38]ZrO_2, [39]TiO_2, [40]Y_2O_3, [41]V_2O_5 etc. which when doped to barium magnesium tantalates improved their microwave dielectric properties. But the action of these dopants are different in different dopant conditions and the exact role of a dopant in the parent matrix is still regarded as a matter of debate. Chai et al.[42] found that when tetravalent impurity was added to BMT, the cation ordering is changed from 1:2 to 1:1 but the larger amount of these additives make them disordered. They asserted that a size limit of $B^{4+} > 0.693$? is being required to stabilize the 1:1 ordering. In 1997, Youn at al.[43] observed that when trivalent ions like La^{3+} is doped to $Ba(Mg_{1/3}Ta_{2/3})O_3$ the 1:2 and 1:1 states of ordering are coexisting. Recently, Ra and Phule [44] investigated the correlation

between dielectric loss and long range cation ordering in BMT who arrived at the conclusion that it is not cation order but point defects generated at the time of material synthesis, controls the dielectric loss factor of BMT ceramic.

3. 3 SYNTHESIS OF STOICHIOMETRIC $Ba(Mg_{1/3}Ta_{2/3})O_3$ CERAMICS

3. 3. 1 Solid State Ceramic Routes

3. 3. 1. 1 One Step Process

The phase diagrams of BaO-MgO-Ta_2O_5 have not been reported until now, but the binary phase diagrams of [45] BaO-MgO system, [46] MgO-Ta_2O_5 system and [47] Ta_2O_5-$MgTa_2O_6$ systems are already reported in which the liquid phase formation temperatures are 1500^oC, 1600^oC and 1750^oC respectively. Thus it is evident that the long time processing or calcination over 40 hours, above 1500 degrees can result in the evaporation of BaO-MgO melt [46]. The material formation mechanism and reaction kinetics of $Ba(Mg_{1/3}Ta_{2/3})O_3$ was first investigated by Lu and Tsai [86] who calculated the activation energy for material formation as 257 kJ/mol. They could calculate formation temperature as ~ 800 ^oC which agreed well with experiment. Zhao et al.[48] synthesized BMT at a still lower temperature using hydrated Ta_2O_5 in the solid state ceramic route.

3. 3. 1. 2 Two Step Process

The high sintering temperature and unnecessary formation of additional phases put several constrains on the solid state synthesis of $Ba(Mg_{1/3}Ta_{2/3})O_3$ ceramics. Even in mixed oxide route, earlier reports suggests that a careful design of the reaction sequence can effectively bring down processing temperature of this ceramic and suppress the additional phases. In 1997, Li [49] suggested that phase pure $Ba(Mg_{1/3}Ta_{2/3})O_3$ ceramics can be synthesized in a two step process: (i) synthesis of $MgTa_2O_6$ reacting MgO and Ta_2O_5 in the ratio 1:1 and then mixing it with $BaCO_3$ in the ratio 1:3 at a relatively lower temperature. This intermediate compound with coulombite structure is a good dielectric resonator with high Q factor and positive temperature coefficient of resonant frequency[50]. Later on, Liang et al.[51] succeeded in controlling the formation of $Ba_5Ta_4O_{15}$ additional phase whose formation is not easy to restrict in the reaction sequence of conventional ceramic route.

3. 3. 1. 3 Experimental

(i) One Step Process : Recently, our research group [52] proved that phase pure ordered BMT can be processed by strictly controlling the synthesizing conditions. The synthesis of $Ba(Mg_{1/3}Ta_{2/3})O_3$ was carried out through a solid state ceramic route as described in Chapter 2, section 2.1.2.1 to 2.1.2.7. The reaction mixture was calcined in platinum crucible in the range 600-1400^oC for 4 hours with an increment of 50^oC. The phase evolution of the BaO-MgO-Ta_2O_5 mixture at various temperatures was analyzed using XRD and DTA/TGA analysis.

(ii) Two Step Process: To synthesize $MgTa_2O_6$, stoichiometric amounts of $(MgCO_3)_4$. $Mg(OH)_2.5H_2O$ and Ta_2O_5 are mixed in 1:1 ratio between MgO and Ta_2O_5. The reaction mixture was calcined at 1200^oC for 8 hours with intermediate grinding. The phase purity of $MgTa_2O_6$ was confirmed using XRD. It is ground thoroughly in an agate mortar and mixed with $BaCO_3$ in the molar ratio $BaCO_3$:$MgTa_2O_6$ = 3:1. The mixture was then heated at temperatures 600, 700, 800, 900, 1000 and 1100. The optimum calcination temperature was determined as the lowest temperature at which the phase pure BMT was formed.

The BMT samples synthesized through (a) single step process and (b) two step process are sintered in air at temperature 1625 and 1550^oC respectively for 2 hours. The microwave dielectric properties of the cylindrical pucks were determined using standard resonance techniques described in section Chapter 2, Sections 2.2.2 to 2.2.4. The sintered samples were annealed at 1450^oC for 40 hours. The crystal structure was determined using powder diffraction technique as discussed in Section Chapter 2, Section 2.3.1. The crystallite size of the precursor powder was determined using Debye-Scherrer formula[53]

3. 3. 1. 4 Results and Discussion

The phase evolution and reaction sequence of $Ba(Mg_{1/3}Ta_{2/3})O_3$ using powder diffraction pattern is plotted as a function of temperature is shown in Fig. 3.3. The XRD patterns suggest that the formation of $Ba(Mg_{1/3}Ta_{2/3})O_3$ is starting above 800^oC. But even at temperatures above 900^oC trace amounts of Ta_2O_5 and $BaTa_2O_6$ are present which will be completely eliminated only at a heat treatment above 1100^oC. To understand the emergence

barium tantalate additional phases we need to examine the reaction sequence that lead to the formation of $Ba(Mg_{1/3}Ta_{2/3})O_3$. The reaction sequence of $Ba(Mg_{1/3}Ta_{2/3})O_3$ is believed to be as follows:

$BaCO_3 + Ta_2O_5 \longrightarrow BaTa_2O_6 + CO_2$ |

$BaTa_2O_6 + 3BaCO_3 \longrightarrow Ba_4Ta_2O_9 + 3CO_2$ |

$Ba_4Ta_2O_9 + 1/3MgO + O_2 \longrightarrow Ba(Mg_{1/3}Ta_{2/3})O_3 + 1/3\ BaTa_2O_6 + 3BaO$

$BaTa_2O_6 + 1/3MgO \longrightarrow Ba(Mg_{1/3}Ta_{2/3})O_3 + 1/3Ta_2O_5$

$BaO + Ta_2O_5 \longrightarrow BaTa_2O_6$

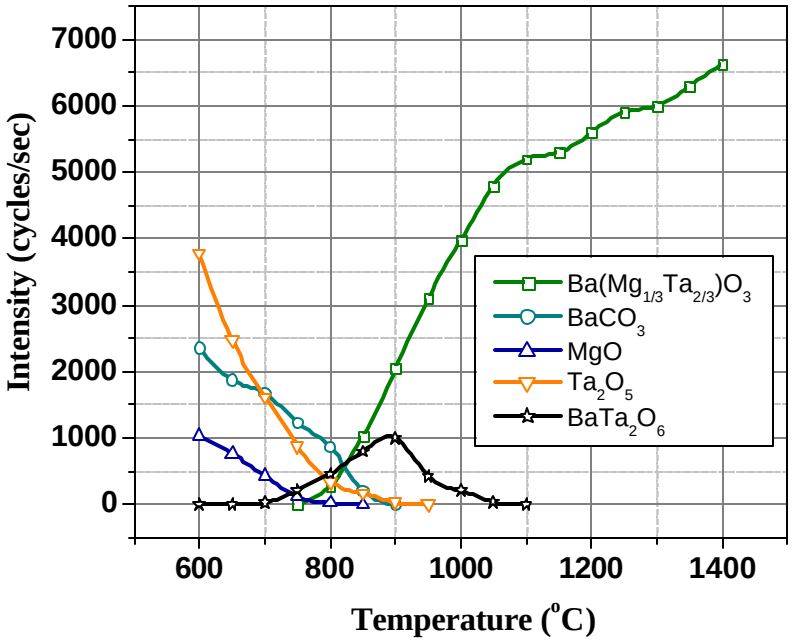

Fig. 3.3 Variation of most intense (*hkl*) reflection in the reaction sequence of $Ba(Mg_{1/3}Ta_{2/3})O_3$ as a function of temperature.

According to the above reaction sequences as reported by as suggested by Fang et al.[54], as 1 mole of the BMT is formed, 0.33 mole of Ta_2O_5 or $BaTa_2O_6$ is formed. May be this is the reason why the secondary phase $BaTa_2O_6$ can be formed above 700°C (see Fig. 3.3). Trace amount of $Ba_4Ta_2O_9$ can also be formed. But it should be noted that if the reaction between $BaTa_2O_6$ and $Ba_4Ta_2O_9$ can result in the formation $Ba_5Ta_4O_{15}$ or $Ba_7Ta_6O_{22}$ which is stable even at high temperatures [55]. From $Ba_5Ta_4O_{15}$ and $Ba_7Ta_6O_{22}$ it is very difficult to

form BMT because they have to make contact with MgO to form BMT by long range solid state diffusion process. Hence the chances of formation of these barium tantalate phases have to be minimized to yield high quality BMT phase.

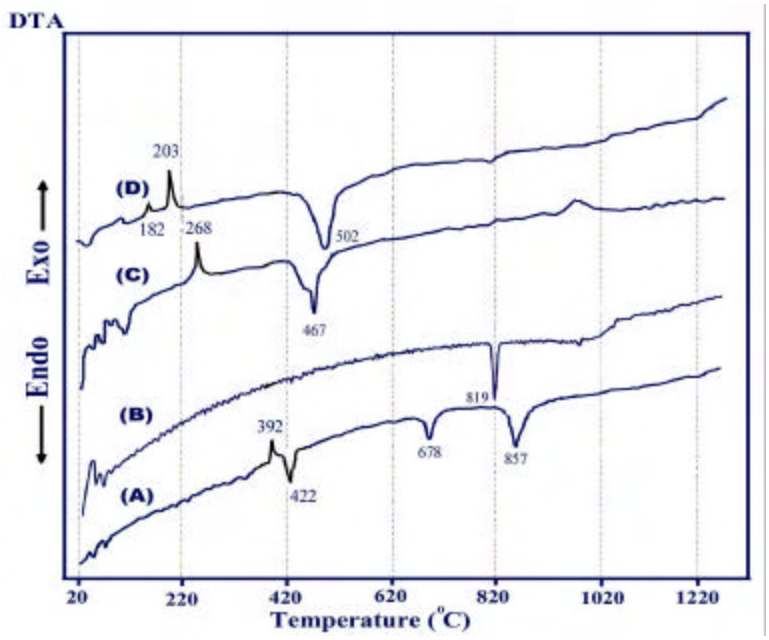

Fig. 3. 4 DTA profiles of the formation of BMT powder prepared through (A) One Step Process, (B) Two Step Process,(C) Citrate Gel and (D) Precipitation

The differential thermal analysis curve of BMT prepared through different synthesizing routes is given in Fig. 3.4. The material formation of BMT ceramics through one step and two step solid state reactions are shown in Figs. 3.4 (A) and (B) respectively. In the DTA for single step solid state synthesis of BMT, an exothermic peak around 392^{o}C is seen which may be attributed to the evolution of CO_2 from $BaCO_3$. The endothermic peak at 425^{o}C is believed to be the evolution of hydroxylated water from reactant $(MgCO_3)_4.Mg(OH)_2.5H_2O$. The endothermic dip for material formation of $Ba(Mg_{1/3}Ta_{2/3})O_3$ is at 857^{o}C which has been confirmed from the variation of the relative intensities of X-ray diffraction profiles as given in Fig. 3.3.

The DTA profile of BMT prepared through a two step process is given in Fig. 3.4 (B). The plot which show the reaction sequence between $BaCO_3$ and coulombite phased $MgTa_2O_6$, show a sharp endothermic peak at 819^{o}C heralding the formation of single phase

$Ba(Mg_{1/3}Ta_{2/3})O_3$. It must be noted that this temperature is lower than the phase formation temperature (857°C) of single step process.

The density of as sintered pure PMT in process 1 is 7.21 g/cm^3 which on annealing at 1450 yields 7.244 g/cm^3. On the other hand the densification of pure BMT prepared through coulombite phase is 7.118 g/cm^3. But it must be remembered that the particle size is smaller (210 nm) for this process compared to the former. Moreover the sintering of two step BMT compacts can be performed at a relatively lower temperature (1550°C).

The X-ray diffraction profiles of BMT prepared through single and two step solid state processes are given in Fig. 3.5. The powder diffraction pattern (JCPDS File Card No. 18-176) of as sintered BMT sample is given in Fig. 3.5. The X-ray diffraction profile presented in BMT (a) is for unannealed specimen which shows only a feeble presence of superstructural reflections. The emergence of superstructure reflections are visible in BMT (b) of Fig. 3. 5, which is believed to be due to cation ordering as described in Section 3. 2. 3.

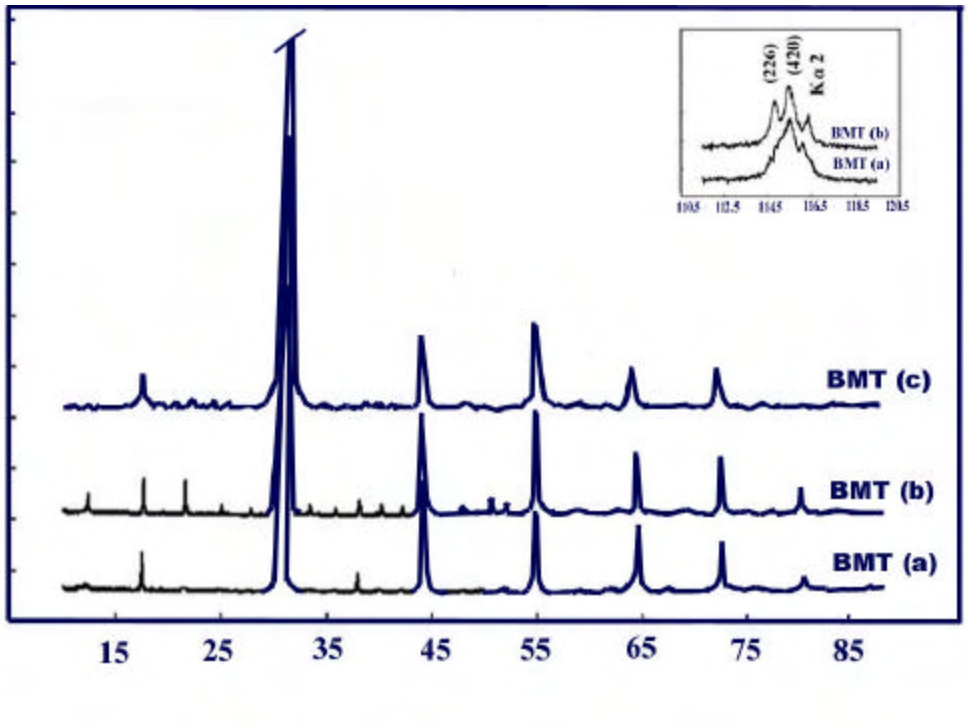

Fig. 3. 5 Powder Diffraction pattern of BMT prepared through dry synthesis route BMT(a) - as sintered BMT; BMT(b) - BMT annealed at 1450°C for 40 hours and BMT(c) – BMT synthesized though two step process. Inset represents the splitting of 422 and 266 lines due to ordering

The XRD pattern of unannealed BMT prepared through a two step procedure is given in BMT (c) of Fig. 3.5. Even though no additional phases were visible the intensities of prominent lines are relatively low and broad which is believed to be due to the incomplete material formation process that can be compensated through multiple calcination. As discussed in Section 3.2.3, the cation ordering in 1:2 ordering bring about a lattice distortion, resulting in the splitting of the (266) and (422) diffraction lines (see the inset of Fig.3.5). The properties of $Ba(Mg_{1/3}Ta_{2/3})O_3$ ceramics prepared through different synthesizing techniques are given in Table 3.1.

Table 3. 1 Properties of $Ba(Mg_{1/3}Ta_{2/3})O_3$

Properties	Solid State		Chemical Route	
	One Step	Two Step	Precipitation	Citrate Gel
Sintering Temp. (^oC)	1625	1550	1600	1550
Bulk Density (g/cm^3)	7.244	7.118	7.215	7.089
Dielectric Constant	24.4	24.1	26.5	23.4
Q_u xf (GHz)	100500	96000	11325	34450
τ_f (ppm/^oC)	8.01	11.2	16.1	6.5
Order Parameter	0.97	0.91	*	*
Cell Parameter Ratio (c/a)	1.2254	1.2251	1.2231	1.2198
Average Particle Size (nm)	451	210	56	34

* Highly disordered

The unloaded quality factor of as sintered BMT prepared through single step conventional ceramic route is $Q_u$xf = 80,000 GHz, which on annealing at 1450^{o}C for 40 hours yields 100,500 GHz. The dielectric properties such as Q factor and dielectric constant of a dielectric resonator ceramic depends on the density of the sintered specimen[56]. The relatively lower densification (93 % of the theoretical density) may be reason behind the relatively lower values of quality factor ($Q_u$xf = 96,000 GHz) for BMT synthesized through the multi step process. The cation ordering of coulombite phase BMT too was lower (0.91) compared to BMT prepared through single step process. The solution chemistry offers alternate methods to prepare complex oxide powders with smaller particle size and higher reactivity which is discussed in the following section

3. 3. 2 Chemical Routes to Synthesize $Ba(Mg_{1/3}Ta_{2/3})O_3$

`The surface area of the ceramic powder derived through solid state reaction technique is relatively lower and hence the particles can offer lesser points of contacts which is vital for effective sintering reactions to take place[57]. In addition to that the homogeneity of particle size distribution and high temperature of formation makes the solid state ceramic techniques unpopular for the synthesis of advanced dielectric ceramics[58] like $Ba(Mg_{1/3}Ta_{2/3})O_3$. So alternate chemical techniques [59, 60] like molten salt, precipitation, sol-gel, hydrothermal and combustion, have been worked out in the synthesis of complex perovskites. We attempted two wet chemical methods such as co-precipitation and a modified citrate gel techniques to synthesis $Ba(Mg_{1/3}Ta_{2/3})O_3$ ceramics at low temperatures.

3. 3. 2. 1 Precipitation Synthesis

The co precipitation is a simultaneous precipitation of a normally soluble component with a macro-component from the same solution by the formation of mixed crystals, by adsorption, occlusion or mechanical entrapment.

There are several reports [61] on solution co precipitation synthesis which also been regarded as a useful tool for improving the characteristics of low loss ceramic powders. The semi-precipitation method using oxine [62] is considered as a first attempt in literature for the synthesis of $Ba(Mg_{1/3}Ta_{2/3})O_3$ powders. In this process, magnesium and tantalum cations are precipitated by using oxine, and then the precipitates are subsequently mixed with $BaCO_3$. Due to the insufficient mixing between precipitates and $BaCO_3$, the synthesis temperature has to be raised to as high as 1300°C for complete generation of $Ba(Mg_{1/3}Ta_{2/3})O_3$. There have been other attempts to prepare BMT through alternate precipitation techniques[63], but none of these techniques could fetch a higher quality factor than that obtained through solid state technique.

For obtaining densified monophasic $Ba(Mg_{1/3}Ta_{2/3})O_3$ ceramics with highly ordered structure from inexpensive raw materials, we have developed a co-precipitation process. This process involves simultaneous precipitation of the constitute cations to overcome the insufficient mixing of cations, which occurs in the semi precipitation process.

3. 3. 2. 2 Citrate Gel Synthesis

The sol–gel process, using alkoxides, can effectively reduce the formation temperature and facilitate sintering; however, the stringent operation conditions involved due to the high sensitivity of alkoxides to moisture, as well as the high cost of alkoxides, limit usage of this process in industry. On the other hand when inorganic salts are used in the sol-gel process, the consequent presence of polymers tends to retard the decomposition of $BaCO_3$, thus increasing the temperature for synthesizing $Ba(Mg_{1/3}Ta_{2/3})O_3$.

The sol-gel process synthesis of BMT using alkoxide precursor method has been attempted by Katayama et al [64] from the hydrolysis of barium magnesium and tantalum ethoxides. Later on Renoult et al.[65] also reported the synthesis of $Ba(Mg_{1/3}Ta_{2/3})O_3$ through alkoxide hydroxide process. Apart from these attempts there has been many reports about the nano synthesis of BMT ceramics [66, 67]. In all the cases the microwave dielectric properties are poor which is still a matter of much scientific debate. In sol-gel process, the adjacent ions can immediately react with each other at a relatively low temperature[68]. But this method is not cost effective. The pechini or citrate gel process is usually considered to have the advantage of mixing ions on the atomic scale in the liquid state, so it is easy to control accurately the composition of the powder. However, there are many types of cation citrate complexes in the solution, so the concentration of citric acid could affect the formation of citrate complexes and further affect precipitation and segregation during gelling and charring, respectively [69]. It is considered that both citrate to metal ratio and pH value of the initial solution are most important to get a clear gel with no precipitation. There has been a previous report on the synthesis BMT through citrate gel technique[70] but in that paper the microwave dielectric properties of the chemically derived BMT ceramics was not reported. Hence we revisited the problem and attempted to synthesis BMT though a modified citrate gel route.

3. 3. 2. 3 Experimental

(i) Co-Precipitation

Barium Nitrate [$Ba(NO_3)_2$], Magnesium Nitrate [$Mg(NO_3)_2$] and Tantalum Penta Chloride [$TaCl_5$] are used as the starting material for the Precipitation Synthesis of BMT.

Alkaline conditions were used to the final precipitation of $Ba(Mg_{1/3}Ta_{2/3})O_3$ precursor, since both barium and magnesium are alkaline metals, rendering them soluble in acidic or neutral medium and requiring strongly alkaline conditions to ensure their complete precipitation. The reaction sequence and the flow chart of the experimental procedure of (i) Precipitation and (ii) Citrate Gel are as follows :

Reaction Sequence

$$3Ba(NO_3)_2 + 2TaCl_5 + Mg(NO_3)_2 \xrightarrow{H_2C_2O_4} 3BaMg_{1/3}Ta_{2/3}(C_2O_4)_3$$

$$3BaMg_{1/3}Ta_{2/3}(C_2O_4)_3 \xrightarrow[-\ CO_2]{H_2C_2O_4} 3\ Ba(Mg_{1/3}Ta_{2/3})O_3$$

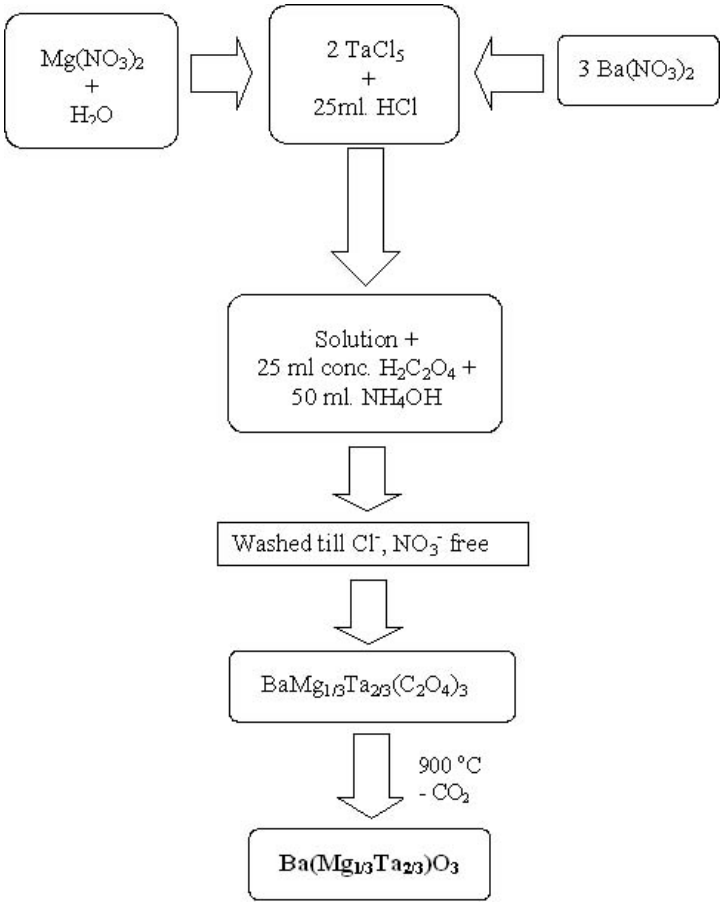

(ii) Citrate Gel Route

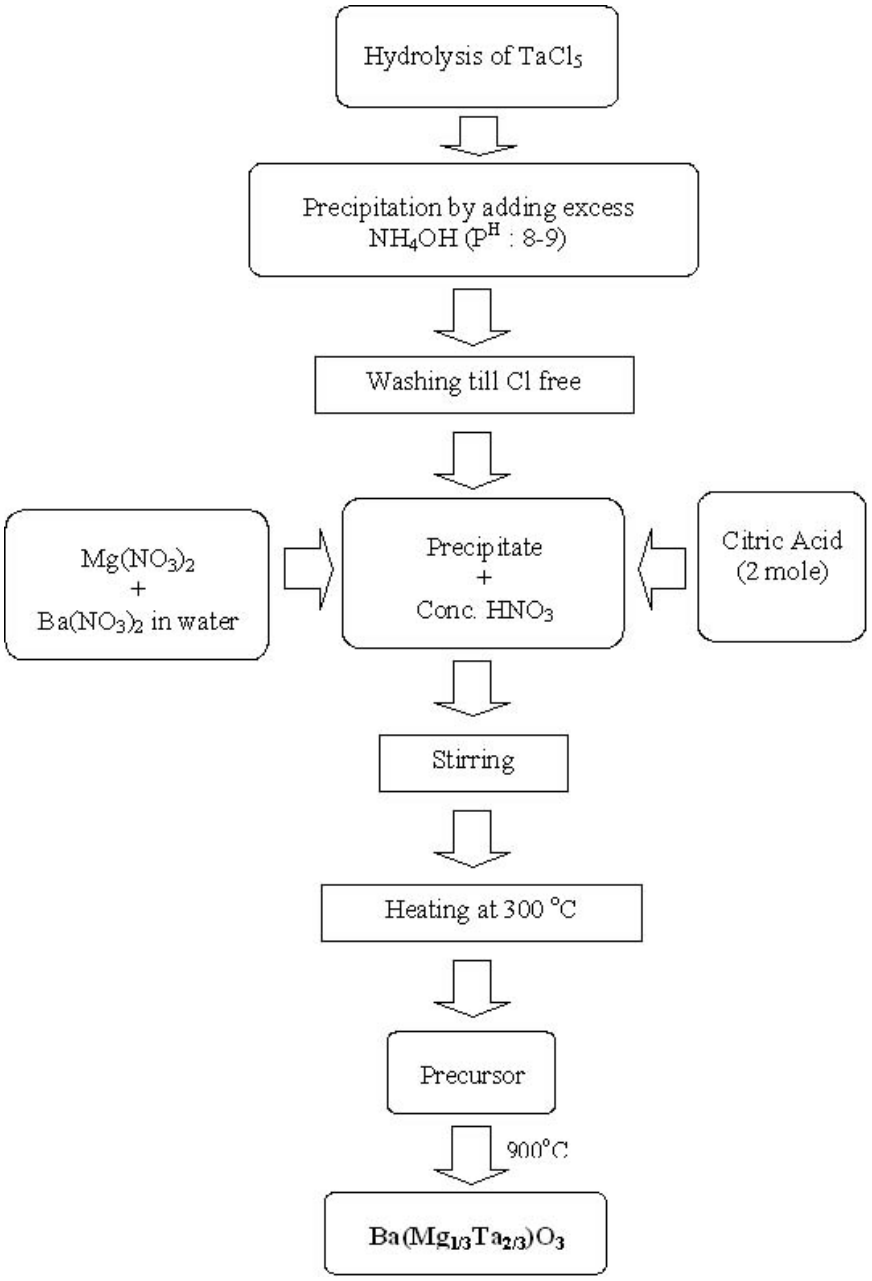

3. 3. 2. 4 Results and Discussion

The DTA thermogram of BMT prepared through Citrate Gel and Precipitation techniques are given as (C) and (D) respectively in Fig. 3.4. In Fig. 3.4 (D) for precipitation synthesis route, the exotherm at 182°C is beloved to be due to the liberation of 3 moles of CO_2 from $BaMg_{1/3}Ta_{2/3}(C_2O_4)_3$. This is followed by the volatisation of the carbonates which is marked by a strong exothermic peak at 203°C. The material formation in co-

precipitation route is occurring at 502^{o}C which is much lower than the formation temperature (> 800^{o}C) in solid state reaction techniques. The achievement in reducing the synthesis temperature is believed to result from the improvement in overall mixing homogeneity of cations and enhanced reactivity of starting materials [71]. The self propagating combustion synthesis is operating at a lower temperature as shown in Fig.3.4 (C). The exotherm at 268^{o}C is corresponding to the burnout temperature of citrate polymer. In this case the product formation temperature is at 467^{o}C which is indicated by a strong endothermic dip in the DTA curve.

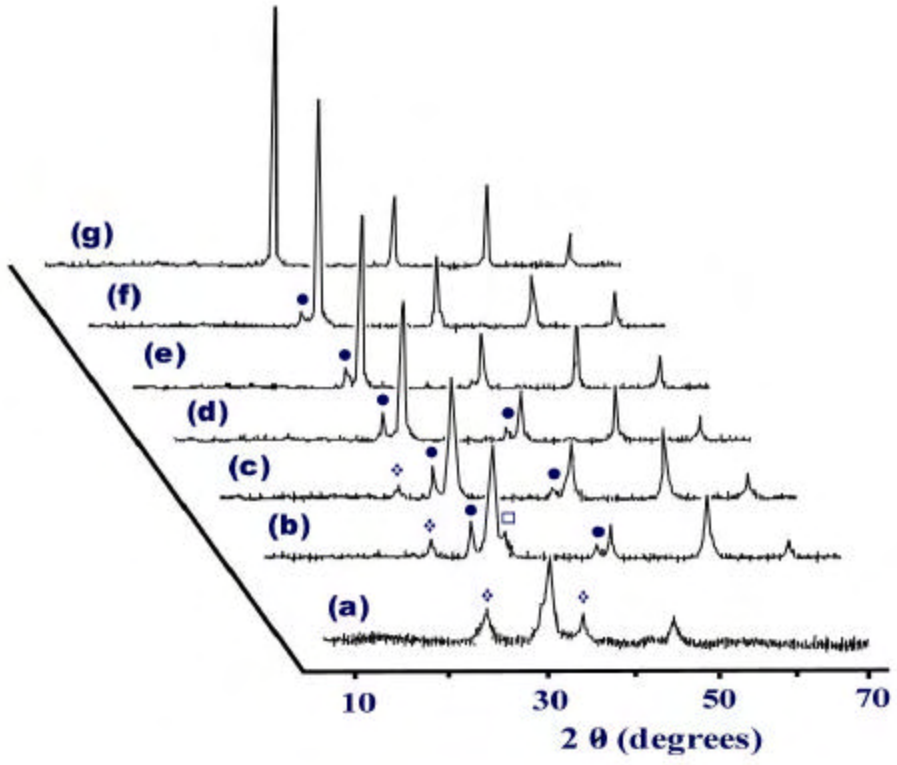

Fig. 3.6 Powder Diffraction patterns of BMT synthesized through co-precipitation method (a) for the precursor heated at 600, (b) 700, (c) 800, (d) 900, (e)1000, (f) 1200 and 1400^{o}C. ❖ represents $BaCO_3$, ● represents $Ba_5Ta_4O_{15}$ and □ $MgTa_2O_6$

Fig.3.6 represents the XRD profiles BMT prepared through homogeneous precipitation synthesis, heated at various temperatures from 600^{o}C to 1400^{o}C. At low processing temperatures (~ 600^{o}C), unreacted barium oxalate precursor converts to carbonate whose presence is detected in the powder diffraction pattern. As the temperature is increased, owing to the insufficient mixing of cations in the precipitate, diffraction peaks

for $MgTa_2O_6$ and $Ba_5Ta_4O_{15}$ are detected. The former reacts with $BaCO_3$ to form BMT but $Ba_5Ta_4O_{15}$ is present in the powder even when heated at temperatures as high as 1200°C. The calcination at extremely higher temperatures (1400°C) only can yield phase pure BMT. Thus the co-precipitation technique is found to be less attractive as a useful low temperature synthesizing technique for preparing BMT. A recent study[72] on the co-precipitation also confirms the observation of high calcination temperature requirement of BMT.

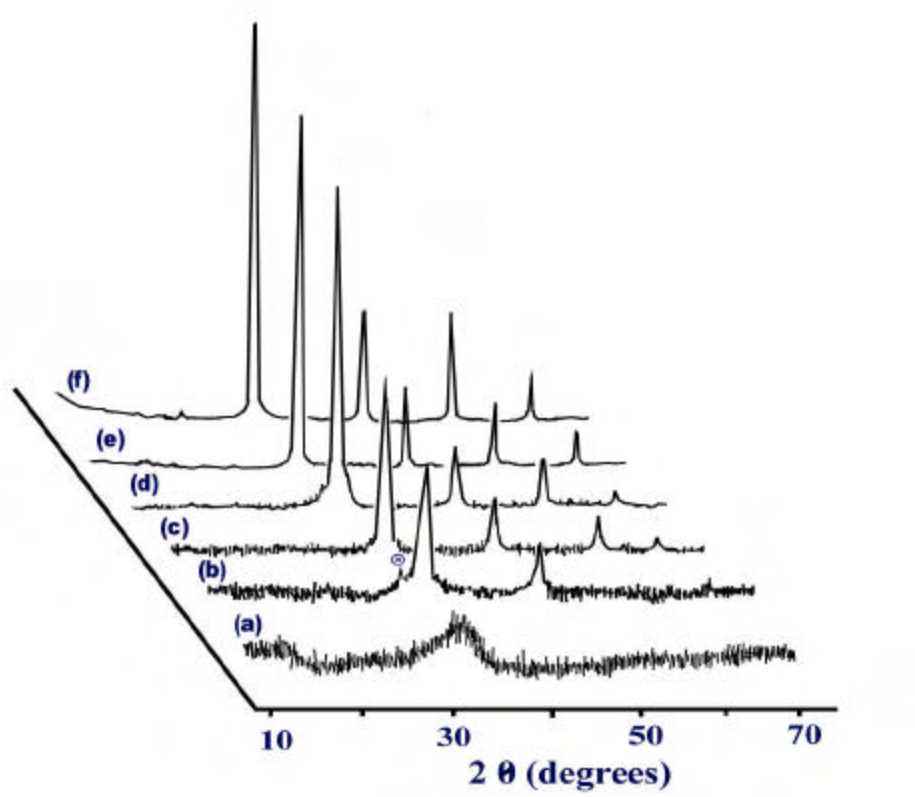

Fig. 3. 7 Powder Diffraction patterns of BMT synthesized through citrate gel method (a) for the precursor heated at 500, (b) 600, (c) 700, (d) 800, (e)900, (f)1000°C. ⊗ stands for $BaTa_2O_6$

The material formation sequence of BMT prepared through citrate gel route is given in Fig. 3.7. Here also presence of $BaTa_2O_6$ was detected at a calcination temperature of 600°C but it vanishes at high temperatures. Even at temperature as low as 700°C, phase pure BMT can be synthesized. So unlike co precipitation, citrate gel method is a useful technique to synthesize nanocrystalline $Ba(Mg_{1/3}Ta_{2/3})O_3$ powder. The average particle size of the chemically derived powder was determined as 56 nm and 34 nm respectively using

co-precipitation and citrate gel techniques. It is interesting to study the microwave dielectric properties of BMT prepared through solution methods.

In spite of the efforts by a number researchers, the microwave dielectric properties of BMT prepared through wet methods remained surprisingly poor even after long time annealing, compared to their solid state counterparts. The cation ordering is poor in chemically derived BMT specimen (see Table 3.1). In our investigations, the unloaded quality factor for co-precipitated BMT is 11,325 GHz. As a general trend, the densification is poor in both cases. The quality factor for BMT in citrate route is slightly higher ($Q_u$xf = 34,450 GHz) compared to co-precipitated BMT specimen (see Table 3.1). Further work is needed to be done to probe the reasons behind the poor display of dielectric properties in specimen prepared with chemical methods.

3. 4 EFFECT OF NON-STOICHIOMETRY IN $Ba(Mg_{1/3}Ta_{2/3})O_3$

3. 4.1 Introduction

One way to improve the sinterability is to enhance the material transport processes in the dielectric through altering the material's stoichiometry. The effect of off-stoichiometry on the dielectric properties have been discussed by many authors [73, 74] in a wide range of materials. Historically, Desu and O'Bryan[75] made the first attempt in correlating the phenomenon of the excellent microwave quality factor of a prominent complex perovskite candidate $Ba(Zn_{1/3}Ta_{2/3})O_3$ (BZT) with B-site cation non-stoichiometry. They could explain the low loss property on the basis of ZnO evaporation. This investigation was further extended by Kawashima[76] who found that inhomogeneous densification was achieved by ZnO evaporation which can be compensated by muffling in ZnO, but the quality factor decreased. Subsequently in 1996, Choi et al.[77] revisited this problem in BZT using transmission electron microscopy who observed a new type of ordering along the <110> direction apart from the formation of $Ba_{0.5}TaO_3$ and $Ba_3TaO_{5.5}$ phases in zinc defiant samples. The effect of a slight non stoichiometry and chemical inhomogeneity on the order-disorder phase transformation has been studied[78] in complex perovskite $Ba(Ni_{1/3}Nb_{2/3})O_3$ and $Ba(Zn_{1/3}Nb_{2/3})O_3$. In yet another significant attempt, Paik et al.[79] investigated the effect of Mg deficiency on the microwave dielectric properties of complex

perovskite $Ba(Mg_{0.33}Nb_{0.67})O_3$. In this report the authors claimed an improvement in density and unloaded Q factor for x= 0.02 in $Ba(Mg_{0.33-x}Nb_{0.67})O_3$ which was expected to be due to enhanced grain boundary mass transport generated by lattice defects. It may be noted that the volatilization of MgO[80] in $Ba(Mg_{1/3}Ta_{2/3})O_3$ at high temperature leads to the formation of secondary phases. Later on Tochi [81]observed that the sinterability of BMT could be improved with the addition of the extra phase $BaTa_2O_6$ that formed during calcination even though there has been previous reports that presence of the extra phase $BaTa_2O_6$ in BMT would cause degradation of the microwave Q factor. In addition to that there were previous reports [82, 83] that among the three starting materials, the reactivity of MgO is inferior to $BaCO_3$ and Ta_2O_5. In the conventional sintering processes, the reaction between the latter two give rise to Ba-Ta-O satellite phases which is detrimental to the microwave dielectric properties of the ceramic [84]. An improvement in the degree of 1: 2 ordering and sinterability was proposed by Lu and Tsai [85] in Ba-deficient $Ba(Mg_{1/3}Ta_{2/3})O_3$ ceramics, but they didn't throw light into the effects of this A-site cation deficiency on the microwave dielectric properties of BMT. The effect of Mg deficiency on the microwave dielectric properties of BMT was also investigated by a couple of research groups [86, 87] who found that MgO-deficient specimen showed faster grain growth rate than stoichiometric BMT. However off-stoichiometric samples showed lower Q values.

The brief discussion made above suggests that the effect of B-site deficiency improves the dielectric properties in $Ba(Zn_{1/3}Ta_{2/3})O_3$ while it is detrimental to the dielectric quality factor in $Ba(Mg_{1/3}Ta_{2/3})O_3$. This drew our special attention into the complex relationship between stoichiometry and microwave loss quality of complex perovskite $Ba(Mg_{1/3}Ta_{2/3})O_3$ ceramics. In the next section, the effect of Ba and Mg non-stoichiometries on the densification, microstructure, structural ordering and microwave dielectric properties of $Ba(Mg_{1/3}Ta_{2/3})O_3$ is discussed. The effects of nonstoichiometry and associated lattice distortion on the vibrational modes of BMT crystal are studied by laser Raman scattering.

3. 4. 2 Ceramic Preparation

The non-stoichiometric compositions based on $Ba(Mg_{0.33-x}Ta_{0.67})O_3$ [x = -0.015, -0.010, -0.005. 0.0, 0.005, 0.010, 0.015, 0.020, 0.025 and 0.030] and $Ba_{1-x}(Mg_{0.33}Ta_{0.67})O_3$

[x = -0.015, -0.010, -0.005. 0.0, 0.0025, 0.005, 0.0075, 0.010, 0.015, 0.020, 0.025 and 0.030] were prepared by the conventional solid-state ceramic route as described in Chapter. 2, Sections 2.1.2.1 to 2.1.2.7.. The homogenized stoichiometric mixture was calcined at 1200^{o}C for 10 hours. The uniaxially pressed pellets were sintered at 1600^{o}C for 4 hours. The sintered specimens were annealed at 1450^{o}C for 40 hours to enhance cation ordering. The cation ordering and lattice distortion were analyzed by an X-ray diffractometer (Rigaku – Dmax 1C, Japan) using Cu Kα radiation. The surface morphology of the thermally etched sintered samples were analyzed using scanning electron microscope (SEM S-2400, Hitachi, Japan). The approximate ionic concentration of the specimen were measured using SEM/EDX facility with Oxford ISIS software.

The dielectric properties ε_r and τ_f of the materials were measured in the microwave frequency range using resonance technique as described Chapter 2, Sections 2.2.2 to 2.2.5. Micro-Raman scattering spectra were recorded using a *Jobin-Yvon* LABRAM-HR spectrometer, equipped with a 1800 grooves/mm diffraction grating, a liquid-N_2-cooled CCD detector and a confocal microscope (100 × objective).

3. 4. 3 Results and Discussion

3. 4. 3. 1 Densification, Structural Order and Microstructure

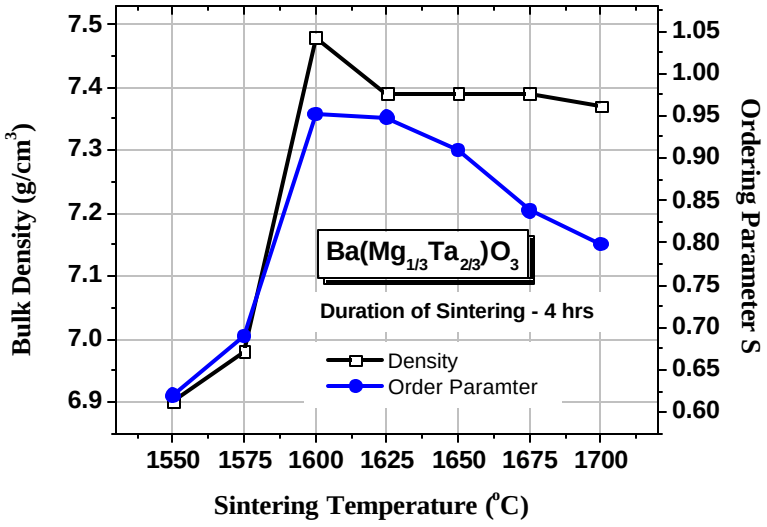

Fig. 3. 8 Variation of bulk density and ordering parameter of $Ba(Mg_{0.3283}T_{0.67})O_3$ with sintering temperature

The Fig. 3. 8 represents the variation of the bulk density and cation ordering parameter with sintering temperature of x = 0.005 in $Ba(Mg_{0.33-x}Ta_{0.67})O_3$. It is evident that both ordering and density are increasing with sintering temperature and reach maximum values at 1600°C. A slight non stoichiometry of MgO can bring about two effects in the ceramic: (i) appearance of additional phase such as $BaTa_2O_6$ and $Ba_5Ta_4O_{15}$ (ii) improvement of the sinterability by bulk diffusion due to vacancies created by MgO loss. It is expected that the latter phenomenon might have contributed to the improvement of density at high sintering temperature at 1600°C. The specimens used in this investigation are sintered at 1600°C where the dielectric properties are also found to be better. It must be noted that sintering the ceramic at temperature above 1650°C is not desirable, as it will breed porosity and correspondingly density decreases.

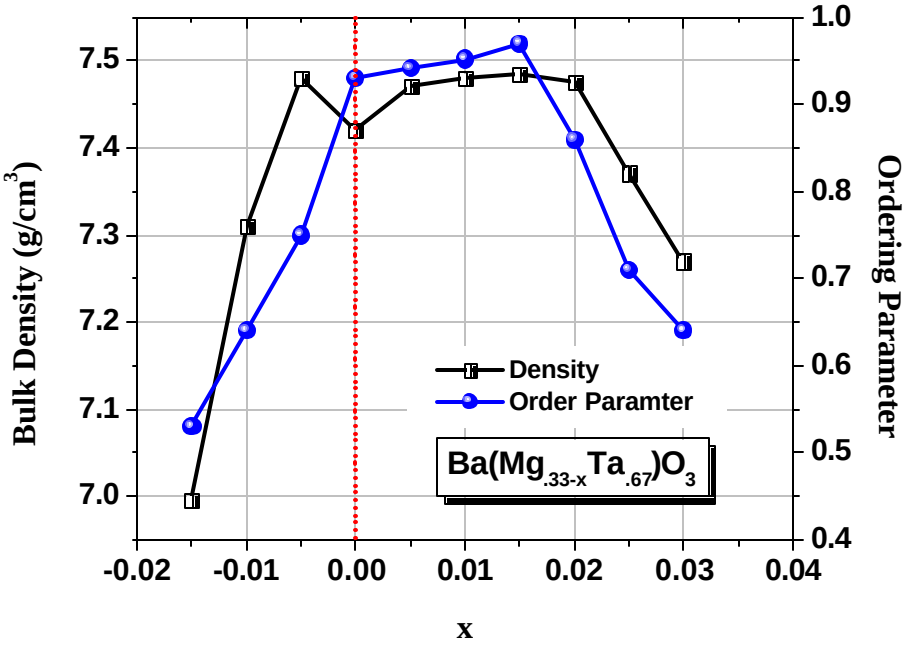

Fig. 3. 9 Variation of bulk density and ordering parameter of $Ba(Mg_{0.33-x}T_{0.67})O_3$ with x

The bulk density of BMT is more or less invariant with Mg deficiency upto x=0.02 in $Ba(Mg_{0.33}Ta_{0.67})O_3$ as shown in Fig. 3. 9. The densification reaches maximum value of 7.485 g/cm^3 for x=0.015 in $Ba(Mg_{0.33-x}Ta_{0.67})O_3$ which is about 98 % of the theoretical density (7.625 g/cm^3) of stoichiometric BMT. For higher values of (x >0.2 in $Ba(Mg_{0.33-x}$

$Ta_{0.67})O_3$) the density decreases due to the formation of additional phases like $BaTa_2O_6$ and $Ba_5Ta_4O_{15}$. In addition to that it has been well established[88] that greater extent of nonstoichiometry results in lattice distortion which can hinder the diffusion mechanism for densification. In a recent publication [89] Lu and Chang found that the densification phenomenon of complex perovskite $Pb(Mg_{1/3}Nb_{2/3})O_3$ (PMN) was considerably improved with the addition of small amount of MgO. This suppressed the grain growth phenomena that could have been occurred in pure PMN. A similar observation was made in Mg excess $Ba(Mg_{0.33}Ta_{0.67})O_3$ ceramics, where the density is slightly higher for x = -0.005 than pure BMT. The higher percentage of excess MgO (x >0.05 in $Ba(Mg_{0.33-x}\ Ta_{0.67})O_3$)would remain in the grain boundary, significantly hinder the diffusion mechanism and the migration of grain boundary thereby decreasing the density of the specimen. It must be noted that the densification mechanism and cation ordering phenomenon does not bear a one to one correspondence in Mg offstoichiometric compositions. The cation ordering (see Fig. 3. 9) which is a microscopic phenomenon, is reaching its maximum value (0.97) for x=0.015 in $Ba(Mg_{0.33-x}Ta_{0.67})O_3$) while ordering is poor for pure and MgO excess specimens.

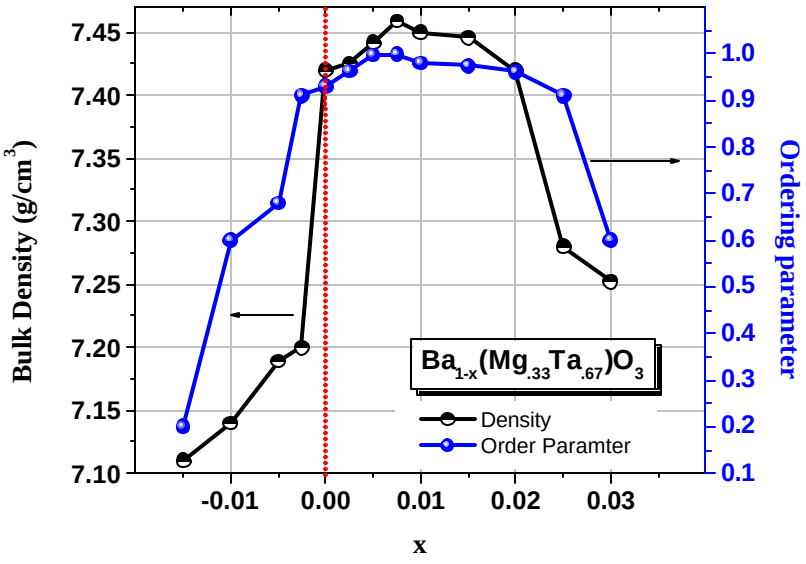

Fig. 3. 10 Variation of bulk density and ordering parameter of $Ba_{1-x}(Mg_{0.33}T_{0.67})O_3$ with x

The evolution of density and cation ordering in Ba off-stoichiometric BMT is given in Fig. 3.10. The sintered specimens show a trend of densification in slightly Ba deficient samples. The bulk density is maximum (7.459 g/cm^3 which is about 97.8 % of the x ray density of stoichiometric BMT sample) for x = 0.0075 in $Ba_{1-x}(Mg_{0.33}Ta_{0.67})O_3$. The densification is decreased as the barium content is decreased below x= 0.02 in $Ba_{1-x}(Mg_{0.33}Ta_{0.67})O_3$ which can be attributed to the formation of additional phases like $MgTa_2O_6$. A similar observation in non--stoichiometric BMT was reported by Lu and Tsai [86] who found an increase in densification for x = -0.005 in $Ba_{1+x}(Mg_{0.33}Ta_{0.67})O_3$. The density of samples with surplus Ba content show poor densification. This result is consistent with the similar observation made in $Ba(Zn_{0.33}Ta_{0.67})O_3$ by Kawashima [77] who observed a degradation in the shrinkage of BZT samples with excess Ba content. The cation ordering parameter shows reasonably better values in Ba deficient samples in comparison with Mg deficient ones. The ordering parameter for x=0.0, 0.0025, 0.005, 0.0075 and 0.01 are 0.93, 0.963, 0.997, 0.999 and 0.98 respectively. On the other hand, the addition of excess Ba ions damage the 1: 2 cation ordering (see Fig.3.10). It is expected that a part of excess barium ion might enter B-site in $Ba(Mg_{0.33}Ta_{0.67})O_3$ and disturb the cation ordering between magnesium and tantalum[77].

In this investigation it was found that one composition each in Mg and Ba deficient perovskites ($Ba(Mg_{0.3183}Ta_{0.67})O_3$ and $Ba_{0.9925}(Mg_{0.33}Ta_{0.67})O_3$) have exhibited excellent properties. So it is imperative to analyze the chemical compositions of these ceramics in detail. The surface ionic concentration of the above compositions are studied quantitatively using Energy Dispersive X-ray analysis. Figs. 3.11 (a) and 3.11 (b) gives the EDX spectra of $Ba(Mg_{0.3183}Ta_{0.67})O_3$ and $Ba_{0.9925}(Mg_{0.33}Ta_{0.67})O_3$ ceramics sintered at 1600^{o}C for 4 hours. The ratio between relative concentration of B-site ions Mg/Ta = 0.0474, which confirms the lower concentration of Mg^{2+} ions in the specimen. It must be noted that the concentration of Mg ions is slightly less than the expected Mg concentration as per the stoichiometry of $Ba(Mg_{0.3183}Ta_{0.67})O_3$ [= 0.06142] which may be attributed to the volatisation of MgO at 1600 ^{o}C. A similar observation of non stoichiometry created by the high temperature MgO loss has been reported [80] earlier in BMT. On the other hand the ratio Mg/Ta is slightly higher [0.0753] than expected [0.0672] in $Ba_{0.9925}(Mg_{0.33}Ta_{0.67})O_3$ (see Fig. 3.11 (b)) which may be understood as a result of the substitution of Mg in vacant Ba-

sites to form a possible composition $Ba_{1-x/3}\ Mg_{x/3}[Mg_{(1-x)/3}Ta_{2/3}]O_3$. But this process could take place only at a very slow pace due to the difference in ionic radii between Ba^{2+} (1.35 Å for six coordination[90]) and Mg^{2+} (0.72 Å for six

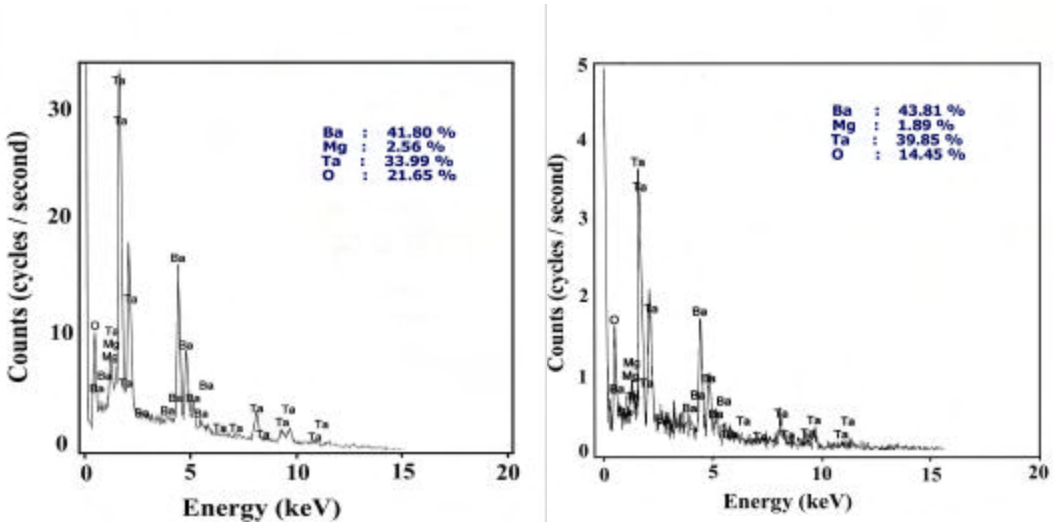

Fig. 3. 11 (a) EDX spectrum of $Ba(Mg_{0.3183}Ta_{0.67})O_3$ and (b) $Ba_{0.9925}(Mg_{0.33}Ta_{0.67})O_3$ ceramics sintered at 1600°C for 4 hours

coordination). The possible representations of Mg deficient compositions are (i) $Ba[(Mg_{1/3})_xBa_xTa_{2/3}]O_3$ and (ii) $Ba[\square_xMg_{1/3-5x/3}Ta_{2/3}+2_{x/3}]O_3$ ($\square$ = magnesium vacancy) which can be assumed [76, 77] similar to Zn deficient $Ba(Zn_{1/3}Ta_{2/3})O_3$. The second proposed structure is also reasonable as the ionic radii of Mg and Ta are comparable and the lattice positions of magnesium and tantalum are at random at the early stages of synthesis[91]. It must be noted that the cation non-stoichiometry in $Ba(Mg_{0.33}Ta_{0.67})O_3$ is compensated as a manifestation of the oxygen anion concentration in BMT lattice. So the more appropriate representations of the non--stoichiometric BMT are $Ba(Mg_{0.33-x}Ta_{0.67})O_{3\pm d}$ and $Ba_{1-x}(Mg_{0.33}Ta_{0.67})O_{3\pm d}$, where d determines the oxygen non-stoichiometry which can be determined using semi empirical methods[92]. Even though this oxygen non stoichiometry has drastic effects on the dielectric properties, we avoid the representation of non-stoichiometric BMT for the sake of simplicity.

The XRD patterns of typical Mg deficient, Ba deficient and stoichiometric $Ba(Mg_{0.33}Ta_{0.67})O_3$ are given in Fig. 3. 12. In the powder pattern recorded from pure BMT,

presence of superstructure reflections are visible which means that the stoichiometric BMT is reasonably well ordered. This observation is consolidated by Figs. 3.9 & 3.10 from which it is understood that the ordering parameter of pure BMT is 0.93. As the Mg content is decreased upto x=0.015

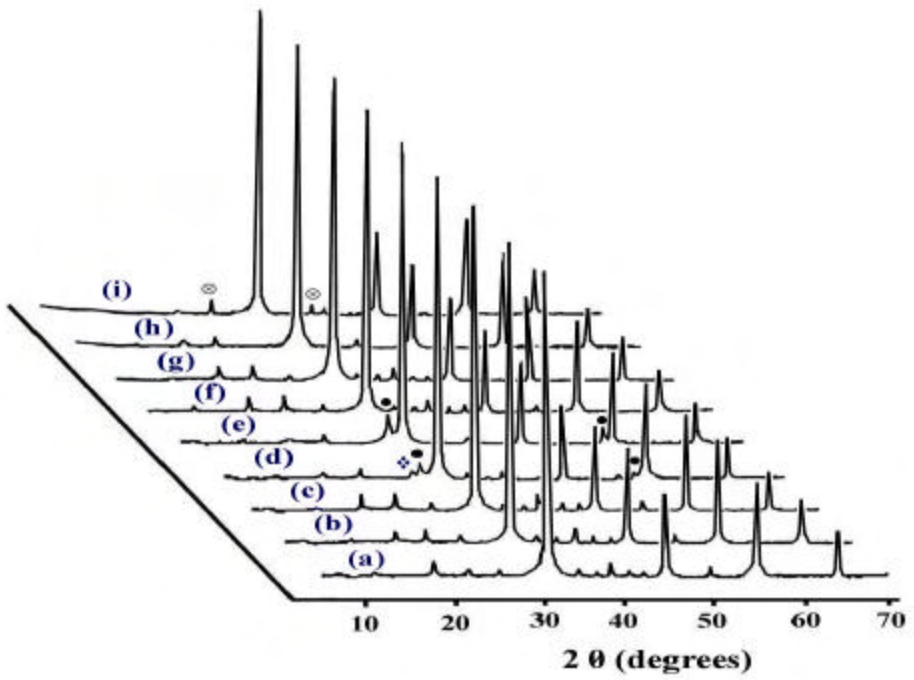

Fig. 3. 12 Powder diffraction patterns of some typical non--stoichiometric compositions of BMT. (A) Pure $Ba(Mg_{0.333}Ta_{0.667})O_3$, (B) $Ba(Mg_{0.3233}Ta_{0.667})O_3$, (C) $Ba(Mg_{0.3183}Ta_{0.667})O_3$, (D) $Ba(Mg_{0.3133}Ta_{0.667})O_3$, (E) $Ba(Mg_{0.3033}Ta_{0.667})O_3$, (F) 0.9925 $Ba(Mg_{0.3183}Ta_{0.667})O_3$, (G) 0.99 $Ba(Mg_{0.3183}Ta_{0.667})O_3$, (H) 0.98$Ba(Mg_{0.3183}Ta_{0.667})O_3$, (I) 0.97 $Ba(Mg_{0.3183}Ta_{0.667})O_3$. ● stands for $Ba_5Ta_4O_{15}$, ❖ for $BaTa_2O_6$, ⊗ $MgTa_2O$

in $Ba(Mg_{0.33-x}Ta_{0.67})O_3$ (see Fig. 3. 12(c)) the intensity of 1:2 superstructure lines increases, but no traces of any additional phases are visible within the limits of experimental error. But a larger level of Mg deficiency x > 0.015 will initiate the formation of additional phases like [17] $BaTa_2O_6$ and [93] $Ba_5Ta_4O_{15}$ whose presence is reported to deteriorate the dielectric quality factor in BMT. The loss of B" site ion in 1:2 type Ba based complex perovskites may result in formation of additional phases like [94] $Ba(B'_{1/8}B"_{3/4})O_3$ whose crystal structure has been reported by Abakumov et al [95]. Recently Davies et al.[96] confirmed the formation of $Ba_8ZnTa_6O_{24}$ in Zn deficient $Ba(Zn_{0.33}Ta_{0.67})$ dielectrics. This compound has a hexagonal perovskite structure (space group P63cm) with an eight-layer

$(cchc)_2$ close-packed arrangement of BaO_3 layers. In a separate investigation, Bieringer et al.[97] also explored the non-stoichiometry and ordered domain growth aspects of zinc deficient BZT in the light of the newly formed complex perovskite $Ba_8ZnTa_6O_{24}$ phase. But the present study does not favour the formation of a possible compound like $Ba_8MgTa_6O_{24}$ in Mg deficient perovskites. On the hand the x-ray diffractogram of typical Ba deficient BMT ceramics (see Fig.3.12(f-i)) shows comparatively better cation ordering of B-site cations which is evidenced by the appearance of discrete ±1/3{hkl} superlattice reflections perpendicular to e.g. <111> and <11$\bar{1}$>. The samples are free of additional phases for $x \leq 0.025$. However decreasing the barium concentration below a threshold level will result in the formation of additional phases like $MgTa_2O_6$ (see Fig. 3.12(i)).

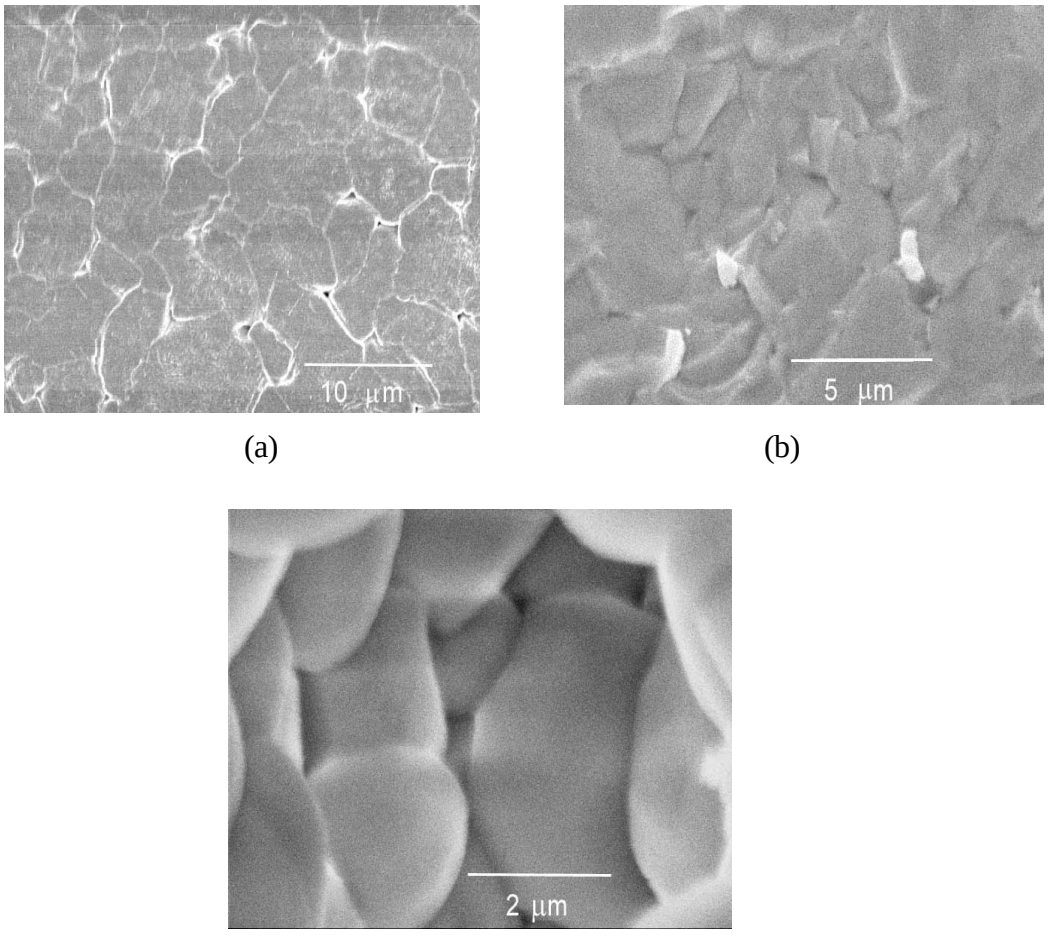

(a) (b)

(c)

Fig. 3. 13 Scanning electron micrographs of (a) $Ba(Mg_{0.3183}Ta_{0.667})O_3$ (b) $Ba(Mg_{0.3483}Ta_{0.67})O_3$ (c) $Ba_{0.9925}(Mg_{0.33}Ta_{0.67})O_3$ ceramics

Fig. 3. 13 presents the scanning electron micrographs of three non--stoichiometric specimens sintered at 1600°C. The surface morphology recorded from a typical Mg deficient BMT ($Ba(Mg_{0.3183}Ta_{0.667})O_3$) sample is given in Fig. 3.13(a). There has been previous reports [91] that the grain growth will be more rapid in Mg deficient BMT ceramics, consequent to the formation of sandwich type precipitates of $Ba_5Ta_4O_{15}$ within the matrix grain. Here also it is evident that the average grain size of BMT grain is about 5-8 μm in Mg deficient specimens with reasonably good close packing of grains. It must be remembered that in our experiment the additional phases like $BaTa_2O_6$ and $Ba_5Ta_4O_{15}$ have started appearing in the sintered grain only for x>0.015 in $Ba(Mg_{0.33-x}Ta_{0.67})O_3$. On the other hand addition of excess MgO is also not beneficial to the densification of BMT as the sample presented in Fig. 3.13(b) is showing symptoms of a possible liquid phase sintering. The additional MgO in $Ba(Mg_{0.3483}Ta_{0.67})O_3$ may retard the excessive grain growth that could have been happened by forming a vitreous phase with matrix components. Moreover additional MgO precipitates are visible in the electron micrograph. This is in disagreement to the observations of Lee et al. [91] who reported that the surplus MgO added to BMT will precipitate on the matrix grain surface and impede grain growth. Fig. 3.13(c) represents the surface morphology of $Ba_{0.9925}(Mg_{0.33}Ta_{0.67})O_3$ which is taken from a fractured surface. Here no additional phases are visible in the SEM picture and the grain size is around 2-3 μm. A previous report [91] on the Ba-deficient BMT ceramics observed the presence of magnesium rich small darker grains which is appeared as a solidified liquid. But no evidence of liquid phase sintering was revealed in Ba deficient BMT samples.

Since sintering occurs through mass transport and the rate of mass transport depends on the defect mechanism of ionic crystals, the crystal defect occurring even at the time of calcinations can control the sintering behaviour of BMT. Based on the powder diffraction analysis, three cases can be considered for the dominant defect types in calcined BMT powder : (a) A site vacancy is the major defect (b) B site (B' or B") vacancy is the major defect and (c) both A and B sites occur simultaneously. One of these cases plays a major role during sintering process[98]. In complex perovskite $Ba(Zn_{1/3}Ta_{2/3})O_3$ ceramics Desu and O'Bryan[75] observed that prolonged sintering up to 100 hours increased the unloaded quality factor. They attributed this phenomenon to the loss of ZnO and the subsequent

replacement of Zn^{2+} ions by Ba^{2+} ions in the perovskite unit cell. This result in the expansion of the unit cell along body

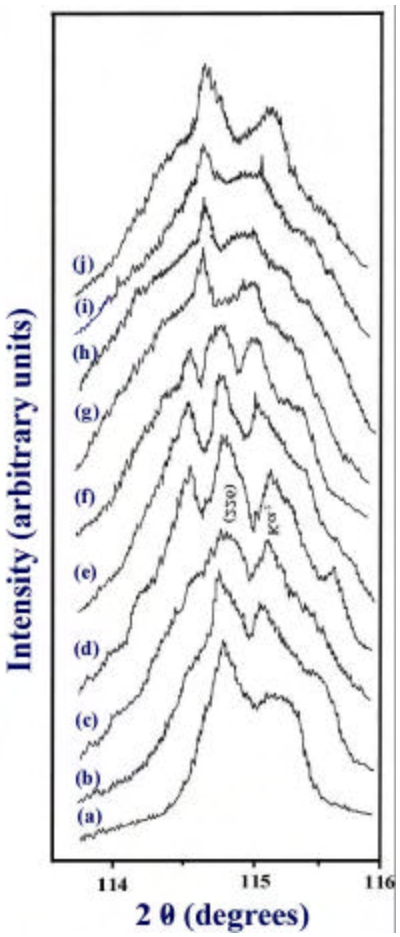

Fig. 3.14

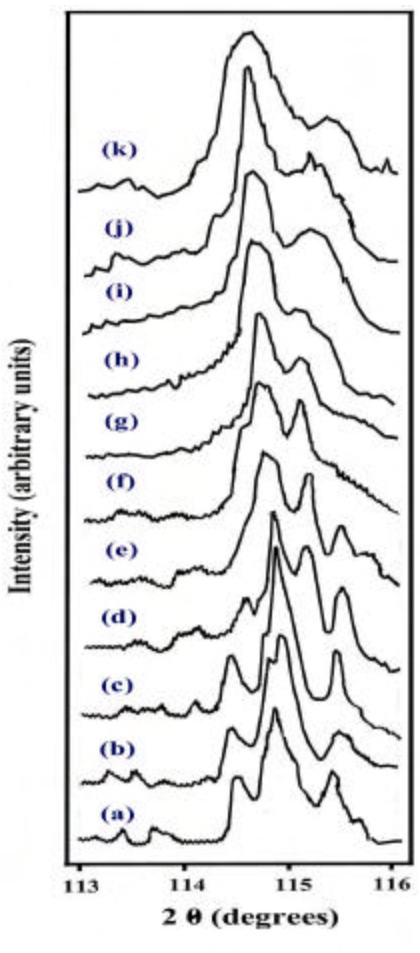

Fig.3.15

Fig. 3. 14 X-ray diffraction line profiles of 422 and 266 reflections for $Ba(Mg_{0.33-x}Ta_{0.67})O_3$ for x= (a) 0.03, (b) 0.025, (c) 0.02, (d) 0.015, (e) 0.01, (f) 0.005, (g) 0.0, (h) -0.005, (i) -0.010 and (j) -0.015

Fig. 3.15 X-ray diffraction line profiles of 422 and 266 reflections for $Ba_{1-x}(Mg_{0.33}Ta_{0.67})O_3$ for x= (a) 0.0025, (b) 0.005, (c) 0.0075, (d) 0.01, (e) 0.015, (f) 02, (g) 0.025, (h) 0.03, (i) -0.005, (j) -0.01 and (k) –0.015.

diagonal <111> direction and in the splitting of the (422) and (226) powder diffraction lines in accordance with lattice distortion. Hence it is expected that the B' ion non-stoichiometry may have a vital role on the sinterability and microwave dielectric properties

of $Ba(B'_{1/3}Ta_{2/3})O_3$ [B'=Mg, Zn]. The splitting of the profiles of (422) and (266) reflections due to the lattice distortion of non- stoichiometric $Ba(Mg_{0.33-x}Ta_{0.67})O_3$ and $Ba_{1-x}(Mg_{0.33}Ta_{0.67})O_3$ for different values of x is shown in Figs. 3.14 and 3.15 respectively. The XRD patterns shown in Fig. 3.14 are recorded with a slow scan of 2Θ =1 degree/minute. For stoichiometric BMT the two profiles are not distinguishable from standard Ka_2 line, which has apparently no lattice distortion. It is observed that splitting is more pronounced for x = 0.015 in $Ba(Mg_{0.33-x}\ Ta_{0.67})O_3$ (see Fig. 3.14(d)). A similar phenomena was observed in Ba- deficient complex perovskites, where the maximum line splitting was observed for x= 0.0075 in $Ba_{1-x}\ (Mg_{0.33}Ta_{0.67})O_3$ (see Fig. 3.15 (c)). It is interesting to note that the rise and fall of the ordering parameter as a function of non-stoichiometry x in $Ba(Mg_{0.33-x}Ta_{0.67})O_3$ and $Ba_{1-x}(Mg_{0.33}Ta_{0.67})O_3$ (see Figs Figs. 3.9 and 3.10) is in accordance with variation of the lattice distortion given in 3.14 & 3.15 where the splitting of the profiles of (422) and (266) reflections is maximum.

Table 3. 2 Unit cell properties of $Ba(Mg_{0.33-x}Ta_{0.67})O_3$ and $Ba_{1-x}(Mg_{0.33}Ta_{0.67})O_3$ for different values of x

x	$Ba(Mg_{0.33-x}Ta_{0.67})O_3$			$Ba_{1-x}(Mg_{0.33}Ta_{0.67})O_3$		
	a (Å)	**c (Å)**	**c/a**	**a (Å)**	**c (Å)**	**c/a**
-0.0150	5.7814	7.0678	1.2225	5.7832	7.0711	1.2226
-0.0100	5.7819	7.0680	1.2224	5.7821	7.0709	1.2228
-0.0050	5.7821	7.0671	1.2222	5.7810	7.0714	1.2232
0.0000	5.7720	7.0699	1.2249	5.7720	7.0699	1.2249
0.0025	------	-------	--------	5.7724	7.0711	1.2249
0.0050	5.7802	7.0799	1.2249	5.7757	7.0800	1.2258
0.0075	------	-------	--------	5.7749	7.0802	1.2260
0.0100	5.7818	7.0811	1.2247	5.7788	7.0784	1.2248
0.0150	5.7818	7.0845	1.2252	5.7799	7.0780	1.2246
0.0200	5.7820	7.0849	1.2252	5.7805	7.0762	1.2241
0.0250	5.7824	7.0833	1.2249	5.7823	7.0771	1.2233
0.0300	5.7835	7.0821	1.2245	5.7819	7.0691	1.2226

The ordering of Mg and Ta results in the expansion of the original unit cell along the <111> direction[99] so that the value of *c/a* assumes a value greater than √(3/2) =1.22474. It is interesting to note that the value of the cell parameter c also increases from 7.0699 to 7.0845 Å when x changes from 0.0 to 0.015 and the cell parameter ratio *c/a* increases upto x = 0.015 (Table. 3.2). On the other hand the lattice parameter ratio is poor for MgO sufficient samples. In Ba deficient samples the *c/a* ratio increases with x and reaches a maximum value. So it is expected that B site cation is fully ordered for the complex perovskite composition $Ba_{0.9925}(Mg_{0.33}Ta_{0.67})O_3$. As general rule, the increase of deviation from the ideal stoichiometry would cause an increase of the volume of the unit cell in complex perovskites. This is in contrast with the observations made in other lattice systems like spinels where the cation nonstoichiometry increases the average oxidation state of transition metal ions in the spinel structure. Therefore, shrinkage of the lattice with increasing nonstoichiometry may be resulted which is caused by lattice relaxation due to the missing of cations, by stronger interaction between anions and cations[100].

3. 4. 3. 2 Microwave Dielectric Properties

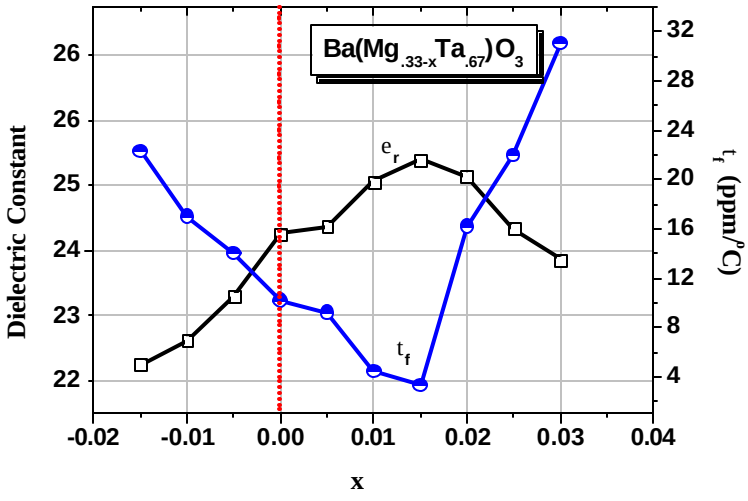

Fig. 3.16 Variation of e_r and t_f of $Ba(Mg_{0.33-x}T_{0.67})O_3$ with x

It has been reported that the vacancies created at the A site in complex perovskite plays a crucial role in controlling their dielectric properties[101]. The variation of the

dielectric constant and τ_f with x in $Ba(Mg_{0.33-x}Ta_{0.67})O_3$ is plotted in Fig. 3.16. The dielectric constant steadily increases as the magnesium deficiency increases. The increase in e_r are in agreement with increase in density. The presence of porosity decreases the e_r since the $e_r(air) = 1$. The magnesium deficiency resulted in enhanced material transport and densification, which is understood to be the reason for increase of dielectric constant in the region $0.0 \leq x \leq 0.015$. For $x > 0.015$, the dielectric constant decreases further due to the presence of $Ba_5Ta_4O_{15}$ whose presence has been confirmed though XRD technique. It must be noted that adding excess of MgO resulted in the decrease of dielectric constant, which is due to the liquid phase sintering and precipitation of MgO on the surface of BMT grains (see Fig. 3.13 (b)). The temperature coefficient of resonant frequency (τ_f) is 8 ppm/^oC for the stoichiometric composition $Ba(Mg_{0.33}Ta_{0.67})O_3$ sintered at 1600^oC/4 hrs (see Fig.3.16). It approaches a minimum value of 4.2 ppm/^oC for x=0.015 in $Ba(Mg_{0.33-x}Ta_{0.67})O_3$. As the value of x increases further τ_f also increases. For x=0.03 the value of τ_f increased 31 ppm/^oC. There are reports that the deficiency of B-site ion in some other complex perovskites like $Pb(Zn_{1/3}Nb_{2/3})O_3$, also decreased its dielectric constant[102]. The addition of excess amount of MgO also results in the increase of τ_f. The variation of the temperature coefficient suggests that higher τ_f values are a consequence of greater lattice distortion.

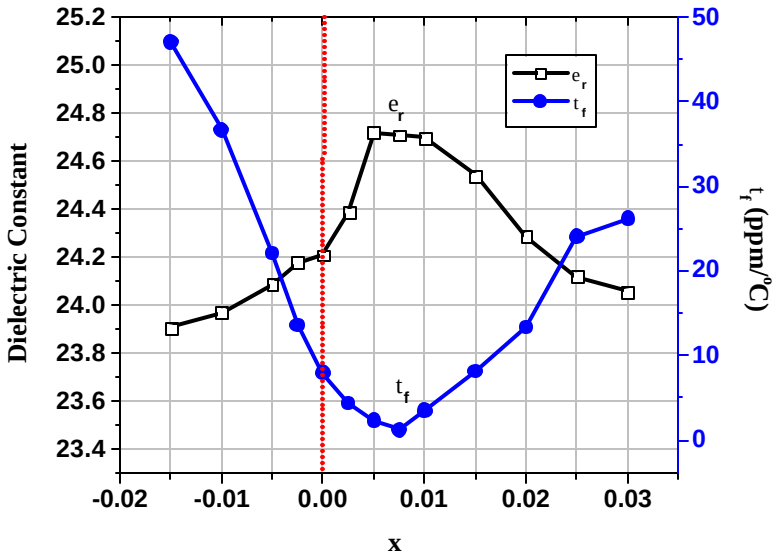

Fig. 3. 17 Variation of e_r and t_f of $Ba_{1-x}(Mg_{0.33}T_{0.67})O_3$ with x

The variation of dielectric constant and temperature coefficient of resonant frequency of Ba-deficient BMT samples are given in Fig.3.17. It is clear that the dielectric constant of the specimens increases with slight barium non- stoichiometry. Here the best dielectric constant (24.2) is measured for stoichiometric BMT while that for the highest level of non--stoichiometry (x= 0.03 in $Ba_{1-x}(Mg_{0.33}Ta_{0.67})O_3$) is 24.06. As seen from the Fig. 3.17, decrease of dielectric constant for Ba rich specimens, is mainly due to poor densification (see Fig. 3.10). It is interesting to note that the temperature coefficient of resonant frequency of Ba deficient samples first decreases and reaches a minimum of 1.2 ppm/^oC for x=0.0075 in $Ba_{1-x}(Mg_{0.33}Ta_{0.67})O_3$. The τ_f of Ba excess BMT is increasing rapidly reaching 47.1 ppm/^oC for x = -0.015 in $Ba_{1-x}(Mg_{0.33}Ta_{0.67})O_3$.

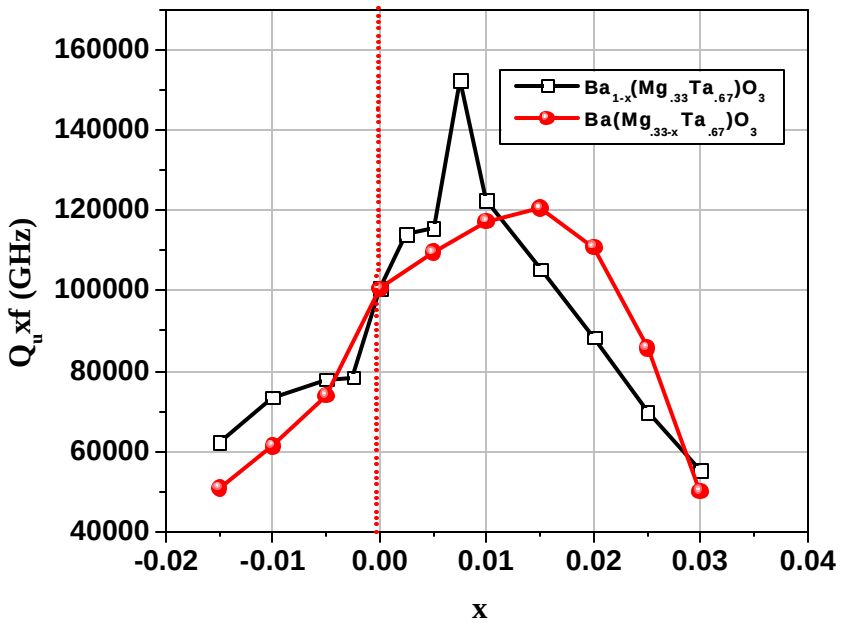

Fig. 3. 18 Variation of Q_ux f of $Ba(Mg_{0.33-x}T_{0.67})O_3$ and $Ba_{1-x}(Mg_{0.33}T_{0.67})O_3$ with x

The microwave quality factor of barium and magnesium non-stoichiometric BMT samples are given in Fig.3. 18. A slight non-stoichiometry may be beneficial for enhanced material transport. The extensive deviation from stoichiometry and associated point defects is correlated to in complex perovskite $BaMg_{0.33}Ta_{0.67})O_3$ can give rise to additional loss in BMT. Rong et al.[103] emphasized that the major cause for dielectric loss in complex perovskites is the enhanced concentration of point defects. The $Q_u$xf of pure stoichiometric

BMT is 100,500 GHz. A slight decrease of Mg concentration (x=0.015 in $Ba(Mg_{0.33-x}Ta_{0.67})O_3$) the BMT ceramic observes a marginal increase in quality factor as $Q_u$xf reaches 120,500 GHz. The Mg deficiency and excess Mg will introduce series of lattice defects in the crystal apart from the distortion of the octahedral skeleton of oxygen. Consequently the quality factor decreases. On the other hand the unloaded quality factor increases with small percentages of Ba deficiency. The quality factor of the fully ordered $Ba_{0.9925}(Mg_{0.33}Ta_{0.67})O_3$ is $Q_u$xf =152,580 GHz. With further increase of x the quality factor decreases, reaches $Q_u$xf =55,570 GHz for x=0.03 in Ba_{1-x} $(Mg_{0.33}Ta_{0.67})O_3$. The quality factor of Ba rich compositions are comparatively lower than Ba deficient samples.

3. 4. 3. 3 Raman Spectra of Non-stoichiometric BMT

The vibrational spectra of complex perovskite-type compounds are functions of both disordered and ordered regions with a particular symmetry, allowing the appearance of specific Raman scattering. Thus, in real systems, a combination of ordered and disordered regions difficult the analysis of Raman data in such materials[104]. The effects of ordering on the Raman spectra of $Ba(Mg_{1/3}Ta_{2/3})O_3$ ceramics have been studied by Siny et al.[105] They found that four strong Raman lines were detected in BMT irrespective of whether 1:2 ordering was found by X-ray diffraction. If the Mg and Ta ions are randomly distributed, the structure should be a cubic perovskite with the space group *Pm3m* (O_h^1), which has no Raman-active modes; 1:2 ordering distorts the structure to $P\bar{3}m1$ (D_{3d}^3), which gives $G_{Raman} = 4A_{1g} + 5E_g$, i.e., nine Raman-active modes. Siny et al. [105] attribute the four strong Raman lines to domains of 1:1 ordering with a superstructure, *Fm3m* (O_h^5) symmetry, and $G_{Raman} = A_{1g} + E_g + 2F_{2g}$. The authors identified these vibrations with the four Raman lines that are characteristic of BZT and BMT. In addition, three extra lines between 100 and 300 cm^{-1} are observed in these two compounds. These are particularly prominent in samples with high *Q* values, and may originate from the complete 1:2 order in the B-sublattice, as a result of the $P\bar{3}m1$ space symmetry.

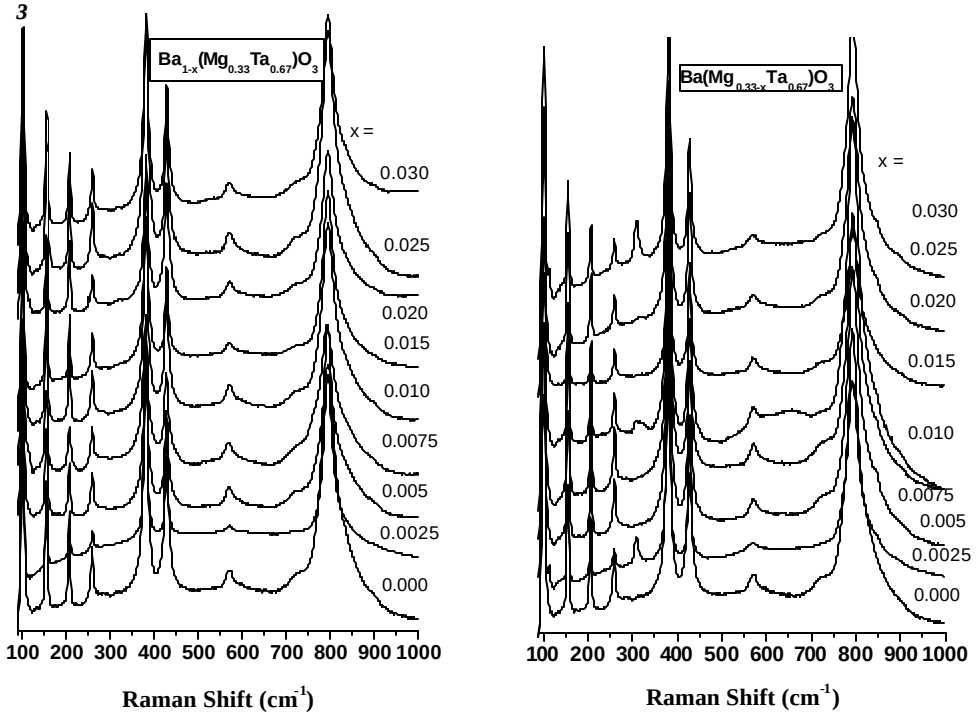

Fig. 3. 19 Raman spectra of (a) Ba- and (b) Mg- deficient BMT ceramics. (The Raman intensities are in log scale.)

Figs. 3.19 (a) and (b) present the Raman spectra of Ba-deficient and Mg-deficient BMT ceramics, respectively. The intensities are in log scale to reveal details in the weaker lines, as well as in the strongest ones. Apparently, the samples have a very good ordered structure because the Raman peaks are of narrow line-width. As it can be seen, four intense lines, related to the 1:1 ordering in the B- sublattice, can be observed in all materials, together with three lines between 150-300 cm^{-1} and one broad line around 570 cm^{-1}. The Raman phonon with the lowest energy near 105 cm^{-1} corresponds to the A_{1g}(Ba) and E_g(Ba) modes (motion of Ba ions against the oxygen octahedral); the bands at about 380 and 430 cm^{-1} are related to internal vibrations of oxygen octahedra, A_{1g}(O) and $2E_g$(O), respectively; the broad band at 795 cm^{-1} corresponds to A_{1g}(O); and the lines at 160, 210, 260 and 570 can be associated to the E_g(O), E_g(Ta) and A_{1g}(Ta) in 1:2 ordered perovskites. Thus, from the results of Raman spectroscopy, the nonstoichiometric BMT ceramics studied in the present work present a high ordering degree, in agreement with the X-ray diffraction results.

Let us now consider the effects of the nonstoichiometry on our Raman spectra. The spectra of Ba-deficient BMT ceramics look very similar (Fig. 3. 19 (a)), with few important differences in samples with $x = 0.0075$ and $x \geq 0.02$. For the first sample, a broad band at 120 cm^{-1} appeared, while bands around 312 cm^{-1} can be seen for $x \geq 0.02$. These extra lines can be associated to lattice distortions for less deficient ceramics (Mg could move to the *A* site) and to the presence of second phases ($MgTa_2O_6$) detected by X-ray diffraction for $x \geq 0.02$ (Fig. 3.12). The region of the spectra between 90 and 170 cm^{-1} was carefully studied in order to understand the influence of nonstoichiometry in the Raman scattering of Ba-deficient ceramics. The results are displayed in Fig. 3.20 (a), where it can be seen in detail the broad line at 120 cm^{-1} for $x = 0.0075$ and the splitting in the lowest energy modes A_{1g}(Ba) and E_g(Ba) at 103 and 106 cm^{-1}, commonly observed as a single band.

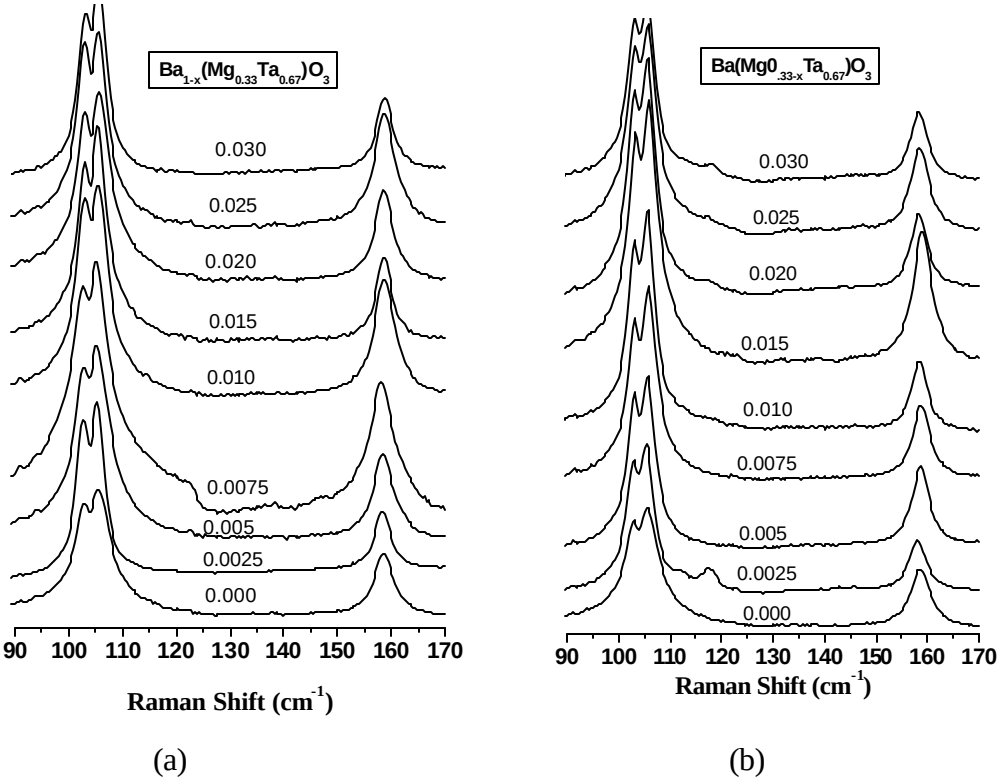

Fig. 3. 20 Raman results for (a) Ba-and (b) Mg -deficient samples in the region 90-170 cm^{-1} (The Raman intensities are in log scale)

Mg-deficient samples (Fig. 3. 19 (a)) present extra weak lines at 112 and 118 cm^{-1} and a strong extra line at 313 cm^{-1} for x = 0.0025, a very low magnesium deficiency. This result is probably due to the lattice distortion from the Ba movement towards the B' site, activating forbidden bands (infrared-active bands). Increasing the Mg deficiency, the extra bands tend to vanish for x < 0.015; at this value, the spectra is almost identical to the stoichiometric BMT. For deficiencies higher than 0.020, the bands appear probably due to distortions from the second phases verified by X-ray diffraction, $Ba_5Ta_4O_{15}$ and $BaTa_2O_6$ (Fig. 3.12). As also investigated in Ba-deficient samples, the region 90-170 cm^{-1} is depicted in Fig. 3. 20 (b) for all Mg-deficient ceramics, showing the splitting of the A_{1g}(Ba) and E_g(Ba) modes together with the extra lines at 112 and 118 cm^{-1} for x = 0.0025 and weak bands at 118 cm^{-1} for $x \geq 0.02$.

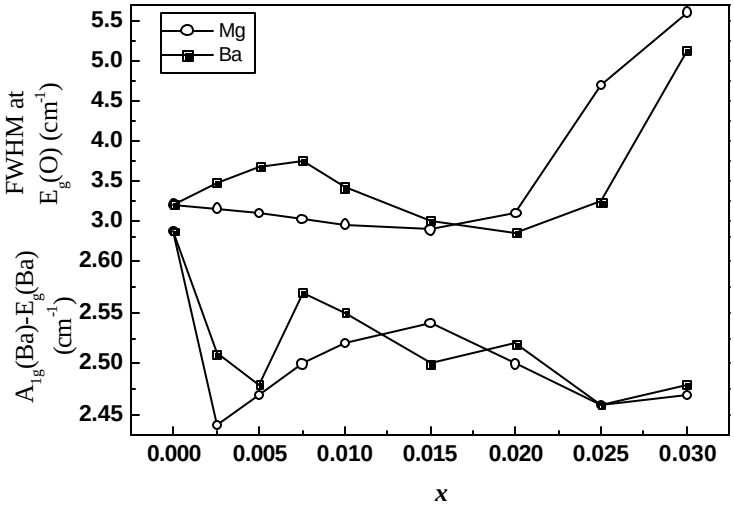

Fig. 3. 21 Full width at half maximum (FWHM) of the E_g(O) mode around 157 cm^{-1} and A_{1g}(Ba)-E_g(Ba) distance (modes around 106 and 103 cm^{-1}), for the BMT materials, as a function of cation deficiency.

The variations of Raman lines and the full width at half-maximum (FWHM) are important fingerprints to study the phonons in samples with different compositions, particularly those related to cation deficiency. These nonstoichiometric samples present ion movements that lead to lattice distortions, which can be observed by Raman spectroscopy. In this work, Raman modes and FWHM for all bands associated with the

normal modes of oxygen and barium were investigated in detail. Vibrations associated to Ta atomic motion are expected to show relatively small changes or to be quasi-invariant. Fig. 3. 21 presents the FWHM for the band at 157 cm^{-1}, E_g(O) mode, which showed a pronounced variation with nonstoichiometry. Also, the difference between the frequencies for the A_{1g}(Ba) and E_g(Ba) modes is plotted for all samples. It was verified that the FWHM increased for $x < 0.0075$ in Ba-deficient ceramics, decreasing in more cation deficient samples. The huge increase for the materials with lower Ba contents ($x = 0.025$ and 0.030) can be related to the presence of a secondary phase ($MgTa_2O_6$). Conversely, Mg-deficient ceramics exhibit a decreasing tendency of FWHM of this mode with nonstoichiometry until $x < 0.015$, followed by increasing due to the secondary phases $Ba_5Ta_4O_{15}$ and $BaTa_2O_6$. Raman splitting observed for the lowest frequency A_{1g}(Ba) and E_g(Ba) bands (around 105 cm^{-1}) presented a curious behavior. Considering only the nonstoichiometric samples, we note that a maximum difference between the frequencies of these bands is observed at $x = 0.0075$ in Ba-deficient samples and at $x = 0.015$ in Mg-deficient materials.

Raman results can be now correlated to the microwave properties of the nonstoichiometric BMT ceramics. The compositions $Ba_{0.9925}(Mg_{0.333}Ta_{0.667})O_3$ and $Ba(Mg_{0.318}Ta_{0.667})O_3$ presented the highest ordering degree and the more pronounced splitting of the (422) and (226) diffraction lines from all samples studied. This result is an indicative of the lattice distortion caused by the cation deficiency. Also, these BMT compounds presented maximum values of dielectric constant, quality factor and τ_f close to zero. Thus, nonstoichiometry showed advantages in terms of the microwave properties. Raman analyses verified evidences of lattice distortion in both Ba and Mg-deficient ceramics. According to Kawashima,[76] the nonstoichiometry lead to an increase in the degree of 1:1 B-site ordering. However, in the present work, the modes associated to the 1:1 ordered phase do not present a significant change. On the other hand, Desu and O'Bryan [75] proposed that Ba replaced the B' cation, causing a distortion, since the ionic radius of Ba^{+2} (1.42 Å) is larger than that of Mg^{+2} (0.72 Å). Such distortions, also verified by X-ray diffraction (Figs. 9 and 10), would change the frequency of the vibrations of the oxygen octahedra, which could explain the variations in Raman spectra observed in Fig. 3. 19 (a) and (b)

3. 5 CONCLUSIONS

- The reaction sequence of BMT synthesized through two different solid state routes (single step & coulombite) are investigated. It was found that the properties of BMT prepared through single step solid state ceramic route (ε_r = 24.4, Q_u x f = 100,500 GHz and τ_f= +8 ppm/^oC) is superior over that made through two step coulombite process (ε_r = 24.1, Q_u xf = 96000 GHz and τ_f= +11.2 ppm/^oC).
- Two chemical synthesizing routes (co-precipitation and citrate gel) were also attempted to make nanostructured BMT. In both cases, the microwave dielectric properties of the samples are very poor in spite of their smaller particle size.
- The complex relationship between stoichiometry and microwave loss quality of complex perovskite $Ba(Mg_{1/3}Ta_{2/3})O_3$ ceramics is investigated. The influence of A and B-site cation non-stoichiometry on the sinterability and microwave dielectric properties of low loss ceramic barium magnesium tantalate is explored by deliberately altering the barium and magnesium ion concentration. The ceramics are synthesized using the mixed oxide route and their microwave dielectric properties are determined. It is found that density increases with slight non-stoichiometry (x=0.015) of Mg^{2+} concentration which is caused by enhanced material transport due to vacancies. The addition of MgO in large excess amount will develop inefficient liquid phase sintering of BMT which deteriorates its densification and microwave dielectric properties. Small deviation from stoichiometry is found to increase density and cation ordering parameter and also improve τ_f and Q factor.
- The improvement of the microwave dielectric properties is more for Ba deficient specimen compared to Mg deficient ones. However large deviations from stoichiometry considerably deteriorate the microwave dielectric properties. The microwave dielectric properties of fully ordered $Ba_{0.9925}(Mg_{0.33}Ta_{0.67})O_3$ is given by e_r = 24.71, τ_f = 1.2 ppm/^oC, $Q_u$xf = 152,580 GHz, which is the best among the non-stoichiometric samples studied in this investigation. The cation ordering between Mg^{2+} and Ta^{5+} ions reaches a maximum for x = 0.015 in $Ba(Mg_{0.33}Ta_{0.67})O_3$ which also shows relatively better microwave dielectric properties [e_r = 25.12, τ_f = 3.3 ppm/^oC and $Q_u$xf = 120,500 GHz] compared to stoichiometric BMT.

- Variations in Raman spectra of nonstoichiometric BMT ceramics were described and correlated to changes in the nature of cation ordering. Although the results showed a highly ordered 1:2 structure (all Raman-active bands are present), normal modes related to lattice distortions appeared for samples with low levels of cation deficiency and/or secondary phases. The increase in the frequency of the E_g(Ba) mode around 106 cm^{-1}, as well as the band width variations observed in the E_g(O) mode around 157 cm^{-1} coincide with the highest *Q* verified for the compositions $Ba_{0.9925}(Mg_{0.333}Ta_{0.667})O_3$ and $Ba(Mg_{0.318}Ta_{0.667})O_3$.

3. 6 REFERENCES

1. W. Wong-Ng, T. Holesinger, G. Riley, and R. Guo (Eds), *Perovskite Oxides for Electronic Energy Conversion, and Energy Efficiency Applications*, Ceramic Transactions,104, American Ceramic Society, Westerville, USA (2000).

2. M.J. Rosseinsky, Materials Network on Perovskite Oxides, http://www.ssci.liv.ac.uk/~perox/ perovskiteintro.html

3. R.M. Hazen, *Sci. Am.*, **258**, 74-81 (1988).

4. B.M. Goldschmidt, Geochemische Verteilungsgesetse der Elementer VII, *Strifter Norske Videnskaps-Akademi Klasse I, Mat. Naturvid. KI.*, 2, Oslo (1926).

5. K. Uchino, *Piezoelectric Actuators and Ultrasonic Motors*, Kluwer Academic Press, Boston (1996)

6. R. Roy, *J. Am. Ceram. Soc*., **37**, 581-84 (1954).

7. F.S. Galasso, J. R. Barrante and Lewis Katz, *J. Am. Chem. Soc*., **83**, 2830-32 (1961).

8. F. S. Galasso, L. Katz and R. Ward, *J. Am. Chem. Soc*., **81**, 820-23 (1959).

9. T. Nagai, M. Sugiyama, M. Sando and K. Niihara, *Jpn. J. Appl. Phys*., **36**, 1146-53 (1997).

10. F. S. Galasso and J. Pyle, *Inorg. Chem*., **2**, 482-84 (1963).

11. F. S. Galasso and J. Pyle, *J. Phys. Chem*., **67**, 1561-62 (1963).

12. F. S. Galasso and J. Pinto, *Nature*, **307**, 567-69 (1965).

13. R. H. Mitchel, *Perovskites, Modern and Ancient*, Almaz Press Inc., Thunder Bay, Ontario, Canada (2002).

14. H. Vincent, C. Perrier, P. L'Heritier, M. Labeyrier, *Mater. Res. Bull.*, **28**, 951-58 (1993).

15. A. J. Jacobson, B. M. Collins and B. E. F. Fender, *Acta, Cryst*., **B32**, 1083-86 (1993).

16. B. P. Burton, *Phys. Rev. B*, **58**, 6087-91 (1999).

17. Z-R. Liu, J-S. Liu, B-L. Su and X-W. Zhang, *Phys. Rev. B*, **61,** 11918-21 (2000).

18. M. U. Cohen, *Rev. Sci. Instrum*., **6**, 68-73 (1963).

19. K. Matsumoto, T. Hiuga, K. Takada and H. Ichimura, *Proc. Sixth IEEE International Symposium on Application of Ferroelectrics*, Institute of Electrical and Electronic Engineers, Bethlehem, PA, (1986).

20. K.-J. Hoon, K.-Y. Kim and H. Kim, *Jpn. J. Appl. Phys*., **35,** 3947-53 (1996).

21. S. Kawashima, M. Nishida, I. Ueda, H. Ouchi and S. Hayakawa, *Proc. of the 1st meeting on Ferroelectric Mater. and their Applications*, p. 293-96, Keihin Printing Co. Ltd., Kyoto, (1977).

22. S. Nomura, K. Toyama and K. Kaneta, *Jpn. J. Appl. Phys*., **21**, L 624-26 (1982).

23. S. Nomura and Y. Konishi, *Low Loss microwave dielectric (tantalate) material*. US 4, **487**, 842-50 (1984).

24. M. Sugiyama, T. Inuzuka and H. Kubo, *Ceram. Trans*., **15**, 153-66 (1990).

25. K. Wakino and H. Tamura, *Ceram. Trans*., **15**, 305-14 (1990).

26. T. Tsnooka, *TFCC Rev*., **7**, 229-33 (1997).

27. E. S. Kim, K. H. Jo and K.H. Yoon, *Inter. Ceram. Monogr*., **1**, 486-91 (1994).

28. K. Matsumoto and T. Hiuga, *Seramikkusu*, **22**, 676-82 (1987).

29. K. Kageyama, *Funtai Oyobi Funmatsu Yakin*, **40**, 614-17 (1993).

30. S. Komeneni, I. R. Abothu, A. V. P. Rao, *J. Sol-Gel Sci. Technol*., **15**, 263-70 (1999).

31. A. Dias, V. T. L. Buono, V. S. T. Ciminelli, R. L. Moreira, *J. Eur. Ceram. Soc*., **19**, 1027-31 (1999).

32. H. M. Shirey, *Low temperature Synthesis of the Microwave Dielectric Material, Barium Magnesium Tantalate (BMT),* M.S. Thesis, University of Pittsburg (2003).

33. C-M. Cheng, Y-T. Hsieh and C-F. Yang, *Ceram. Inter*., **28**, 255-60 (2002).

34. K. P. Surendran and M. T. Sebastian, *Proc. National Symposium on Advances in Microwave and Lightwaves,* October 13-14, University of Delhi South Campus, New Delhi (2003).

35. L-C Tien , C-C Chou and D-S Tsai, *Ceram. Inter*., **26**, 57-62 (2000).

36. E-S. Kim, J-B. Kim and K-H. Jo, *Ceram. Trans*., **32**, 231-40 (1993).

37. K. H. Yoon, D. P. King and E. S. Kim, *J. Am. Ceram. Soc*., **77**, 1062-66 (1994).

38. W-A. Lan, M-H. Liang, C-T. Hu, K-S Liu and I-N.Lin, *Mater. Chem.Phys.*, **79**, 266-69 (2003)

39. C. H. Choi, C.H. Choi, S. Nahm. Y.W. Song, *J. Kor. Phys. Soc*, **35**, S410-14 (1999).

40. M-H. Liang, C-T. Hu; C-G. Chiou, H-Y Chang; I-N. Lin, *Ferroelectrics*, **231**, 691-96 (1999).

41. C-L. Huang, K-H. Chiang, S-C Chuang, *Mater. Res. Bull.*, (in press) (2004).

42. L. Chai, M. A. Akbas and P. K. Davies, *Proc. Solid State Chemistry of Inorganic Materials*, p. 443-48, 2-5 December, Boston, (1996).

43. J. Youn, K. S. Hong, and H. Kim, J. Mater. Res., **12**, 589-92 (1997).

44. S.-H. Ra and P. P. Phule, *J. Mater. Res*., **14**, 4259-65 (1999).

45. H. Von, Wartenburg and E. Prophet, *Phase Diagrams for Ceramists* 1975 Supplement, Edited by E.M. Levin, C.R. Robbins, H. F. McMurdie and M. K. Reser, The American Ceramic Society, Ohio, Fig.274, p. 113 (1964).

46. B. W. King, J. Schultz and E. Prophet, *Phase Diagrams for Ceramists* 1975 Supplement, Edited by E. M. Levin, C. R. Robbins, H. F. McMurdie and M. K. Reser, The American Ceramic Society, Ohio, Fig. 273, p.113 (1964).

47. J. J. L. Andre, *Phase Diagrams for Ceramists*, 1975 Supplement, Edited by E. M. Levin, C. R. Robbins, H. F. McMurdie and M. K. Reser, The American Ceramic Society, Ohio, Fig. 205, p. 96, (1964).

48. M. Zhao, J. Bian, Y. Wang, Y. Yao, W. Wu and Z. Yin, *Ferroelectrics*, **230**, 145-50 (1999).

49. M. Li, *Ferroelectrics*, **195**, 87-91 (1997).

50. J-W. Choi, S. Kucheiko, S-J. Yoon, H-J. Kim and K. H. Yoon, *J. Am, Ceram. Soc*., **84**, 2570-72 (2001).

51. M-H. Liang, C-G. Chiou, Y-N. Tsai, C-T. Hu and I. N. Lin, *Ferroelectrics*, **238**, 81-89 (2000).

52. K. P. Surendran, Manoj Raama Varma, P. Mohanan and M. T. Sebastian, *Proc. National Conference on Recent Advances in Materials Processing (RAMP-2001)* Sept. 7-8, Annamalainagar, India (2001).

53. D. M. Moore and R.C. Reynolds Jr., *X-Ray Diffraction and the Identification and Analysis of Clay Minerals.* Oxford University Press, New York (1989).

54. J-A. Lee, J-J. Kim, H-Y. Lee, T-H. Kim, T-G. Choy, *J. Kor. Ceram. Soc.*, **31**, 1561-69 (1994).

55. Y. Fang, A. Su, S. Ouyang and J. J. Oh, *J. Eur. Ceram. Soc*., **21**, 2745-50 (2001).

56. S. J. Penn, N. McN Alford, A. Templeton, X. Wang, M. Xu, M. Reece and K. Schrapel, *J. Am. Ceram. Soc*., **80**, 1885-90 (1997).

57. H. Schmalzried, *Sold State Reactions*, Academic Press, New York, (1974)

58. P. Nanni, M. Viviani and V. Buscaglia, *Synthesis of Dielectric Ceramic Materials, Handbook of Low and High dielectric Constant and their Applications,* Ed. H.S. Nalwa, Vol.1, Materials and Processing, Academic Press, New York, (1999).

59. M. Thirumal, P. Jain & A. K. Ganguli, *Mater. Chem. Phys.,* **70**, 7-10 (2001).

60. D. W. Johnson Jr., *Am. Ceram. Soc. Bull*., **6**4, 1597-1603 (1985).

61. K. A. Evans and N. Brown, *Speciality Inorganic Chemicals*, Ed. R. Thompson, Royal Society of Chemistry, London, pp.164-95 (1981).

62. K. Kakegawa, T. Wakabayashi and Y. Sasaki, *J. Am. Ceram. Soc*., **69**, C 82-C 83 (1986).

63. Y. Chuanren, Q. Guangyu, Z. Dayu, Y. Wennan, G. Fujun, *J. Chinese Ceram. Soc*., **27**, 143-49 (1999).

64. S. Katayama, I. Yoshinaga, N. Yamada and T. Negas, *J. Am. Ceram. Soc*., **79**, 2059-64 (1988).

65. O. Renoult, J-P. Boilot, F. Chaput, R. Papiernik, L.G. Hubert-Pfalzgraf and M. Lejeune, *Ceramics, Today-Ceramics Tomorrow*, (Ed.)P. Vincentini, Elsevier Science Publishers, Amsterdam (1991).

66. Y-C. Lee, M-H. Liang, C-T. Hu and I-N. Lin, *J. Eur. Ceram. Soc*.,**21**,755-58 (2001).

67. I. S. Abouthu, S. Komeneni, D. S. Paik and H. S. Jentsch, *J. Electroceram*., **3**, 65-

71 (1999).

68. D. Hennings and W. Mayer, *J. Sol. St. Chem*., **26**, 329-38 (1978).

69. Z. Haijun, J. Xiaolin, Y. Yongjie, L. Zhanjie, Y. Daoyuan and L. Zhenzhen, *Mater. Res. Bull.,* **39**, 839-50 (2004).

70. J. Bian, M. Zhao and Z. Yin, *Mater. Lett*., **34**, 275-79 (1998)

71. I. Mclaren and C.B. Ponton, *J. Mat. Sci*., **33**, 17-22 (1998).

72. F. Gu, Y. Shen and X. Liang, *Mater. Sci. Engg.B*, **99**, 453-56 (2003).

73. D. Shima and S. M. Haile, *Solid. St. Ion.*, **97**, 443-55 (1997).

74. K. Mizumoto and S. Hayashi, *Solid. St. Ion*., **116**, 263-69 (1999).

75. S. B. Desu and H. M. O'Bryan, *J. Am. Ceram. Soc.*, **68**, 546-51, (1985).

76. S. Kawashima, *Am. Ceram. Soc. Bull*., **72**, 120-26 (1993).

77. S. J. Choi, S. Nahm, M. H. Kim and Byun, *J. Kor. Ceram. Soc*., **2**, 242-45 (1996).

78. K.S. Hong, I. T. Kim, and S.J. Yoon, *J. Mater. Sci*., **30**, 514-21 (1995).

79. J. H. Paik, S. Nahm, J. D, Bylin, M. H. Kim and H. J. Lee, *J. Mat. Sci. Lett*., **17**, 1777-80 (1998).

80. C. Yang, D. Zhou, C. Huang and G. Qin, *J. Adv. Mater*., **31**, 8-11 (1998).

81. K. Tochi, *J. Ceram. Soc. Japan*, **100**, 1464-66 (1992).

82. I. Amato and A. Negro, *J. Less Com. Met.*, **20**, 37-48 (1970).

83. K. Kusumoto and T. Sekiya, *Mater. Res. Bull.*, **33**, 1367-75 (1998).

84. Y. Fang, A. Hu, S. Ouyang, and J. J. Oh, *J. Eur. Ceram. Soc*., **21**, 2745–50 (2001).

85. C.-H. Lu and C.-C. Tsai, *J. Mater. Res*., **5**, 1219-27 (1996).

86. J. B. Byun, S. Nahm, D. W. Lee, Y. S. Kim, M. H. Kim and H. J. Lee, *Proc. 9th International Meeting on Ferroelectricity.* 24-29, 1997, Seoul, Korea (1997).

87. J-A. Lee, J-J. Kim, H-Y. Lee, T-H. Kim, T-G. Choy, *J. Kor. Ceram. Soc*., **31**, 1299-1306 (1994).

88. J. K. Burdett and J. F. Mitchell, *Prog. Solid State Chem*., **23**, 131-70 (1995).

89. C-H. Lu and D-P. Chang, *Mater. Sci. Engg. B*, **64**, 195-98 (1999).

90. R. D. Shannon, *Acta Cryst*., **A32**, 751-67 (1976).

91. J-A. Lee, J-J. Kim, H-Y. Lee, T-H. Kim and T-G. Choy, *J. Kor. Ceram. Soc.*, **31**, 1561-69 (1994).

92. Z. Yang and Y.S. Lin, *Solid St. Ionics*, **150**, 245–54 (2002).

93. M-H. Liang, C-T. Hu, C-G. Chiou, Y-N. Tsai and I-N. Lin, *Jpn. J. Appl. Phys.*, **38**, 5621-24 (1999).

94. V. Tolmer and G. Desgardin, *J. Am. Ceram. Soc*., **80**, 1981–91 (1997).

95. A. M. Abakumov, G. V. Tendeloo, A. A. Scheglov, R. V. Shpanchenko and E.V. Antipov, *J. Solid State Chem.*, **125**, 102–07 (1996).

96. P. K. Davies, A. Borisevich and M. Thirumal, *J. Eur. Ceram. Soc.* **23**, 2461-66 (2003).

97. M. Bieringer, S. M. Moussa, L. D. Noailles, A. Burrows, C. J. Kiely, M. J. Rosseinsky and R. M. Ibberson, *Chem. Mater*., **15**, 586-97(2003)

98. H. J. Youn, H. Y. Kim and H. Kim, *Jpn. J. Appl. Phy*s., **35**, 3947-53 (1996).

99. E. S. Kim and K. H. Yoon, *Ferroelectrics*, **133**, 187-92 (1992).

100. S-H. Kang, H-I. Yoo, and H. M. Park, *J. Mater. Res*., **14**, 4070-74 (1999).

101. O. Bidault, E. Husson, A.Morell, *J. Appl. Phys.*, **82**, 5674-79 (1997).

102. S. Qu, F. Gao, Z. Yang, J. Xue and C. Tian, *Ceram. Inter.*, **30**, 307- 10 (2004).

103. G. Rong, N. Newman, B. Shaw and D. Cronin, *J. Mater. Res.*, **14**, 4011-19 (1999).

104. R. L Moreira, F. M. Matinaga and A. Dias, *Appl. Phys. Lett*., **78** 428-32 (2001).

105. I. G. Siny, R. Tao, R.S. Katiyar, R. Guo and A.S. Bhalla. *J. Phys. Chem*. *Solids*, **59**, 181-95 (1998).

CHAPTER 4

EFFCECT OF DOPANTS IN $Ba(Mg_{1/3}Ta_{2/3})O_3$ CERAMICS

This Chapter deals with the doping aspects of BMT. The effect of dopants such as $MnCO_3$, NiO, ZnO, Co_3O_4, Al_2O_3, Ga_2O_3, Fe_2O_3, In_2O_3, Nd_2O_3, Bi_2O_3, TiO_2, SnO_2, ZrO_2, HfO_2, CeO_2, V_2O_5, Sb_2O_3, Nb_2O_5, WO_3 and MoO_3 with different oxidation states and ionic radii on the densification, structural ordering and microwave dielectric properties of $Ba(Mg_{1/3}Ta_{2/3})O_3$ is investigated. It is found that dopants such as Sb_2O_5, $MnCO_3$, ZrO_2, WO_3 and ZnO improve the microwave dielectric properties of BMT. A correlation between the microwave dielectric properties of BMT and ionic radii of the dopant has been established. The variation of the dielectric properties of pure and doped BMT at cryogenic temperatures are also discussed.

4. 1 INTRODUCTION

Dielectric resonator has achieved an important position, as the key element in microwave integrated circuits and in microwave filters. As it has been outlined in Chapter 3, $Ba(Mg_{1/3}Ta_{2/3})O_3$ is one of the most extensively studied $Ba(B'_{1/3}B''_{2/3})O_3$-type complex perovskites and has the highest quality factor among the microwave dielectric ceramics. The discovery[1] of this low loss complex perovskite has turned out to be a breakthrough in the research on microwave dielectrics, as until now there is no other dielectric resonator material, which can dwarf BMT in dielectric properties. However, the sintering conditions for obtaining high performance BMT ceramic is very stringent because of its poor sinterability, which is thought to be due to the formation of some special satellite secondary phases in the calcined powders. Usually BMT is made by solid state reaction route, but the sintering temperature is often higher than 1600 °C. Solution chemistry offers alternative approaches like sol-gel technique for synthesis of BMT powders. But the chemical synthesis of BMT was not the most appropriate method for industrial production due to the complexity of the procedures involved, high cost of production and comparatively poor microwave dielectric properties[2] (see Chapter 3, Section 3.3.2).

The first reported study on the effect of dopants on $Ba(Mg_{1/3}Ta_{2/3})O_3$ was made by Nomura[3] who found that doping with Mn (1 mole %) not only promotes sinterability by lowering the sintering temperature but also increases the unloaded Q value appreciably. Later on Matsumoto [4] studied doping effects of SnO_2 in BMT which too yielded excellent microwave dielectric properties. In that report it has been revealed that on addition of 10 and 15 mole % of $BaSnO_3$ into $Ba(Mg_{1/3}Ta_{2/3})O_3$ ceramics, the Q value reached as high as 33000 at 10 GHz and the t_f approached negative values. In another report [5]Yoon et al. added hexavalent WO_3 in the form of $BaWO_4$ and found that addition of barium tungstate up to 5 mole % increased the lattice constant ratio (*c/a*), ordering parameter, density and dielectric quality factor due to the increase in the substitution of Ta^{5+} by W^{6+} from the melted $BaWO_4$ at above 1430^{o}C. The effect of nickel on the microwave dielectric properties of BMT has also been studied [6] and found that the dielectric properties such as e_r and t_f were slightly increased with the substitution of Ni^{2+} ion at Mg^{2+} site in $Ba(Mg_{1/3}Ta_{2/3})O_3$ but Q decreased. It is well understood [59] that NiO and MgO form ideal solid solutions due to their matching ionic radii (0.69 for Ni and 0.72 for Mg Å

respectively) of cations. But doping of NiO in BMT complex perovskites damaged their dielectric properties which resulted in the appearance of needle shaped grains of magnesium and tantalum rich phases [7, 8]. The effects of low melting additive [9] such as NaF reduced the processing temperature of BMT but the formation of additional phases such as Na_3TaO_4 should be suppressed to achieve high Q stable phase. Chai et al. [10, 11] reported that with the addition of tetravalent ions, the 1: 2 ordering of B-site cation in complex perovskite $Ba(Mg_{1/3}Ta_{2/3})O_3$ ceramics was transformed into 1:1 ordering with the partial substitution of Zr^{4+}, Ce^{4+} and Sn^{4+} to the $(Mg_{1/3}Ta_{2/3})^{4+}$ site but no such ordering transformation was observed with Ti^{4+} addition. However, this report provided no information as to how the microwave dielectric properties of BMT vary with B-site substitution. The effect of Ga_2O_3 on the physical and microwave dielectric properties of BMT was investigated by Shirey[12] in which the author reported that in spite of a reduction in sintering temperature, the unloaded quality factor deteriorated with Ga addition. The densification and quality factor of low loss BMT was also reported [13] to be improved with the addition of Y_2O_3. A recent investigation[14] suggested that the addition of pentavalent impurity like V_2O_5 did not significantly affected the temperature coefficient of resonant frequency but it improved the microwave quality factor consequent to the substitution of V^{5+} in the Ta^{5+} site.

Hence from a brief literature survey made above, it is clear that even though this ceramic possess the highest Q factor in literature, a comprehensive effort is needed to correlate the complex relationship between the structure and low loss nature of $Ba(Mg_{1/3}Ta_{2/3})O_3$ which is a challenging problems in the science of dielectric materials. A number of parameters starting from the synthesizing stage, up to the final high temperature densification have to be controlled to achieve high Q phase in BMT ceramics [15, 16]. The origin and purity of the initial raw materials also have a considerable influence on the sinterability. Moreover the particle size of the starting materials, sintering temperature, sintering duration and annealing etc. make substantial influence on the long range cation ordering and microwave quality factor of BMT [17] when it is prepared through solid state reaction technique. Though many research groups have studied the effect of various additives on the microwave dielectric properties and sinterability of BMT, the doping was performed under different conditions: sometimes before

calcination and sometimes after. Hence the reported Q values show a wide scatter, which may either be due to the errors in various measuring techniques or due to variations in the synthesizing conditions. To overcome this difficulty, we carried out a comprehensive investigation in which aliovalent and isovalent additives are added to calcined BMT under similar conditions in a systematic way. The objective of this study is to investigate the effect of various dopants of different ionic radii and valency on the densification, sinterability, dielectric properties in BMT. The complex relationship between dielectric loss and the order-disorder transformation on the B-site cations in BMT ceramic materials is also presented in this chapter. The optimization of the synthesizing conditions were done prior to the doping.

4. 2 SYNTHESIS AND CHARACTERIZATION

The $Ba(Mg_{1/3}Ta_{2/3})O_3$ precursor was prepared through the conventional solid state ceramic technique as described in Chapter. 2. 1, Sections 2. 1. 2. 1 to 2. 1. 2. 7. The calcination temperature was done at 1200^{o}C for 10 hours with intermediate grinding. The dopants added to BMT were categorized based on their stable valency a high temperatures. The calcined BMT precursor was divided into several batches and different mole % of divalent (MnCO3, NiO, ZnO and Co_3O_4), trivalent (Al_2O_3, Ga_2O_3, Fe_2O_3, In_2O_3, Nd_2O_3 and Bi_2O_3), tetravalent (TiO_2, SnO_2, ZrO_2, $CeO_{2-\delta}$ and HfO_2), pentavalent (V_2O_5, Sb_2O_3 and Nb_2O_5) and hexavalent (WO_3 and MoO_3) dopants were added it. The sintering temperature was optimized at 1625 ^{o}C. The well sintered samples were annealed at 1450 ^{o}C for 40 hours to relieve the lattice strain and to enhance cation ordering mechanism. The powdered samples were used for analyzing the X-ray diffraction patterns using CuK_α radiation (Philips X-Ray Diffractometer). The lattice parameters were determined using the least mean square technique. The degree of ordering in BMT is calculated by comparing the relative density of [*100*] super lattice diffraction peak to that of the [*110, 102*] diffraction as described in Chapter 3, Section 3.2.3. A few typical sintered samples were thermally etched for 30 minutes at a temperature of about 1575 ^{o}C and the surface morphology was studied using a scanning electron microscope Hitachi SEM Model No. S-4300.

The dielectric properties ε_r and τ_f of the materials were measured in the microwave frequency range using resonance technique [18, 19, 20] as described Chapter 2, Sections 2.2.2 to 2.2.5.

4. 3 RESULTS AND DISCUSSION

4. 3. 1 Effect of Dopants on the Structure of BMT

Wang et al. theoretically studied [21] effect of A-site and B-site doping in complex perovskites. They postulated that in ionic systems like perovskites, the cation ordering related structural stability is mainly monitored by electrostatic Madelung energy in addition to the minor contributions of other energies like covalent and elastic strain energies. Accordingly dopants of any valency substituted on the A-site of $A(B'_{1/3}B''_{2/3})O_3$ do not promote 1:2 ordering while an acceptor dopant such as Na^+ on the A site leads to 1:1 ordering. The 1:1 ordering of B' and B" ions in a face centered superlattice like BMT, generates space charge that dominate the kinetics of the ordering process and inhibit the development of ordering process [22, 23, 24]. Chen et al.[25] observed that by introducing Na^+ on the A-site of $Pb(Mg_{1/3}Nb_{2/3})O_3$ the above said charge effect is increased and cation ordering is suppressed. The problem of A-site substitution of 1:2 ordered perovskites with alkali metals have been studied in Ba-based microwave dielectrics also. Lee[26] et al. found that a reduction in degree of cation ordering was observed when K_2O was doped to $Ba(Zn_{1/3}Ta_{2/3})O_3$ (BZT) whose cation partially substitute the site of Ba^{2+} ion to form composition $K_xBa_{1-x}(Zn_{(1-x)/3}Ta_{(2+x)3})O_3$. In addition to that, Dupont et al.[27] confirmed that a 1:1 mixture of Na^+ and La^{3+} in A site of BMT is apparently effective in destabilizing the 1:2 layering of the B-site cation and favors a 1:1 ordering due to high charge imbalance between A' and A" cations. Yet another significant observation was made by Wu et al.[28] who found the quality factor of BMT reduced to alarmingly low values and densification was hindered when NaF was added to BMT. The recent research trends points out that presence of alkali metals in low loss DR have been found to be detrimental to their microwave dielectric properties[29]. So in this investigation, we deliberately avoided the doping of monovalent alkali metals into $Ba(Mg_{1/3}Ta_{2/3})O_3$.

Table 4. 1 Impurity content in starting materials for the synthesis of BMT (*all results are in ppm*)

Impurity	$BaCO_3$	$(MgCO_3)_4.Mg(OH)_2.5H_2O$	Ta_2O_5
Sr	500	20	-
Ca	50	3,900	-
Fe	50	100	7
Ni	-	-	4
Cr	-	-	5
Ti	20	20	< 10
Nb	-	-	275
Pb	100	< 10	-
Na	< 100	< 40	-
K	< 20	< 5	-

Before studying the effect of impurities on $Ba(Mg_{1/3}Ta_{2/3})O_3$ ceramics, it is imperative to analyze the impurity level of the starting materials for its synthesis. The purity level of the main raw materials such as $BaCO_3$, $(MgCO_3)_4.Mg(OH)_2.5H_2O$ and Ta_2O_5 are analysed using Inductively Couple Plasma (ICP) Optical Emission Spectra (Perkin Elmer) which is given in Table 4.1. It must be noted that the impurity level of $(MgCO_3)_4$. $Mg(OH)_2.5H_2O$ was higher than the other two (i.e. $BaCO_3$ and Ta_2O_5) in which a substantial amount of $CaCO_3$ was present.

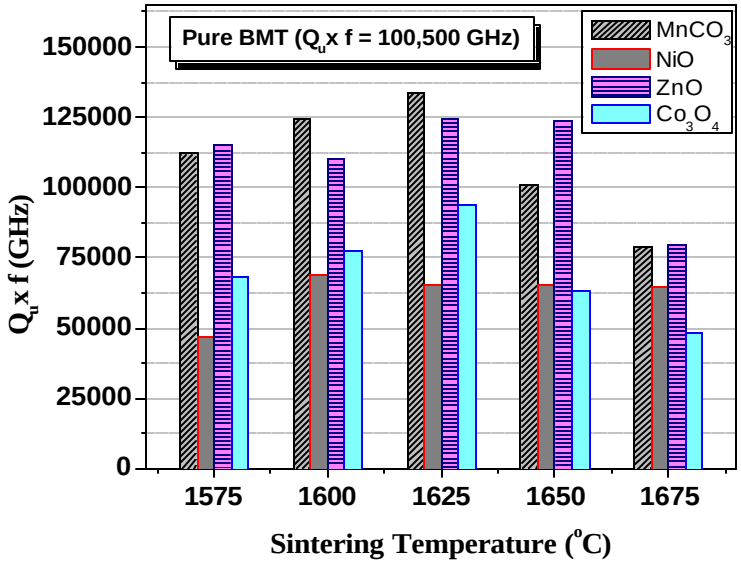

Fig. 4. 1 Variation of the unloaded Q factor of BMT doped with 0.5 mole % divalent additives such as $MnCO_3$, NiO, ZnO and Co_3O_4, with sintering temperature

The dopants used in this investigation are classified as a function of their stable oxidation states as divalent, trivalent, tetravalent, pentavalent and hexavalent. Aliovalency and comparable ionic size with B-site cations are taken as the basic criterion for selecting dopants in this study. It should be noted that Co_3O_4 which is a mixture of major CoO and Co_2O_3 has been categorized as a divalent metal oxide. On the other hand CeO_2 which stores and releases oxygen via the redox shift between Ce^{+4} and Ce^{+3} under oxidizing and reducing conditions respectively, undergoes a partial phase transition consequent to the reduction[30] of Ce^{4+} to Ce^{3+} in the range 573-873 K. However cerium oxide has been considered as a tetravalent impurity with chemical formula $CeO_{2-\delta}$ in this study. Sb_2O_3 is regarded as a pentavalent impurity even though it is trivalent at room temperature.

The processing conditions of doped $Ba(Mg_{1/3}Ta_{2/3})O_3$ dielectrics are optimized for best dielectric properties at microwave frequency region. Fig. 4. 1 represents a plot of unloaded quality factor of BMT samples doped with divalent metal oxides such as MnCO3, NiO, ZnO and Co_3O_4. The doped samples are sintered at different temperatures in the range 1575-1675^oC for 4 hours and annealed at 1450^oC for 40 hours. It must be remembered that for pure BMT, the best sintering temperature was 1650^oC for 4 hours. On the other hand, the measured microwave quality factor is maximum when the uniaxially pressed compacts are sintered at 1625^oC except for NiO which shows slightly better properties at 1600 ^oC. Thus it is evident that doping with suitable metal oxides decreases the processing temperature of ceramics. For the sake of comparison we report the dielectric properties of samples sintered at 1625 ^oC. At high temperatures of sintering above 1625 ^oC, the dielectric properties deteriorate mainly due to exaggerated grain growth (see Fig. 4. 1).

The X-ray diffractograms of BMT doped with 5 mole % of different additives is given in Fig 4. 2. Fig. 4. 2 (A) represent the XRD patters of the unannealed ceramic which was sintered at 1625^oC and Fig. 4. 2 (B) for a similar sample annealed at 1450 ^oC for 40 hours. The superstructure structure reflections are clearly seen Fig. 4. 2 (B). This observation is attributed to the existence of small 1:2 ordering domains which grow at higher temperatures on annealing. During the process of cation ordering, the unit cell expends and resulting in the formation of weaker maxima occur at $\{h \pm ?\ , k \pm ?\ , l \pm ?\ \}$ in

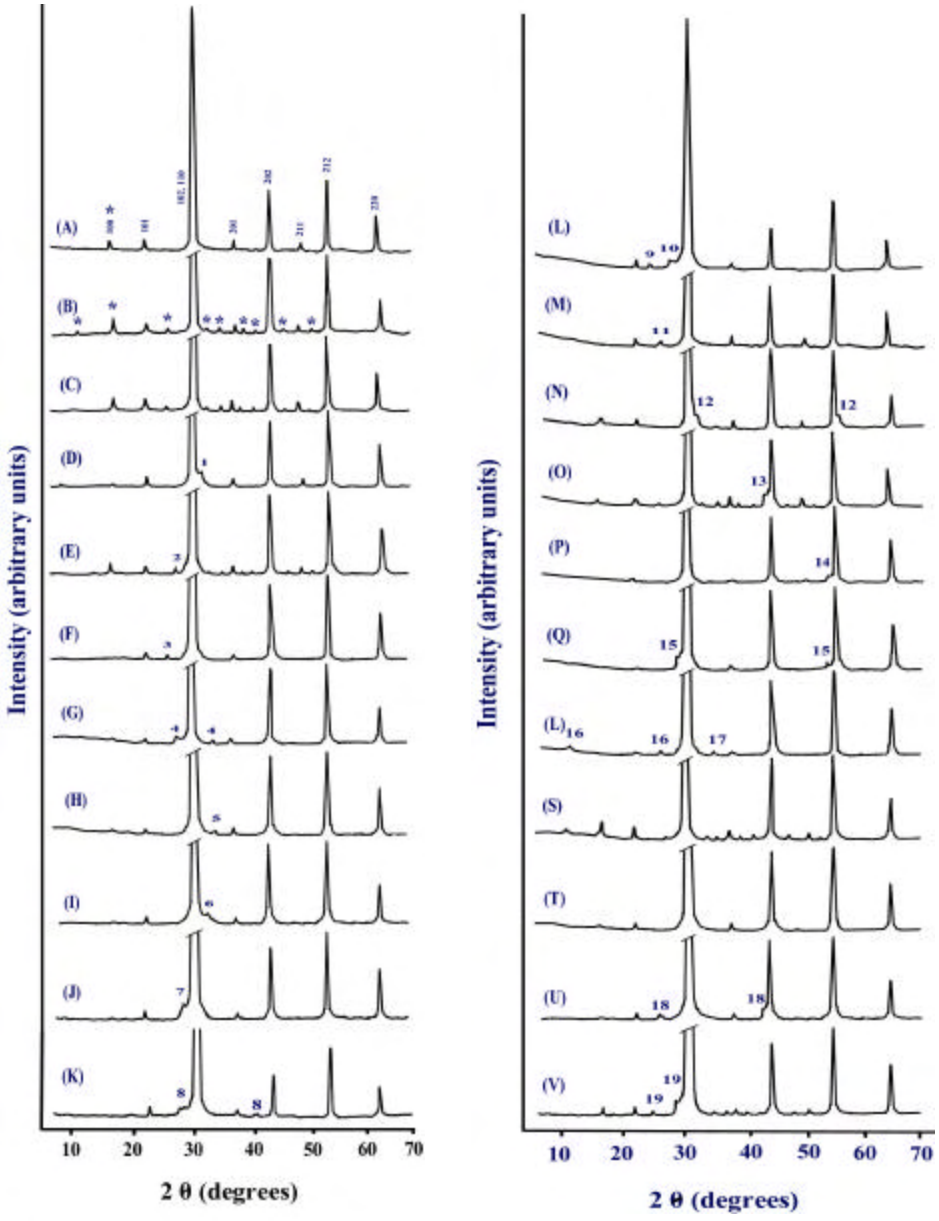

Fig. 4. 2 Powder Diffraction pattern of BMT doped with 5 mole % of the additives: (A) Pure and Unannealed, (B) Pure and Annealed, (C) BMT doped with $MnCO_3$, (D) NiO, (E) ZnO, (F) Co_3O_4, (G) Al_2O_3, (I) Fe_2O_3, (J) In_2O_3, (K) Nd_2O_3, (L) Bi_2O_3, (M) CeO_2, (N) TiO_2, (O) SnO_2, (P) ZrO_2, (Q) HfO_2, (R) V_2O_5, (S) Sb_2O_3, (T) Nb_2O_5, (U) WO_3, (V) MoO_3. 1 stands for $Ba_3NiTa_2O_9$, 2 for $Ba_4Ta_2O_9$, 3 for $BaCoO_{2.93}$, 4 for $Ba_{10}Al_2O_{13}$, 5 for $BaGa_{12}O_{19}$, 6 for $Fe_4Ta_2O_9$, 7 for $InTaO_4$, 8 for Nd_2O_3, 9 for Bi_2O_3, 10 for $BaBiO_3$, 11 for $BaCeO_3$, 12 for $BaTiO_3$, 13 for $BaSnO_3$, 14 for Ba_2HfO_4, 15 for $BaZrO_3$, 16 for BaV_3O_8, 17 for $VTaO_4$, 18 for $BaWO_4$, 19 for $BaMoO_4$. * represent superstructural reflections

addition to the strong intensity maxima at allowed {*h*, *k*, *l*} position. When BMT is doped with $MnCO_3$ no traces of additional phases are observed in the entire range of doped BMT with comparatively higher degree of cation ordering (0.802) which is reflected as

the appearance of superstructure reflections (see Fig. 4.2 (C)). The addition of divalent NiO resulted in the formation of additional phases with higher concentration (5 mole %). Here the additional line was formed at 2T = 31.15 degrees, which may be either $Ba_3Ni_3O_6$ (JCPDS File Card No. 4-684) with a strong line at 2T = 31.27 or $Ba_3NiTa_2O_9$ at 2T = 31.05 (JCPDS File Card No. 18-181) (see Fig. 4.2 (D)). The doping of ZnO does not form any additional phases with it (Fig. 4. 2 (E)) may be due to the volatisation of ZnO [31] but for higher percentages of the dopant, satellite phases of $Ba_4Ta_2O_9$ appears as seen from the X-ray diffractogram. This may be attributed to the volatisation of MgO at elevated temperatures which is consistent with the observation[32] made before. The addition of Co_3O_4 does not damage its ordering up to 2 mole % but at 5 mole % a slight percentage of $BaCoO_{2.93}$ (JCPDS File Card No. 26-144) is appeared in the XRD pattern (Fig. 4.6 (F)).

The effect of addition of trivalent impurities such as Al, Ga, Fe, In, Nd and Bi on the sintered phase structure is given in Figs. 4.2 (G) to 4.2 (L) for the highest concentration (5 mole %). Owing to the limitations of XRD as a comprehensive tool for structural analysis, the possibility of trivalent ion substituting at any of the B-site in BMT could not be explored, but it is expected that bigger trivalent dopant ions like Nd and Bi can go into the A-site to form a structure $Ba_{1-3x}(Nd/Bi)_{2x}(Mg_{1/3}Ta_{2/3})O_3$. The formation of additional phases may be probably the reason behind the poor ordering of B-site cations in BMT doped with trivalent ions. The presence of unreacted Al_2O_3 (JCPDS File Card No. 26-31) is detected in samples doped with 1 mole % and 2 mole % of the Al_2O_3 additive. But as the concentration of alumina increases it reacts with A- site cation of BMT and the additional phase like $Ba_{10}Al_2O_{13}$ (JCPDS File Card No. 28-121) are formed during sintering (Fig. 4.2 (G)). The Ga doping in $Ba(Zn_{1/3}Ta_{2/3})O_3$ has been proved to be beneficial [33, 34] due to the enhanced cation ordering on annealing below its order–disorder transition temperature which allows long range co-operative distortion of the TaO_6 octahedra, resulting in the correct coordination environment for a d^0 transition metal [37]. But in complex perovskite $Ba(Mg_{1/3}Ta_{2/3})O_3$ ceramics, the presence of Ga did not aid in improving the microwave dielectric properties. On the other hand the presence of $BaGa_{12}O_{19}$ (JCPDS File Card No. 26-147) is detected in the XRD spectrum of the sintered samples (Fig. 4. 2 (H)). The presence Fe_2O_3 has been proved to be beneficial to

some low loss ceramics like Titania[35] as an excellent oxidizer but they could not impart a commendable effect in BMT ceramics. Instead a higher concentration of Fe_2O_3 doping results in a reaction of the dopant with the matrix forming $Fe_4Ta_2O_9$ (JCPDS File Card No. 19-633) as seen from Fig. 4. 2 (I). Doping with Indium oxide also damages the cation ordering in BMT ceramics consequent to the formation of additional phase $InTaO_4$ (JCPDS File Card No. 25-391) (see Fig. 4. 2 (J)). Of the trivalent additives we have used in this investigation, the only additive which have the ionic radii close to 1 ? are Nd^{3+} (0.983 ?) and Bi_2O_3 (1.03 ?) which are likely to substitute the Ba site in $Ba(Mg_{1/3}Ta_{2/3})O_3$. This effect has resulted in the modification of the lattice parameters (see Table 4.3). The XRD pattern suggests (Fig. 4. 2 (K)) that presence of unreacted Nd_2O_3 (JCPDS File Card No. 6-408) and Nd_3TaO_7 (JCPDS File Card No. 38-1414) are visible at 5 mole percentage of the doping. In a previous report [36], a bigger trivalent ion like La^{3+}doped in BMT results in the formation of a 1:1 ordered structure coexisting with 1:2 ordered phase. It is evident that addition of trivalent Bi_2O_3 severely damages the cation ordering arrangement of BMT on higher concentration of the dopant as there are hardly any superstructure reflections in the XRD pattern (Fig. 4. 2 (L)). In addition to that, formation of impurity phases like $BaBiO_3$ (JCPDS File Card No. 35-1020) has been present in the XRD pattern. It is worthwhile to note that presence of minor amount of 1:1 ordered peak has been detected in samples doped with bigger trivalent cations such as Nd and Bi between 2T = 18-19 degrees which may be the superstructure line ½(111)*. But on doping with 5 mole % of the additives, the 1:2 reflections (100)* as well as ½(111)* vanishes (see Fig. 4. 2).

The effect of small amount of tetravalent impurities like Ti, Sn, Zr and Ce on the order-disorder phase transformation of $Ba(Mg_{1/3}Ta_{2/3})O_3$ have been investigated before[37]. In this report the authors pointed out that bigger tetravalent cations like Zr^{4+} or Sn^{4+} induces a 1:1 ordering in the crystal lattice while undersized cations like Ti^{4+} promotes a disordered structure. The cerium oxide which bears multiple oxidation states of 3 and 4, which can form possible configurations $Ba[(Mg_{1-x}Ce_x)_{1/3}Ta_{2/3}]O_{3-d}$ or $Ba(Mg_{1/3}Ta_{2/3})_{1-x}Ce_xO_3$ if it reacts with the BMT matrix. A recent investigation by [38] Santha et al. proved that the oxidation and reduction of CeO_2 plays a great role in controlling the microwave dielectric loss aspects that ceramic. So the reaction sequence of this oxide when doped in

BMT seems highly complex which evidently resulted in the formation of a new perovskite $BaCeO_3$ (JCPDS File Card No. 22-74) phase (Fig. 4. 2 (M)). The doping of TiO_2 damages the cation ordering of BMT as seen from Table 4.4. Presence of rutile (JCPDS File Card No. 21-1276) is observed for BMT doped with 2 mole % TiO_2 but it vanished at 5 mole % doping. In this case on the other hand, the formation of barium titanate, $BaTiO_3$ (JCPDS File Card No. 34-129) is detected in the XRD (Fig. 4. 2 (N)). On doping of BMT with SnO_2 has been beneficial to stabilize the cation ordering in BMT which may promotes 1:1 as per the previous report in a similar investigation. Perovskite phase $BaSnO_3$ (JCPDS File Card No. 15-780) was detected as a major additional line in the XRD pattern (see Fig.4. 2 (O)). The effect of the zirconia doping in the form of low loss perovskite impurity $BaZrO_3$ has been a thoroughly studied feature which contributes to the cation ordering phenomenon in BMT. In their paper[10] Chai et al. found that in (1-x)$Ba(Mg_{1/3}Ta_{2/3})O_3$-x$BaZrO_3$ system, the range stability of the trigonal 1:2 ordered phase is very narrow. Samples with x=0.05 in the above equation are comprised of a two phase mixture of 1:2 perovskite and a cubic 1:1 ordered structure ($Fm\bar{3}m$) with unit cell parameter $a = 2\ a_{subcell}$. Surprisingly enough, the $BaZrO_3$ doped BMT samples with high Q factor has a significant level of long range cation order which raised serious doubts about the origin of dielectric loss in this low loss $Ba(Mg_{1/3}Ta_{2/3})O_3$ dielectric ceramic. In a similar investigation in complex perovskite $Ba(Zn_{1/3}Ta_{2/3})O_3$ dielectrics Davies et al. [39]observed discrete 1:1 fcc ordered reflections in (1-x)$Ba(Zn_{1/3}Ta_{2/3})O_3$–x$BaZrO_3$ (BZT-BZ) ceramics. The 1:1 ordering in BZT-BZ however, is stabilized by charge compensation on the B-site, $[Zn^{2+} + (1/4)\ Zr^{4+}]$:$Ta^{5+}$ and encouraged by the similar cation radii of Zn^{2+} and Zr^{4+} (~ 0.75 Å). In a recent publication Ra and Phule [40]investigated the correlation between dielectric loss and long range cation ordering in BMT doped with $BaZrO_3$. The duo observed that 4 mole % BZ doped BMT showed a high quality factor (Q = 28300±8500) even when the cation ordering parameter is 0.49±0.13. So they arrived at the conclusion that it is not cation order but point defects generated at the time of material synthesis, controls the dielectric loss factor of BMT ceramic. They attributed the improvement of microwave quality factor during annealing to the changes in the concentration of point defects like oxygen vacancies that occur during heat treatments. In a recent publication Lan et al. [41]who investigated the effect of Zr doping in BMT, found

out that additional phases like $Ba_5Ta_4O_{15}$ which was detrimental to the microwave dielectric properties were suppressed on Zr addition. Hence they concluded that it is the presence of additional phases and not the cation ordering that controls the dielectric loss factor of BMT. In our investigation it was revealed that the ordering parameter steadily decreased with increasing concentration of Zr additive and for 5 mole % of the dopant the B site cations are observed to be disordered. Still the XRD pattern shows the formation of $BaZrO_3$ (JCPDS File Card No. 6-399) phases (Fig.4. 2 (P)). Interestingly, the higher percentage of HfO_2 additives does not form any simple perovskite additional phases. Instead Ba_2HfO_4 (JCPDS File Card No. 22-63) was the secondary phase detected in their corresponding XRD pattern (Fig. 4. 2 (Q)). Presence of weak diffraction line corresponding to 1:1 ordered is detected in BMT with 5 mole % of ZrO_2 and HfO_2.

The addition of pentavalent impurities is resulted in a partial substitution at Ta-site in $Ba(Mg_{1/3}Ta_{2/3})O_3$. In a recent report the Huang[14] et al. observed an improvement in the dielectric properties of BMT with low melting V_2O_5 addition which has been attributed to the substitution of smaller V_2O_5 (ionic radius 0.54 ?) ion in the Ta site (ionic radius 0.64 ?). This observation is in agreement with the finding of Galasso and Darby[42] who postulated that cation ordering decreases when the charge or ionic difference between the B-site cation decreases. In our observation we found that the cation ordering and related dielectric properties are poor (see Table. 4. 5) for V_2O_5 doped samples and the reasons for this may be attributed to the formation of additional phases. Apart from that the intensity of additional phases like BaV_3O_8 (JCPDS File Card No. 26-1038) and $VTaO_4$ (JCPDS File Card No. 24-1261) increases with increasing V_2O_5 addition (Fig. 4.6(R)). The XRD pattern of BMT doped with 5 mole % of Sb_2O_3 is given in (Fig. 4. 2 (S)). It is well known that at high temperatures, the oxidation state of Sb will be converted to 5 which may partially replace the Ta-site in BMT. Here the XRD pattern is well ordered and no trace of any additional peak is visible in the XRD spectrum which is reflected in the excellent microwave dielectric properties of BMT ceramics doped with Sb_2O_3. In the case of Sb_2O_3 doping, the size difference between partially substituted Sb^{5+} ion (0.6 ?) in the Ta^{5+} site with Mg^{2+} ion (0.72 ?) is 0.12 which effectively promotes the cation ordering. This result is consistent with the observation made by [43] Desu and O'Bryan that long range cation ordering in depends not only on the charge difference but

also on the ionic radius difference between B-site ions. The doping with Nb_2O_5 also does not form any additional phase with BMT (Fig. 4.2 (T)) which is understood since Nb^{5+} is having identical ionic radius with Ta^{5+} (0.64 ?).

The addition of hexavalent impurities like WO_3 and MoO_3 are also forming additional phases when doped in higher percentages (5 mole %). Kim et al.[44] found that WO_3 doping enhances the 1:2 ordering of BMT due to the greater difference in charge and ionic radius between W^{6+} and Ta^{5+} ions when the latter substitutes at the Ta-site. In the present study it was revealed that the influence hexavalent dopants enhances the B site cation ordering in complex perovskite $Ba(Mg_{1/3}Ta_{2/3})O_3$ due to obvious reasons of increased charge difference, between the additive cation and divalent Mg in the B' site of BMT. Formation of $BaWO_4$ (JCPDS File Card No. 8-457) is confirmed in the XRD pattern of 5 mole % WO_3 doped BMT (see Fig. 4. 2 (U)). $BaMoO_4$ (JCPDS File Card No. 28-147) is suspected to be the additional line present in the XRD pattern recorded from BMT samples doped with MoO_3 (Fig. 4. 2 (V)).

4. 3. 2 Effect of Dopants on Densification

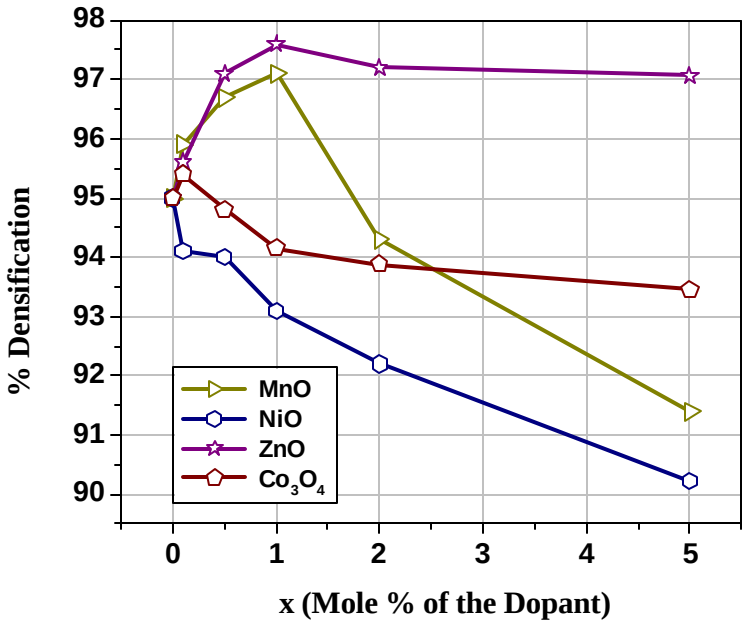

Fig. 4. 3 Variation of densification of BMT with concentration of divalent dopant

It is well evident that the addition of dopant ions in to BMT slightly modify the lattice parameter of its unit cell and hence the x-ray density has been calculated for each mole percentage of the additive. Fig. 4. 3 represents the variation of the percentage densification of BMT doped divalent impurities such as $MnCO_3$, NiO, ZnO and Co_3O_4. The densification is comparatively larger for ZnO and $MnCO_3$ up to 1.0 mole %. But the addition of impurities in large amount have a detrimental effect on material densification as it may breed grain growth. NiO doping resulted in poor densification in BMT. A previous report observed [45] that excess doping of NiO in BMT resulted in low densification and deterioration of dielectric properties due to lattice distortion. In complex perovskite $Ba(Mg_{1/3}Nb_{2/3})O_3$ ceramics when doped with Co_3O_4, presence of additional phase $Ba_5Nb_4O_{15}$ has been noticed, which inhibited the densification mechanism in the ceramic. But in our experiment on Co_3O_4 doping in BMT, no barium tantalate formation was observed but maximum density reached is only 95.5 % for 0.1 mole % of the additive.

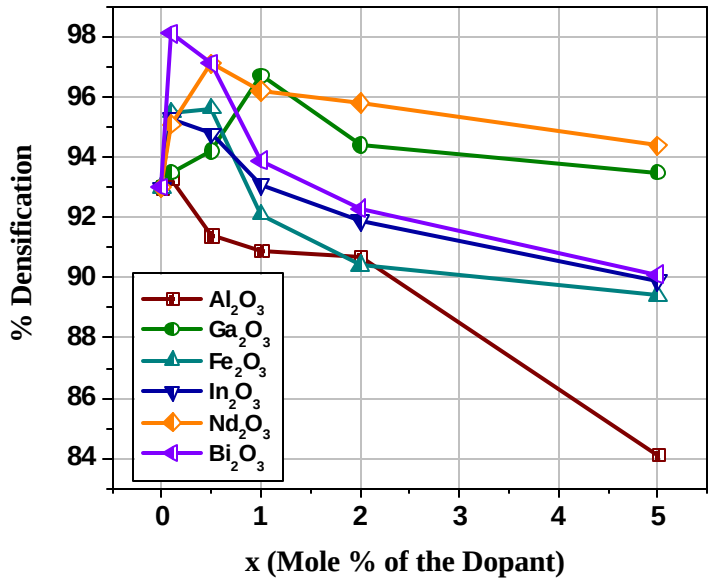

Fig. 4. 4 Variation of densification of BMT with concentration of trivalent dopant

The densities for BMT samples doped with trivalent impurity are slightly improved only for small amount of the additive (0.1 mole %) as seen Fig. 4.4. The

densification is very poor for Al_2O_3 doped samples where density steadily falls from 93 % to 84 % of their theoretical density which is attributed to the formation of barium aluminate. Apart from Nd^{3+} and Bi^{3+} ions, all other dopants in this family possibly can go into the B-site of the complex perovskite. But it is well analyzed that the coexistence of 1:1 ordering with 1:2 ordered domains occur when trivalent ion like La doped in BMT [46] which deteriorate the dielectric properties. It is interesting to note that densification behaviour of Bi_2O_3 dopant in BMT is best among the trivalent dopants we used in this study, which is believed to be due to liquid phase sintering. Nevertheless, it could not bring about any improvement in the dielectric properties of BMT ceramics.

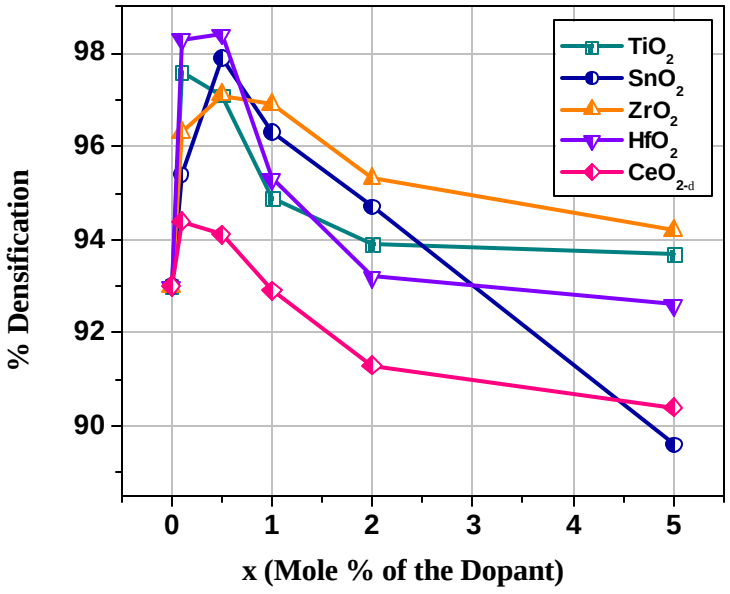

Fig. 4. 5 Variation of densification of BMT with concentration of tetravalent dopant

The densification trend of BMT doped with additives with an oxidation state 4 is given in Fig. 4. 5. The tetravalent additives perform fairly well in densifying the BMT matrix for 0.1 and 0.5 mole % of the additives such as TiO_2, SnO_2, ZrO_2, $CeO_{2-\delta}$ and HfO_2. On addition of more than 0.5 mole % of the dopant, the density decreases, due to obvious reasons of formation of secondary phase $BaMO_3$ (M=Ti, Sn, Zr, Ce and Hf) as shown in Fig.4. 5. The decrease of density of BMT dielectric with overdoping of

tetravalent impurities is more prominent in SnO_2 which has only 89.6 % of the theoretical density for 5 mole % of the dopant.

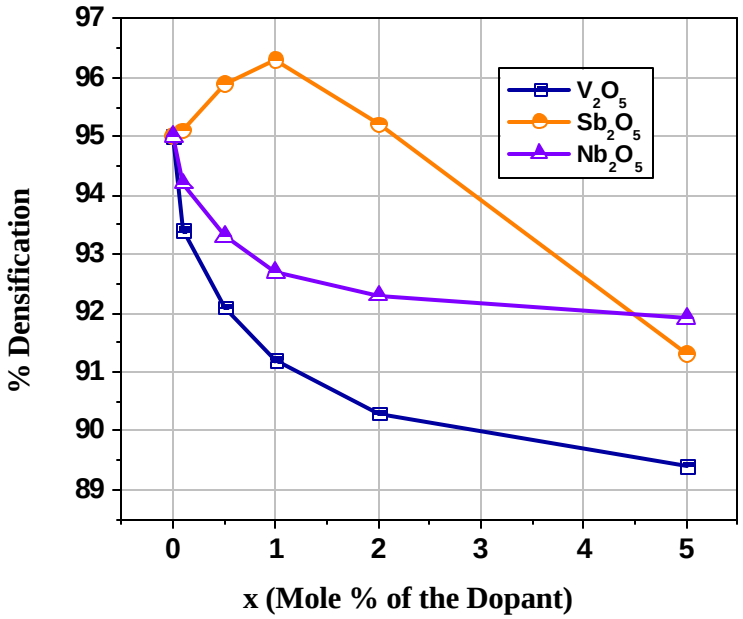

Fig. 4. 6 Variation of densification of BMT with concentration of pentavalent dopant

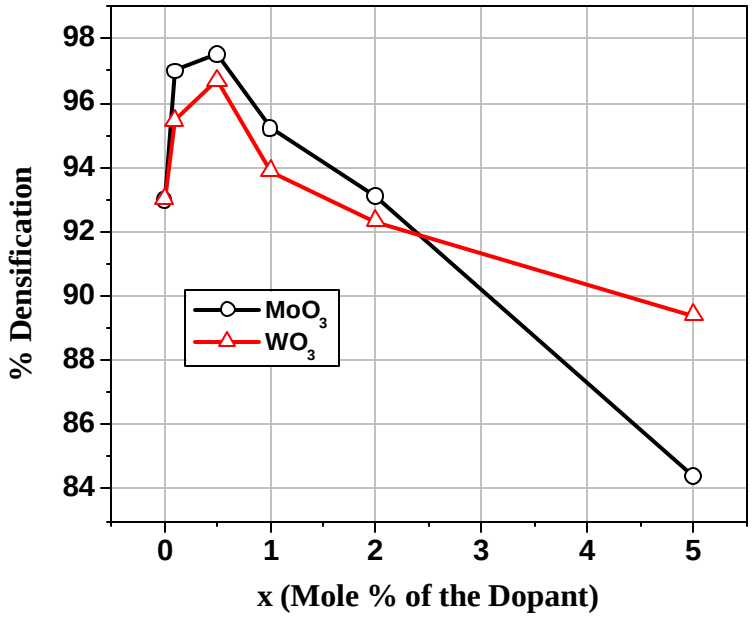

Fig. 4. 7 Variation of densification of BMT with concentration of hexavalent dopant

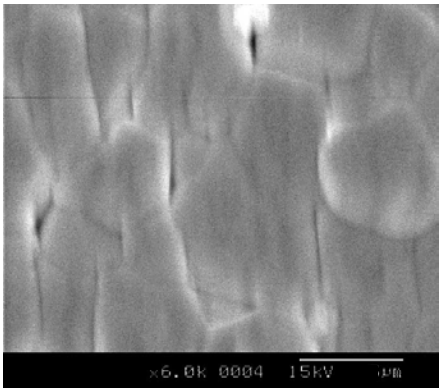

(a)

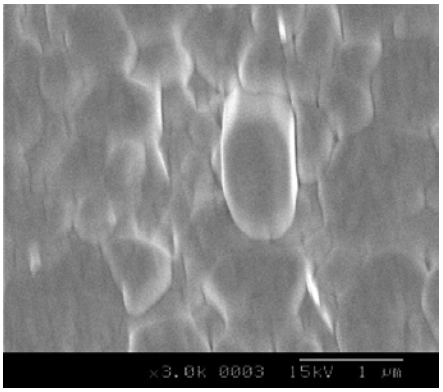

(b)

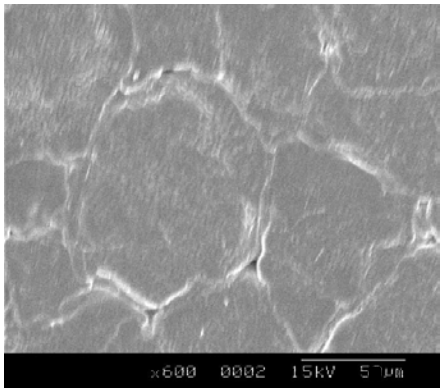

(c)

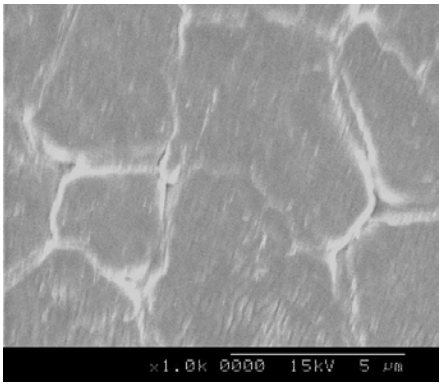

(d)

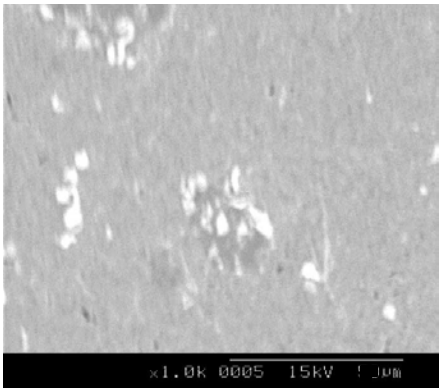

(e)

Fig. 4. 8 Scanning electron micrographs of BMT ceramic doped with (a)SnO_2, (b)Nd_2O_3 (c)ZrO_2, (d)$MnCO_3$ and (e) Bi_2O_3 sintered at 1625°C for 4 hours

The variation of percentage densification as a function of the mole % of the pentavalent additive is given in Fig. 4.6. The densification behaviour of Sb_2O_3 is good among pentavalent additives, whose cation is likely to replace Ta^{5+} in $Ba(Mg_{1/3}Ta_{2/3})O_3$. The liquid phase formed by melting of Sb_2O_3 is providing an ideal wetting medium for

vitreous sintering which can act as a short circuit media for materials transport from one matrix grain to other. Hence it can bring about improvement in the densification of BMT. A similar observation of good densification in complex perovskite was reported [47] in $Ba(Ni_{0.6}Zn_{0.4})_{0.33}Nb_{0.67})O_3$ when it is doped with Sb_2O_3. On the other hand, the doping with V_2O_5 does not improve the density as it resulted in the formation of additional phases such as BaV_3O_8 and $VTaO_4$ (see Fig. 4.2 (R)). This result stands as contradictory with a recent observation made by Huang et al.[14] who observed an increase in the density and dielectric properties of BMT with V_2O_5 addition for obvious reasons of liquid phase sintering and partial substitution of V^{5+} at the Ta^{5+} site. The doping of BMT with Nb_2O_5 also does not improve the densification mechanism of BMT.

The densification trend of hexavalent impurities WO_3 and MoO_3 in BMT are plotted Fig. 4. 7. After an initial improvement with smaller percentage of the additives, the density deteriorates with further addition. The presence of additives like WO_3 on the microwave dielectric properties of BMT has been well investigated aspect and many authors points out that partial substitution of aliovalent ion W^{6+} in the Ta^{5+} site act as a point defect and invites efficient material transport [5, 44]. The improvement in density for small amount of WO_3 and MoO_3 may be understood as a consequence of this phenomenon. Yoon et al. [48] observed that a simultaneous addition of BaO and WO_3 into BMT can improve its densification and microwave dielectric properties since the additive BaO/WO_3 will act as a low melting medium to enhance liquid phase sintering. The addition of MoO_3 by 5 mole % resulted in partial deformation of the samples due to melting when sintered at 1625^oC. The formation of the additional phase $BaMoO_6$ along with melting of the samples resulted in the poor show of density of BMT (84 % of the theoretical density) doped with 5 mole % of MoO_3.

4. 3. 3 Microstructural Analysis

The surface morphology of a few typical doped BMT samples were given in 4.12. It is found that the addition of 0.5 mole % of SnO_2 into the BMT resulted in better densification characteristics as seen from Fig. 4.8. The grains are upto 2-3 μm in size. One of the functions[49] of an ideal dopant is to control the particle coarsening and thereby enhance densification. Doping BMT with 2 mole % of Nd_2O_3 will lead to exaggerated

Table 4. 2 Unit cell properties of BMT doped with divalent impurities

BMT + Dopant	Mole % of Additive	Cell parameter a (?)	Cell parameter c (?)	c/a	Cell Volume (?)^3	X – Ray Density (g/cm^3)	Ordering Parameter
	0.1	5.7832	7.0852	1.2251	205.213	7.636	0.999
$MnCO_3$	0.5	5.7831	7.0840	1.2249	205.172	7.637	0.992
	1.0	5.7850	7.0861	1.2249	205.367	7.630	0.945
	2.0	5.7852	7.0796	1.2237	205.193	7.636	0.925
	5.0	5.7855	7.0774	1.2233	205.151	7.638	0.802
	0.1	5.7877	7.0867	1.2244	205.576	7.622	0.785
	0.5	5.7876	7.0791	1.2231	205.349	7.630	0.588
NiO	1.0	5.7899	7.0752	1.2219	205.399	7.628	----
	2.0	5.7895	7.0696	1.2211	205.208	7.636	----
	5.0	5.7898	7.0691	1.2209	205.215	7.635	----
	0.1	5.7874	7.0857	1.2243	205.526	7.624	0.930
	0.5	5.7870	7.0877	1.2248	205.556	7.623	0.995
ZnO	1.0	5.7871	7.0799	1.2233	205.336	7.631	0.891
	2.0	5.7869	7.0795	1.2233	205.254	7.634	0.882
	5.0	5.7881	7.0751	1.2223	204.746	7.653	0.556
	0.1	5.7871	7.0834	1.2239	205.438	7.627	0.892
	0.5	5.7877	7.0839	1.2239	205.495	7.625	0.901
Co_3O_4	1.0	5.7889	7.0848	1.2239	205.606	7.621	0.556
	2.0	5.7891	7.0734	1.2219	205.290	7.632	0.124
	5.0	5.7889	7.0727	1.2217	205.255	7.634	-----

grain growth as clear from Fig. 4. 8(b). This phenomenon is detrimental to the dielectric properties of the low loss ceramic. There are previous reports[50] that addition of Nd_2O_3 in BMT will form a liquid phase which prevents further densification of the ceramic. The Fig. 4.8(c) represents the surface morphology of BMT samples doped with 5 mole % ZrO_2. From the figure it is evident that addition of ZrO_2 into the low loss dielectric promoted grain growth but no additional phases even though XRD analysis (Fig. 4.2) confirms the presence of $BaZrO_3$ at 5 mole % doping. A polycrystalline structure with bigger grain is equivalent to a single crystal with lower defect levels. Such a sintering condition will be congenial for good dielectric properties. The surface micrograph corresponding to BMT with addition of 1 mole % of $MnCO_3$ also presented a well packed grain structure with relatively bigger grains. On the other hand, addition of certain dopants like Bi_2O_3 promotes liquid phase sintering as they melt at a temperature much lower than 1625^{o}C (see Fig. 4.8 (e). But due to the inefficient wetting of the BMT matrix, the densification remains poor in this case. The Bi_2O_3 additive reacts with matrix and forms additional phase which can be clearly seen in the scanning electron micrograph.

4. 3. 4 Cation Ordering Studies

Table 4. 3 Unit cell properties of BMT doped with trivalent impurities

BMT + Dopant	Mole % of Additive	Cell parameter a (?)	Cell parameter c (?)	c/a	Cell Volume (?)^3	X-Ray Density (g/cm^3)	Ordering Parameter
	0.1	5.7823	7.0824	1.2248	205.068	7.641	0.783
	0.5	5.7804	7.0799	1.2229	204.862	7.648	0.452
Al_2O_3	1.0	5.7915	7.0771	1.2219	205.567	7.622	0.265
	2.0	5.7917	7.0773	1.2219	205.587	7.621	0.260
	5.0	5.7922	7.0769	1.2217	205.611	7.621	-----
	0.1	5.7873	7.0862	1.2244	205.531	7.624	0.986
	0.5	5.7872	7.0822	1.2237	205.410	7.628	0.988
Ga_2O_3	1.0	5.7885	7.0801	1.2231	205.442	7.627	0.875
	2.0	5.7885	7.0800	1.2231	205.439	7.627	0.352
	5.0	5.7892	7.0725	1.2216	205.271	7.633	-----
	0.1	5.7820	7.0809	1.2246	205.004	7.643	0.892
	0.5	5.7891	7.0789	1.2227	205.449	7.627	0.751
Fe_2O_3	1.0	5.7921	7.0776	1.2219	205.625	7.620	0.231
	2.0	5.7998	7.0780	1.2203	206.183	7.599	-----
	5.0	5.7993	7.0783	1.2205	206.178	7.600	-----
	0.1	5.7873	7.0861	1.2244	205.530	7.624	0.712
	0.5	5.7881	7.0774	1.2227	205.335	7.631	0.297
In_2O_3	1.0	5.7889	7.0725	1.2216	205.249	7.634	-----
	2.0	5.7893	7.0705	1.2213	205.220	7.635	-----
	5.0	5.7892	7.0703	1.2212	205.207	7.636	-----
	0.1	5.7871	7.0799	1.2233	205.336	7.631	0.957
	0.5	5.7888	7.0769	1.2225	205.371	7.629	0.945
Nd_2O_3	1.0	5.7881	7.0751	1.2223	204.746	7.653	0.949
	2.0	5.7898	7.0690	1.2209	205.214	7.635	0.223
	5.0	5.7892	7.0699	1.2212	205.196	7.636	----
	0.1	5.7842	7.0782	1.2237	205.082	7.640	0.744
	0.5	5.7873	7.0790	1.2231	205.325	7.631	0.341
Bi_2O_3	1.0	5.7873	7.0701	1.2216	205.066	7.641	-----
	2.0	5.7871	7.0700	1.2216	205.049	7.641	-----
	5.0	5.7866	7.0704	1.2218	205.026	7.642	-----

Tables 4. 2 to 4. 6 represent the properties of the unit cell parameters of BMT as a function of mole percentage of the additives. For pure ordered complex perovskite $Ba(Mg_{1/3}Ta_{2/3})O_3$ dielectric ceramics sintered at 1625 ^oC the unit cell parameters assuming a hexagonal superstructure are a = 5.7807 Å and c = 7.084 Å. The x-ray density of pure BMT = 7.625 g/cm^3, assuming the molecular weight to be 314.596 grams [51]. When the samples are annealed at 1450 ^oC for 40 hours, the modified cell parameters are a = 5.7878 Å and c = 7.093 Å so that c/a = 1.2255.

Table 4. 4 Unit cell properties of BMT doped with tetravalent impurities

BMT + Dopant	Mole % of Additive	Cell parameter a (?)	Cell parameter c (?)	c/a	Cell Volume (?)^3	X – Ray Density (g/cm^3)	Ordering Parameter
	0.1	5.7877	7.0868	1.2244	205.579	7.622	0.483
TiO_2	0.5	5.7871	7.0858	1.2244	205.508	7.625	0.252
	1.0	5.7871	7.0855	1.2243	205.499	7.625	-----
	2.0	5.7865	7.0802	1.2235	205.303	7.633	-----
	5.0	5.7842	7.0789	1.2238	205.102	7.634	-----
	0.1	5.7831	7.0831	1.2248	205.146	7.638	0.975
	0.5	5.7834	7.0829	1.2247	205.161	7.638	0.922
SnO_2	1.0	5.7871	7.0799	1.2233	205.336	7.631	0.897
	2.0	5.7888	7.0770	1.2225	205.375	7.629	0.756
	5.0	5.7893	7.0771	1.2224	205.412	7.628	0.437
	0.1	5.7899	7.0908	1.2247	205.852	7.612	0.852
	0.5	5.7945	7.0925	1.2240	206.229	7.598	0.597
ZrO_2	1.0	5.7951	7.0788	1.2215	205.873	7.611	0.524
	2.0	5.7951	7.0787	1.2214	205.870	7.611	0.202
	5.0	5.7973	7.0772	1.2203	205.983	7.609	-----
	0.1	5.7891	7.0789	1.2227	205.449	7.627	0.564
	0.5	5.7880	7.0741	1.2222	205.232	7.635	0.443
HfO_2	1.0	5.7901	7.0741	1.2217	205.374	7.629	-----
	2.0	5.7903	7.0738	1.2216	205.387	7.629	-----
	5.0	5.7921	7.0733	1.2211	205.500	7.625	-----
	0.1	5.7801	7.0781	1.2245	204.788	7.651	0.965
	0.5	5.7834	7.0756	1.2234	204.949	7.645	0.922
$CeO_{2-\delta}$	1.0	5.7833	7.0755	1.2234	204.946	7.645	0.911
	2.0	5.7880	7.0741	1.2222	205.232	7.635	0.465
	5.0	5.7945	7.0790	1.2216	205.836	7.612	-----

It is well reported the presence of a dopant impairs the lattice parameters if it goes into the lattice site of the matrix. The accurate determination of the crystallographic lattice parameters in complex perovskites needed to be determined using refinement technique like [52]Rietvield method, we arrived at our conclusions based on analytic calculations using XRD data of the doped samples sintered at 1625 ^oC. The cell parameters reported in this dissertation have been derived from powder diffraction data of all the diffraction lines in the range 2T = 5-70 degrees and then taking the weighted average.

The unit cell parameters *a* and *c* are modified slightly by divalent ion doping as seen from Table. 4.2. When BMT is doped with $MnCO_3$, the lattice parameter ratio (*c/a*) is calculated as 1.2251, 1.2239 and 1.2249 for 0.1 0.5 and 1.0 mole % of the dopant. This implies that a partial substitution of Mg^{2+} with Mn^{2+} enhances the cation ordering in

$Ba(Mg_{1/3}Ta_{2/3})O_3$ which is confirmed by larger values of ordering parameter. The cation order is decreased with higher concentration of the $MnCO_3$ dopant which is reflected in the decline of the dielectric properties of BMT. Addition of NiO has been detrimental to its cation ordering and dielectric properties in the sense that the additional phase $Ba_3Ni_3O_6$ melt at 1100 ^oC [53] which does not favor liquid phase sintering. This observation is consistent with a previous report by Kim et al.[6] who noticed the appearance of needle shaped grains when NiO was added to BMT. The addition of ZnO resulted in better ordered structure for BMT but it could not fetch much improvement in its dielectric properties. It must be noted that among all the trivalent impurities we studied in this work, not even a single dopant improved the 1:2 cation arrangement in BMT so that *c/a* is greater than 1.2247. This observation categorically points out that the trivalent additives are unsuitable for complex perovskite $Ba(Mg_{1/3}Ta_{2/3})O_3$ ceramics.

The effect of ABO_3 perovskite additives on the order-disorder phase transition of BMT has been well investigated by various research groups[10, 11, 54]. In most of these works, it has been revealed that on higher percentage of the substitution of the tetravalent additive at the B-site, appearance of 1:1 ordered domains along with 1:2 ordered superstructure. In a significant work Davies[55] proved that the size of M^{4+} cation in (1-x) $Ba(Mg_{1/3}Ta_{2/3})O_3$–$xBaM^{4+}O_3$ (cation with an oxidation state 4) plays a critical role in the formation of the 1:1 ordered structure. The introduction of a larger dopant such as Ce (0.87 Å) or Zr (0.72 Å) removes the 1:2 order in BMT and stabilizes a region of 1:1 order that is upto 25 mole % substitution. In our investigation, the ordering parameter of Sn doped ceramic is comparably better (see Table 4. 4) which is thought to be due to 1:2 ordering of the hexagonal perovskite. The ordering parameter of BMT doped with TiO_2 is poor which is reflected in the dielectric properties of these ceramic at microwave frequencies. This may be due to the presence of additional phase $BaTiO_3$ which is lossy with high dielectric constant.. The cation ordering decreases 0.952 to zero when the concentration of the ZrO_2 dopant increases from 0.1 to 5.0 mole %. On the other hand the cation ordering is poor in HfO_2 doped complex perovskites. It is worthwhile to note that an insignificant presence of diffraction line corresponding to 1:1 ordered is observed in BMT when it is doped with 5 mole % of ZrO_2 and HfO_2. The doping of BMT with TiO_2 presented a disordered perovskite structure (see Fig. 4.6). According to Chai et al.[11], in

BMT ceramics the 1:1 cation ordering is mainly promoted by tetravalent cations with ionic radius > 0.69 Å and a cation additive smaller than this may result in the random distribution of the B-site cation. This indirectly substantiate the disordered perovskite structure of BMT with TiO_2 additive since the ionic radius of Ti^{4+} is 0.605 Å.

Table 4. 5 Unit cell properties of BMT doped with pentavalent impurities

BMT + Dopant	Mole % of Additive	Cell parameter a (?)	Cell parameter c (?)	c/a	Cell Volume (?)^3	X-Ray Density (g/cm^3)	Order Parameter
	0.1	5.7835	7.0781	1.2238	205.021	7.642	0.827
	0.5	5.7837	7.0766	1.2235	205.000	7.643	0.785
V_2O_5	1.0	5.7834	7.0756	1.2234	204.949	7.645	0.334
	2.0	5.7841	7.0751	1.2231	204.985	7.644	0.320
	5.0	5.7842	7.0704	1.2223	204.856	7.649	0.331
	0.1	5.7795	7.0811	1.2252	204.833	7.650	0.978
	0.5	5.7803	7.0799	1.2248	204.855	7.649	0.999
Sb_2O_3	1.0	5.7805	7.0795	1.2247	204.857	7.649	0.991
	2.0	5.7822	7.0767	1.2238	204.896	7.647	0.753
	5.0	5.7839	7.0765	1.2234	205.011	7.643	0.608
	0.1	5.7871	7.0799	1.2233	205.336	7.631	0.856
	0.5	5.7887	7.0770	1.2225	205.366	7.630	0.774
Nb_2O_5	1.0	5.7893	7.0771	1.2224	205.412	7.628	0.350
	2.0	5.7889	7.0744	1.2221	205.305	7.632	0.221
	5.0	5.7928	7.0730	1.2210	205.541	7.623	-----

The effect of doping of pentavalent ions into BMT on the unit cell parameters is given in Table 4. 5. It is evident that the doping of Sb_2O_3 is found to be excellent among the 20 dopants we used in this investigation in terms of the dielectric properties it exhibits in the microwave frequency region. BMT samples added with 0.1, 0.5, 1.0, 2.0 and 5.0 mole % of antimony trioxide have cation ordering parameter 0.978, 0.999, 0.971, 0.753 and 0.608 as seen in Table. 4.5. The unit cell parameter ratio (c/a) also has values greater than $\sqrt{(3/2)}$ = (1.2247) up to 1.0 mole % of the dopant addition which clearly confirms the expansion of the unit cell diagonal along the <111> direction to form a hexagonal superstructure. The doping of V_2O_5 and Nb_2O_5 did not produce any significant contribution towards the long range ordering of the complex perovskite.

It should be noted that the addition of hexavalent impurity can result in partial substitution of the B" site in BMT. On doping BMT with WO_3, the unit cell retains its ordered hexagonal structure ($P\bar{3}m1$) upto 1.0 mole % of the additive which has been

substantiated by an enhanced cation ordering as shown in Table 4.6. On the other hand the cation ordering is appreciably high only for 0.1 mole % of MoO_3 additive. The long range order and dielectric properties deteriorates with further addition of the dopant. The addition of dopants make more pronounced effects on the microwave dielectric properties of BMT which is discussed in the next section.

Table 4. 6 Unit cell properties of BMT doped with hexavalent impurities

BMT + Dopant	Mole % of Additive	Cell parameter a (?)	Cell parameter c (?)	c/a	Cell Volume (?)^3	X-Ray Density (g/cm^3)	Ordering Parameter
	0.1	5.7810	7.0809	1.2249	204.933	7.646	0.970
WO_3	0.5	5.7811	7.0812	1.2249	204.949	7.646	0.989
	1.0	5.7825	7.0821	1.2247	205.074	7.641	0.974
	2.0	5.7859	7.0820	1.2240	205.313	7.632	0.675
	5.0	5.7860	7.0832	1.2242	205.065	7.641	0.362
	0.1	5.7815	7.0811	1.2247	204.974	7.645	0.885
	0.5	5.7877	7.0795	1.2232	205.367	7.630	0.559
MoO_3	1.0	5.7876	7.0770	1.2228	205.288	7.633	0.576
	2.0	5.7869	7.0776	1.2230	205.256	7.634	0.540
	5.0	5.7892	7.0725	1.2216	205.271	7.633	0.538

4. 3. 4 Microwave Dielectric Properties

The main objective of this investigation is to improve the dielectric properties of BMT at microwave frequencies for practical applications. In this investigation, it should be remembered that the intrinsic purity of the raw materials used in the solid state synthesis of BMT has a significant role in controlling its dielectric loss phenomena. The microwave dielectric properties of pure BMT ceramic samples sintered at 1625 ^oC for 4 hours before annealing are e_r = 24.3, $Q_u$xf = 80,000 GHz and t_f= 7 ppm/^oC. On annealing the samples at 1450 ^oC for 40 hours (which has been the optimized condition for annealing), the dielectric properties are e_r = 24.4, $Q_u$xf = 100,500 GHz and t_f= 8 ppm/^oC.

4. 3. 4. 1 Divalent Additives

Fig. 4.9 shows microwave dielectric properties of BMT ceramics doped with divalent dopants such as $MnCO_3$. NiO, ZnO and Co_3O_4. The measured [56] dielectric

constants are corrected for porosity. The ionic polarisabilities of the dopant cations Mn, Ni, Zn and Co are 2.64, 1.23, 2.04 and 1.65 respectively. The dielectric constant of 0.5

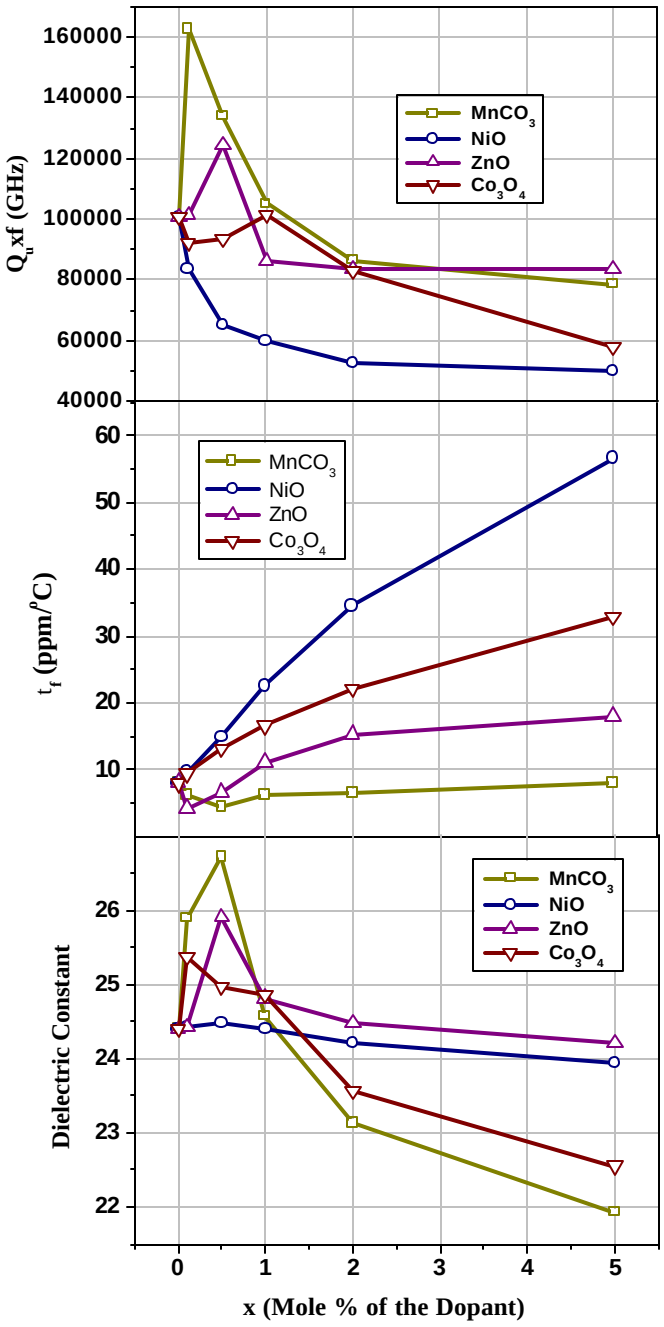

Fig. 4. 9 Variation of dielectric properties of BMT with the addition of divalent dopant

mole % Mn^{2+} and Zn^{2+} doped BMT samples increase to 26.7 and 25.9 respectively. With higher concentration of the dopant ions, the measured dielectric constant decrease which may be due to high temperature phenomena like abnormal grain growth. For Ni and Co additives, the dielectric constant decreases with larger amount of doping which is consistent with previous reports[57] on effects of Co/Nb substitution in BMT.

It is well known that the temperature coefficient of resonant frequency is intimately related to the coefficient of linear expansion (a) and the temperature coefficient of dielectric constant (t_e). In 1994, Colla et al.[58] suggested a macroscopic model for temperature coefficient of complex perovskite compounds which assumed three factors that have a major contribution to the change in temperature coefficient of dielectric constant (t_e). They are (a) volume expansion coefficient, (b) variation in total polarisability with volume expansion and (c) variation of the total polarisability with temperature. It has been established that chemical doping impairs the ordering of complex perovskite $Ba(Mg_{1/3}Ta_{2/3})O_3$, but the linear expansion coefficients of the ordered and disordered BMT are almost same. So the first term (a) does not have any contribution on t_e. Therefore the variation in t_e with ordering can be attributed to the change in ionic polarisability with respect to volume expansion (b) and temperature (c). Here it is expected that the partial substitution of divalent impurities in magnesium site of BMT results in lattice distortion. Hence the t_e becomes more negative as the percentage of the dopant increases. This accounts for the high increase of t_f values with the addition of NiO, Co_3O_4 and ZnO. For $MnCO_3$ additives however the measured t_e values are less than 8 ppm/^oC.

The quality factor of the samples depend on a number of parameters like purity of the raw materials, synthesizing conditions and final densification. The Mn doped BMT samples are showing high quality factor of $Q_u$xf = 162,800 GHz for 0.1 mole % of the additive which is consistent with the report of Nomura[3]. The quality factor is decreased with further increase of the dopant. The ZnO doped samples (0.5 mole %) have also reasonably good quality factor ($Q_u$xf = 124,550 GHz). Among the divalent dopants we studied, the lowest Q is found for NiO doped samples as seen from Fig. 4.9. It is quite surprising that despite having ideal solid solution characteristics[59], the chances of Ni substitution for Mg site in BMT is very poor and hence it may form additional needle

shaped tantalate phases [6]. A similar observation was made in $Ba(Zn_{1/3}Ta_{2/3})O_3$ by Rong et al.[7] who found that a significant increase in the level of point defects is observed in BZT when it is doped with Ni.

4. 3. 4. 2 Trivalent Dopants

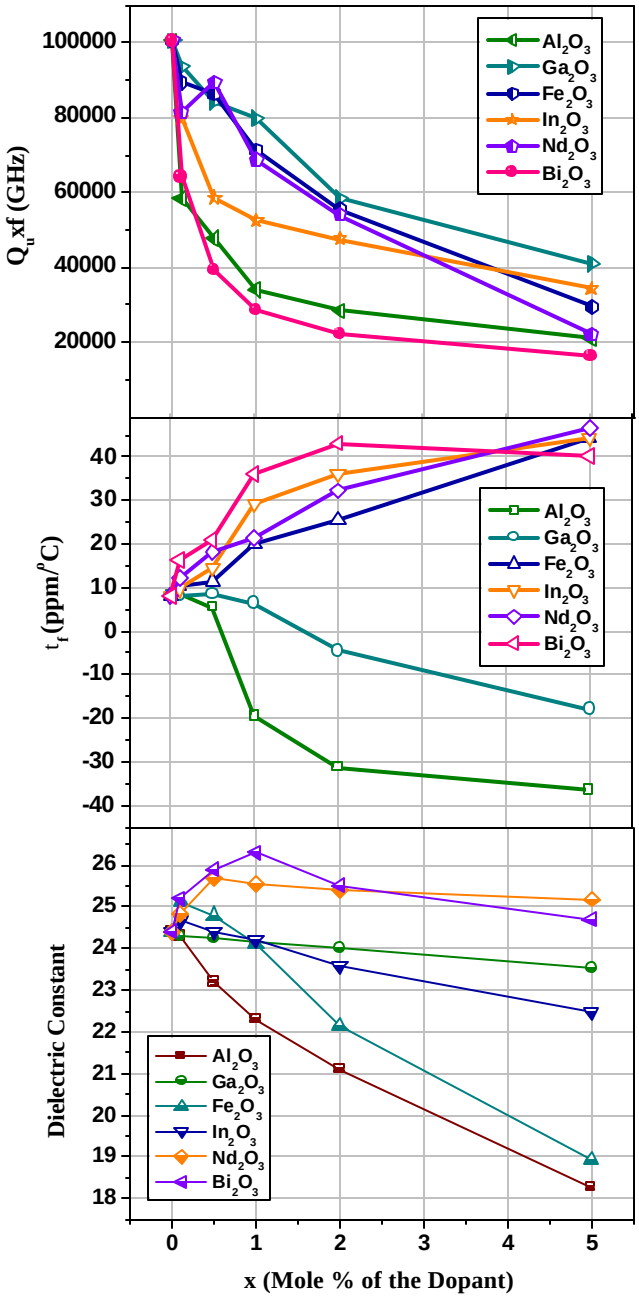

Fig. 4. 10 Variation of the microwave dielectric properties of BMT with trivalent impurity addition.

The microwave dielectric properties of $Ba(Mg_{1/3}Ta_{2/3})O_3$ dielectrics doped with dopants with oxidation state 3 are found to be comparatively poor as shown in Fig. 4.10. This is attributed to the formation of lossy additional phases. The dielectric constant of Bi and Nd doped ceramics show higher values which can be attributed to the high dielectric polarisabilities (6.12 and 6.15 respectively) of these cations. It is worthwhile to note that if the trivalent dopant's ionic polarisability is lower than the average polarisability (= 3.693) of the B-site cation in BMT, then the measured dielectric constant decreases. The dielectric constant decreases for higher concentration of the additive due to the formation of secondary phases (see Fig. 4. 2).

The temperature coefficient of resonant frequencies of BMT as a function of trivalent dopant is given in Fig. 4.10 Except for Al_2O_3 and Ga_2O_3, the doped samples show high positive τ_f values. Since Al_2O_3 being a negative τ_f dielectric resonator[29] whose presence is detected in XRD of the doped sample along with $Ba_{10}Al_2O_{13}$ phases, the fall in τ_f may be understood. In Ga doping τ_f approaches negative values which can be due to the formation of additional phase $BaGa_{12}O_{19}$ that may be a negative τ_f material. For other dopants such as Fe_2O_3, Al_2O_3, In_2O_3 and Nd_2O_3, the high positive values of τ_f is observed.

It is evident that the effect of doping of ions with stable oxidation state 3 is found to be disastrous to the microwave quality factor of BMT. As it is clear from Fig. 4.10, that unloaded quality factor of all the samples decreases with doping. A previous study [54] on the effect of trivalent Nd_2O_3 on BMT revealed that even when the ordering parameter is close to 1, the quality factor shows extremely low values ($Q_u$xf < 7000 GHz) due to the formation of secondary phases. The fall in quality factor is believed to be due to the cation order transformation from 1:2 to 1:1 ordering.

4. 3. 4. 3 Tetravalent Dopants

The effect of tetravalent impurities like Zr and Ti, on the dielectric loss factor of complex perovskites have been studied by a many research groups [10, 11] due to the pivotal role of these dopants in initiating and controlling the phase transition of the complex perovskites from 1:2 to 1:1 symmetry. The dielectric properties of tetravalent impurity

added BMT measured at microwave fequency is plotted in Fig. 4.11. The dielectric constants of all doped BMT samples are increased as compared for pure BMT, except

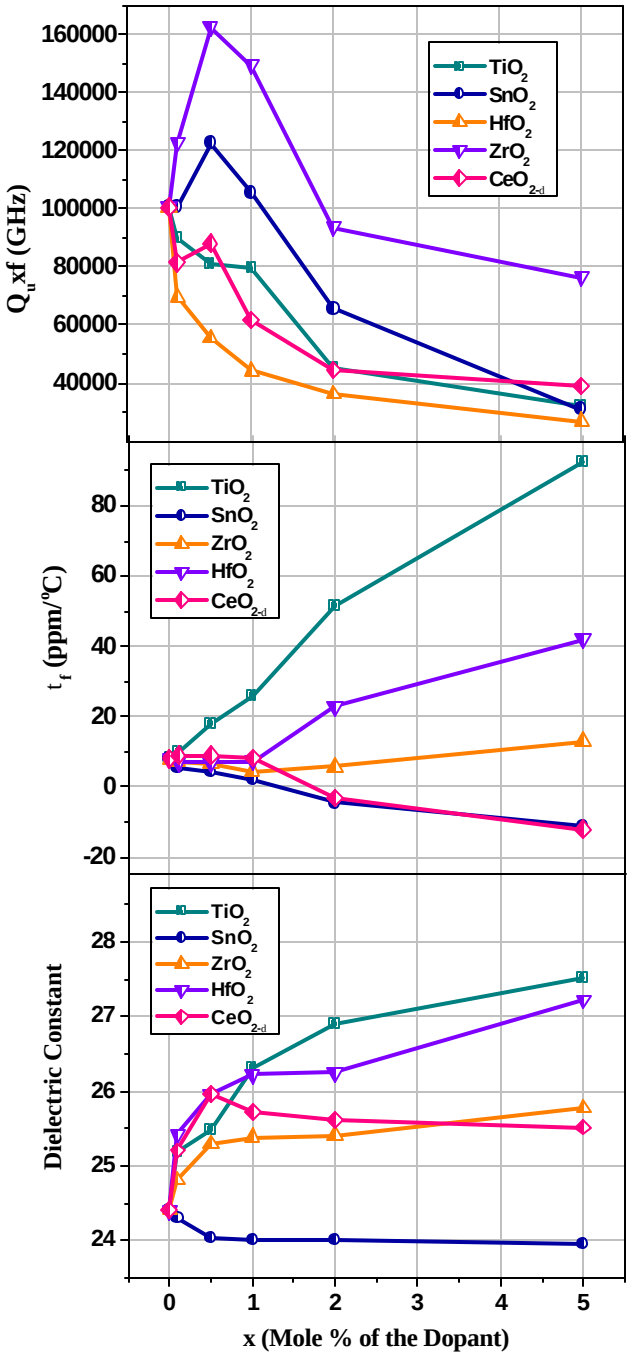

Fig. 4. 11 Variation of the microwave dielectric properties of BMT with the addition of tetravalent impurity

for SnO_2 addition. The dielectric polarisability of Zr (3.25) is more than Ti (2.93), but the dielectric constant of samples doped with 5 mole % TiO_2 has higher values (27.5) than that doped with an identical concentration of ZrO_2 (25.8). The increase in dielectric constant is believed to be of lattice distortion of the perovskite structure due to the substitution of tetravalent cation doping. Lan et al [60] also observed a small enhancement of dielectric constant of BMT with Zr doping. There have been previous reports made about the improvement of dielectric properties of BMT with TiO_2 and SnO_2 doping[61]. It is worthwhile to note that on titania doping in BMT, a ferroelectric $BaTiO_3$ is formed which is reported[62] to have very high dielectric constant (4000-10000). This observation indicates that additional phases formed during higher percentage of doping have more influence on the dielectric constant than the individual ionic polarisability of the dopant.

The effect of SnO_2 and CeO_2 on BMT decreases the τ_f to negative values. This observation is consistent with a previous observation by Matsumoto [4] who noted that, apart from improving quality factor, the τ_f of BMT decreases to negative values on doping with $BaSnO_3$. The titania and hafnia doping increase the τ_f of BMT dielectric due to the greater lattice distortion imparted in the disordered perovskite. For 1 mole % of ZrO_2 dopant the τ_f value of BMT decrease to 4.5 ppm/^oC and then increases to 13 ppm/^oC on further addition of the dopant.

The cation ordering transformation from 1:2 to 1:1 arrangement plays a significant role in the microwave quality factor of BMT doped with tetravalent impurities. A previous report [40] suggest that the cation ordering is not a vital factor that controls the microwave dielectric properties of BMT. Instead, loss factor is more controlled by point defects that are introduced as a result of non-stoichiometry, impurities in raw material and processing. They believe that quality factor improvement after long period annealing may be more linked to the changes in the concentration of such point defects (e.g. oxygen vacancies) that occur during such heat treatments. In our investigation we found that the $Q_u$xf reaches its maximum value (162,500 GHz) for 0.5 mole % of ZrO_2 dopant where the ordering parameter is 0.897. For higher concentration of the dopant, the Q factor decreases where the cation ordering is also poor. A recent study [41] suggests that the fall in quality factor with higher concentration of Zr may be more likely due to the formation of Ba-Ta-O secondary phase than reduction in the

ordering parameter. But in our study of Zr doping in BMT no barium tantalate secondary phase was detected apart from perovskite $BaZrO_3$. The microwave quality factor of BMT doped with titania, hafnia and ceria are poor. On the other hand 0.5 mole % of SnO_2 improved the quality factor of BMT from its undoped quality factor of 100,500 GHz to 122,500 GHz.

4. 3. 4. 4 Pentavalent Dopants

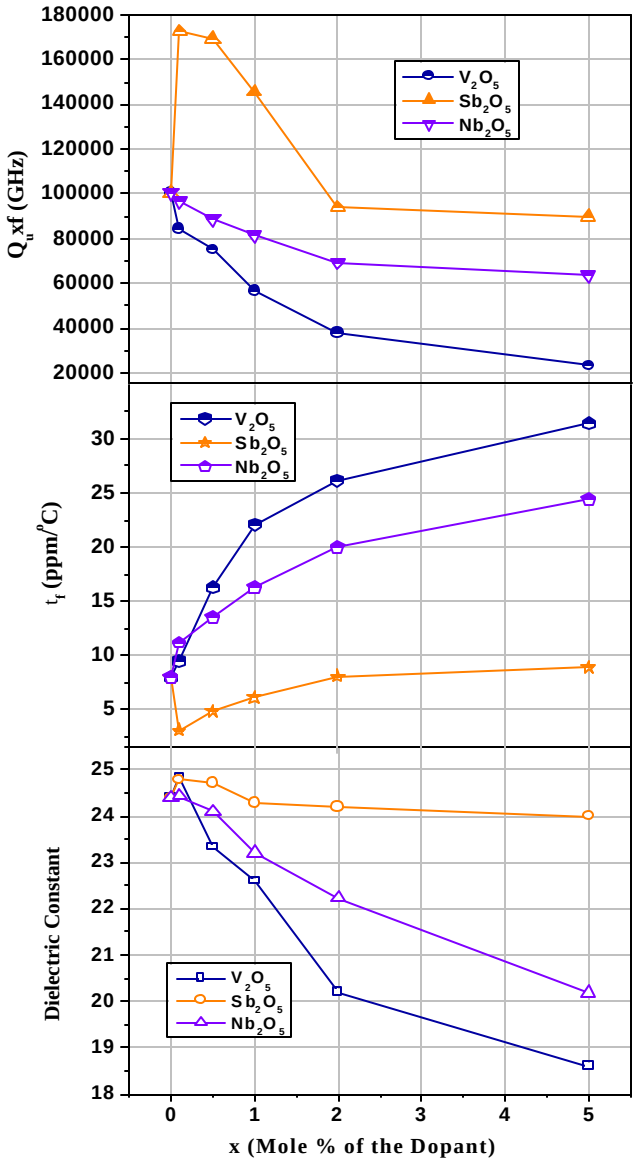

Fig. 4. 12 Variation of the microwave dielectric properties of BMT with the addition of pentavalent impurity

The effect of pentavalent dopant addition on the microwave dielectric properties of BMT is plotted in Fig. 4.12. It is well known that all the three additives used in this investigation (Sb_2O_3, V_2O_5 and Nb_2O_5) are low melting and can aid liquid phase sintering. The partial substitution of Sb in Ta site has been beneficial in increasing the dielectric constants of the doped samples with Sb_2O_3 addition. On the other hand the measured dielectric constant decreases with increasing V_2O_5 concentration. This is due to the substitution of a less polarisable V ion (polarisability = 2.92) at Ta site (polarisability = 4.73). The dielectric constant of BMT samples decreases slightly with Nb_2O_5 addition, despite a complete replacement of Ta with Nb to form $Ba(Mg_{1/3}Nb_{2/3})O_3$ which has a relatively high dielectric constant of 32. A similar effect of decrease in dielectric constant for small percentage of Nb ions in BMT has already been reported [63].

The t_f increase monotonously with increase in the V_2O_5 and Nb_2O_5 content. This observation is in agreement with a recent observation that temperature coefficient of resonant frequency increases with V_2O_5 addition[14]. The τ_f values are 3.1 and 4.9 ppm/^oC when BMT is doped with 0.1 and 0.5 mole % of Sb_2O_3 additive.

The quality factor of BMT doped with 0.1 mole % of Sb_2O_3 is found to be the best ($Q_u$xf =172,500) among all the additives we studied. But the density is maximum for 1 mole % of the additive (see Fig. 4. 6) where the quality factor- frequency product is only 145,500 GHz. It is worthwhile to note that the cation ordering is greater for samples doped with Sb_2O_3 additive (see Table 4. 5). For other additives V_2O_5 and Nb_2O_5, the loss factor increases with dopant concentration. The lowering of Q with V_2O_5 addition disagrees with a recent observation by Huang et al.[14] who observed an enhancement of the quality factor with V_2O_5 incorporation due to the liquid phase sintering.

4. 3. 4. 5 Hexavalent Dopants

The microwave dielectric properties of the BMT ceramics doped with MoO_3 and WO_3 are given in Fig. 4.13. For 0.1 mole % of MoO_3 additive the dielectric constant increases from 24.4 to 25.17 and then decreases on further addition. On the other hand the dielectric constant steadily increases to 25.7 up to 2 mole % of the WO_3 additives and then decreases which may be due to the formation of $BaWO_4$ (also see Fig. 4. 2).

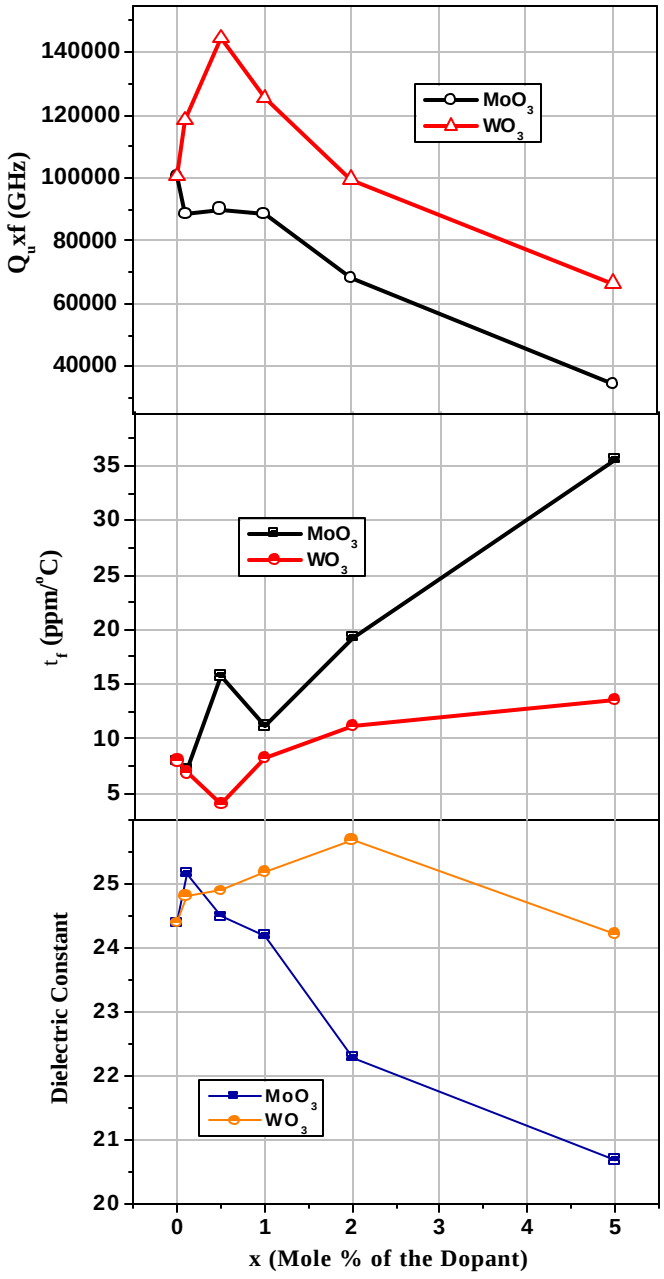

Fig. 4. 13 Variation of the microwave dielectric properties of BMT with the addition of hexavalent impurity.

The t_f of 0.5 mole % WO_3 doped sample decreases to 4.1 from 8 ppm/^oC and then increases with overdoping. But the variation of τ_f with MoO_3 doping shows an irregular trend which is believed to be due to the effect of Ba_2MoO_6 additional phase.

The ionic radii of W^{6+}, Ta^{5+} and Mg^{2+} with a coordination number 6 are 0.58, 0.64 and 0.72 Å respectively. A partial substitution of W^{6+} at Ta^{5+} site not only bring about a charge difference of 4 between B' and B" site cations, but the ionic radius difference also increases from 0.08 to 0.14 Å. Kim et al. proved that this substitution produces the positively charged W in Ta sites with a concomitant generation of tantalum vacancies and mobile oxygen vacancies for the ionic charge compensation. This ionic compensation mechanism relieves the electrostatic repulsion associated with the formation of the positively charged sites and thus promotes the growth of 1:2 ordered domain. In the present investigation WO_3 doping initiates reasonably good ordering in BMT, but the ordering effect is poor with MoO_3 doping (see Table 4.6). The quality factor frequency product of 0.5 mole % WO_3 doped BMT are 144,500 GHz. The quality factor MoO_3 doped samples are in general poor due to the lossy effects of the additional phase formed during doping. It is interesting to note that the effect of WO_3 doping in $Ba(Mg_{1/3}Nb_{2/3})O_3$ is also brings about good structural ordering and microwave dielectric properties[64].

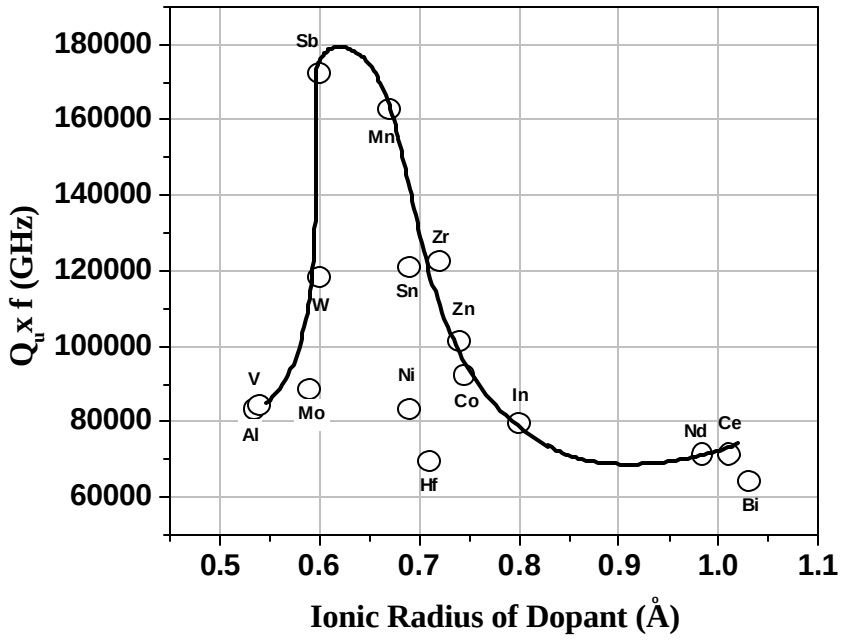

Fig. 4. 14 Plot of ionic raius of the dopant versus quality factor of BMT ceramic

Based on the results and discussion made above, we explored a possible relationship between ionic radius of the dopant and the quality factor of BMT samples

added with different dopants. The average ionic radius of B-site cation of BMT (i.e. $Mg_{1/3}Ta_{2/3}$) is calculated as 0.653 Å. A plot of the unloaded quality factor of BMT ceramic doped with 0.1 mole % of the dopants as a function of ionic radius of the dopants is given in Fig.4.14. In general when the ionic radius of the dopants are between 0.6 and 0.7 Å (i.e. close to the average ionic radii of the B-site ion in BMT) the quality factor reaches maximum values. However not all the cations with ionic radius between 0.6 and 0.7 (like Ga(0.64 Å), Nb (0.64 Å) and Fe (0.645Å)) are favorable for improving the properties in BMT.

4. 3. 4. 6 Dielectric Properties at Cryogenic Temperatures

The cryogenic behaviour of dielectric properties of single crystals has generated a lot of academic interest[65] which can throw light into the intrinsic dielectric loss factor of crystals. The dielectric properties of some of the polycrystalline ceramics like alumina and titania were studied at subzero temperatures[66]. However, not much work has been done on the low temperature behaviour of BMT ceramics.

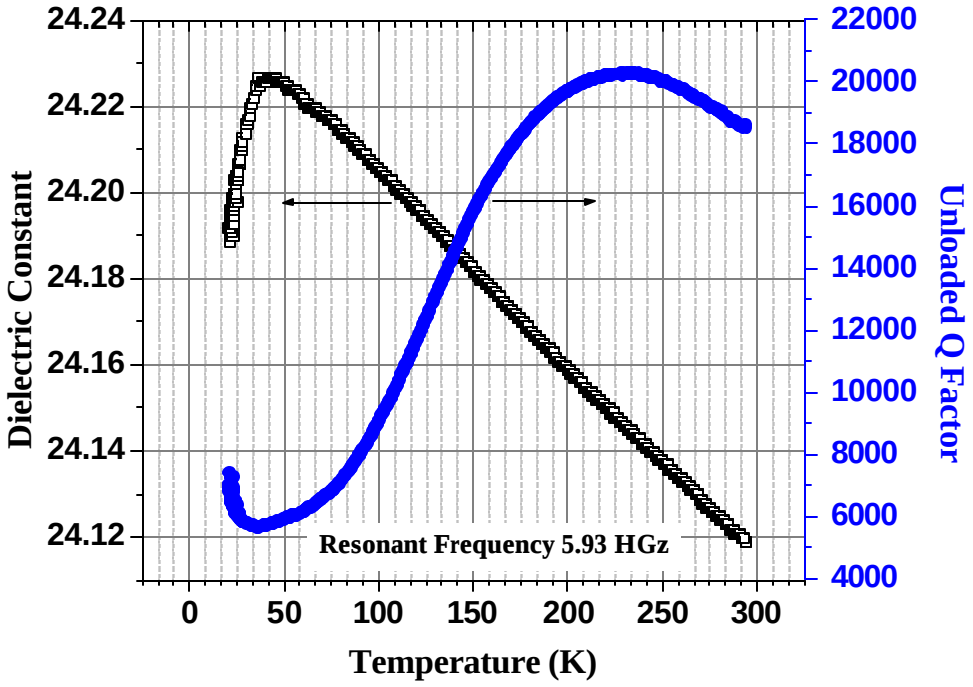

Fig. 4. 15 Variation of the dielectric constant and quality factor of pure BMT sintered at 1625°C (unannealed)

In an ideal crystal the main reason for dielectric loss at microwave frequency is due to the interaction of the microwave field with the lattice vibration. Hence the quality factor increases at cryogenic temperature. The intrinsic Q factor of a low loss material is limited by the loss tangent of the dielectric which in turn depends on the unharmonicity terms in the potential energy term when a pair of atoms are at a mean separation[67]. The unharmonicity terms in the lattice vibrational energy term of a dielectric decrease with decrease in temperature in accordance with second low of thermodynamics. The frequency dependence of dielectric loss tangent is given by[68]

$$\tan\delta = \frac{\omega\gamma}{\omega_T^2} \tag{4.1}$$

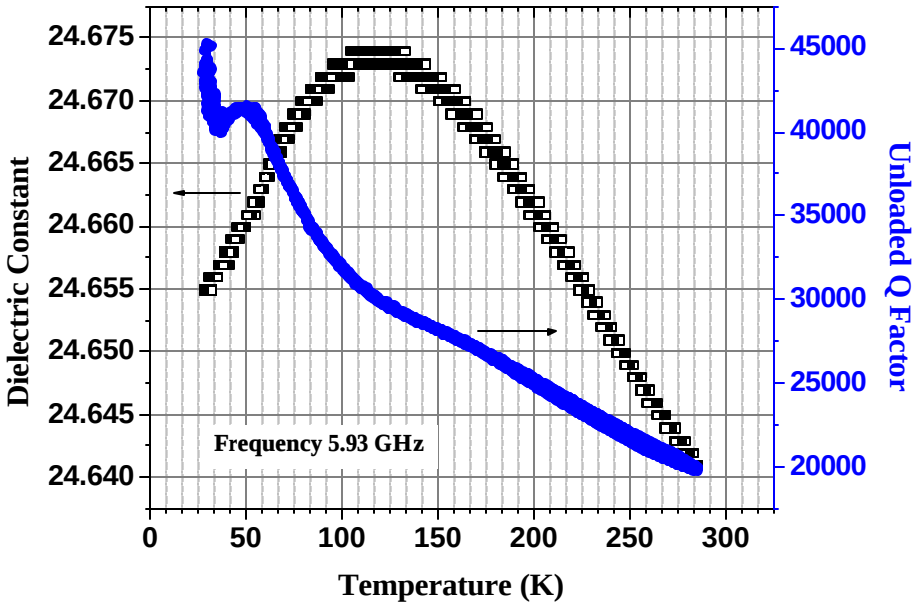

Fig. 4. 16 Variation of dielectric constant and quality factor of BMT doped with 0.5 mole % of $MnCO_3$ at cryogenic temperatures

where γ is the damping constant, ω_T is the resonant frequency of the optical mode of the lattice vibration, whose derivation is given in Chapter1, Section 1.3.1. The damping constant γ is proportional to the square of the third harmonic term and to temperature.

We have investigated the effect of the doping on the microwave dielectric properties of BMT cryogenic temperatures down to 20 K. Fig.4.15 represents the variation of dielectric constant and quality factor of unannealed BMT in the temperature range 20 K to 300 K. Here the dielectric loss of BMT increases with decrease of temperature due to the presence of paramagnetic impurities[69]. In addition to that an unannealed BMT sample may contain a lot of point defects like oxygen vacancies[70] which also decrease the quality factor at sub-zero temperatures. Fig. 4.20 represents the variation of dielectric constant and quality factor of BMT doped with 0.5 mole % of $MnCO_3$ at cryogenic temperatures. Doping with oxygen supplier like $MnCO_3$ annihilates the oxygen vacancies in the crystal and annealing increases the cation ordering in the crystal lattice of BMT. These combined effect of these two phenomena resulted in the increase of microwave quality factor as the temperature approaches absolute zero.

4. 4 CONCLUSIONS

- The structural and microwave dielectric property modifications in BMT as a result of doping with inorganic oxides is investigated in this chapter. The main objectives of this investigation were (i) to search for the best dopant which can improve the microwave dielectric properties of BMT, (ii) to probe the correlation between 1:2 structural order and dielectric loss complex perovskite (iii) to probe whether there exist any possible relationship between the microwave dielectric properties of BMT and the ionic radius of the dopant added and (iv) to study the variation of the dielectric properties of BMT at cryogenic temperature.
- BMT ceramic precursor was synthesized using solid state reaction technique. Dopants such as $MnCO_3$, NiO, ZnO, Co_3O_4, Al_2O_3, Ga_2O_3, Fe_2O_3, In_2O_3, Nd_2O_3, Bi_2O_3, TiO_2, SnO_2, ZrO_2, HfO_2, CeO_2, V_2O_5, Sb_2O_3, Nb_2O_5, WO_3 and MoO_3 were added to calcined precursor and sintered at 1625^oC for 4 hours. The sintered samples were annealed at 1450^oC to enhance the cation ordering. The phase evolution and unit cell properties of the doped samples are studied using powder diffraction method and the surface morphology of the sintered samples were

studied using scanning electron microscope. The dielectric properties of the sintered samples were characterized in the microwave frequency region.

- With the addition of dopants the optimized sintering temperature was reduced to 1625^{o}C. The microwave dielectric properties of pure BMT ceramic sintered at 1625 and annealed at 1450 for 40 hrs are e_r = 24.4, $Q_u$xf = 100,500 GHz and t_f= 8 ppm/^{o}C. With the addition of 0.1 mole % of the divalent impurity $MnCO_3$, the dielectric properties of BMT was improved to e_r = 26.72, $Q_u$xf = 162,800 GHz, and t_f = 6.3 ppm/^{o}C. The addition of tetravalent impurities bring about noticeable influence on the cation ordering of BMT ceramics. The cation ordering is poor (0.597) for BMT added with 0.5 mole % of ZrO_2 but the dielectric properties are appreciably higher (e_r = 25.29, $Q_u$xf = 162,500 GHz, and t_f= 4.5 ppm/^{o}C). The densification and dielectric properties of BMT is reaching their maximum values with Sb_2O_3 addition. The microwave dielectric properties of BMT when doped with 0.1 mole of Sb_2O_3 are given as e_r = 24.78, $Q_u$xf = 172,500 GHz, and t_f = 3.1 ppm/^{o}C. The addition of hexavalent impurities imparts better ordering in BMT due to the greater charge difference between B-site cation. The microwave dielectric properties of BMT doped with 0.5 mole % of WO_3 are e_r = 24.9, $Q_u$xf = 144,500 GHz, and t_f = 4.1 ppm/^{o}C.
- The microwave quality factor of the doped BMT ceramics show a proportionate dependence on the ordering of B-site cations except for tetravalent additives. For tetravalent dopants like ZrO_2, the high quality factor is observed even for samples with a lower ordering parameter.
- The average ionic radius of B-site cation of BMT (i.e. $Mg_{1/3}Ta_{2/3}$) is calculated as 0.653 Å. It is observed that when the ionic radii of the dopants are between 0.6 and 0.7 Å (i.e. close to the average ionic radii of the B-site ion in BMT) the quality factor touches maximum values.
- The quality factor of as sintered pure BMT decreases when the sample is cooled below 0 ^{o}C. On the other hand when Mn doped and annealed BMT is cooled to cryogenic temperatures, the unloaded quality factor increases.

4. 5 REFERENCES

1. S. Nomura, K. Toyama and K. Kaneta, *Jpn. J. Appl. Phys*., **21**, L 624–26 (1982)

2. S. Katayama, I. Yoshinaga, N. Yamada and T. Nagai, *J. Am. Ceram. Soc.*, **79**, 2059-64 (1996).

3. S. Nomura, *Ferroelectrics*, **49**, 61-70 (1983).

4. H. Matsumoto, H. Tamura and K. Wakino, *Jpn. J. Appl. Phys*., **30**, 2347-49 (1991).

5. K. H. Yoon, D. P. King and E. S. Kim, *J. Am. Ceram. Soc*., **77**, 1062-66 (1994).

6. E. S. Kim and K.H. Yoon, *J. Mater. Sci.*, **29**, 830-34 (1994).

7. G. Rong, N. Newman, B. Shaw and D. Cronin, *J. Mater.Res*., **14**, 4011-19 (1999).

8. S. Y. Cho, H. J. Yoon, K. S. Hong, I. T. Kim, and Y. H. Kim, *J. Mater. Res*., **12**, 1558-62 (1997)

9. X. M. Chen and Y. J. Wu, *J. Mater. Sci. Mater. Electron*., **7,** 369-73(1996).

10. L. Chai, M. A. Akbas, P. K. Davies and J. Parise, *Mater. Res. Bull*., **32**, 1261-69 (1997).

11 L. Chai and P. K. Davies, *Mater. Res. Bull*., **33**, 1283-92 (1998).

12. H. M. Shirey, *Low temperature Synthesis of the Microwave Dielectric Material, Barium Magnesium Tantalate (BMT)*, M.S. Thesis, University of Pittsburg, (2003).

13. M-H. Liang, C-T. Hu, C-G. Chiou, H-Y. Chang and I-N. Lin, *Ferroelectrics*, **231**, 691-96 (1999).

14. C-L. Huang, K-H. Chiang, S-C. Chuang, *Mater. Res. Bull.* (in press) (2004).

15. T. V. Kolodiazhnyi, A. Petric, G.P. Johari and A. G. Belous, *J. Eur. Ceram. Soc*., 22, 2013-21 (2002).

16. Y. Yang, D. Zhou, C. Huang and G. Qin, *J. Adv. Mater*., **31,** 8-11 (1999)

17. K. P. Surendran, Manoj Raama Varma , P. Mohanan and M. T. Sebastian, *Proc. National Conference on Recent Advances in Materials Processing (RAMP-2001*, Sept. 7-8, Annamalainagar, India (2001)

18. B. W. Hakki and P. D. Coleman, *IRE Trans. on Microwave Theory Tech*., **MTT-8**, 402-10 (1960).

19. W. E. Courtney, *IEEE Trans. on Microwave Theory Tech.*, **MTT-18**, 476-85 (1970).

20. J. Krupka, K. Derzakowski, B. Riddle and J. Baker-Jarvis, *Meas. Sci. Technol.*, **9**, 1751-56 (1998).

21. Q. Wang, H. Rushan and Z. Z. Gan, *J. Am. Ceram. Soc*., **75**, 2881-82 (1992).

22. A. D. Hilton, D. J. Barber, C. A. Randall and T. R. Shrout, *J. Mater. Sci.*, **25**, 3461- 66 (1990).

23. L. J. Lin, and T. B. Wu, *J. Am. Ceram. Soc*., **73**, 1253-56 (1990).

24. N. Setter and L. E. Cross, *J. Appl. Phys.*, **51**, 4356-60 (1980).

25. J. Chen, H.M. Chan and M. P. Harmer, *J. Am. Ceram. Soc*., **72**, 593-98 (1989).

26. C-C. Lee, C-C. Chou and D-S. Tsai, *J. Am. Ceram. Soc*., **80**, 2885- 90 (1997).

27. L. Dupont, L. Chai and P.K. Davies. *Mater. Res. Soc. Symp. Proc*., *Solid State Chemistry of Inorganic Materials-II,* **547,** 93-98 (1999).

28. Y. J. Wu and X. M. Chen, Mater. Sc. Engg. B, **100**, 244-47 (2003).

29. S. J. Penn and N. M. Alford, *High Dielectric Constant, Low Loss Dielectric Resonator Materials,* Final Report: EPSRC Grant GR/K-70649, EEIE, South Bank University, London (2000).

30. C. Binet, M. Daturi and J-C Lavalley, *Catalysis Today,* **50**, 207-25(1999)

31. S. Kawashima, *Am. Ceram. Soc. Bull*., 72, 120-26, (1993).

32. C. Yang, D. Zhou, C. Huang and G. Qin, *J. Adv. Mater.*, **31**, 8-11 (1998).

33. I. M. Reaney, P. L. Wise, I. Qazi, C. A. Miller, T. J. Price, D. S. Cannell, D. M. Iddles, M. J. Rosseinsky, S. M. Moussa, M. Bieringer, L. D. Noailles and R.M. Ibberson, *J. Eur. Ceram. Soc*., **23**, 3021-34 (2003).

34. S. J. Webb, J. Breeze, R. J. Scott, D. S. Cannell, D. M. Iddles and N. M. Alford, *J. Am. Ceram. Soc*., **85**, 1753-56 (2002).

35. A. Templeton, X. Wang, S. J. Penn, S. J. Webb, L. F. Cohen and N.

McN. Alford, *J. Am. Ceram. Soc*., **83**, 95-98 (2000).

36. J. Youn, K. S. Hong, and H. Kim, *J. Mater. Res.*, **12**, 589-92 (1997).

37. L. Chai, M. A. Akbas and Peter. K. Davies, *Proc. International Conference on Solid State Chemistry of Inorganic Materials*, p. 443-48, 2-5 Dec, Boston, (1996).

38. N. Santha, M. T. Sebastian, P. Mohanan, S. Kamba, J. Petzelt, N. M. Alford, R. C. Pullar, V. Sharma. *J. Am. Ceram. Soc*, **87,** 1233-37 (2004).

39. P. K. Davies, J. Tong and T. Negas, *J. Am. Ceram. Soc*., **80**, 1727-40 (1997).

40. S.-H. Ra and P. P. Phule, *J. Mater. Res*., **14**, 4259-65 (1999).

41. W-A. Lan, M-H. Liang, C-T. Hu, K-S Liu and I-N. Lin, *Mater. Chem. Phys*., **79**, 266-69 (2003).

42. F. S. Galasso and W. Darby, *J. Phys. Chem*., 66 (1962) 131-133

43. S. B. Desu and H. M. O'Bryan, *J. Am. Ceram. Soc*., **68**, 546-61 (1985).

44. Y. K. Kim, K. M. Lee and H.M. Jang, *J. Mater. Sci*., **35**, 4885-93 (2000).

45. E-S. Kim, J-B. Kim and K-H. Jo, *Ceram. Trans*., **32**, 231-40 (1993)

46. L-C. Tien, C-C. Chou and D-S. Tsai, *J. Am. Ceram. Soc.*, **83**, 2074–78 (2000).

47. J. H. Lee, Y. I. Jang, H. J. Youn, J. W. Jang and B. K. Kim, *J. Mater. Sci.*, **34**, 625-28 (1999).

48. K. H. Yoon, S. J. Yoo, W. S. Kim, J. B. Kim and E. S. Kim, *Jpn. J. Appl. Phys*., **38**, 5616-20 (1999).

49. M. F. Yan, *Solid State Sintering, Advances in Ceramics*, Ceramic Powder Science, (American Ceramic Society, Westerville, Ohio) **21**, p. 635-69 (1987).

50. X. Hu, X. M. Chen and Y. J. Wu, *Mater. Lett*., **54**, 279-83 (2002).

51. F. S. Galasso, *Perovskites and High Tc. Superconductors*, Gordon and Breach Scientific Publishers, New York, (1990).

52. H. Vincent, C. Perrier and M. Labeyrie, *Mater, Res. Bull.*, **28**, 951-58 (1993).

53. J. J. Lander, *Phase Diagram for Ceramics*, Edited by E. M. Levin, C. R. Robbins, H. F. McMurdie and M. K. Reser, (American Ceramic Society) p. 118 (1975).

54. H. Tamura, T. Konoike and S. Takehiro, *J. Am. Ceram. Soc*., **67**, C 59-61 (1984).

55. P. K. Davies, *Ceram. Trans*., **53**, 137-51 (1995).

56. S. J. Penn, N. M. Alford, A. Templeton, X. Wang, M. Xu, M. Reece and K. Schrapel, *J. Am. Ceram. Soc*., **80**, 1885-88 (1997).

57. M. K. Lee, J. H. Chung, K. W. Ryu and Y. H. Lee, *Proceedings of the 30th International Symposium on Electrical Insulating Materials*, Toyohashi, Japan, Sept.27-30 (1998).

58. E. L. Colla, I. M. Reaney and N. Setter, *Ferroelectric*s, 154, 1173-80 (1994).

59. M. W. Barsoum, *Fundamentals of Ceramics*, McGraw Hill, New York (2002).

60. W-A. Lan, M-H. Liang, C-T. Hu, K-S. Liu and I-N. Lin, *Mater. Chem. Phys*., **79**, 266-69 (2003).

61. C. H. Choi, S. Nahm. Y.W. Song *J. Kor. Phys. Soc.*, **35**, S410-S414 (1999).

62. Jonas P. Grigas, *Microwave Dielectric Spectroscopy of Ferroelectrics and Related Materials (Ferroelectricity & Related Phenomena S.* , Taylor & Francis, New Jersey (1996).

63. M. Thirumal, G. S. Murugan, K. B. R. Varma, A. K. Ganguli, *Mater. Res. Bull*., **35**, 2423–30 (2000).

64. Z.-Q. Tian, H.-X. Liu and H-T. Yu *Mater. Chem. Phys.*, **86**, 228-32 (2004).

65. V. Gurevich and A. K. Tagantsev, *Sov. Phys.JETP*, **64**, 142-151 (1986).

66. N. M. Alford, S. J. Penn, A. Templeton, X. Wang and S. Webb, *Proc. 9th World Ceramic Congress and Forum on New Materials (CIMTEC),* Florence, Italy, 14-19 June (1998).

67. V. B. Braginsky, V. S. Ilchenko, K. S. Bagdassarov, *Phys. Lett*., **120**, 300-05 (1987).

68. K. Wakino, M. Murata and H. Tamura, *J. Am. Ceram. Soc*., **69**, 34-37 (1986).

69. S. R. Stein, *Proceedings of the 29th Annual Frequency Control Symposium,* (Electronic Industries Association, Washington, D.C., p. 321-29, (1975).

70. K. Wakino and H. Tamura, *Ceram. Trans*., **15**, 305-14 (1990).

CHAPTER 5

EFFECT OF GLASS FLUXING IN $Ba(Mg_{1/3}Ta_{2/3})O_3$ CERAMICS

The liquid phase sintering of $Ba(Mg_{1/3}Ta_{2/3})O_3$ using glass additives such as B_2O_3, SiO_2, B_2O_3-SiO_2, ZnO-B_2O_3, 5ZnO-$2B_2O_3$, Al_2O_3-SiO_2, Na_2O-$2B_2O_3.10H_2O$, BaO-B_2O_3-SiO_2, MgO-B_2O_3-SiO_2, PbO-B_2O_3-SiO_2, ZnO-B_2O_3-SiO_2 and $2MgO$-$2Al_2O_3$-$5SiO_2$ is investigated in this Chapter. The aims of the research work on BMT with glass addition are (a) to reduce the preparation temperature of BMT and thereby the cost of production without any deterioration in the microwave dielectric properties, (b) to probe the relation between structural order and quality factor, (c) to suppress the formation of secondary phases such as barium tantalates which are detrimental to the microwave quality factor and (d) to improve the microwave dielectric properties of BMT. The influence of the above mentioned glasses on the phase structure, densification, cation ordering and microwave dielectric properties of BMT ceramics are discussed. The results of this investigation are useful for identifying the ideal liquid phase sintering medium in developing Low Temperature Co-fired Ceramics (LTCC) using BMT.

5. 1 INTRODUCTION

In producing miniaturized devices, ceramic multilayer structures with low sintering temperatures are needed because they can be co-fired with low-loss conductors like silver or copper. Low Temperature Co-fired Ceramic (LTCC) technology offers significant benefits over other established packaging technologies for high density, high RF and fast digital applications requiring hermetical packaging and good thermal management[1]. Many new ceramic-glass compositions[2] have recently been developed for microwave applications, especially low permittivity (ε_r) materials using alumina and suitable glass combinations, but also higher dielectric constant materials in the range 20–100 with low dielectric loss. As described in Chapter 3, Section 3.2, $Ba(Mg_{1/3}Ta_{2/3})O_3$ (abbreviated as BMT) has stimulated a surge of interest for their excellent dielectric properties. But the sintering temperature of these ceramics are above 1600 ^oC which pose practical difficulties for them to be used for LTCC applications which demands low temperature sintering between 850 and 950°C for co-firing with high conductivity metals.

A number of strategies have been worked out to reduce the sintering temperature of low loss materials like (a) chemical synthesis [3, 4, 5] (b) using starting powders with smaller particle size[6] and (c) liquid phase sintering [7] by adding low melting additive into the ceramic. As outlined in Chapter 3, Section 3.3.2, the chemical synthesis of BMT is not a suitable method for industrial production due to the complexity of the procedures involved, high cost of production and comparatively poor microwave dielectric properties[8]. Chen[9] et al. used NaF as the low melting additives for BMT which suppressed the formation of barium tantalate secondary phases, but the formation of Na_3TaO_4 on the surface has to be controlled to ensure the formation of completely ordered $Ba(Mg_{1/3}Ta_{2/3})O_3$. Boric oxide and copper oxide are the well-known liquid phase sintering promoters. But there are reports[2] that multi-component glasses are more effective than single component glass to reduce the sintering temperature of ceramics without considerably damaging the physical properties of the matrix. Recent research trends suggest that glass addition is a useful tool for producing low loss ceramics like [10,11]$(Zr,Sn)TiO_4$, [12,13,14]$Ba_2Ti_9O_{20}$, [15,16,17]$BaTi_4O_9$ and [18,19,20]$(Mg_{0.5}Ca_{0.5})TiO_3$ at relatively low temperatures of sintering. As an initial study on the interaction of a glass flux with complex perovskite $Ba(Mg_{1/3}Ta_{2/3})O_3$ ceramic, Cheng et al.[21,22] observed that adding

MgO-CaO-Al_2O_3-SiO_2 (MCAS) glass to BMT decreased the sintering temperature down to 1300 ^oC but the $Q_u$xf value has been considerably lowered (9700 GHz) which cannot be afforded in industrial production. In a recent research report Pollet et al.[23] suggested that a combination of B_2O_3 and $LiNbO_3$ can act as a good medium for liquid phase sintering in BMT but the densification (< 95 %) and quality factor are not good for applications in multilayer devices. So the search for the right glass composition which aids the vitreous sintering of fully ordered BMT without affecting the low loss quality of the ceramic is a highly challenging problem in microwave ceramics.

After conducting a detailed investigation on the dielectric properties of glasses at ultra-high frequencies, Navias et al.[24] noted that the dielectric losses of borosilicate glasses are comparatively lower than alkali containing glasses. This is due to the fact that in the latter, alkali ions which are weakly held in the glassy network, absorb energy and eventually give rise to dielectric loss. On the other hand, borosilicate glasses [25, 25] have continuous atomic structures, with SiO_4 and BO_3 configurations joined to form (-Si-O-B-O-) linkages, will have high electrical resistance and low dielectric loss. In a recent study[26], the microwave dielectric properties of a few borosilicate glasses (BaO-B_2O_3-SiO_2, PbO-B_2O_3-SiO_2 and ZnO-B_2O_3-SiO_2) have been reported in which it was observed that the t_f of all these glasses are negative. As cited above, a large number of papers were published on the interaction of glasses with low loss microwave dielectrics. But the vitreous phase densification and dielectric loss aspects of silicate/borate and borosilicate glasses in complex perovskites such as $Ba(Mg_{1/3}Ta_{2/3})O_3$ which can provide useful information to research on LTCC materials, has not been discussed before. Hence we have carried out a comprehensive investigation on the liquid phase sintering effects in BMT using a number of glass systems such as B_2O_3, SiO_2, B_2O_3-SiO_2, ZnO-B_2O_3, $5ZnO$-$2B_2O_3$, Al_2O_3-SiO_2, Na_2O-$2B_2O_3.10H_2O$, BaO-B_2O_3-SiO_2, MgO-B_2O_3-SiO_2, PbO-B_2O_3-SiO_2, ZnO-B_2O_3-SiO_2 and $2MgO$-$2Al_2O_3$-$5SiO_2$ in an effort to find out an ideal glass system which promotes liquid phase sintering without deteriorating the microwave dielectric properties. The aims of the research work on BMT with glass addition are (a) to reduce the preparation temperature of BMT and thereby the cost of production without any deterioration in the microwave dielectric properties, (b) to probe the relation between structural order and quality factor, (c) to suppress the formation of secondary phases such

as barium tantalates which are detrimental to the microwave quality factor and (d) to improve the microwave dielectric properties of BMT. The influence of the above mentioned glasses on the phase structure, densification, cation ordering and microwave dielectric properties of BMT ceramics are discussed.

5. 2 EXPERIMENTAL

The glass powders used in this investigation were divided into three category : [i] Primary Glasses such as B_2O_3 (abbreviated as B), SiO_2 (S) [ii] Binary Glasses such as B_2O_3-SiO_2 (BS), ZnO-B_2O_3 (ZB), $5ZnO$-$2B_2O_3$ (5Z2B), Al_2O_3-SiO_2 (AS), Na_2O-B_2O_3 (NB), and [iii] Ternary Glasses such as BaO-B_2O_3-SiO_2 (BBS), MgO-B_2O_3-SiO_2 (MBS), PbO-B_2O_3-SiO_2 (PBS), ZnO-B_2O_3-SiO_2 (ZBS) and $2MgO$-Al_2O_3-$5SiO_2$ (MAL). For synthesizing glasses, high purity (99.9 %) oxides/carbonates were weighed stoichiometrically and mixed for two hours in an agate mortar with pestle using deionised water as the medium. It was then melted in a platinum crucible above their deformation temperature (see Table 5.1), quenched and powdered. The formation of the glass was confirmed using powder diffraction method. To measure the dielectric properties of the glasses, the powders were added with PVA binder, compacted uniaxially to form thin cylindrical pucks with 14 mm diameter and 1 mm thickness at a pressure of 100 MPa and were sintered at temperatures less than their respective deformation points (see Table 5.1). The polished thin pellets were electroded by coating silver on both sides in the form of ceramic capacitors and were used for dielectric measurements at low frequencies (50Hz-13MHz) using an impedance analyzer (HP 4102 A - LF).

The $Ba(Mg_{1/3}Ta_{2/3})O_3$ precursor was prepared through the conventional solid state ceramic technique as described in Chapter. 2, Sections 2.1.2.1 to 2.1.2.7. The calcination temperature was 1200^{o}C for 10 hours with intermediate grinding. The calcined powder was then mixed with different weight percentages of the glass and ground for 2 hours. The green density of the uniaxially pressed glass added ceramic pucks were measured using dimensional method. These compacts were sintered in the temperature range 1300-1500^{o}C for 4 hours in air at a heating rate of 10^{o}C/hour. The sintered samples were then cooled to 800^{o}C at a slow rate of 60^{o}C per hour to enhance cation ordering. The sintering temperature is optimized for each glass ceramic compositions. The bulk density of the

sintered samples were measured using Archimedes method. The powdered samples were used for analyzing the X-ray diffraction patterns using CuK_α radiation (Philips X-Ray Diffractometer). The sintered samples were thermally etched for 30 minutes at a temperature of about 25 ^oC below the sintering temperature and the surface morphology was studied using a scanning electron microscope Hitachi SEM Model No. S-4300.

Table 5.1 Properties of glasses

Glass code	Composition (approx.) (mole %)	Density (g/cm^3)	Softening Temp. (^oC)	ε_r	Tan d (at Frequency)	Ref
B	99:B_2O_3	2.46	450	2.47	5.5 x10^{-3}(1MHz)	51
S	99:SiO_2	2.60	1600	3.7	4.0 x10^{-4} (1 MHz)	31
BS	40:B_2O_3, 60:SiO_2	2.23	820	4.6	9.0 x10^{-4} (1 MHz)	51
ZB	50:ZnO, 50:B_2O_3	3.61	610	6.9	9.4 x10^{-3} (16 GHz)	27
5Z2B	71:ZnO, 29:B_2O_3	2.19	567	4.21	3.3 x10^{-3}(1MHz)	51
AS	50:Al_2O_3, 50:SiO_2	2.60	850	8.06	9.7x10^{-3}(1MHz)	51
NB	8:Na_2O, 15:B_2O_3, 77:H_2O	2.80	75	10.2	2.1 x10^{-1}(1MHz)	51
BBS	30:BaO, 60:B_2O_3, 10:SiO_2	3.40	627	7.2	4.4 x10^{-3} (15 GHz)	27
MBS	40:MgO, 40:B_2O_3, 20:SiO_2	3.18	950	5.01	2.3 x10^{-3}(1MHz)	51
PBS	40:PbO, 40:B_2O_3, 20:SiO_2	4.31	448	12.9	7.1x10^{-3} (12GHz)	27
ZBS	60:ZnO, 30:B_2O_3, 10:SiO_2	3.60	582	7.5	10.7 x10^{-3}(15GHz)	27
MAS	22.:MgO, 22:Al_2O_3, 6:SiO_2	2.30	1350	4.5	7.0 x10^{-4}(1MHz)	52

The dielectric properties ε_r and τ_f of the materials were measured in the microwave frequency range using resonance technique[27, 28, 29] as described Chapter 2, Sections 2.2.2 to 2.2.5.

5. 3 RESULTS AND DISCUSSION

5. 3. 1 Densification

The dielectric properties of most of the ternary glasses we used in this investigation have been reported [25, 30] earlier and hence we synthesized those compositions, which exhibited relatively better dielectric properties at microwave frequencies. Very recently, Cheng[31] et al. made a remarkable observation that the reactivity and wettability of sol-gel derived glasses were inferior to quenched ones. Hence in this investigation, quenched glass compositions were used. Table 5.1 gives the physical and electrical properties of the glasses used. The major problem with the solid state sintering of BMT is that the

sintering temperature of this ceramic is above 1600 ^{o}C and long time annealing upto several days is needed for achieving ordered phase of BMT. This results in two effects:

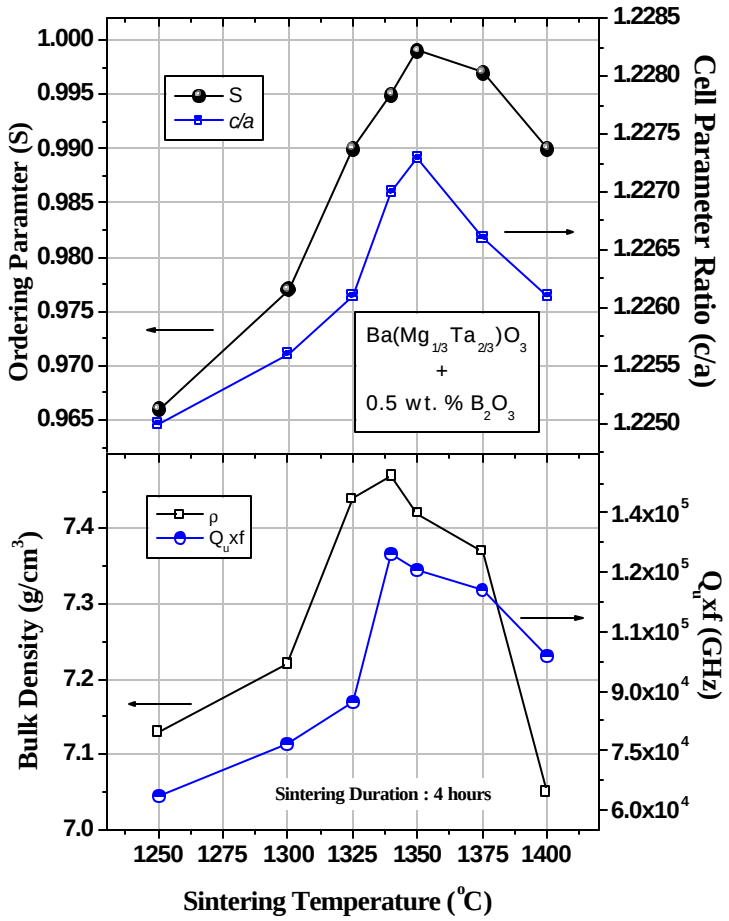

Fig.5. 1 The variation of bulk density, quality factor, cation ordering and unit cell parameter ratio of $Ba(Mg_{1/3}Ta_{2/3})O_3$ added with 0.5 wt. % of B_2O_3 with sintering temperature

(a) The particle coarsening and consequent generation of porosity occurs when the ceramic is heat treated at high temperatures for long periods of time which is detrimental to the microwave dielectric properties of the sintered ceramic and (b) secondly the volatilization of the Mg^{2+} ions occurs which results in the formation of low Q secondary phases such as $BaTa_2O_6$ and $Ba_5Ta_4O_{15}$ which too is undesirable[32]. So for obvious reasons, the low temperature sintering of low loss BMT ceramic is of high importance, which can be achieved through vitreous phase sintering. But excess addition of glass has

been proved to increase the dielectric loss quality of the ceramic, nonetheless a reduction in the sintering temperature.

Table 5. 2 Sintering, densification and unit cell properties of $Ba(Mg_{1/3}Ta_{2/3})O_3$ fluxed with Primary Glasses

BMT + Glass	Wt. % of Additive	Sinter. Temp. (°C)	Green Density (g/cm^3)	Theor. Density (g/cm^3)	Axial Shrinkage	Radial Shrinkage	Sintered Density (g/cm^3)	c/a
	0.1	1375	4.974	7.609	72.3	82.2	7.480	1.2272
	0.2	1350	4.984	7.593	72.6	82.5	7.510	1.2268
B_2O_3	0.5	1350	4.981	7.546	72.0	81.6	7.441	1.2273
	1.0	1325	4.992	7.469	72.0	82.1	7.440	1.2270
	2.0	1300	4.989	7.323	74.2	83.4	7.200	1.2271
	0.1	1500	4.452	7.619	73.1	83.7	7.390	1.2257
	0.2	1475	4.447	7.595	74.1	83.3	7.380	1.2251
SiO_2	0.5	1460	4.436	7.552	74.5	84.6	7.301	1.2248
	1.0	1450	4.431	7.482	74.8	85.3	7.225	1.2246
	2.0	1450	4.430	7.396	75.1	86.8	7.015	1.2241

It has been observed that introducing a glassy material into matrix plays a pivotal role in controlling the phase evolution and densification phenomena in BMT. As a typical case, the behavior of sintered density and microwave quality factors of BMT mixed with 0.5 wt.% B_2O_3 as a function of sintering temperature is presented in Fig. 5.1. The bulk density increased with sintering temperature, reached a maximum (7.47 g/cm^3) at 1340 ^oC and then decreased with further increase in temperature. At low sintering temperatures, the microwave quality factors were lower due to poor densification and the formation of a number of additional phases. As the sintering temperature rose from 1250 to 1340^oC, the value of $Q_u$xf was improved from 63,500 GHz to 124,700 GHz. Increasing the sintering temperature above 1350^oC resulted in grain growth which was proved to be detrimental to the dielectric properties. The $Q_u$xf decreased when sintered above 1350^oC.

The effect of primary, secondary and ternary glasses on the processing temperature, densification and lattice parameters of BMT are given in Tables 5.2, 5.3 and 5.4. In this investigation it has been observed that addition of primary glasses like B_2O_3 up to 2 wt % can bring down the sintering temperature from 1625 to 1300^oC without appreciable deterioration in the microwave dielectric properties. The addition of silica glass did not result in appreciable lowering of the sintering temperature (see Table 5.2) may be due to the high melting point of SiO_2 (1600^oC). Moreover, doping of SiO_2 to a

ceramic matrix may promote anomalous grain growth[33] which would result in porosity. In Sodium Borate Glass, the basic structure contains chains of interlocking $BO_2(OH)$ triangles and $BO_3(OH)$ tetrahedrons bonded to chains of sodium and water octahedrons (Table 5.3). Since the alkali ions are weakly held in the glassy network[34], its melting point is the lowest (75°C) among the glass systems we have studied. Hence the fluxing of BMT with sodium borate glass lowers the temperature to 1300°C. However it could not help in densifying the BMT ceramics may be because of its poor solubility in this glass. On the other hand in ternary glasses, it is generally agreed that large metal ions are held more firmly in the glass network [25]. The addition of ternary glasses did not reduce the sintering temperature to values less than 1300°C (Table 5.4).

Table 5. 3 Sintering, densification and unit cell properties of $Ba(Mg_{1/3}Ta_{2/3})O_3$ fluxed with Binary Glasses

BMT + Glass	Wt. % of Additive	Sinter. Temp. (°C)	Theor. Density (g/cm^3)	Green Density (g/cm^3)	% Axial Shrinkage	% Radial Shrinkage	Sintered Density (g/cm^3)	c/a
	0.1	1370	7.597	4.484	73.0	82.2	7.394	1.2256
	0.2	1360	7.588	4.480	72.8	82.5	7.395	1.2252
BS	0.5	1360	7.534	4.522	72.7	81.6	7.350	1.2253
	1.0	1350	7.449	4.472	73.3	81.9	7.330	1.2251
	2.0	1340	7.284	4/470	73.7	83.5	7.281	1.2252
	0.1	1420	7.617	4.823	72.1	82.7	7.429	1.2267
	0.2	1410	7.608	4.864	72.0	82.0	7.452	1.2267
ZB	0.5	1410	7.583	4.855	72.5	82.6	7.444	1.2264
	1.0	1400	7.542	4.847	72.6	82.2	7.431	1.2256
	2.0	1375	7.462	4.825	74.2	85.3	7.421	1.2255
	0.1	1400	7.606	4.872	73.3	82.8	7.438	1.2270
	0.2	1375	7.587	4.877	73.0	82.7	7.465	1.2271
5Z2B	0.5	1360	7.532	4.868	72.5	82.5	7.496	1.2269
	1.0	1350	7.442	4.861	71.3	82.4	7.442	1.2272
	2.0	1330	7.271	4.862	71.5	82.4	7.270	1.2263
	0.1	1475	7.610	4.751	73.5	83.5	7.417	1.2256
	0.2	1450	7.596	4.727	73.4	83.5	7.366	1.2255
AS	0.5	1440	7.552	4.732	73.5	84.7	7.285	1.2252
	1.0	1425	7.482	4.741	72.8	85.1	7.260	1.2253
	2.0	1420	7.347	4.740	71.5	86.6	7.157	1.2247
	0.1	1350	7.612	4.261	72.5	82.2	7.414	1.2252
	0.2	1325	7.599	4.272	72.4	82.0	7.302	1.2248
NB	0.5	1320	7.560	4.252	73.2	82.3	7.210	1.2241
	1.0	1310	7.497	4.248	73.7	82.9	7.070	1.2239
	2.0	1300	7.376	4.246	74.4	83.3	6.893	1.2220

The theoretical density (D) of the BMT-Glass ceramics is calculated using the following equation :

$$D_{th} = \frac{W_1 + W_2}{\left[\frac{W_1}{D_1} + \frac{W_2}{D_2}\right]} \quad (5.1)$$

where W_1 and W_2 are the weight percentage of the BMT matrix and glass with densities D_1 and D_2 in the mixture respectively. The theoretical density of undoped BMT was calculated as 7.625 g/cm^3 using powder diffraction pattern of the sample sintered at 1650^{o}C and annealed at 1450^{o}C for 40 hours. The green and sintered densities of various glass added ceramic samples were given in Table 5. 2, 5. 3 and 5. 4. A comparative study

Table 5. 4 Sintering, densification and unit cell properties of $Ba(Mg_{1/3}Ta_{2/3})O_3$ fluxed with Ternary Glasses

BMT + Glass	Wt. % of Additive	Sintering Temp. (^{o}C)	Theor. Density (g/cm^3)	Green Density (g/cm^3)	Axial Shrinkage	Radial Shrinkage	Sintered Density (g/cm^3)	c/a
	0.1	1390	7.615	4.414	72.3	82.5	7.402	1.2275
	0.2	1390	7.606	4.405	72.3	82.2	7.427	1.2266
BBS	0.5	1380	7.578	4.395	72.7	81.3	7.424	1.2267
	1.0	1375	7.532	4.385	73.6	83.0	7.413	1.2267
	2.0	1350	7.444	4.392	74.6	83.3	7.402	1.2262
	0.1	1460	7.614	4.195	72.4	83.8	7.401	1.2278
	0.2	1430	7.606	4.202	72.3	83.6	7.419	1.2277
MBS	0.5	1425	7.572	4.203	71.9	83.9	7.421	1.2274
	1.0	1425	7.521	4.198	72.9	82.6	7.426	1.2277
	2.0	1410	7.422	4.196	74.3	85.2	7.312	1.2272
	0.1	1410	7.619	5.050	72.9	83.4	7.411	1.2253
	0.2	1375	7.613	5.041	73.0	83.6	7.400	1.2262
PBS	0.5	1335	7.596	5.124	72.4	83.8	7.381	1.2261
	1.0	1325	7.567	5.109	73.2	82.5	7.300	1.2268
	2.0	1300	7.511	5.104	73.5	82.7	7.224	1.2252
	0.1	1375	7.616	4.277	71.6	82.3	7.399	1.2264
	0.2	1360	7.608	4.338	70.5	81.5	7.485	1.2265
ZBS	0.5	1335	7.583	4.361	72.3	82.4	7.484	1.2267
	1.0	1335	7.542	4.331	72.2	83.6	7.447	1.2270
	2.0	1330	7.461	4.361	73.4	83.7	7.403	1.2257
	0.1	1450	7.608	4.056	74.5	83.2	7.389	1.2253
MAS	0.2	1435	7.589	4.158	74.7	82.4	7.341	1.2243
	0.5	1425	7.538	4.209	75.4	83.2	7.224	1.2244
	1.0	1410	7.454	4.201	75.7	83.3	7.152	1.2239
	2.0	1410	7.294	4.216	75.9	83.5	7.003	1.2241

of the variation of green density with respect to additives revealed that maximum green density (above 65 % of their respective theoretical densities) is observed for BMT doped with PbO-B_2O_3-SiO_2 glass which on sintering, resulted in a final densification of about

97 % of their theoretical densities. Doping with zinc borate glasses (ZnO-B_2O_3, $5ZnO$-$2B_2O_3$) also showed good green densities. The sintered density is maximum (98.7 %) for 0.2 wt % B_2O_3 added ceramic. It should be noted that it is difficult to densify BMT more than 97 % by conventional methods without the help of suitable dopants. It is well known that low contact angle, low dihedral angle and high solubility of the solid in the liquid are essential for achieving high sintered density in glass added materials. In such cases, the transient glassy phase formed at a lower temperature would act as a short circuit medium for grain to grain materials transport[35]. The primary glass B_2O_3 is regarded as a typical glass network former that has a lower glass transition temperature[36]. It is generally agreed that a non-wetting glassy network leads to porosity and hence the densification will be lower if the solubility of the ceramic in the liquid phase is poor. This could be the reason behind the poor densification of SiO_2, Na_2O-$2B_2O_3$.$10H_2O$ and $2MgO$-$2Al_2O_3$-$5SiO_2$. The percentage shrinkage along the axial and radial directions is defined as

$$\text{Percentage shrinkage} = \frac{Sintered \quad dimension \quad \text{x} \quad 100}{Green \quad dimension} \tag{5.2}$$

which is given in Tables 5.2, 5.3 and 5.4. It is expected that during sintering, the shrinkage along the axial component is more than that along the radial component. This is due to the gravitational effects which are more pronounced during liquid phase sintering[37]. In liquid phase sintering the densification occurs through the enhanced rearrangement of particles through low viscous liquid and eventually removes pores in the solid bodies. The evolution of the densification from green to sintered ceramic can be studied using a densification factor (DF) which is given by[38]

$$\text{DF} = \frac{D_m - D_g}{D_{Th} - D_g} \tag{5.3}$$

where D_m is the measured sintered density, D_g the green density of the pressed compact, and D_{th} the theoretical density calculated by the mixing rule (Eq. 5.1). Fig. 5.2 shows the

variation of the densification factor as a function of the weight percentages of primary, binary and ternary glass additives in BMT. For primary glass additive B_2O_3, the DF

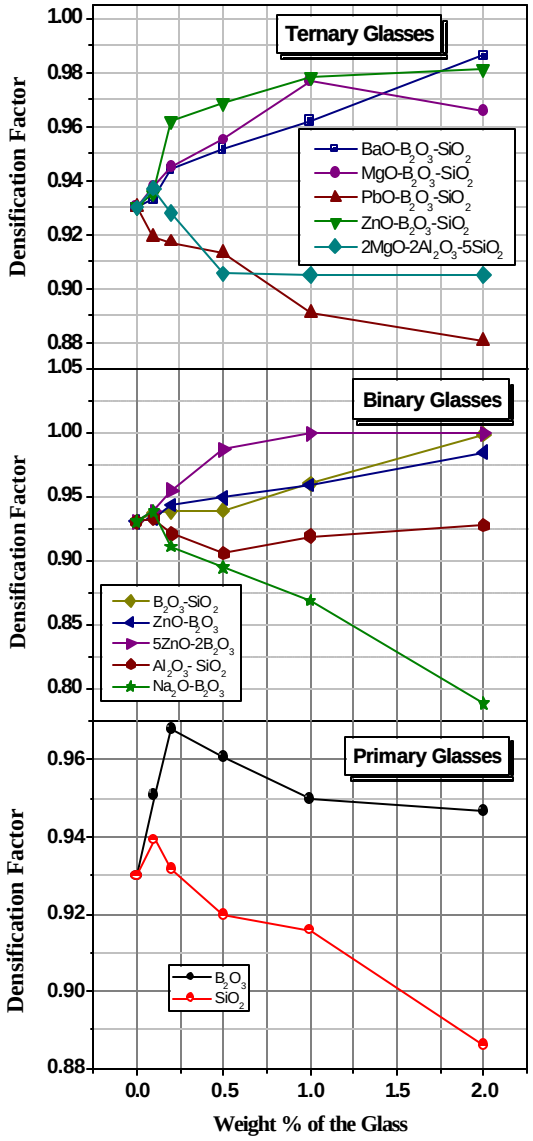

Fig. 5. 2 The variation of the densification factor (DF) as a function of the weight % of the glass additives in primary, binary and ternary glasses

increases first to 0.968 (for 0.2 wt. % B_2O_3) from 0.93 (undoped BMT) and then decreased to 0.946 with higher additive concentration (for 2 wt. % B_2O_3). On the other hand, the DF decreased with the SiO_2 addition. For zinc borate and borosilicate glasses the densification factor increases while it decreased on aluminosilicate glass addition up

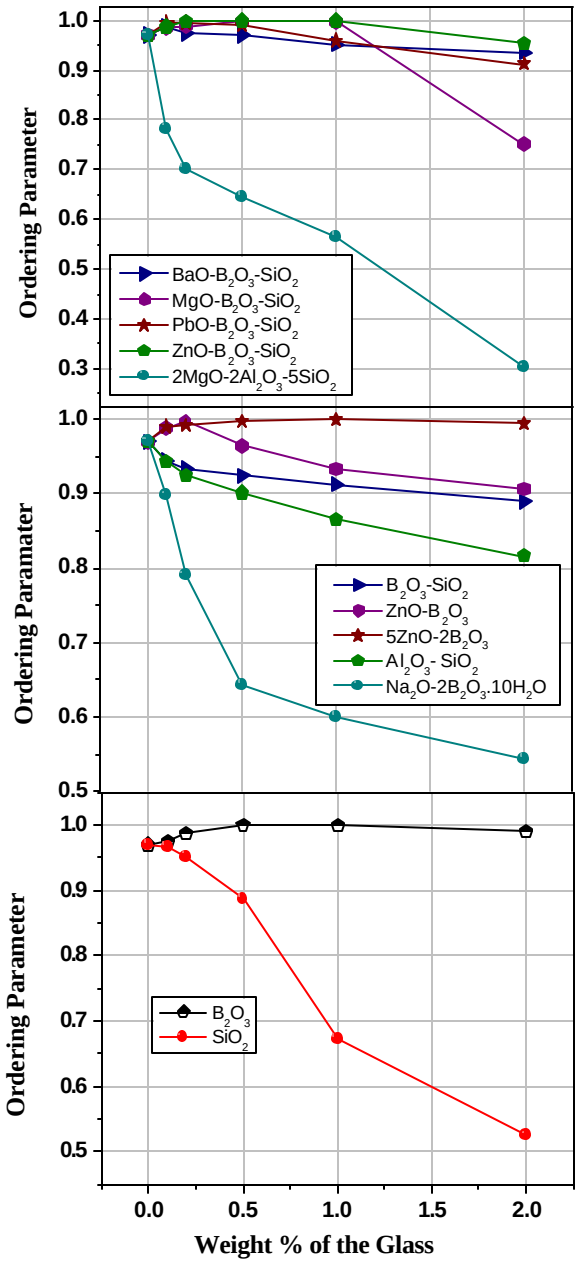

Fig. 5. 3 The variation of the cation ordering parameter (S) as a function of the weight % of the glass additives in primary, binary and ternary glasses

to 0.5 wt % and then increases thereafter. A monotonous decrease of densification factor was observed for alkali borate glass addition. With exceptions of $PbO\text{-}B_2O_3\text{-}SiO_2$ and $2MgO\text{-}2Al_2O_3\text{-}5SiO_2$, the densification factor increased with additive concentrations

(Fig. 2). Being a function of green density, slight errors in the measurement of green density can reflect in the calculated values of densification factor. So the anomalous variation of densification factor in the case of some glass additives need not always represent the sinterability of the glass ceramic. But generally DF can be considered as a tool to test the wettability of the glass with the ceramic.

5. 3. 2 X-Ray Diffraction Analysis

It is known that BMT can exist in ordered and disordered forms. In the high-temperature disordered phase, the Mg^{2+} and Ta^{5+} cations are randomly distributed on octahedral sites of the perovskite subcell which raises the symmetry of the system to cubic (cubic space group *Pm3m*). The ordering increases with the long time annealing. In the low-temperature ordered form (trigonal space group $P\bar{3}m1$) the Mg^{2+} and Ta^{5+} cations are distributed on individual (111) planes of the perovskite subcell with alternating {Mg, Ta, Ta} layers. This is the 1:2 ordered configuration with the ordered phase is having a hexagonal superstructure. Prolonged annealing results in the expansion of the units cell along the (111) direction so that the unit cell parameter ratio (*c/a*) has a value greater than √(3/2) = (1.2247). To quantitatively examine the degree of ordering, Matsumoto[39] et al. originally defined the ordering parameter for BMT using the following equation

$$S = \sqrt{\frac{(I_{(100)} / I_{(110),(102)})_{observed}}{(I_{(100)} / I_{(110),(102)})_{theoretical}}} \qquad (5.4)$$

The theoretical value of the ratio of the integral intensity of super structural reflection line (100) to that of (110,102) line, $(I_{100} / I_{110,102})_{theoreticd}$ is 8.3 %. This value was modified to 6.2 % by Youn [40] et al. and the ordering parameters reported in this paper are calculated using the equation

$$S = \sqrt{\frac{28.13 \times I_{(100)} / I_{(110),(102)}}{1.814 - I_{(100)} / I_{(110),(102)}}} \qquad (5.5)$$

Several authors[41,53] determined the cation ordering parameters in BMT by calculating the ratio of intensities of (100) super structure line and the fundamental reflection line (110, 102) by using Eqs. (5.4) and (5.5). Since the intensity of the ordering reflection line (100) is proportional to the difference in atomic scattering factors of Mg and Ta in complex perovskite BMT their intensities may be relatively lower. The ratio of the unit cell parameters (*c/a*) of BMT added with primary, binary and ternary glass systems are given in Tables 5.2, 5.3 and 5.4. This investigation gave no evidence about the substitution of Zn, Al etc. ions from the glass at the Mg site in $Ba(Mg_{1/3}Ta_{2/3})O_3$. However the X-ray diffraction study cannot reveal any useful information when the substitution level is very small. But it has been revealed that certain glasses can control the order-disorder phase transformation of BMT. The variation of the cation ordering parameter (S) with concentration of the glass addition is given in Fig. 5.3. The addition of 0.5 wt. % B_2O_3 increases the ordering parameter from 0.970 (undoped BMT) to 0.999. The ordering decreases to 0.991 on 2 wt. % B_2O_3 glass addition. On the other hand the cation ordering was severely damaged with SiO_2 addition. The *c/a* ratio also followed a trend similar to cation ordering parameter with glass incorporation (see Tables 5.2, 5.3 and 5.4). For B_2O_3-SiO_2, Al_2O_3-SiO_2 and Na_2O-$2B_2O_3.10H_2O$ the ordering parameters decreased with glass addition, while for zinc borate glasses, (ZnO-B_2O_3 and $5ZnO$-$2B_2O_3$) the cation ordering increased for small amount of glass content and the decreased with higher concentration. In the case of ternary glass systems, except BaO-B_2O_3-SiO_2 and $2MgO$-$2Al_2O_3$-$5SiO_2$ the cation ordering of BMT increased with an increase in glass content up to 1 wt. % and then decreased (Fig. 5. 3).

As discussed in Chapter 3, Section 3. 2. 4, a number of investigators established [42, 43] that formation of satellite secondary phases such as $Ba_5Ta_4O_{15}$, $Ba_4Ta_2O_9$, $BaTa_2O_6$ etc. during solid state synthesis of BMT, are detrimental to its densification, cation ordering and microwave dielectric properties. Fig. 5. 4 shows the powder diffraction profiles of 0.5 wt % B_2O_3 added BMT calcined at 1200 ^oC and sintered at temperatures 1250, 1300, 1325, 1340, 1350, 1375 and 1400 ^oC. Many investigators analyzed the solid state reaction mechanism of BMT which is reported to be highly complex. Fang[44] et al. reported that $BaTa_2O_6$ and $Ba_4Ta_2O_9$ are the two intermediate phase resulting from the reaction between $BaCO_3$ and Ta_2O_5. In principle, they on reaction with MgO forms the

desired end compound $Ba(Mg_{1/3}Ta_{2/3})O_3$. However in a previous report the same authors cautioned [45] that there are chances when these two intermediates react each other to form $Ba_5Ta_4O_{15}$ and $Ba_7Ta_6O_{22}$. From $Ba_5Ta_4O_{15}$ and $Ba_7Ta_6O_{22}$, it is very difficult to form BMT because the reactants are stable even at high temperature and the reaction needs to occur through a solid

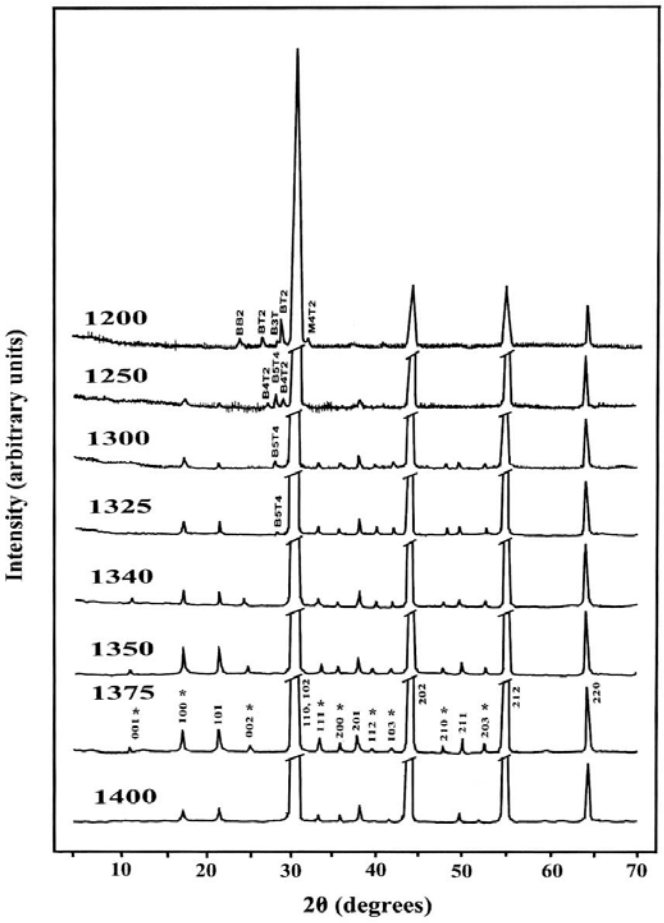

Fig. 5. 4 Powder diffraction patterns of $Ba(Mg_{1/3}Ta_{2/3})O_3$ doped with 0.5 wt % of B_2O_3 glass at various sintering temperatures. (* represent superstructure reflections) The abbreviations stand for BB2-BaB_2O_4, BT2-$BaTa_2O_6$, M4T2-$Mg_4Ta_2O_9$, B3T-$Ba_3TaO_{5.5}$, B4T2-$Ba_4Ta_2O_9$, B5T4-$Ba_5Ta_4O_{15}$

state diffusion process. The mechanism for these reactions is not clear; however, it is reasonable to assume that they have to make contact with MgO to form BMT by long-distance diffusion. If these two compounds are formed in the precursor powder during the calcination processes, they will maintain growth during sintering and finally present as secondary phases in the sintered body.

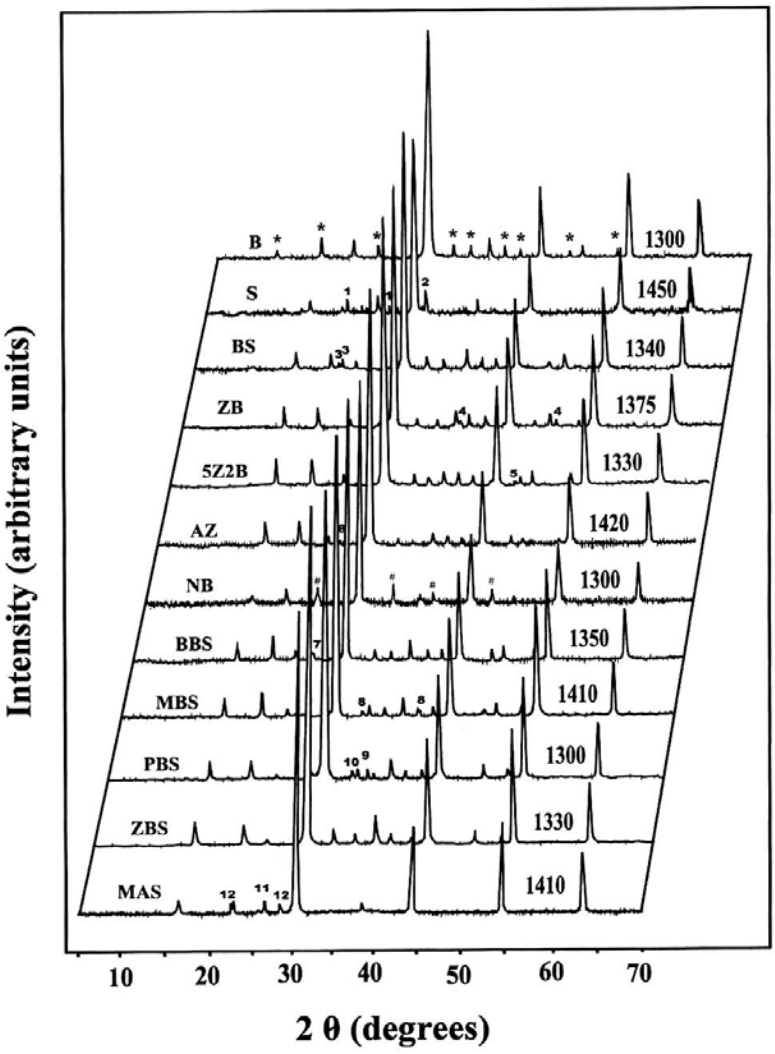

Fig. 5. 5 Powder diffraction pattern of $Ba(Mg_{1/3}Ta_{2/3})O_3$ doped with 2 wt. % of various glasses. (* represent superstructure reflections and # represent unknown peaks) The peak numbers stands for 1- $Ba_3Si_5O_{13}$, 2- $MgSiO_3$, 3- B_2SiO_5, 4- $Zn(BO_2)_2$, 5- ß-$Zn_5B_4O_{11}$,6-Al_2SiO_5, 7- $Ba_3B_6Si_{12}O_{16}$, 8- $Mg_3(BO_3)_2$, 9- $Pb_5Si_2O_7$, 10-PbB_4O_7, 11-$BaMgSi_4O_{10}$, 12-$Mg_2Al_4Si_5O_{18}$

The XRD pattern recorded from samples sintered at 1200^oC suggested that with addition of 0.5 wt. % B_2O_3 into the matrix, satellite phases such as $BaTa_2O_6$, $Ba_3TaO_{5.5}$ and $Mg_4Ta_2O_9$ were detected in the samples in small amounts (Fig. 5. 4). These phases might have formed as a result of an incomplete solid state reaction when the samples were calcined at 1200 ^oC. At still higher temperatures, the phases such as $BaTa_2O_6$ could be transformed into the desired $Ba(Mg_{1/3}Ta_{2/3})O_3$ or could remain in the samples as additional phase, which in turn can decrease the dielectric Q factor of the material. It is

expected that the possible formation of the transient liquid phases like BaB_2O_4 might have helped the materials transport. However such a phase was not detected in the present XRD profile. When the samples were sintered at 1250^oC, the additional phases formed were $Ba_5Ta_4O_{15}$ and $Ba_4Ta_2O_9$. Apart from these, the samples revealed an ordered perovskite structure with superstructure reflections visible in the XRD pattern. At 1325 ^oC, the XRD profile represented only single phase BMT with no trace of additional phases like $Ba_5Ta_4O_{15}$. This indicates that in presence of a vitreous medium, stable phases like $Ba_5Ta_4O_{15}$ can react with MgO to form stable $Ba(Mg_{1/3}Ta_{2/3})O_3$ which is very difficult to occur in ordinary high temperature solid state reaction synthesis[45]. Sintering at higher temperatures retains the ordered structure, but the bulk density decreases which can be due to grain growth (Fig. 5. 1). Furthermore, this observation confirms a recent finding by Cheng[22] et al. that the presence of satellite phases in BMT can be eliminated by glass fluxing. It must be noted that even for higher percentage of B_2O_3 addition no traces of glassy phases noticed in the XRD. This confirms the volatisation of B_2O_3 at high temperatures after the formation of a transient vitreous phase which enables efficient particle rearrangement and material transport during sintering. It is also evident that ordering parameter (S) and the unit cell parameter ratio (*c/a*) of BMT doped with 0.5 wt. % B_2O_3 glass were increased with sintering temperature and approached its maximum value at 1350^oC. Increasing the sintering temperature above 1350^oC deteriorated the cation ordering (see Fig. 5. 1 and Table 5. 2). A similar observation regarding the suppression of barium tantalate phases were observed with other glass systems like $5ZnO\text{-}2B_2O_3$ and $ZnO\text{-}B_2O_3\text{-}SiO_2$ (the XRD profiles are not given here). It was also observed that with 0.5 wt. % $PbO\text{-}B_2O_3\text{-}SiO_2$ glass fluxing, a small trace of $Ba_7Ta_6O_{22}$ was noticed in their respective powder patterns besides the usual $BaTa_2O_6$. The diffraction peaks of $Ba_7Ta_6O_{22}$ and $BaTa_2O_6$ disappeared on the addition of 1 mole % of $PbO\text{-}B_2O_3\text{-}SiO_2$ glass.

Fig. 5. 5 describes the XRD patterns recorded from BMT fluxed with 2 wt. % different glasses. It is observed that addition of certain glasses of about 2 wt. % gave rise to a number of additional phases formed may be due to the decomposition of some glasses at high temperatures and their consequent reaction with the matrix phase. The slow cooling (60 ^oC per hour) of the glass ceramic after sintering could lead to the

formation of these crystalline phases. Doping up to 0.5 wt. % primary glasses like B_2O_3 will not form any additional phase but will act as a sintering aid. Addition of B_2O_3 glass in excess of 2 wt. % will result in the formation of BaB_4O_7 (JCPDS File Card. No. 15-862) secondary phases and decreased the dielectric Q factor. No additional phases were observed when the samples were sintered at 1300 ^oC (see Fig. 5.5). As the concentration of SiO_2 in BMT increases, additional lines corresponding to $Ba_3Si_5O_{13}$ (JCPDS File Card. No. 26-179) and a weak line for $MgSiO_3$ (Card. No. 19-768) appeared in the powder diffraction profile. The crystalline phase of borosilicate glass (B_2SiO_5, JCPDS File Card No. 42-392) was visible in the XRD pattern of BMT (Fig. 5.5) doped with 2 wt. % B_2O_3-SiO_2. The two diffraction peaks for $Zn(BO_2)_2$ (Card. No. 39-1126) and ß-$Zn_5B_4O_{11}$ (Card. No. 9-153) were appeared in their respective powder diffraction patterns when BMT is doped with them up to 0.5 wt. %. But no such additional peaks are visible when the samples are doped upto 2.0 wt. % (see Fig. 5.5 and SEM picture 5.6(b)). Formation of crystalline Al_2SiO_5 (Card. No. 38-471) may be the reason for the decrease of density for higher concentration of Al_2O_3-SiO_2 doped samples. It is also observed that addition of borax glass (Na_2O-$2B_2O_3.10H_2O$) severely damaged the cation ordering of BMT and powder diffraction patterns presents no superstructure reflection peaks when the ceramic is doped with it in excess of 2.0 wt.%. A few unidentified additional diffraction lines were present in the profile which could not be indexed using any of the standard schemes of indexing. This observation was consolidated by the low value of the cation ordering parameter (0.544) (Fig. 5. 3). The addition of ternary glasses resulted in the formation of a number of additional lines. When BMT was fluxed with 0.1 wt.% of BaO-B_2O_3-SiO_2 a small diffraction line corresponding to $BaSi_4O_9$ (Card. No. 15-386) appeared in the XRD pattern (Fig. 5. 5) which could be the reason behind the anomaly in its dielectric constant. Doping of BMT with more than 0.2 wt. % of BaO-B_2O_3-SiO_2 resulted in the formation of $Ba_3B_6Si_{12}O_{16}$ (Card No. 6-351). Even a small concentration of MgO-B_2O_3-SiO_2 resulted in the formation of $Mg_3(BO_3)_2$ (Card No. 33-858) whose intensity was diminished with more MBS concentration. This is suspected to be due to the evaporation of the glass during sintering or the reaction with the matrix resulted in the formation of some unidentified phase whose presence could not be detected by XRD. Glass fluxing of BMT with 1 wt. % PBS gave rise

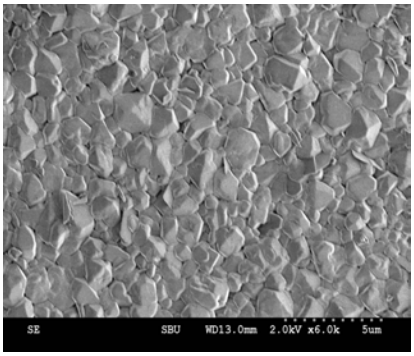

5.6 (a)

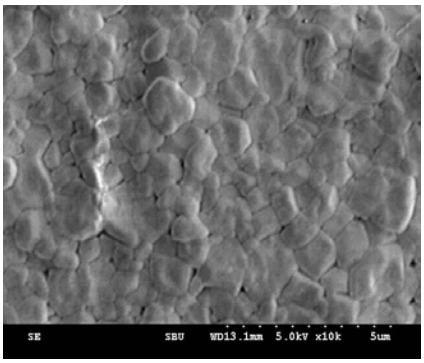

5.6(b)

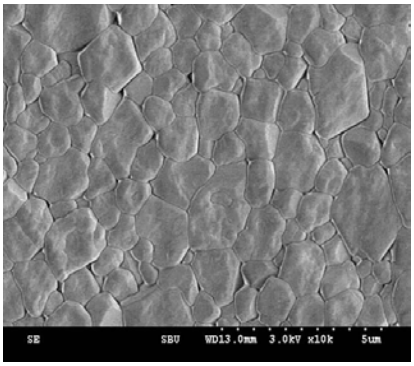

5.6(c)

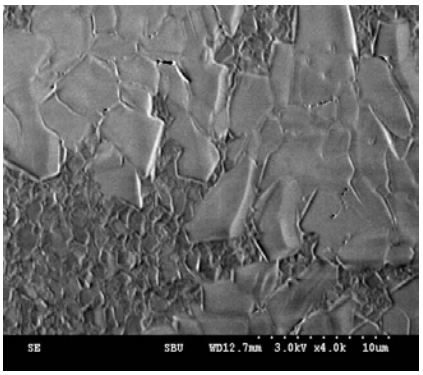

5.6(d)

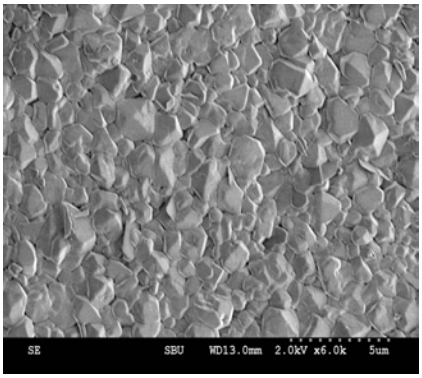

5.6 (e)

Fig. 5. 6 The Scanning Electron Micrographs of $Ba(Mg_{1/3}Ta_{2/3})O_3$ (a) doped with 0.1 wt.% B_2O_3 sintered at 1375 ^oC, (b) doped with 2 wt. % of $5ZnO\text{-}2B_2O_3$ sintered at 1375 ^oC, (c) doped with 2 wt. % of $ZnO\text{-}B_2O_3\text{-}SiO_2$ sintered at 1330 ^oC, (d) doped with 2 wt. % of $PbO\text{-}B_2O_3\text{-}SiO_2$, sintered at 1300 ^oC and (e) undoped $Ba(Mg_{1/3}Ta_{2/3})O_3$ sintered at 1350 ^oC.

to $Pb_5Si_2O_7$ phase (Card. No. 32-538) while with 2 wt. %, an additional phase of PbB_4O_7 (Card. No. 15-278) also appeared in the XRD pattern. The doping with $ZnO\text{-}B_2O_3\text{-}SiO_2$ seems to be most interesting as the formation of the additional phases were not visible in the XRD profiles. For 0.1 wt. % a small trace of Zn_2SiO_4 (Card. No. 24-1467) was detected in the XRD but the additional phase disappears with more addition of ZnO-

B_2O_3-SiO_2. The formation of secondary phases such as $BaMgSi_4O_{10}$ (Card. No. 15-799) was detected at a doping level of 1.0 wt. % $2MgO$-$2Al_2O_3$-$5SiO_2$. One more additional line of crystalline cordierite, $Mg_2Al_4Si_5O_{18}$ (Card. No. 13-293) has appeared in the XRD pattern of BMT doped with cordierite up to 2 wt. % (see Fig. 5.5). This result confirms a recent finding by Cheng[22] et al. who observed that excess presence of cordierite in BMT hindered its densification process and thereby deteriorated the microwave dielectric properties. It is likely that on doping with zinc and aluminium based glasses, a small amount of ions like Zn^{2+} and Al^{3+} can substitute the Mg site in BMT due to their comparable size and charge. It is also possible that small amount of sodium in borax glass can go into the Ba^{2+} site of BMT. But the conventional X-ray diffraction analysis based on powder diffraction methods does not give any information for such a very small amount of substitutions.

5. 3. 3 Microstructural Analysis

The scanning electron micrographs recorded from a few typical samples were presented in Fig. 5. 6. Figure 5. 6 (a) is the electron micrograph of BMT sample doped with 0.1 wt. % of B_2O_3 which was sintered at 1375^oC. The average grain size was about 1 µm. The SEM picture did not show the presence of any additional phases. This may be either due to (i) the amount of glass content was too negligible to be detected or (ii) since the liquid phase sintering is a transient phenomenon, the B_2O_3 melt might have evaporated away after acting as an effective medium for molecular diffusion. Some previous reports[15] on the effects of B_2O_3 in $Ba_2Ti_9O_{20}$, also confirmed that B_2O_3 is volatile during the high temperature sintering above 1200^oC. Fig. 5.6(b) gives the surface morphology of BMT doped with 2 wt. % of $5ZnO$-$2B_2O_3$. Here SEM picture showed closely packed grains. The formation of the low melting phase ß-$Zn_5B_4O_{11}$ has enhanced the densification of BMT by providing a liquid phase medium. The addition of ZnO-B_2O_3-SiO_2 glass has enhanced the densification phenomena through enhanced material transport, as it is clear from Fig. 5.6(c). In this case the friction between the particles during diffusion was significantly reduced. So they can rearrange easily under the action of the compressive stress exerted by the liquid. It should be noted that the bulk diffusion through a liquid is more efficient than a solid. The melted phase of PbO-B_2O_3-SiO_2

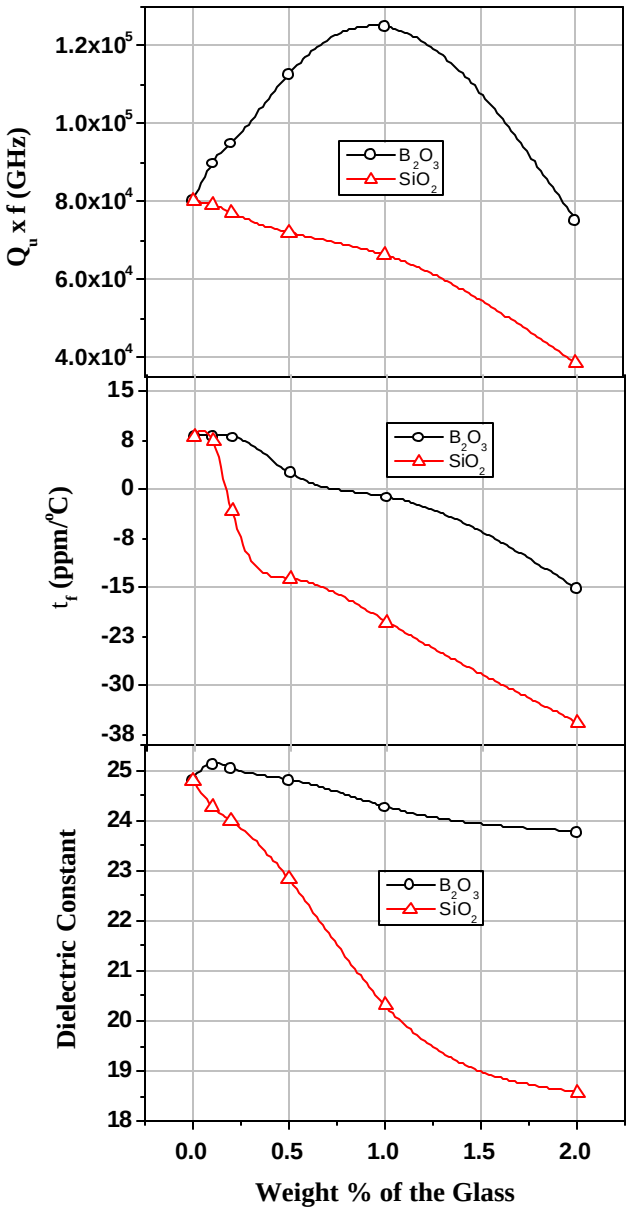

Fig. 5. 7 Variation of microwave dielectric properties of $Ba(Mg_{1/3}Ta_{2/3})O_3$ as a function of primary glass addition

glasses is visible in Fig. 5. 6 (d) which is the micrograph of BMT fluxed with 2.0 wt.% of $PbO\text{-}B_2O_3\text{-}SiO_2$, sintered at 1300°C. The XRD analysis suggests that the additional liquid phase may be either $Pb_5Si_2O_7$ or PbB_4O_7 or a homogeneous mixture between them. Fig. 5.6(e) show the SEM picture of pure BMT ceramic sintered at 1350°C without additives showing a highly porous structure.

5. 3. 4 Microwave Dielectric Properties

The glass assisted sintered ceramics need not necessarily result in the desired improvement in dielectric properties. This is especially true if the dielectric constant and Q factor of the matrix material are lowered by the presence of a continuous low dielectric constant grain boundary phase. To tackle this problem one need to control the grain growth related porosity consequent to glass fluxing and reduce the volume fraction of the low dielectric constant secondary phases formed as a result of the reaction of the vitreous phase with the ceramic. The glass can act either as a fluxing agent for liquid phase sintering or a modifier of the dielectric properties if the glass component is incorporated into the lattice of the ceramic matrix[46]. Therefore the suitable composition of the glass additive and the chemical interaction of the $Ba(Mg_{1/3}Ta_{2/3})O_3$ with glasses are important aspects in understanding, characterizing and controlling their dielectric properties.

5. 3. 4. 1 Primary Glasses

The microwave dielectric properties of undoped $Ba(Mg_{1/3}Ta_{2/3})O_3$ with a densification of 93.1 % of the theoretical density are e_r = 24.8, t_f = 8 ppm/^oC and $Q_u$xf = 80,000 GHz. This sample was sintered at 1600^oC for 4 hours in air. We have also observed[47] that increasing the sintering temperature upto 1650^oC or prolonged annealing upto 40 hours at 1450^oC could increase densification upto 97.5 % and $Q_u$xf to 125,300 GHz. It is worthwhile to note that the doped ceramic samples used in this investigation was not annealed. This is because the sintering temperatures of most of the glass fluxed BMT ceramics were less than 1400^oC while the usual annealing temperature of BMT was 1450-1500^oC. In order to promote cation ordering in complex perovskite BMT the sintered samples were subjected to a very slow cooling rate (1 ^oC/minute). Fig. 5.7 gives the microwave dielectric properties of B_2O_3 and SiO_2 glass added BMT. The dielectric constant increased from 24.8 (pure BMT) to 25.02 when the sample was added with 0.2 wt. % of boric oxide and further addition resulted in a decrease of it. On the other hand the e_r was considerably decreased with SiO_2 addition.

As discussed in Chapter 1, Section 1.3.3, the temperature coefficients of resonant frequency (t_f) and dielectric constant (t_e) are related by

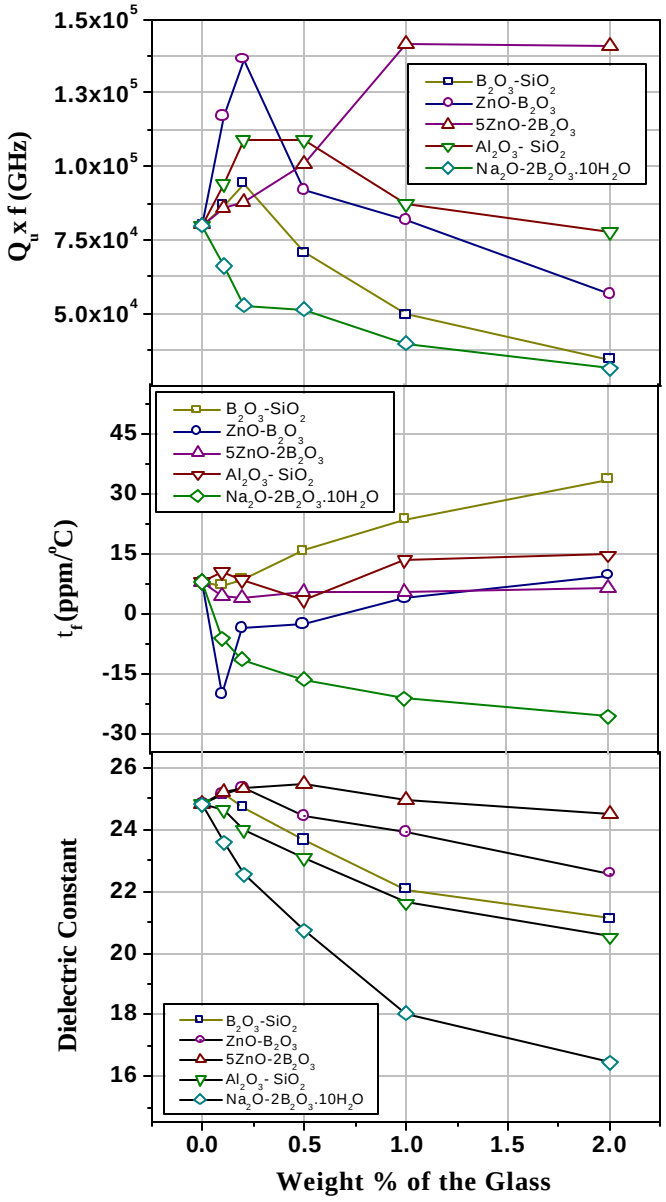

Fig. 5. 8 Variation of microwave dielectric properties of $Ba(Mg_{1/3}Ta_{2/3})O_3$ as a function of binary glass addition

$$\tau_f = -\alpha - \frac{\tau_\varepsilon}{2} \qquad (5.6)$$

where *a* is the thermal expansion coefficient of the glass-ceramic composite. In amorphous materials the dielectric constant increased with temperature due to the relatively weak bonding structure. With a finite value of the thermal expansion

coefficient the t_e will have high positive values which eventually makes t_f of most of the glassy materials negative[27]. The t_f of BMT decreases with B_2O_3 and SiO_2 addition, approached more negative values when doping level of the glass exceeded. It is interesting to note in Fig. 5.7 that t_f was close to zero (+2.4 and -1.3 ppm/^oC respectively) for samples mixed with 0.5 and 1.0 wt. % of B_2O_3.

The quality factor of BMT increased for small amount of B_2O_3. For 0.5 wt. % of B_2O_3 addition $Q_u$xf reached 124,700 GHz. The unloaded quality factor decreased with further addition of B_2O_3 glass where the densification factor also followed a similar trend (see Fig. 5.2). The effect of SiO_2 glass in BMT on the other hand destroyed its cation ordering (see Table 5.2) and severely deteriorated the microwave quality factor (Fig. 5.7).

5. 3. 4. 2 Binary Glasses

The variation of the dielectric properties of BMT as a function of weight percentage of the binary glass additives was given in Fig. 8. In the case of binary systems like $5ZnO\text{-}2B_2O_3$, $ZnO\text{-}B_2O_3$ and $B_2O_3\text{-}SiO_2$, the dielectric constant which is an indicator of the various polarization phenomena of the ceramic, increases slightly with glass addition. On adding 0.5 wt. % of $5ZnO\text{-}2B_2O_3$ glass, the measured values of e_r increased to 25.45 and then gradually decreased to 24.5 with 2.0 wt. % of the additive. The maximum values of e_r for BMT doped with $B_2O_3\text{-}SiO_2$ and $ZnO\text{-}B_2O_3$ were 25.12 and 25.34 for 0.1 and 0.2 wt.% of the additives respectively. For all other binary glasses the dielectric constant decreased with increasing concentration of the glass additive. For sodium diborate decahydrate glass, the lowest value of dielectric constant was observed as 16.4 (for 2 wt. % of the $Na_2O\text{-}2B_2O_3.10H_2O$). It is worthwhile to note that the behavior of dielectric constants of the glass fluxed ceramics do not exhibit any direct relationships with the intrinsic dielectric properties of the glass systems (Table 5.1).

Unlike primary glasses, anomalous behavior of t_f is observed when BMT is doped with binary glass compositions. In the case of borosilicate glass, the t_f increased with glass content and approached values as high as +33.6 ppm/^oC (for 2.0 wt. % $B_2O_3\text{-}SiO_2$) while for the same concentration of aluminosilicate it is 14.8 ppm/^oC. For very small amount of $ZnO\text{-}B_2O_3$, the t_f has negative values while it increased to 9.8 ppm/^oC with 2.0 wt. % glass addition. The t_f first decreased to 3.4 and then increased to 14 ppm/^oC with

aluminosilicate glass doping. The irregular variation of t_f in some added ceramics are attributed to the formation of additional phases formed as result of the reaction of the glass with BMT matrix. In the case of sodium borate addition, the t_f of BMT showed negative values (see Fig. 5.8). Among binary glass compositions, the temperature coefficient of resonant frequency showed steady values only in the case of $5ZnO\text{-}2B_2O_3$ addition.

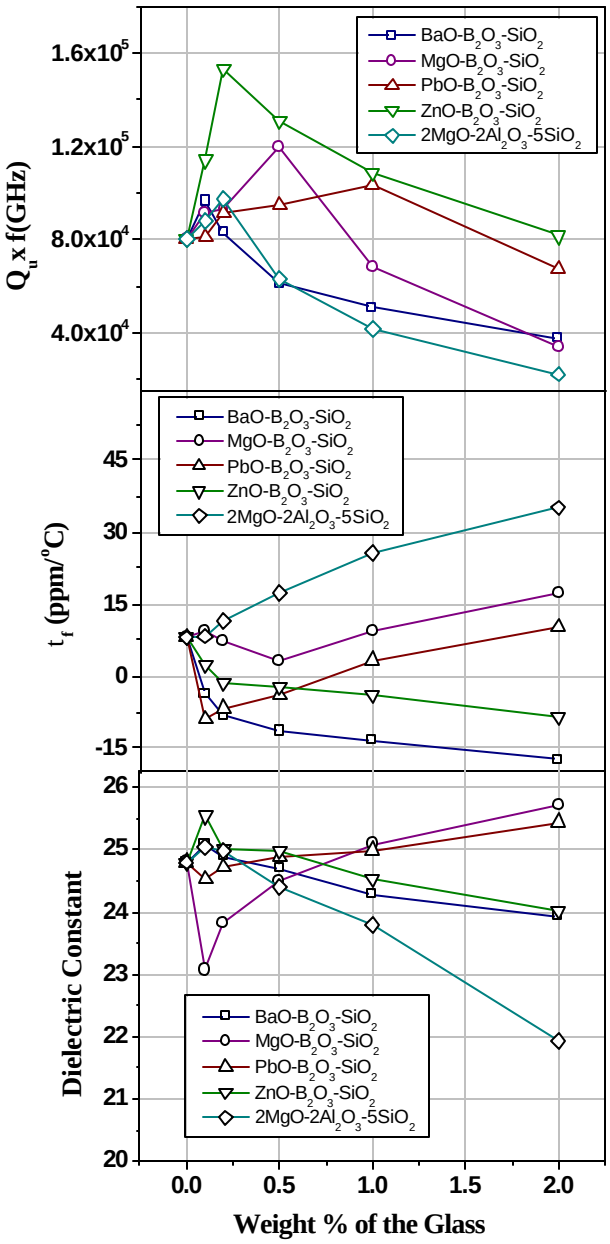

Fig. 5. 9 Variation of the microwave dielectric properties of BMT with ternary glass addition

The unloaded quality factor of BMT increased to $Q_u$xf = 136,500 GHz with 0.2 wt. % of $ZnO\text{-}B_2O_3$ addition. With small amount of $Al_2O_3\text{-}SiO_2$ addition a slight improvement of microwave quality factor ($Q_u$xf = 109,200 GHz) was observed. It is interesting to note that the quality factor of BMT increased steadily with $5ZnO\text{-}2B_2O_3$ content. It is believed that the formation of the low melting ß-$Zn_5B_4O_{11}$ has been beneficial to the materials transport mechanism in these glass fluxed ceramics. The best microwave property among binary glass added BMT ceramic was recorded for 1.0 wt. % $5ZnO\text{-}2B_2O_3$ addition where the $Q_u$xf was 141,800 GHz. The addition of alkali glass was found to deteriorate the microwave dielectric properties of $Ba(Mg_{1/3}Ta_{2/3})O_3$ ceramics. The XRD studies revealed the presence of unidentified compositions. In alkali borate glass [25], the oscillation of the alkali ion was limited by crystal bonding while in the vitreous state they were loosely held in the interstices of the glassy network which were relatively free to oscillate with external field. This can lead to extensive dielectric losses. When such lossy amorphous material was incorporated in to the low loss BMT, the dielectric loss quality of the latter can increase.

5. 3. 4. 3. Ternary Glasses

The influence of the additional satellite phases formed consequent to the interaction of the glass with the ceramic matrix played a significant role in controlling the microwave dielectric properties of the ternary glass fluxed BMT. The evolution of the dielectric properties of BMT added with ternary glass compositions are given in Fig. 9. For glass systems like $BaO\text{-}B_2O_3\text{-}SiO_2$, $ZnO\text{-}B_2O_3\text{-}SiO_2$ and $2MgO\text{-}2Al_2O_3\text{-}5SiO_2$ the dielectric constant slightly increases for small values of the glass content and then decreases as the presence of glass in the mixture increases. But the percentage decrease in e_r is more for cordierite glass which can be due to the formation of additional phases such as $BaMgSi_4O_{10}$. For $MgO\text{-}B_2O_3\text{-}SiO_2$ addition, e_r decreased to 23.02 with 0.2 wt. % of the glass due to the formation of $Mg_3(BO_3)_2$ phase and then increased. In the case of $PbO\text{-}B_2O_3\text{-}SiO_2$ doping also, the dielectric constant decreased slightly which may be due to the formation of $Pb_5Si_2O_7$ and PbB_4O_7 phases.

The temperature coefficient of resonant frequency of the glasses decreased from 8 to -17.4 ppm/^oC for $BaO\text{-}B_2O_3\text{-}SiO_2$ and to -8.6 ppm/^oC for $ZnO\text{-}B_2O_3\text{-}SiO_2$ when they

were added up to 2 wt. %. A minimum t_f value of 1.3 ppm/^oC has been found in 1.0 wt. % of $PbO-B_2O_3-SiO_2$ glass mixed BMT. It has already been reported [27] that the temperature coefficient of all these glasses were negative. The $MgO-B_2O_3-SiO_2$ fluxed BMT showed an initial dip in the t_f values which may be due to the presence of $Mg_3(BO_3)_2$ secondary phase. It is interesting to note that a similar anomaly has been observed in the variation of dielectric constant of BMT with $MgO-B_2O_3-SiO_2$ glass incorporation. The temperature coefficient of resonant frequency of cordierite ($Mg_2Al_4Si_5O_{18}$) doped BMT was positive and increased with increasing amount of cordierite. This is surprising since cordierite is reported [52] to have a negative t_f.

The unloaded quality factor of 0.2 wt. % $ZnO-B_2O_3-SiO_2$ glass added BMT was around $Q_u$xf = 152,800 GHz. This result is most interesting as it revealed that this ternary glass system provides an ideal wetting medium for the liquid phase sintering of complex perovskite $Ba(Mg_{1/3}Ta_{2/3})O_3$. The XRD patterns showed no additional peaks except superstructure reflections representing a completely ordered crystal structure formed with cation ordering parameter 0.999 (Fig.3). There has been similar reports about the ideal wetting characteristics of $ZnO-B_2O_3-SiO_2$ with other low loss ceramics like [48] TiO_2 and [20] $MgTiO_3$-$CaTiO_3$. It must be noted that the addition of other ternary additives also resulted in an increase in the $Q_u$xf value from 80,000 GHz (of pure unannealed BMT). The best quality factors measured with the addition of other ternary glass dopants were given by $Q_u$xf = 96,500 for $BaO-B_2O_3-SiO_2$ (0.2 wt. %), 119,900 for $MgO-B_2O_3-SiO_2$ (0.5 wt. %), 103,100 for $PbO-B_2O_3-SiO_2$ (1.0 wt. %) and 97,300 for $2MgO-2Al_2O_3-5SiO_2$. The microwave quality factor of most of the glass added dielectrics decreased when the doping level of the glass increased due to the formation of the satellite phases formed. It is worthwhile to remember that Cheng [22] et al. made a similar observation, who attributed the poor performance of dielectric properties of BMT fluxed with $MgO-CaO-SiO_2-Al_2O_3$ (MCAS) was probably due to the decomposition of MCAS glass into cordierite phase which can eventually damage the microwave quality factor of the ceramic. As a general rule, in glasses the main cause of dielectric loss is associated with deformation loss mechanism [27] and introduction of a lossy glass in to the ceramic may aggravate the loss of the ceramic.

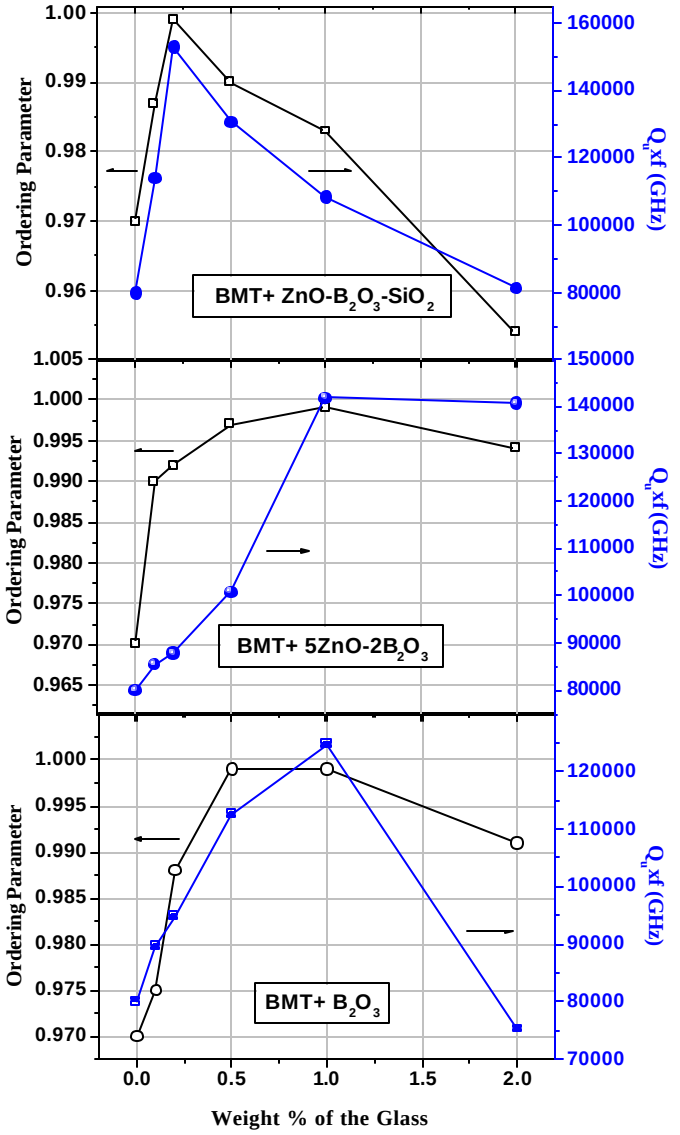

Fig. 5. 10 Variation of unloaded quality factor and ordering parameter of BMT doped with B_2O_3, $5ZnO\text{-}2B_2O_3$ and $ZnO\text{-}B_2O_3\text{-}SiO_2$ additives

In a previous report, Ra et al.[53] suggested that B-site cation ordering is not the primary factor that influences the observed microwave dielectric loss in BMT. They attributed dielectric loss of this ceramic to the atomic level point defect induced from raw material impurities, processing etc. The variation of the cation ordering factor and unloaded quality factor of three typical glasses such as B_2O_3 (primary), $5ZnO\text{-}2B_2O_3$ (binary) and $ZnO\text{-}B_2O_3\text{-}SiO_2$ (ternary) are plotted in Fig. 5.10. Since the variation of the

quality factor and cation ordering parameter follows a more or less similar trend within the limits of experimental error, it is evident that B-site cation ordering of Mg^{2+} and Ta^{5+} is the fundamental requirement for high quality factor in complex perovskite $Ba(Mg_{1/3}Ta_{2/3}O)_3$ ceramics. Moreover this result gives justification to the procedure of calculation of ordering parameter using Eqs. 5.4 and 5.5 which use the ratio of intensity of superstructure (100) line and fundamental reflection (110,102).

It must be remembered that the reduction in sintering temperature in this research report was not sufficient enough for applications in multilayer structures using LTCC technique where the sintering temperature must be less than 961^oC which is the melting point of silver electrode. Furthermore, the amount of liquid phase content was not adequate for complete liquid phase sintering to occur. But in most of the advanced ceramics, the amount of liquid phase produced at the time of firing is kept typically below 5 vol. % to safeguard the physical or electrical properties from deterioration as a result of additional phase formation at the grain boundaries[37]. The present investigation is useful in selecting the right glass compositions that aid vitreous sintering in complex perovskite $Ba(Mg_{1/3}Ta_{2/3}O)_3$ ceramics.

5. 4 CONCLUSIONS

- The effect of glass fluxing on the phase evolution, densification, cation ordering, microstructure and microwave dielectric properties of BMT is investigated. In conventional solid state synthesis, sintering at high temperatures 1625-1675^oC for several hours and annealing upto several days are needed to stabilize the ordered high Q phase of BMT ceramics. The sintering temperature of BMT ceramics was reduced to about 1300^oC from 1650^oC with glass additives. The BMT ceramics when doped with glass systems such as B_2O_3, $ZnO\text{-}B_2O_3$, $5ZnO\text{-}2B_2O_3$ and $ZnO\text{-}B_2O_3\text{-}SiO_2$ and sintered in the temperature range 1300-1450^oC showed ordered perovskite structure without any annealing. Thus the cost of production of BMT can be reduced by using glass additives without any deterioration in the microwave dielectric properties
- Best Densification of about 98.7 % of the theoretical density was observed for B_2O_3 added ceramics. Reasonably good densification was observed for ZnO-

B_2O_3-SiO_2, $5ZnO$-$2B_2O_3$ glass additives. Densification of BMT was poor with SiO_2, Na_2O-$2B_2O_3.10H_2O$ and $2MgO$-$2Al_2O_3$-$5SiO_2$ glass additions.

- Glass addition suppressed the formation secondary phases such as $Ba_5Ta_4O_{15}$ and $Ba_7Ta_6O_{22}$. A small amount of glass additive such as B_2O_3, ZnO-B_2O_3, $5ZnO$-$2B_2O_3$, ZnO-B_2O_3-SiO_2 did not produce additional phases when sintered with BMT while the others such as SiO_2, B_2O_3-SiO_2, Al_2O_3-SiO_2, Na_2O-$2B_2O_3.10H_2O$, BaO-B_2O_3-SiO_2, MgO-B_2O_3-SiO_2, PbO-B_2O_3-SiO_2 and $2MgO$-Al_2O_3-$5SiO_2$ reacted with BMT matrix forming additional phases.
- Certain glasses like B_2O_3, $5ZnO$-$2B_2O_3$, ZnO-B_2O_3-SiO_2 enhanced the cation ordering which had fairly good microwave dielectric properties while some other glasses like SiO_2, Al_2O_3-SiO_2, Na_2O-$2B_2O_3.10H_2O$ and $2MgO$-Al_2O_3-$5SiO_2$ severely destroyed the cation order. This observation emphasized the fact that B-site cation ordering of Mg^{2+} and Ta^{5+} is the fundamental requirement for high quality factor in complex perovskite $Ba(Mg_{1/3}Ta_{2/3}O)_3$ ceramics. The microwave quality factor is found to be directly related to the ordering parameter.
- The microwave dielectric properties of pure unannealed $Ba(Mg_{1/3}Ta_{2/3})O_3$ (e_r = 24.8, t_f = 8 ppm/^oC and $Q_u$xf = 80, 000 GHz) was improved when it was doped with 1.0 wt. % of B_2O_3 ($Q_u$xf = 124,700 GHz, e_r = 24.25, and t_f = -1.3 ppm/^oC). The unloaded Q factor of 0.2 wt. % ZnO-B_2O_3 doped BMT is 136,500 GHz while that of 1.0 wt. % of $5ZnO$-$2B_2O_3$ added ceramic is $Q_u$xf = 141,800 GHz. The best microwave quality factor is observed for ZnO-B_2O_3-SiO_2 (ZBS) glass added ceramics which can act as a perfect liquid phase medium for the sintering of BMT. The microwave dielectric properties of 0.2 wt. % ZBS added BMT dielectric is $Q_u$xf = 152,800 GHz, e_r = 25.54, and t_f = -1.5 ppm/^oC.
- The sintering temperature is brought down to about 1300 from 1650^oC by the addition of a small amount of glass. However this sintering temperature is much higher than that required for LTCC applications. The results indicate that possibility of lowering the sintering temperature further down for LTCC applications by adding large amounts of glasses. Addition of such glasses not only lowers the sintering temperature but also decreases the dielectric constant and quality factor considerably.

5. 5 REFERENCES

1. H. Shomoda, N. Ishitobi, K. Kawamura and M. Kobayashi, *Jpn. J. Appl. Phys*., **31**, 3160-63 (1992).

2. H. Jantunen, *A novel Low Temperature Co-firing Ceramic (LTCC) Materials for Telecommunication Devices*, PhD. Thesis, University of Oulu, Finland (2001).

3. I. Maclaren and C. B. Ponton, *J. Mat. Sci*., **33**, 17-22 (1998).

4. O. Renoult, J-P. Boilot, F. Chaput, R. Papiernik, L. G. Hubert-Pfalzgraf and M. Lejeune, *J. Am. Ceram. Soc.*, **75**, 3337-40 (1992).

5. Chung-Hsin Lu and Chien-Cheng Tsai, *Mater. Sci. Engg. B.*, **55**, 95-101(1998).

6. M-H. Liang, S-Y. Wu, C-T. Hu and I-N. Li, *Mater. Chem. Phys*., **79**, 276-81 (2003).

7. H. M. Shirey, *Low Temperature Synthesis of the Microwave Dielectric Material Barium Magnesium Tantalate*, M.S. Thesis, University of Pittsburgh, (2002).

8. S. Katayama, I. Yoshinaga, N. Yamada and T. Nagai, *J. Am. Ceram. Soc*., **79**, 2059-64 (1996).

9. X. M. Chen and Y. J. Wu, J. Mat. Sci. Mater. Electron., **7**, 427-431 (1996).

10. T. Takada, S. F. Wang, S. Yoshikawa, S-J. Jang and R. E. Newnham, *J. Am. Ceram. Soc.*, **77**, 2485-88 (1994).

11. G. Huang, D. Zhou, J. Xu, X. Chen, D. Zhang, W. Lu and B. Li, *Mater. Sci. Engg. B.*, **99**, 416-20 (2003).

12. C-L Huang, M-H. Weng, C-T. Lion and C-C Wu, *Mater. Res. Bull.*, **5**, 2445-56 (2000).

13. Y-C. Lee, W-H. Lee and F-S. Shieu, *Jpn. J. Appl. Phys.*, **419**, 6049-53 (2002).

14. S-F. Wang, C-C. Chiang, C-H. Wang and J. P. Chu, *J. Mater. Res*., **18**, 201-07 (2003).

15. C-M. Cheng, C-F. Yang, S-H. Lo and T-Y. Tseng, *J. Eur. Ceram. Soc*., **20,** 1061-67 (2000).

16. D-W. Kim, D-G. Lee and K.S. Hong, *Mater. Res. Bull*., **36**, 585-95 (2001).

17. S. G. Lu, K. W. Kwok, H. L. W Chan and C. L. Choy, *Mater. Sci. Engg. B.*, **99**, 491-94 (2003).

18. H. Jantunen, R. Rautioaho, A. Uusimaki and S. Leppavuori, *J. Eur. Ceram. Soc.*, **20**, 2331-36 (2000).

19. H. Jantunen, R. Rautioaho, A. Uusimaki and S. Leppavuori, *J. Am. Ceram. Soc.*, **85**, 697-99 (2002).

20. C-S. Chen, C-C. Chou, C-S. Chen and I-N. Lin, *J. Eur. Ceram. Soc.*, **24**, 1795-98 (2004).

21. C-M. Cheng, Y-T. Hsieh and C-F. Yang, *Ceram. Inter.*, **28**, 255-60, (2002).

22. C.-M. Cheng, Y-T. Hsieh and C-F. Yang , *Mater. Lett.*, **57**, 1471-76 (2003).

23. M. Pollet, S. Marinel, F. Roulland, G. Allainmat, *Mater. Sci. Engg. B.*, **104,** 58-62 (2003).

24. L. Navias and R. L. Green, *J. Am. Ceram. Soc.*, **29**, 267-79 (1946).

25. S. N. Salama, S.M. Salman and H. Darwish, *Ceram. Inter.*, **21**, 159-67 (1995).

26. J-M. Wu and H-L. Huang, *J. Non Cryst. Sol.*, **260,** 116-24 (1999).

27. B. W. Hakki and P. D. Coleman, *IRE Trans. on Microwave Theory Tech.*, **MTT-8**, 402-10 (1960).

28. W. E. Courtney, *IEEE Trans. on Microwave Theory Tech.*, **MTT-18**, 476-85 (1970).

29. J. Krupka, K. Derzakowski, B. Riddle and J. Baker-Jarvis, *Meas. Sci. Technol.*, **9**, 1751-56 (1998).

30. *ATG Powder Glass for CRT, VFD, PDP sealing*, Asahi Techno Glass Corporation, Japan (1990).

31. C-C. Cheng, T-E. Hsieh and I-N. Lin, *J. Eur. Ceram. Soc.*, **24**, 1787-90 (2004).

32. C. Yang, D. Zhou, C. Huang and G. Qin, *J. Adv. Mater.*, **31,** 8 -11 (1998).

33. K-H. Felgner, T. Müller, H. T. Langhammer and H-P. Abicht, *J. Eur. Ceram. Soc.*, **21**, 1657-60 (2001).

34. Y. B. Saddeek, *Physica B: Cond. Matter*., **344**, 163-75 (2004).

35. M. N. Rahaman, *Ceramic Processing and Sintering*, International Edn., Marcel Dekker Inc., New York, p. 516 (1999).

36. J. H. Jean and T. K. Gupta, *J. Mater. Res*. 10 (1995) 1312-20.

37. A. Upadhyaya and R. M. German, *Mater. Chem. Phys*., **67**, 25-31 (2001).

38. S. Mei, J. Yang and José M. F. Ferreira, *Mater. Lett*., **47**, 205-11 (2001).

39. K. Matsumoto, T. Hiuga, K. Takada and H. Ichimura, *Proc. Sixth IEEE International Symposium on Application of Ferroelectrics*, Institute of Electrical and Electronic Engineers, Bethlehem, PA, (1986).

40. H-J. Yoon, K-Y. Kim and H. Kim, *Jpn. J. Appl. Phys*., **35**, 3947-53 (1996).

41. C-H. Lu and C-C. Tsai, *J. Mater. Res*., **11**, 1219-27 (1996).

42. X. M. Chen, Y. Suzuki and N. Sato, *J. Mater. Sci. Mater. Electron*., **5**, 244- 47 (1994).

43. K. Tochi, *J. Ceram. Soc. Jpn. Inter. Edn*., **100**, 1441-43 (1992).

44. Y. Fang, A. Hu, Y. Gu and Y-J. Oh, *J. Eur. Ceram. Soc*., **23**, 2497-02 (2003).

45. Y. Fang, A. Hu, S. Ouyang, J. J. Oh, J. Eur. Ceram. Soc., **21,** 2745–50 (2001).

46. S-F. Wang, T. C. K. Yang, Y-R.Wang and Y. Kuromitsu, *Ceram. Inter*., **27**, 157-62 (2001).

47. K. P. Surendran, M. R. Varma, P. Mohanan and M. T. Sebastian, *Proc. National Conference on Recent Advances in Materials Processing* (RAMP- 2001), Sept. 7-8, Annamalainagar-608002, India (2001).

48. S-H. Yoon, D-W. Kim, S-Y.Cho, K.S. Hong, *J. Eur. Ceram. Soc*., **21**, 2549-52 (2003).

51. K. P. Surendran, M. T. Sebastian, *Dielectric Properties of Glasses in the Frequency Range 50Hz-13MHz*, (unpublished data).

52. R. D. Shannon, A. N. Mariano and G. R. Rossman, *J. Am. Ceram. Soc*., **75**, 2395-99 (1992).

53. S.-H. Ra and P. P. Phule, *J. Mater. Res*., **14**, 4259-65 (1999).

CHAPTER 6

SOLID SOLUTIONS WITH $Ba(Mg_{1/3}Ta_{2/3})O_3$ CERAMICS

This Chapter is an investigation on the effects of B-site substitution on the chemistry and physics of BMT. In this study solid solution phases such as $Ba[Mg_{1/3}Ta_{(1-x)2/3}Ti_{x/3}W_{x/3}]O_3$, $Ba[(Mg_{1/3})_{1-x}Zn_{x/3}Ta_{2/3}]O_3$, $Ba(Mg_{1/3}Ta_{2/3})_{1-x}Ti_xO_3$ and were investigated. The effect of solid solution formation on the densification, the structural phase transition from ordered to disordered structure, tolerence factor, bond valence and microwave dielectric properties of the solid solution phase are also discussed.

6.1 $Ba(Mg_{1/3}Ta_{(2-2x)/3}W_{x/3}Ti_{x/3})O_3$ CERAMICS

6. 1. 1 Introduction

The crystal chemistry of A-site and B-site substitution in Ba-and Pb based complex perovskites is reported[1] to have tremendous influence on its physical and dielectric properties. The cation ordering kinetics in Ba-based and Pb-based ceramics bear marked difference as the latter disorders even at very low temperatures [2]. The partial substitution of Ba with Sr in 1: 2 ordered complex perovskites niobates have been investigated by a number of investigators for possible applications in microwave communication devices[3]. There has been many attempts [4, 5] to predict the microwave dielectric properties by studying the solid solution phases in $Ba_{1-x}Sr_x(Mg_{1/3}Ta_{2/3})O_3$ system which provided valuable information about the structure property relation of low loss complex perovskites. The barium in complex perovskites can be easily substituted with strontium ion as they are isovalent and have comparable ionic radii (1.61 ? and 1.44 ? respectively) which are the two important requirements for a perfect solid solution. This involves a number of microscopic phenomena like tilting of octahedron and order-disorder transition etc. The complete replacement of Ba with Ca in the A-site of BMT was undertaken by Kagata and Kato [6] who found a highest quality factor of Qxf =78,000 GHz for $Ca(Mg_{1/3}Ta_{2/3})O_3$ ceramics. As described in Chapter 3: Section 3. 2. 4 and Chapter 4: Section 4.1, the substitution of a trivalent ion (La) in A-site of BMT results in the coexistence of both 1:1 and 1: 2 ordered domains[7, 8]. The substitution at the B site in Ba-based complex perovskites with tetravalent ion has been one of the most interesting part of the research on complex perovskites as this imparts significant effects on the structural order of these materials[9]. Even partial replacement of $(Mg_{1/3}Ta_{2/3})^{4+}$ with Ti^{4+} can destabilize the crystal structure of BMT ceramics[10].

The microwave dielectric properties of $Ba(Mg_{1/3}Ta_{2/3})O_3$-$A(Mg_{1/2}W_{1/2})O_3$ [A= Ba, Sr and Ca] have been investigated by Furuya and Ochi[11] who found that the presence of $Ba(Mg_{1/2}W_{1/2})O_3$ reduces the temperature coefficient of resonant frequency for BMT. The duo could develop a zero t_f composition for $0.95Ba(Mg_{1/3}Ta_{2/3})O_3$-$0.05Ba(Mg_{1/2}W_{1/2})O_3$ where the $Q_u$xf value is reaching as high as 40,000 GHz. A significant attempt in this direction was done by Takahashi et al.[12] who while investigating the

microwave dielectric properties of (1-x) $Ba(Mg_{1/2}W_{1/2})O_3$-x$BaTiO_3$ ceramics, found that for x= 2/3, the ceramics form a single phase (i.e. $Ba(Mg_{1/3}Ti_{1/3}W_{1/3})O_3$) with low dielectric constant and high quality factor. The above said composition is corresponding to x =1 in the $Ba(Mg_{1/3}Ta_{(2-2x)/3}W_{x/3}Ti_{x/3})O_3$ which is nothing but a solid solution between $Ta_{2/3}$ and $W_{1/3}Ti_{1/3}$ in BMT. So far no useful work has been done on the aspect of simultaneous substitutional characteristics of W and Ti on the Ta site in BMT which has been undertaken in this investigation. The effect of partial to complete substitution of Ta^{5+} with Ti and W in $Ba(Mg_{1/3}Ta_{2/3})O_3$ on the structure, microstructure, cation ordering, bond valence and microwave dielectric properties of the solid solution phases are discussed.

6. 1. 2 Experimental

The $Ba(Mg_{1/3}Ta_{(2-2x)/3}W_{x/3}Ti_{x/3})O_3$ [x = 0.01, 0.02, 0.03, 0.04, 0.05, 0.1, 0.15, 0.2, 0.25, 0.3, 0.4, 0.5, 0.6, 0.7, 0.8, 0.9 and 1.0] ceramics were prepared by the conventional mixed oxide route as described in Chapter. 2, Sections 2.1.2.1 to 2.1.2.7. The reaction mixture was calcined at 1200 ^oC for 10 hours with intermediate grinding. The uniaxially pressed cylindrical compacts were sintered in the temperature range 1500-1600 ^oC for 4 hours in air at a heating rate of 10^oC/hour. The powdered samples were used for analyzing the X-ray diffraction patterns using Cu K_α radiation (Rigaku, Japan) as described in Chapter 2, Section 2. 3. 1.

The dielectric properties ε_r and τ_f of the materials were measured in the microwave frequency range using resonance technique as described Chapter 2, Sections 2. 2. 2 to 2. 2. 5

6. 1. 3 Results and Discussion

The densification behaviour of the solid solution phases is plotted in Fig. 6.1. As given in Chapter 3, Section 3. 3. 4, the theoretical density of BMT is 7.625 g/cm^3 while that of $Ba(Mg_{1/3}W_{1/3}Ti_{1/3})O_3$ [13] is 6.112 g/cm^3. As expected the bulk density of the solid solution phases in $Ba(Mg_{1/3}Ta_{(2-2x)/3}W_{x/3}Ti_{x/3})O_3$ decreases with x.

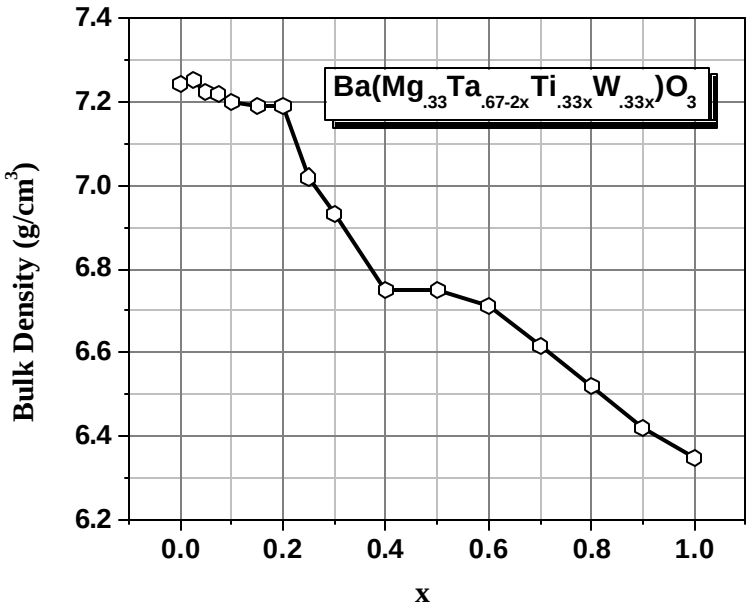

Fig. 6. 1 Variation of bulk density of solid solution phases in $Ba(Mg_{1/3}Ta_{(2-2x)/3}W_{x/3}Ti_{x/3})O_3$ as a function of x

Fig. 6. 2 represents the powder diffraction pattern of $Ba(Mg_{1/3}Ta_{(2-2x)/3}W_{x/3}Ti_{x/3})O_3$ [x =0.1, 0.2, 0.3, 0.4, 0.5, 0.7, 0.9 and 1.0]. The low loss ceramic systems involving $BaO\text{-}xMgO\text{-}yWO_3\text{-}zTiO_2$ [x+y+z=1] has already been investigated by Takahashi et al. [14] who, for x = 0.32, y = 0.32 and z = 0.68 suggested a 1:1:1 cation ordering between Mg-W-Ti along <100> direction. In our investigation, we could index the XRD reflections based on a hexagonal unit cell (a ~ 11.3 Å = 2 x v2 x 4 Å; c ~ 13.9 Å = 2 x v3 x 4 Å) assuming a lattice constant of a ~ 4 Å for the pseudo cubic unit cell [15].The formation of the B-site sublattice was recognized from (00n) line (n = 2, 4, 6…) [14]. When substitution levels of $(Ti_{1/3}W_{1/3})^{3.33+}$ at $(Ta_{2/3})^{3.33+}$ site, presence of unreacted TiO_2 (JCPDS File Card Number 21-1276) was detected in the powder diffraction pattern. A very small percentage of $Ba(Mg_{1/2}W_{1/2})O_3$ (JCPDS File Card Number 16-660) was also detected in the X-ray diffractogram for x = 0.3 in $Ba(Mg_{1/3}Ta_{(2-2x)/3}W_{x/3}Ti_{x/3})O_3$. It is evident from the powder diffraction patterns that the formation of ferroelectric $BaTiO_3$ (JCPDS File Card Number 24-129) takes place for $0.5 \leq x \leq 0.9$, which in turn severely affects the densification and microwave dielectric properties of the solid solution phases

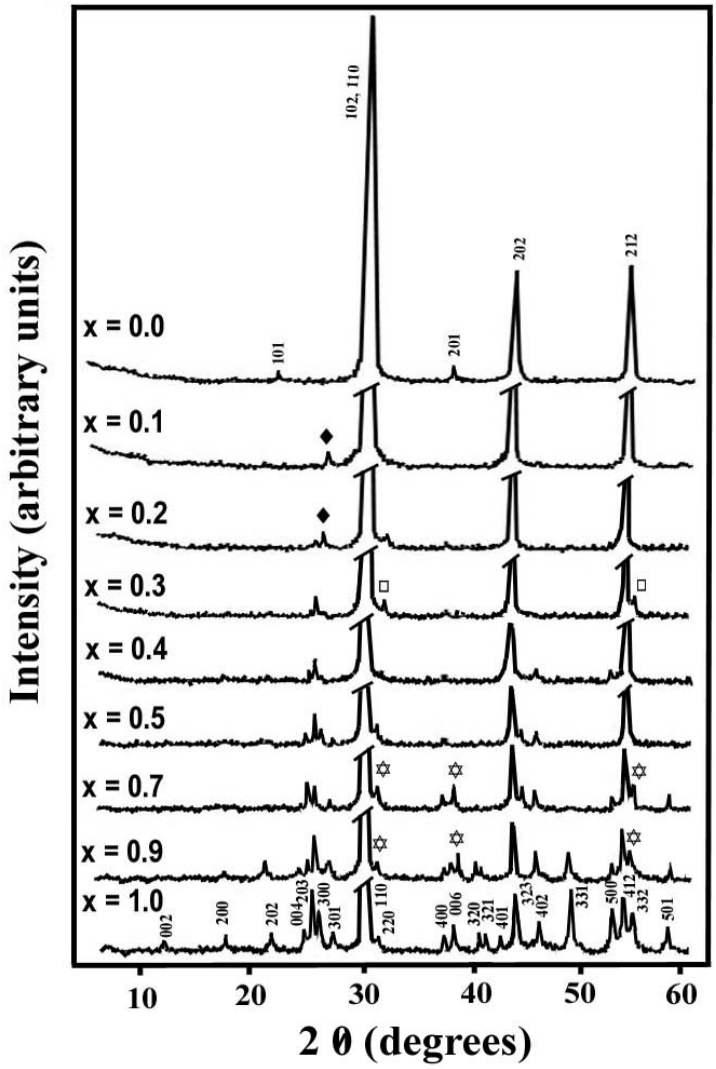

Fig. 6. 2 The powder diffraction pattern of $Ba(Mg_{1/3}Ta_{(2-2x)/3}W_{x/3}Ti_{x/3})O_3$ [x =0.1, 0.2, 0.3, 0.4, 0.5, 0.7, 0.9 and 1.0]. ◆ represents TiO_2, □ $Ba(Mg_{1/2}W_{1/2})O_3$, ✡ $BaTiO_3$

. Fig. 6. 3 represents the scanning electron micrograms recorded from three typical samples for (a) x = 0.05, (b) 0.15 and (c) 1.0 in $Ba(Mg_{1/3}Ta_{(2-2x)/3}W_{x/3}Ti_{x/3})O_3$. Greater densification and best unloaded quality factor are recorded for the composition $Ba(Mg_{0.333}Ta_{0.633}Ti_{0.016}W_{0.016})O_3$ whose average grain size is less than 5 μm. Since no additional phases are visible in the SEM, one can assume that addition of smaller percentages of WO_3/TiO_2 could have resulted in efficient substitution at the Ta site. In the SEM recorded (see Fig. 6. 3(b)) from sample $Ba(Mg_{0.33}Ta_{0.56}Ti_{0.05}W_{0.05})O_3$ a small amount of additional phases are visible which can be either TiO_2 or $BaTiO_3$. It is to be

remembered that this composition stays at the boundary where the t_f approaches zero value. On the other hand the SEM for $Ba(Mg_{0.33}Ti_{0.33}W_{0.33})O_3$ as given in Fig. 6.3(c) presents a porous picture. The phase structure shows signs of a possible liquid phase formed which is on the verge of melt.

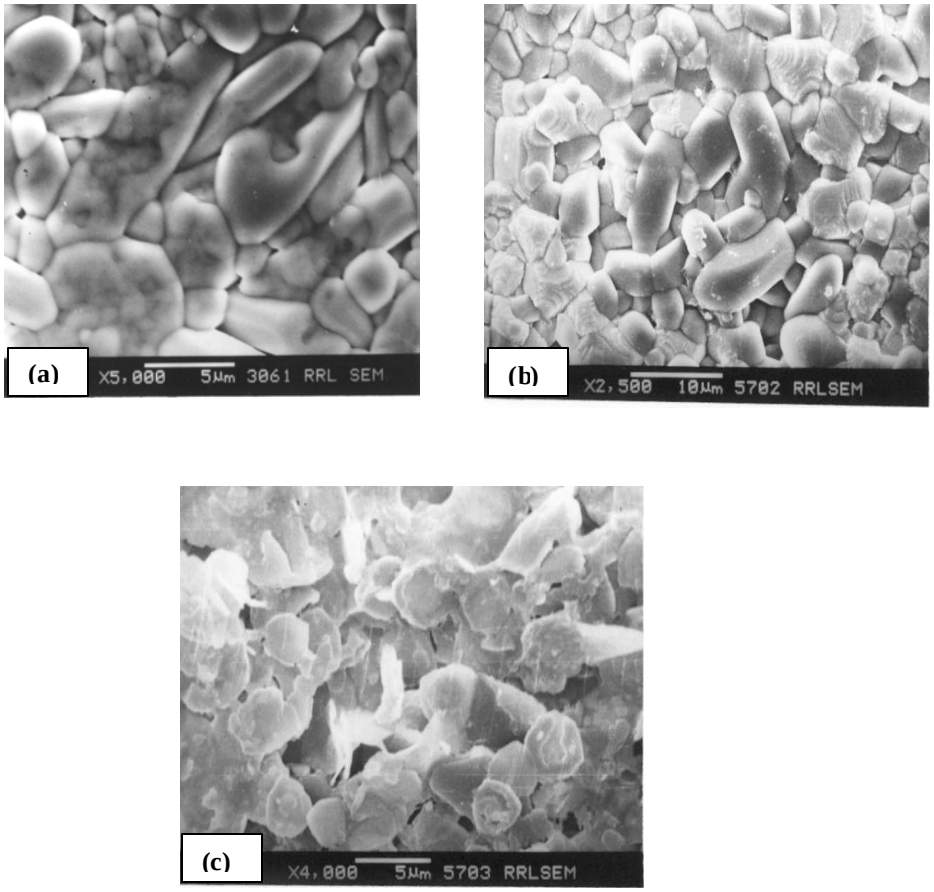

Fig. 6. 3 Typical SEM pictures of (a) $Ba(Mg_{0.333}Ta_{0.633}Ti_{0.016}W_{0.016})O_3$ and (b) $Ba(Mg_{0.33}Ta_{0.56}Ti_{0.05}W_{0.05})O_3$ and (c) $Ba(Mg_{0.33}Ti_{0.33}W_{0.33})O_3$.

The microwave dielectric properties of $Ba(Mg_{1/3}W_{1/3}Ti_{1/3})O_3$ is not as promising as the other end member of the solid solution, $Ba(Mg_{1/3}Ta_{2/3})O_3$. Fig. 6. 4 is a plot describing the variation of the dielectric constant of the solid solution phases with respect to the substitution of W+Ti at the Ta site in BMT. The measured values of dielectric constants were corrected for porosity[16]. At first, the dielectric constant increases to 25.21 for x = 0.05 in $Ba(Mg_{1/3}Ta_{(2-2x)/3}W_{x/3}Ti_{x/3})O_3$ from 24.8 for x=0.0 (i.e. $Ba(Mg_{1/3}Ta_{2/3})O_3$).

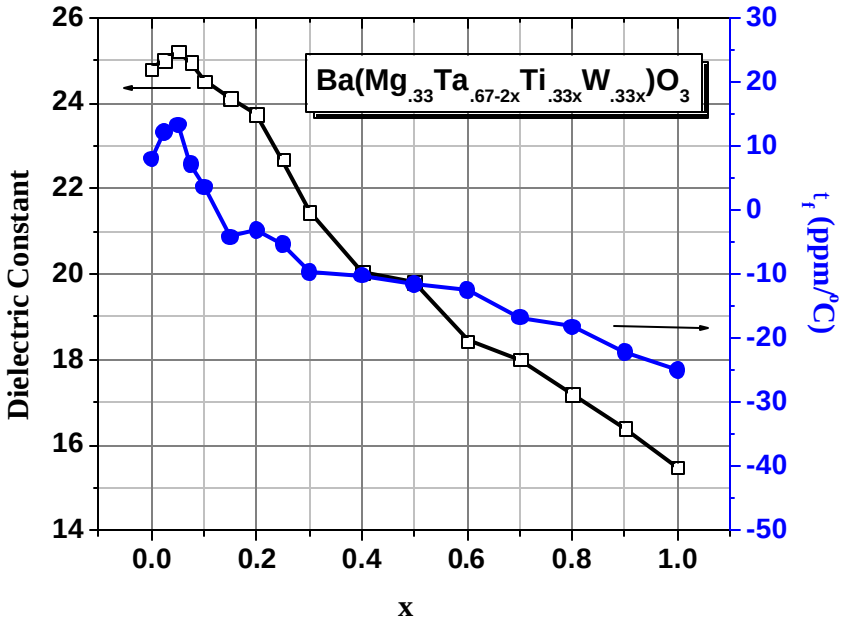

Fig. 6. 4 Variation of the dielectric constant of $Ba(Mg_{1/3}Ta_{(2-2x)/3}W_{x/3}Ti_{x/3})O_3$ as a function of x.

Thereafter the dielectric constant decreases monotonously for higher values of x, reaching 15.4 for $Ba(Mg_{1/3}W_{1/3}Ti_{1/3})O_3$. This dielectric constant for 1:1:1 ordered $Ba(Mg_{1/3}W_{1/3}Ti_{1/3})O_3$ is slightly higher than the value (14.5) published [16] in a previous report. The higher value of the dielectric constant is believed to be due to the presence of $BaTiO_3$ additional phase whose presence may be too low to be detected in XRD analysis.

The temperature coefficient of resonant frequency (t_f) of the solid solution phases is also plotted in Fig. 6.4. The t_f of stoichiometric $Ba(Mg_{1/3}Ta_{2/3})O_3$ is 8 ppm/^oC which increases to 13.3 for x = 0.05 in $Ba(Mg_{1/3}Ta_{(2-2x)/3}W_{x/3}Ti_{x/3})O_3$. It is evident from the Fig. 6.4 that the values of t_f for x=0.1 and 0.15 in $Ba(Mg_{1/3}Ta_{(2-2x)/3}W_{x/3}Ti_{x/3})O_3$ are 3.6 and -4.2 ppm/^oC respectively. This means that the temperature coefficient of resonant frequency is approaching zero between x=0.1 and 0.15 in $Ba(Mg_{1/3}Ta_{(2-2x)/3}W_{x/3}Ti_{x/3})O_3$. In general the t_f values of the solid solution phases will become more and more negative with increasing concentration of $(Ti_{1/3}W_{1/3})^{3.33+}$ at $(Ta_{2/3})^{3.33+}$ site in BMT. The t_f of $Ba(Mg_{1/3}W_{1/3}Ti_{1/3})O_3$ is -25.1 ppm/^oC. This value is higher than -7.6 ppm/^oC in a previous report [14] on the t_f of $Ba(Mg_{1/3}W_{1/3}Ti_{1/3})O_3$.

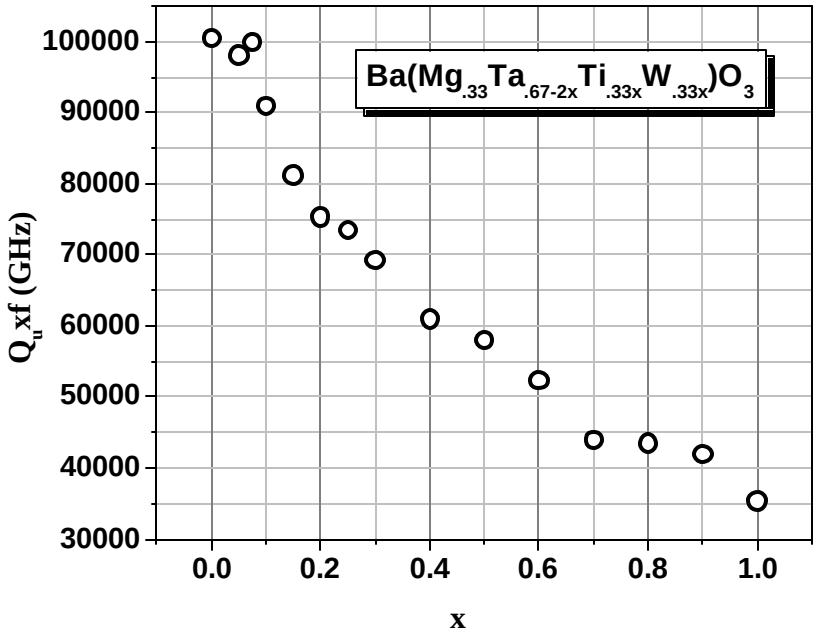

Fig. 6. 5 Variation of the unloaded quality factor of $Ba(Mg_{1/3}Ta_{(2-2x)/3}W_{x/3}Ti_{x/3})O_3$ as a function of x.

The quality factor of a dielectric resonator depends on a number of parameters including the processing conditions, densification etc. As it is clear from Fig.6.1, the densification of the sintered specimen are poor for the ($W_{1/3}Ti_{1/3}$) rich compounds. The unloaded quality factor of the solid solution phases are plotted in Fig. 6. 5. It is evident that the quality factor of $Ba(Mg_{1/3}W_{1/3}Ti_{1/3})O_3$ is inferior to that of $Ba(Mg_{1/3}Ta_{2/3})O_3$ ceramics. The quality factor of $Ba(Mg_{1/3}Ta_{2/3})O_3$ is $Q_u$xf = 100500 GHz while that of $Ba(Mg_{1/3}W_{1/3}Ti_{1/3})O_3$ is 35,400 GHz. It worthwhile to note that zero t_f compositions in the solid solution ($0.1<x<0.15$ in $Ba(Mg_{1/3}Ta_{(2-2x)/3}W_{x/3}Ti_{x/3})O_3$) the quality factor is reasonably high ($Q_u$xf = 80,000 -90,000 GHz).

As discussed in Chapter 3, Section 3. 1. 2, the tolerance factor of the perovskite system $Ba(Mg_{1/3}Ta_{(2-2x)/3}W_{x/3}Ti_{x/3})O_3$) [x = 0.0 -1.0] is given by

$$t = \frac{R_O + R_{Ba}}{\sqrt{2}\ \left[R_O + \left(0.33R_{Mg} + (0.67 - 2x)R_{Ta} + 0.33xR_W + 0.33xR_{Ti}\right)\right]} \qquad (6.1)$$

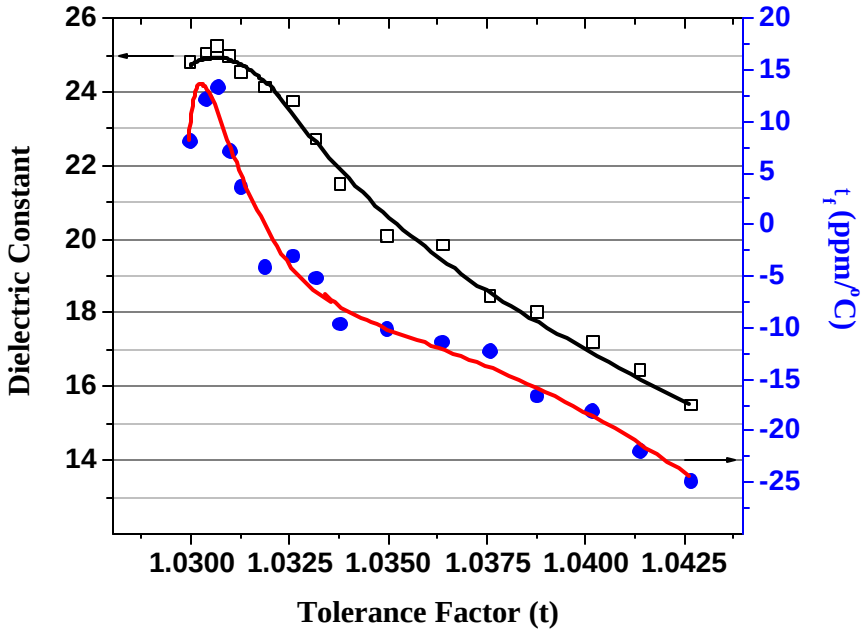

Fig. 6. 6 Variation of the e_r and t_f of $Ba(Mg_{1/3}Ta_{(2-2x)/3}W_{x/3}Ti_{x/3})O_3$ with tolerance factor.

Fig. 6.6 represents the variation of the tolerance factor of BMT with the gradual substitution of $(W_{1/3}Ti_{1/3})^{3.33+}$ at $(Ta_{2/3})^{3.33+}$ site. In a very significant observation, Reaney and Ubic observed[17] that the temperature coefficient of dielectric constant of complex perovskites depends on their tolerance factor which in turn depends on the tilting of the oxygen octahedron. The duo asserted that for a tolerance factor greater than 0.985 belongs to the untilted octahedron perovskites. It is evident that the calculated tolerance factor of $Ba(Mg_{1/3}Ta_{2/3})O_3$ is 1.03 and that of $Ba(Mg_{1/3}Ti_{1/3}W_{1/3})O_3$ is 1.0427, both have untilted octahedron and lower t_e values. Assuming the linear expansion coefficient to be around 10, most of the solid solution phases have negative or close to zero t_f values, which proves that the t_e have smaller values.

The tolerance factor (*t*) of perovskite structure has been reported to be closely related to the tilting of oxygen octahedron [18]. However, it is not enough to explain the change of t_f by the tolerance factor because the effective size of the ion in the center of oxygen octahedra is changed with tilting as reported by Shannon[19]. Moreover there has been previous observation that the temperature coefficient of the resonant frequency of

complex perovskite compounds was associated with the bond valences of the A- and B-sites, as well as the tolerance factor [20]. Considerable amount of work has been done in this regard [21, 22]. Bond valence of an atom *i* with another atom *j* is given by

$$V_{ij} = \exp[R_{ij} - d_{ij}] / b' \qquad (6.2)$$

where R_{ij} is the bond valence parameter, d_{ij} is the bond length between atom i and j and b' is a universal constant commonly taken the value 0.37?.

The total bond valence (V_B) in the perovskite B-site is the sum of all the valences from cationic B-site with the oxygen.

$$V_B = ? \{\exp(R_{B\text{-}O} - d_{B\text{-}O}) / b'\} \qquad (6.3)$$

where $R_{B\text{-}O} = ? R_{ij}$

and the average bond length of B-site cations with oxygen ($d_{B\text{-}O}$) is given as

$$d_{B\text{-}O} = (R_{(Ba)} + R_{(Mg)} + R_{(Ta/Ti/W)}) / 3 + R_O \qquad (6.4)$$

here R represents the radius of corresponding ions in the crystal system. The bond valence of B-site ions was calculated using equations (6.3), (6.4) and (6.5) from the parameters reported by Brown and Altermatt.[23]

The possible dependence of microwave dielectric properties of the solid solution phases in $Ba(Mg_{1/3}Ta_{(2-2x)/3}W_{x/3}Ti_{x/3})O_3$ on the bond valence of B cations is plotted in Fig. 6.7. The bond valence decreases steadily with increasing substitution of Ti and W on the Ta site in BMT. This could be understandable since the effective ionic radii of $(Ti_{1/2}+W_{1/2})^{5+}$ is 0.6025 Å which is less than that of Ta^{5+} (0.64 Å). The decreased ionic radius of $(Ti_{1/2}+W_{1/2})^{5+}$ leads to decreased bond length, which in turn decreases the bond valence of $Ba(Mg_{1/3}Ta_{(2-2x)/3}W_{x/3}Ti_{x/3})O_3$ ceramics with increase in mole fraction of Ti+W. A decrease of bond valence indicate a decreased bond strength at the Ti+W rich region of the solid solution. The lowering bond valence should point towards an increase

of dielectric constant as the constituent ions would become more polarisable if the bonding is weaker. The lower dielectric constant of $Ba(Mg_{1/3}Ti_{1/3}W_{1/3})O_3$ could be due to the 'rattling effect' [24] of the B-site with the substitution of Ti+W at the Ta site of BMT.

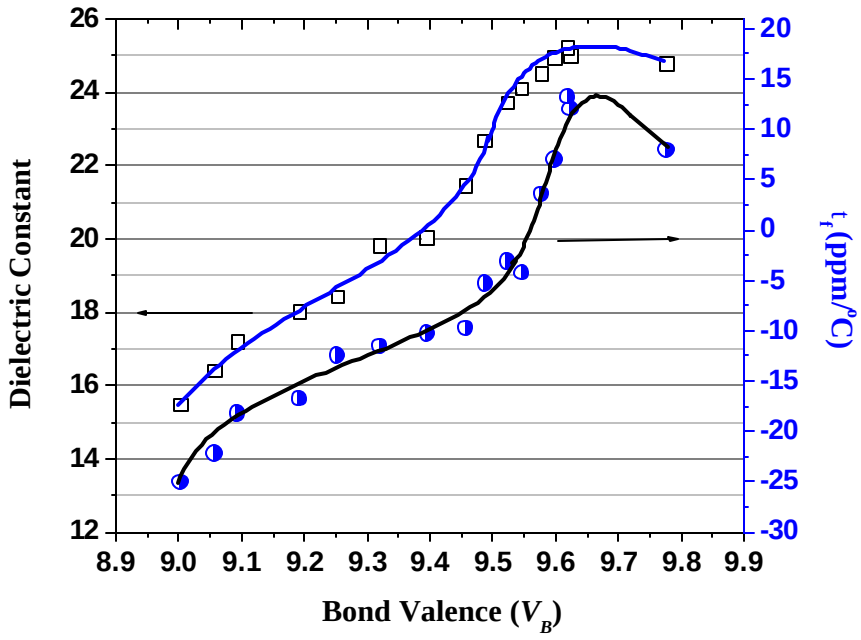

Fig. 6. 7 Variation of the e_r and t_f of $Ba(Mg_{1/3}Ta_{(2-2x)/3}W_{x/3}Ti_{x/3})O_3$ with bond valence.

6. 2 $Ba(Mg_{1/3}Ta_{2/3})_{1-x}Ti_xO_3$ CERAMICS

6. 2. 1 Introduction

The partial substitution of B-site cation with tetravalent ions like Zr, Ti and Hf has been extensively studied in ferroelectric complex perovskites has been studied [25,26, 27, 28] extensively over the last few years. These investigations could throw vital informations on the order-disorder transformations in lead based complex perovskites. As discussed in Chapter 3, Section 3. 2. 4 & Chapter 4, Section 4. 3, the partial replacement of B-site cation with tetravalent impurity impairs the cation ordering, thereby largely affecting their dielectric properties. For example, Chai & Davies observed that when tetravalent impurities were added to BMT, the cation ordering is changed from 1:2 to 1:1 but the greater amount of these substitutions would leave them disordered [29]. In addition

to that they categorically proved that no solid solubility for Zr in the 1:2 ordered BMT [30] while even partial substitution with Ti resulted in the complete disordered perovskite[31]. So a meticulous investigation on the partial to complete solid solubility of the $(Mg_{1/3}Ta_{2/3})^{4+}$ with Ti^{4+} would throw light into the order-disorder transformation of this complex perovskite. In this perspective we attempted to synthesize solid solution phases based on $Ba(Mg_{1/3}Ta_{2/3})_{1-x}Ti_xO_3$ [x = 0.0-1.0]. The range of solid solubility on the densification, cation ordering, tolerance factor, bond valence and microwave dielectric properties are discussed.

6. 2. 2 Experimental

The $Ba(Mg_{1/3}Ta_{2/3})_{1-x}Ti_xO_3$ [x= 0.0, 0.025, 0.05, 0.1, 0.2, 0.3, 0.4, 0.5, 0.6, 0.7, 0.8, 0.9 and 1.0] ceramics were prepared by the conventional mixed oxide route as described in Chapter 2, Sections 2. 1. 2. 1 to 2. 1. 2. 7. The reaction mixture was calcined at 1200 ^oC for 10 hours. The sintering temperature is 1500-1600 ^oC for 4 hours. The powdered samples were used for analyzing the X-ray diffraction patterns using Cu K_α radiation (Philips). The polished samples were thermally etched and their surface morphology and grain structure were analyzed using a scanning electron microscope (JEOL). The solid solution compositions which are not resonating at microwave frequency region were made in the form of thin dielectric capacitors and their dielectric properties were studied using an impedance analyzer (HP 4192 LF)

The dielectric properties ε_r and τ_f of the materials were measured in the microwave frequency range using resonance technique as described Chapter 2, Sections 2.2.2 to 2.2.5.

6. 2. 3 Results and Discussion

The crystal structure of $BaTiO_3$ is reported to be tetragonal [32] in the temperature range $13^oC<T<132\ ^oC$, with unit cell parameters a = 3.99 Å, c= 4.04 Å. In our investigation we got the unit cell parameters of polycrystalline $BaTiO_3$ as a = 4. 0112 Å and c = 4.127 Å. On the other hand as discussed in Chapter 3, Section 3.2, the crystal structure of ordered BMT is hexagonal with a= 5.782 ?, c= 7.067 ? . Fig. 6.8 represents

the variation of the bulk density of solid solution phases in $Ba(Mg_{1/3}Ta_{2/3})_{1-x}Ti_xO_3$ as a function of x. The theoretical densities of the end members are 7.625 (for $Ba(Mg_{1/3}Ta_{2/3})O_3$) and 6.06 g/cm^3 (for $BaTiO_3$) respectively. The densification of ferroelectric $BaTiO_3$ is 5.71 g/cm^3 which is about 92 % of its theoretical density. As expected the density of the solid solution phases decreases with the increase of x.

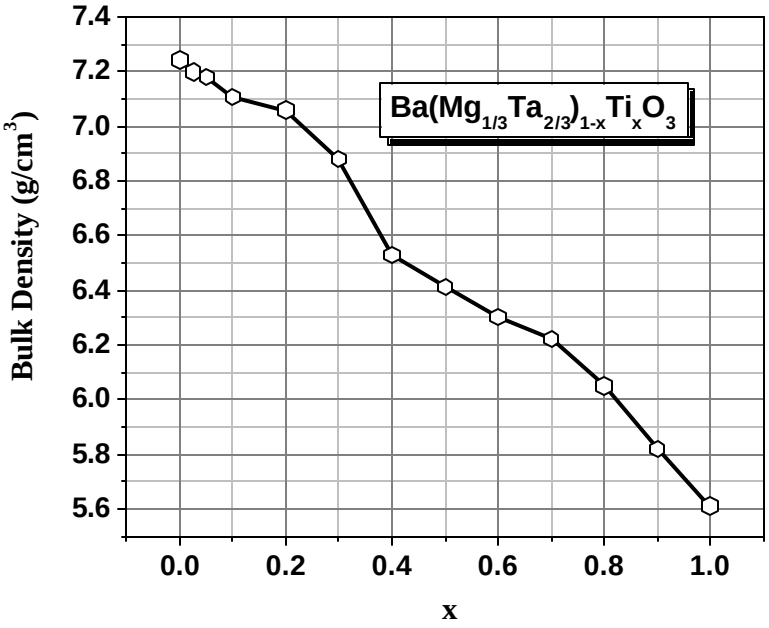

Fig. 6. 8 Variation of bulk density of solid solution phases in $Ba(Mg_{1/3}Ta_{2/3})_{1-x}Ti_xO_3$ with x

Fig. 6.9 (a) represents the SEM pictures of three typical compositions $Ba(Mg_{1/3}Ta_{2/3})_{0.8}Ti_{0.2}O_3$ (b) $Ba(Mg_{1/3}Ta_{2/3})_{0.5}Ti_{0.5}O_3$ and $Ba(Mg_{1/3}Ta_{2/3})_{0.2}$ $Ti_{0.8}O_3$ ceramics sintered at temperatures 1600, 1590 and 1575 ^oC respectively. The incorporation of 20 mole % TiO_2 to BMT (see Fig. 6.9 (a) is appeared to have increased the grain growth in BMT. Hence the grain size is about 5-8 μm. Since no additional phase is visible in the electron micrograph, it is believed that stoichiometric addition of TiO_2 might have resulted in the partial substitution of the B-site (i.e. $Mg_{1/3}Ta_{2/3}$). On the other substitutional addition of TiO_2 by 50 mole % failed to form complete solid solution as the presence of two distinct phases are visible in the SEM (Fig. 6.9 (b). The surface morphology of a typical titanium rich phase ($Ba(Mg_{1/3}Ta_{2/3})_{0.2}Ti_{0.8}O_3$ is presented in Fig. 6.9 (c). It is evident that the major phase ($BaTiO_3$) did not form well defined grains with

comparatively smaller BMT grains are also visible. This composition presents a porous structure.

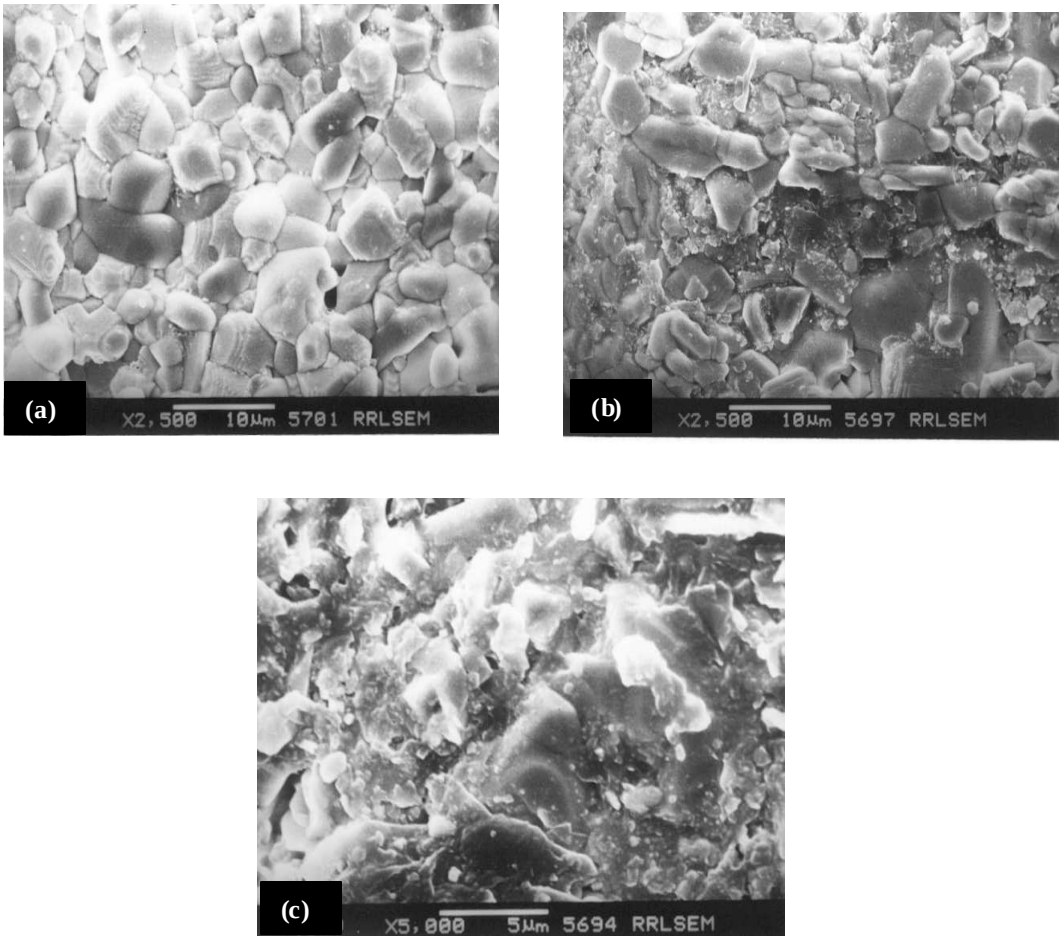

Fig. 6. 9 SEM pictures of (a) $Ba(Mg_{1/3}Ta_{2/3})_{0.8}Ti_{0.2}O_3$ (b) $Ba(Mg_{1/3}Ta_{2/3})_{0.5}Ti_{0.5}O_3$ and $Ba(Mg_{1/3}Ta_{2/3})_{0.2}Ti_{0.8}O_3$ ceramics

The dielectric properties of BMT-BT solid solution is very interesting as there are previous reports [30, 31] that the introduction of this tetravalent cation into the lattice of BMT destabilize its cation ordering mechanism and severely affects its microwave dielectric properties. Fig.6.10 represents the variation of the dielectric constant of BMT with respect to molar addition of $BaTiO_3$. The dielectric constant of the solid solution phases increases with increasing concentration of $BaTiO_3$ as the latter is a well known

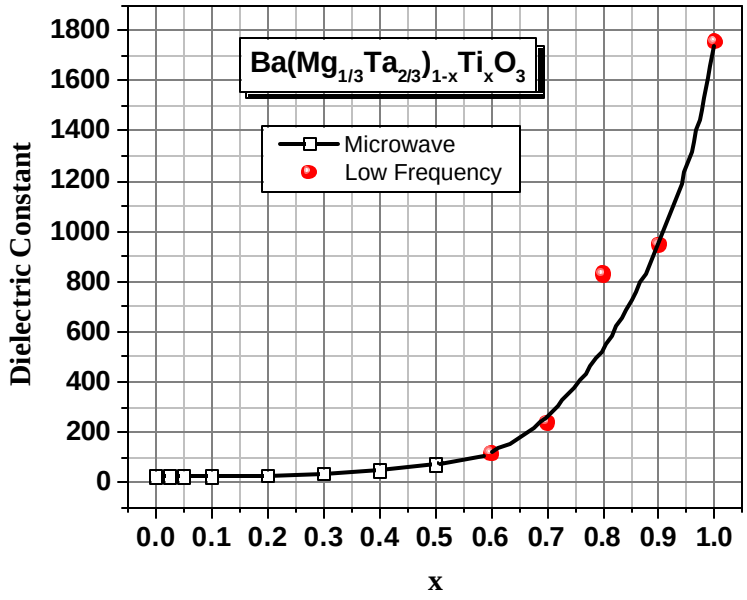

Fig. 6. 10 Variation of dielectric constant of $Ba(Mg_{1/3}Ta_{2/3})_{1-x}Ti_xO_3$ with x

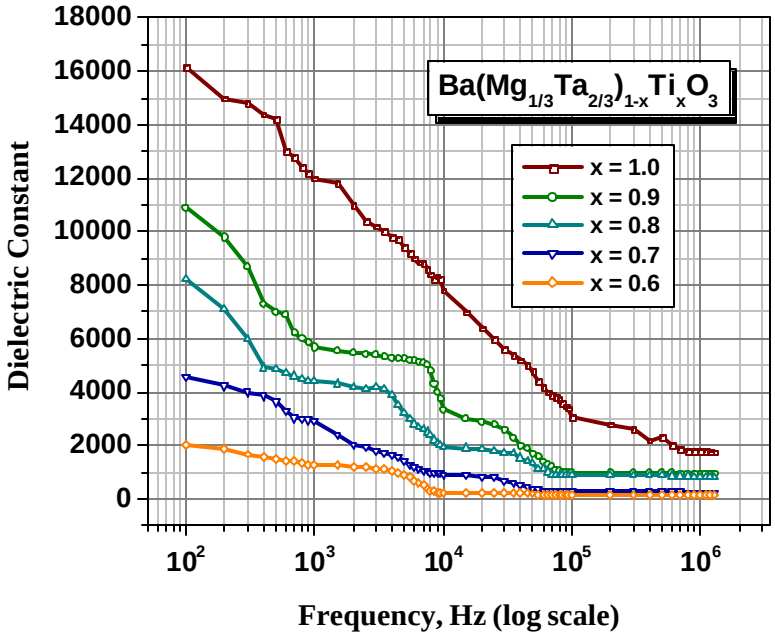

Fig. 6. 11 Variation of the dielectric constant of $Ba(Mg_{1/3}Ta_{2/3})_{1-x}Ti_xO_3$ for 0.5<x<1.0 in the frequency range 500 Hz-13MHz.

ferroelectric material whose dielectric constant is reported [33] to be above 2000. The dielectric constant of the composition $Ba(Mg_{1/3}Ta_{2/3})_{0.5}Ti_{0.5}O_3$ is 73.2. For any

composition with x >0.5 in $Ba(Mg_{1/3}Ta_{2/3})_{1-x}Ti_xO_3$, the dielectric properties are not measurable in the microwave frequency region due to the increase in loss factor. So we adopted low frequency impedance measurement techniques (in the frequency range 500 Hz-13 MHz) to determine the dielectric properties of the compositions for 0.5 < x < 1.0 in $Ba(Mg_{1/3}Ta_{2/3})_{1-x}Ti_xO_3$. The dielectric constant of $BaTiO_3$ was determined as 1756 which is less than previously reported values[34]. This has been attributed to its poor densification.

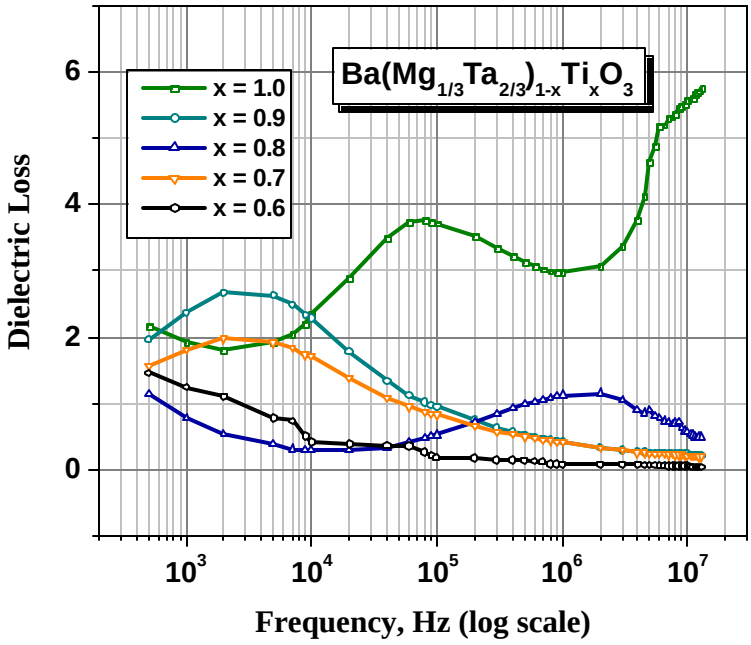

Fig. 6. 12 Variation of the dielectric loss of $Ba(Mg_{1/3}Ta_{2/3})_{1-x}Ti_xO_3$ for 0.5<x<1.0 in the frequency range 500 Hz-13MHz.

The dielectric constant and dielectric loss of the $BaTiO_3$ rich ceramic samples were measured in the frequency range 500 Hz-13 MHz using an impedance analyzer as given Figs. 6.11 and 6.12 respectively. As shown in Fig. 6.11, the dielectric constants of all the ceramic samples were greater at lower frequencies due to their influence of interfacial polarization resulting from the presence of moisture and mobile charge carriers present in the samples. With increase of the applied ac frequency, ionic polarization takes over[35] and the dielectric constant decreases. The values of dielectric constant plotted in Fig. 6.10 are measured at 13 MHz. The dielectric loss vary in a non uniform manner for high dielectric constant specimen for the 0.5 < x < 1.0 in $Ba(Mg_{1/3}Ta_{2/3})_{1-x}Ti_xO_3$ which is

typical characteristics of ferroelectric materials. It is to be noted that all the compositions undergo 'relaxation' at definite frequency ranges which differs from specimen to specimen

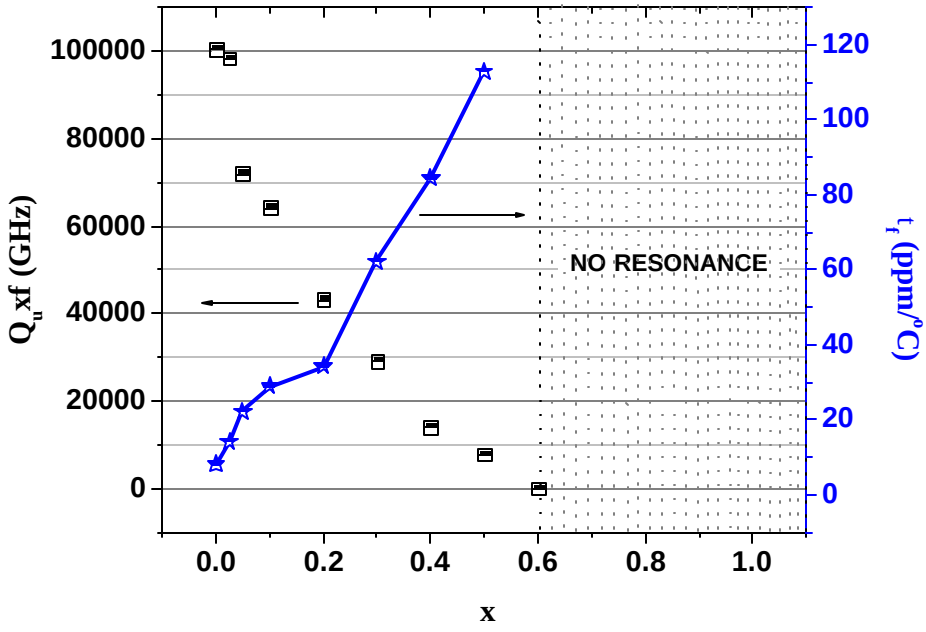

Fig. 6. 13 Variation of t_f and e_r of $Ba(Mg_{1/3}Ta_{2/3})_{1-x}Ti_xO_3$ with x

The microwave quality factor and temperature coefficient of resonant frequency are plotted in Fig. 6.13. It is evident that the quality factor of the specimen decreases as the value of x in $Ba(Mg_{1/3}Ta_{2/3})_{1-x}Ti_xO_3$ increases, while t_f increases. This observation confirms the finding by Andronescu et al.[10] on BMT-BT solid solution who noticed a deterioration of the dielectric properties of BMT with $BaTO_3$ incorporation. A similar view was shared by Choi et al.[36] who noted that addition of excess TiO_2 into BMT, forms $BaTiO_3$ which severely reduces the microwave quality factor this low loss BMT ceramic.

In a previous report Chai and Davies[31] observed that in (1-x) $Ba(Mg_{1/3}Ta_{2/3})O_3$-$xBaTiO_3$ ceramics, a complete solid solution will be possible only up to at a substitution of level of 10 mole % of $BaTiO_3$ in the BMT matrix. The average ionic radius of the ions in the B-site of BMT is 0.653 Å while the ionic radius of Ti^{4+} is 0.605 Å. This means that replacing $(Mg_{1/3}Ta_{2/3})^{4+}$ cation with relatively smaller Ti^{4+} ion will result in destabilizing the ordered perovskite structure owing to the dissimilarity in their ionic size.

This effect can be further elaborated by studying tolerence factor of the solid solution phases. The tolerance factor of stoichiometric BMT is calculated as 1.03 and that of BT is

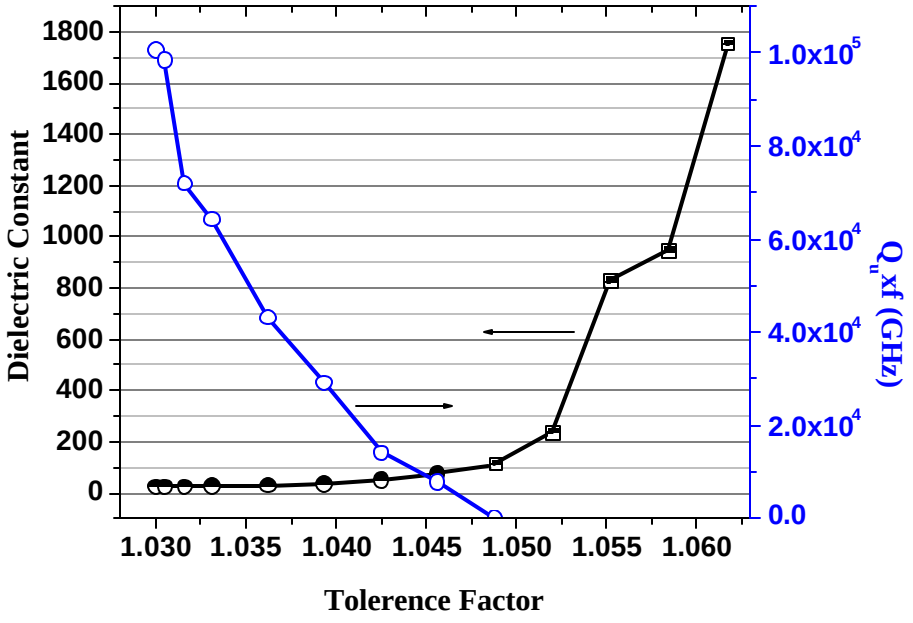

Fig. 6. 14 Variation of dielectric constant and quality factor with tolerence factor of $Ba(Mg_{1/3}Ta_{2/3})_{1-x}Ti_xO_3$ solid solution phases

1.0617 which are calculated using the ionic radii values reported by Shannon [26]. The variation dielectric constant and quality factor of solid solution phases in $Ba(Mg_{1/3}Ta_{2/3})_{1-x}Ti_xO_3$ with tolerance factor are plotted in Fig. 6.14. It is found that the quality factor of the solid solution phases are correlated to their tolerance factor. The resonance vanishes when the tolerance factor the solid solution phases are greater than 1.045. In other words the upper limit of tolerence factor for a partial substitution of tetravalent Ti^{4+} ion at the B-site of BMT is 1.045. For higher level of Ti^{4+} ion will increase the tolerence factor and destabilize the basic perovskite structure into a disordered one.

6. 3 $Ba[(Mg_xZn_{1-x})_{1/3}Ta_{2/3}]O_3$ CERAMICS

6. 3. 1 Introduction

The substitution of Zn in the Mg site in $A(B'_{1/3}Ta_{2/3})O_3$ has attracted a lot of scientific curiosity (due to the structural similarity of the end members but with different

properties) which has been successfully attempted in $Pb(Mg_{1/3}Ta_{2/3})O_3$ relaxor ceramics [37, 38]. In the recent past, a lot of work has been done on the solid solution between Zn and Mg ions in low loss complex oxides [39, 40]. The solid solution between $Ba(Mg_{1/3}Ta_{2/3})O_3$ and $Ba(Mg_{1/3}Nb_{2/3})O_3$ has also been attempted by many investigators [41]. The first reported work on the solid solution between $Ba(Mg_{1/3}Ta_{2/3})O_3$ and $Ba(Zn_{1/3}Ta_{2/3})O_3$ was done by Nomura[42] who observed a monotonous variation of the dielectric properties between BMT and BZT. In that work, with 1.0 mole % Mn addition, the dielectric properties of BMT was reported as e_r = 25, t_f = 4.4 ppm/^oC and Q_u = 16,800 at 10.5 GHz, while that of BZT are e_r = 30, t_f = 0.6 ppm/^oC and Q_u = 14,500 at 11.4 GHz. The intermediate compositions of the solid solution phases exhibits intermediate dielectric properties even though there are marked difference in the ordering characteristics of the two ceramics. For example, Vincent et al.[43] have shown that $Ba_3MgTa_2O_9$ exhibit only partial ordering where as $Ba_3ZnTa_2O_9$ is fully ordered[44]. A significant contribution in this regard was made by Ohuchi et al. [45] who observed an anomalous variation of the microwave Q factor in BMT-BZT solid solution phases. They found that dielectric ceramics with composition 0.5BMT-0.5BZT have excellent dielectric properties (e_r = 27, t_f = 1.95 ppm/^oC and Q_u = 10430 at 12.94 GHz). In a recent report [46] on BMT-BZT solid solution too, anomalous variation of the dielectric constant was observed which demands a more meticulous investigation on this system. So we synthesized solid solution phases $Ba_3Mg_{1-x}Zn_xTa_2O_9$ [x= 0.0, 0.1, 0.2, 0.3, 0.4, 0.5, 0.6, 0.7, 0.8, 0.9 and 1.0] and the influence of the substitution of Zn at Mg site in BMT on the densification, cation ordering, bonding valence, microstructure and microwave dielectric properties of solid solution phases were discussed.

6. 3. 2 Experimental

The $Ba[(Mg_{1-x}Zn_x)Ta_{2/3}]O_3$ [x= 0.0, 0.1, 0.2, 0.3, 0.4, 0.5, 0.6, 0.7, 0.8, 0.9 and 1.0] ceramics were prepared by the conventional mixed oxide route as described in Chapter. 2, Sections 2. 1. 2. 1 to 2. 1. 2. 7. The reaction mixture was calcined at 1200 ^oC. The compacts were sintered in the temperature range 1500-1600 ^oC for 4 hours. The powdered samples were used for analyzing the X-ray diffraction patterns using Cu K_α radiation (Philips).

The dielectric properties ε_r and τ_f of the materials were measured in the microwave frequency range using resonance technique as described Chapter 2, Sections 2. 2. 2 to 2. 2. 5.

6. 3. 3 Results and Discussion

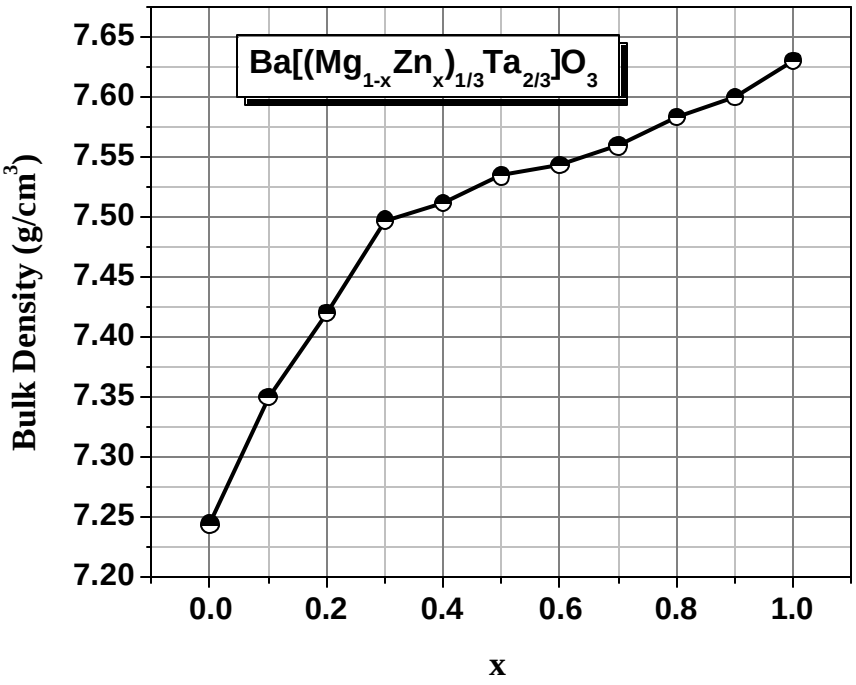

Fig. 6. 15 Variation of bulk density of solid solution phases in $Ba[(Mg_{1-x}Zn_x)Ta_{2/3}]O_3$ with x

The crystal structure of ordered BMT and BZT are hexagonal with space group $P\bar{3}m1$ [47]. The theoretical densities of barium magnesium tantalate[48] and barium zinc tantalate[49] are 7.625 and 7.963 g/cm^3 respectively. Fig. 6.15 represents the variation of the bulk density of the solid solution phases in $Ba[(Mg_{1-x}Zn_x)Ta_{2/3}]O_3$ ceramics with x. It seems that the $Ba(Mg_{1/3}Ta_{2/3})O_3$ and $Ba(Zn_{1/3}Ta_{2/3})O_3$ ceramics are structurally similar and hence their powder diffraction patterns look alike and are not given here. The unit cell properties of BMT-BZT solid solution are given in Table 6.1.

Table 6.1 Unit cell properties of $Ba[(Mg_{1-x}Zn_x)Ta_{2/3}]O_3$ solid solution phases

x in $Ba[(Mg_{1-x}Zn_x)Ta_{2/3}]O_3$	a (Å)	c (Å)	c/a	Cell Volume	Order parameter
0.0	5.7871	7.0892	1.2250	205.606	0.8250
0.1	5.7850	7.0957	1.2265	205.646	0.8793
0.2	5.7901	7.0965	1.2256	206.032	0.8820
0.3	5.798	7.1022	1.2266	206.760	0.8991
0.4	5.7903	7.1049	1.2270	206.289	0.8742
0.5	5.7895	7.1045	1.2271	206.221	0.9450
0.6	5.7851	7.0974	1.2268	205.702	0.9320
0.7	5.7869	7.1053	1.2278	206.059	0.9078
0.8	5.7885	7.1098	1.2282	206.303	0.9217
0.9	5.7893	7.1125	1.2285	206.439	0.9167
1.0	5.7899	7.1178	1.2293	206.636	0.7675

Galasso [50] reported the unit cell parameters of $Ba(Mg_{1/3}Ta_{2/3})O_3$ as a = 5.782 ?, c = 7.067 ? and that of $Ba(Zn_{1/3}Ta_{2/3})O_3$ as a = 5.782 ?, c = 7.097 ?. In our investigation, the unit cell parameters of BMT were measured as a = 5.7871 ?, c = 7.0892 which is in good agreement with previous observations within the limits of experimental error. The cell parameters of BZT were measured as a = 5.7899 ? and c = 7.1178 ?. It is well known that the electrostatic interactions between Mg/Zn and Ta lead to the stabilization of 1:2 long range ordered structure along the <111> direction. From Table 6.1 it is evident that the unit cell expends along the <111> direction so that c/a = 1.2247 in all compositions of the solid solution phases. In general, the unit cell expends with increase in the mole fraction of the Zn in the Mg site of BMT. As shown in Chapter 3, Section 3.2.3, the cation ordering of the BMT is calculated using the following expression [51]

$$S_{BMT} = \sqrt{\frac{(I_{(100)} / I_{(110),(102)})_{observed}}{(6.2/100)}} \qquad (6.5)$$

while that for BZT is calculated by the expression [52]

$$S_{BZT} = \sqrt{\frac{(I_{(100)} / I_{(110),(102)})_{observed}}{(3.7/100)}} \tag{6.6}$$

So the cation ordering parameter of solid solution phases between BMT and BZT are calculated using the empirical relation

$$S = (1\text{-}x)\, S_{BMT} + x\, S_{BZT} \tag{6.7}$$

The calculated values of ordering parameter are given in Table 6.1 from which it is clear that the solid solution phases posses high degree of cation ordering.

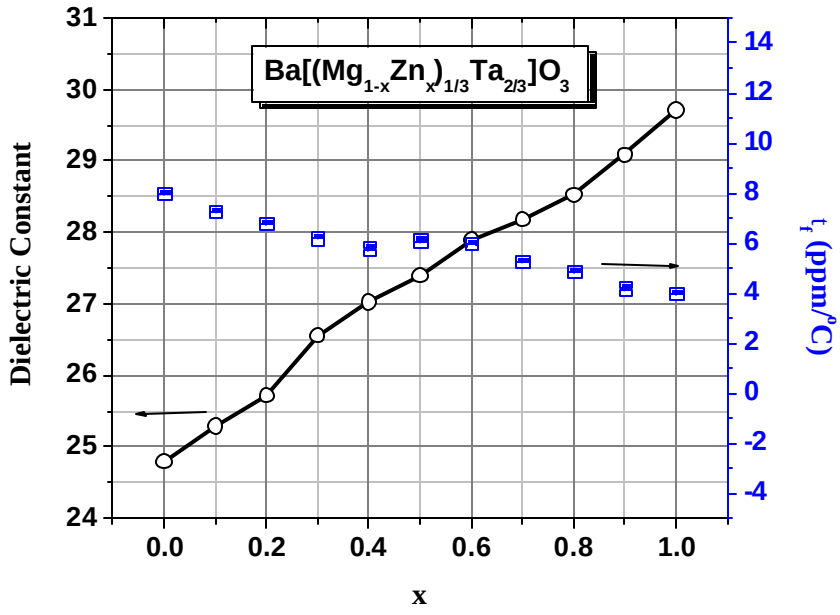

Fig. 6. 16 Variation of e_r and t_f of the solid solution phases in $Ba[(Mg_{1-x}Zn_x)Ta_{2/3}]O_3$ ceramics with x

The dielectric properties of BMT-BZT solid solutions were reported to be ideal for practical applications as both the end members are high Q ceramics with similar structure and very small t_f. The dielectric constant and temperature coefficient of resonant frequency were plotted in Fig. 6.16. The dielectric constant of BMT is 24.8

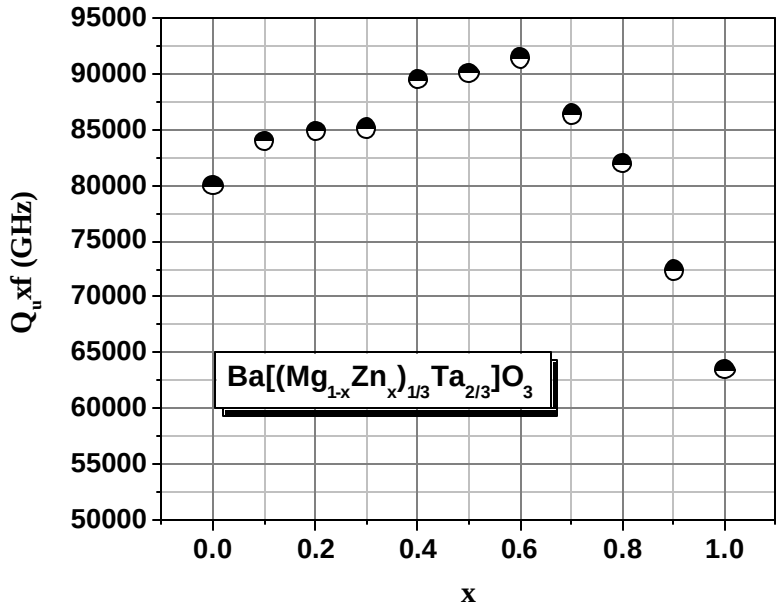

Fig. 6. 17 Variation of the quality factor of the solid solution phases in $Ba[(Mg_{1-x}Zn_x)Ta_{2/3}]O_3$ ceramics with x

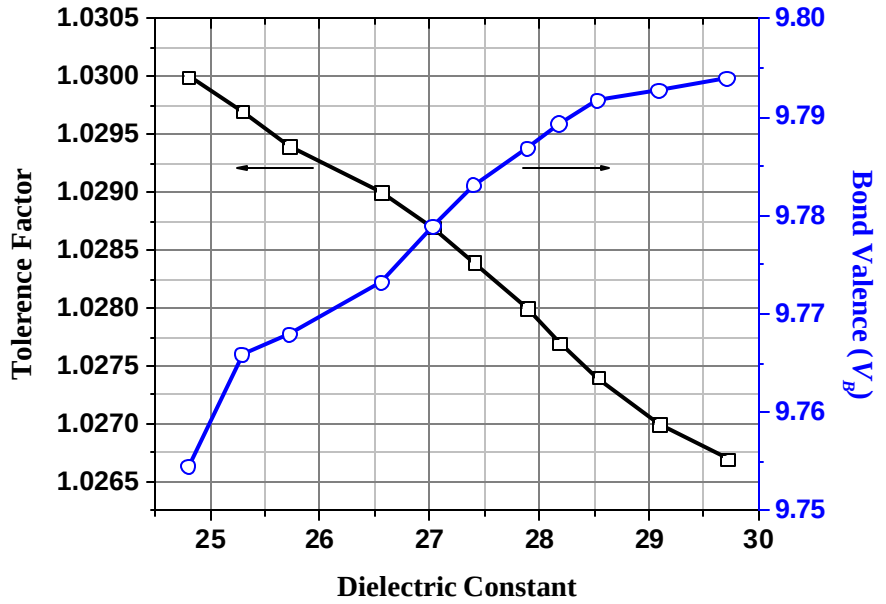

Fig. 6. 18 Variation of the tolerence factor and B -site bond valence of the solid solution phases in $Ba[(Mg_{1-x}Zn_x)Ta_{2/3}]O_3$ ceramics as a function of dielectric constant

while that of BZT is 29.71. The increase of the dielectric constant is monotonous with the increase of x in $Ba[(Mg_{1-x}Zn_x)Ta_{2/3}]O_3$. It is interesting to note that the variation of the

temperature coefficient of resonant frequency of the solid solution is between 8 ppm/^{o}C (for BMT) and 4.1 ppm/^{o}C (for BZT).

The variation of the unloaded quality factor of the solid solution phases are given 6.17. The quality factors of pure unannealed BMT and BZT are $Q_u$xf = 80,000 and 63,500 GHz respectively. The quality factor reaches a maximum ($Q_u$xf= 91,440 GHz) for $Ba[(Mg_{0.4}Zn_{0.6})Ta_{2/3}]O_3$. As the substitution level of Zn at Mg site is greater than x = 0.6, then dielectric loss increases. In a recent study, Shimada[53], using far infrared spectroscopy, established that the damping constants are more for lattice vibrations in BMT-BZT solid solution phases with higher zinc content.

The tolerence factor and the bond valence of the B-site cation of the solid solutions phases $Ba[(Mg_{1-x}Zn_x)Ta_{2/3}]O_3$ are plotted in Fig. 6.18 with respect to the variation of their dielectric constant. It is worthwhile to note that the bond valence of B-site cations which is a yardstick of B-O bond strength, is slightly higher for BZT (9.7939) than BMT (9.7545). Furthermore, the individual ionic polarizability of Zn (2.04) is greater than Mg (1.32) which can conveniently explain the comparatively higher dielectric constant of BZT. The tolerence factor for BMT is 1.03 which is higher than that of BZT (1.0267). It is found that the dielectric constant bears a linear relationship with tolerence factor in BMT-BZT solid solutions.

6. 4 CONCLUSIONS

- The $Ba(Mg_{1/3}Ta_{(2-2x)/3}W_{x/3}Ti_{x/3})O_3$ [x = 0.01, 0.02, 0.03, 0.04, 0.05, 0.1, 0.15, 0.2, 0.25, 0.3, 0.4, 0.5, 0.6, 0.7, 0.8, 0.9 and 1.0] ceramics were prepared by the conventional mixed oxide route and their microwave dielectric properties were studied. The densification is poor at the Ti+W rich compositions. The dielectric constant decreases, while the temperature coefficient of resonant frequency decreases and approaches negative values with increase of x in $Ba(Mg_{1/3}Ta_{(2-2x)/3}W_{x/3}Ti_{x/3})O_3$. The t_f is approaching zero between x = 0.1 and 0.15 in $Ba(Mg_{1/3}Ta_{(2-2x)/3}W_{x/3}Ti_{x/3})O_3$. The microwave dielectric properties of of $Ba(Mg_{1/3}W_{1/3}Ti_{1/3})O_3$ e_r =15.4, t_f -25.1 ppm/^{o}C, $Q_u$xf= 35,400 GHz. For zero t_f compositions in the solid solution ($0.1<x<0.15$ in $Ba(Mg_{1/3}Ta_{(2-2x)/3}W_{x/3}Ti_{x/3})O_3$) have reasonably high ($Q_u$xf = 80,000-90,000 GHz).

- In $Ba(Mg_{1/3}Ta_{2/3})_{1-x}Ti_xO_3$ [x= 0.0, 0.025, 0.05, 0.1, 0.2, 0.3, 0.4, 0.5, 0.6, 0.7, 0.8, 0.9 and 1.0] solid solution the density decreases with increase of substitution of Ti at the B-site of BMT. The dielectric constant of the solid solution phases increases with increasing concentration of TiO_2. The resonance vanishes in the compositions for $0.5<x<1.0$ in $Ba(Mg_{1/3}Ta_{2/3})_{1-x}Ti_xO_3$ due to greater dielectric loss introduced by the presence of lossy $BaTiO_3$ dielectric. The quality factor of the ceramic decreases as the value of x in $Ba(Mg_{1/3}Ta_{2/3})_{1-x}Ti_xO_3$ increases, while t_f increases. A correlation was established between the quality factor of the solid solution phases to their tolerance factor. The upper limit of tolerence factor for a partial substitution of tetravalent Ti^{4+} ion at the B-site of BMT is 1.045.
- In $Ba[(Mg_{1-x}Zn_x)Ta_{2/3}]O_3$ [x= 0.0, 0.1, 0.2, 0.3, 0.4, 0.5, 0.6, 0.7, 0.8, 0.9 and 1.0] solid solution, the density increases as the substitutional level of Zn at Mg site increases. The unit cell parameter ratio *c/a* = 1.2247 in all compositions of the solid solution phases. The unit cell expands with increase in the mole fraction of the Zn in the Mg site of BMT. The dielectric constant increases monotonously with increasing mole fraction of Zn in the Mg site while the values of temperature coefficient of resonant frequency vary between 8 and 4.1 ppm/^oC. The microwave dielectric properties of pure $Ba(Zn_{1/3}Ta_{2/3})O_3$ is e_r = 29.7, t_f = 4.1 ppm/^oC and $Q_u$xf= 63,500 GHz. The quality factor reaches a maximum ($Q_u$xf= 91,440 GHz) for $Ba[(Mg_{0.4}Zn_{0.6})Ta_{2/3}]O_3$.

6. 5 REFERENCES

1. D. J. Barber, K.M. Moulding, J.I. Zhou and M. Li , *J. Mater. Sci.*, **32**, 1531–44 (1997).

2. B. P. Burton, E. Cockayner, *Phys. Rev. B*, **60**, 12542-46 (1999).

3. J. Browne, *Microwaves & RF*, **39**, pp 153-58 (2000).

4. T. Nagai, T. Inuzuka and M. Sugiyama, *Jpn. J. Appl. Phys*., **31**, 3132-35 (1992).

5. J. Venkatesh and V. R. K. Murthy, *Mater. Chem. Phy*., **58**, 276-79 (1999).

6. H. Kagata and J. Kato, *Jpn. J. Appl. Phys*., **33**, 5463-65(1994)

7. J. Youn, K.S. Hong, and H. Kim, *J. Mater. Res*., **12**, 589-92 (1997).

8. H. J. Youn, K.S. Hong, and H. Kim, *J. Kor. Phys. Soc*., **32**, S524-S526 (1998).

9. W. K. Choo, S.B. Park, K. Eo and H. J. Im, *Proc. the 10th US-Japan Seminar on Dielectric & Piezoelectric Ceramics-2001*, p. 79 (2001)

10. C. Andronescu, A. Folea and A. Rahaianu, *Electroceramics –V*, (Ed.) Waser, 73-77 (1994).

11. M. Furuya and A. Ochi, *Jpn. J. Appl. Phys*., **33**, 5482-87 (1994).

12. H. Takahashi, K. Ayusawa and N. Sakamoto, *Jpn. J. Appl. Phys*., **36**, 5597-99 (1997).

13. K. P. Surendran, P. Mohanan and M. T. Sebastian (unpublished data).

14. H. Takahashi, K. Ayusawa and N. Sakamoto, *Jpn. J. Appl. Phys*., **37**, 908-11 (1998).

15. E. J. Fresia, L. Katz and R. Ward, *J. Am. Ceram. Soc*., 81, 478-81 (1959)

16. S. J. Penn, N. M. Alford, A. Templeton, X. Wang, M. Xu, M. Reece and K. Schrapel, *J. Am. Ceram. Soc*., **80**,1885-88 (1997).

17. I. M. Reaney and R. Ubic, *Ferroelectrics*, **228**, 23-38 (1999).

18. I. M. Reaney, E.L. Colla and N. Setter, *Jpn. J. Appl. Phys*., **33**, 3984–90 (1994).

19. R. D. Shannon, *Acta Cryst*., **A32**, 751-67 (1976).

20. N. E. Brese and M. O'Keefe, *Acta Cryst*., **B47,** 192-97 (1991).

21. H. S. Park, K. H. Yoon and E. S. Kim, *J. Mater. Res.* **16**, 817–21(2001).

22. E. S. Kim, Y. H. Kim, J. H. Chae, D. W. Kim and K. H. Yoon, *Mater. Chem. Phys.*, **79**, 230 (2003).

23. I. D. Brown and D. Altermatt, *Acta Cryst*., **B41,** 244-58 (1985).

24. Y. S. Cho, K. H. Yoon, B. D. Lee, H. R. Lee and E. S. Kim, *Ceram. Inter.*, (in press) (2004).

25. X. J. Lu and X.M. Chen, *J. Mater. Res.*, **16**, 2053-56 (2001).

26. Y. Abe, T. Tanaka, K. Kakegawa and Y. Sasaki, *Mater. Lett.*, **47**, 308-13 (2001).

27. J. T. Wang and F. Tang , *Mater. Chem. Phys*., **75**, 86–89 (2002).

28. J-S. Kim and N-K. Kim, *Mater. Res. Bull.*, **35,** 2479–89 (2000)

29. L. Chai, M. A. Akbas and P. K. Davies, *Proc. Solid State Chemistry of Inorganic Materials*, Boston 2-5 December, p. 443-48 (1996).

30. L. Chai, M. A. Akbas P. K. Davies and J. B. Parise, *Mater. Res.Bull.*, **32**, 1261-69 (1997).

31. L. Chai and P. K. Davies, *Mater. Res. Bull*., **33**, 1283-92 (1998).

32. Internet Data, URL : http://www.physoe.com/english/e-010101BaTiO3/0101.htm

33. J. Thongrueng, K. Nishio, Y. Watanable, K. Nagata and T.Tsuchiya, *J. Austr. Ceram. Soc*., **37**, 51-55 (2001).

34. W. J. Merz, *Phys. Rev*., **75**, 687-89 (1949).

35. Kiran S. Pokkuluri, *Effect of Admixtures, Chlorides, and Moisture on Dielectric Properties of Portland Cement Concrete in the Low Microwave Frequency Range*, M S Thesis, Virginia Polytechnic Institute, USA (1998)

36. C. H. Choi, C.H. Choi, S. Nahm and Y. W. Song, *J. Kor. Phys. Soc.*, **35**, S410-S414 (1999).

37. M-C. Chae, S-M. Lim, N-K. Kim and B-O. Park, *Mater. Res. Bull.*, **36**, 2443–51 (2001).

38. S-M. Lim and N-K. Kim, *Mater. Res. Bull.*, **37**, 59-67 (2002).

39. Y. C. Zhang, J. Wang, Z. X. Yue, Z. L. Gui and L. T. Li, *Ceram. Inter.*, **30**, 87-91 (2004).

40. A. Yoshida, H. Ogawa, A. Kan, S. Ishihara and Y. Higashida, *J. Eur. Ceram. Soc.*, **24**, 1765-68 (2004).

41. T-R. Tsai, C-C. Chi, M-H. Liang, C-T. Hu and I-N. Lin, *Mater. Chem. Phys.*, **79**, 169-74 (2003).

42. S. Nomura, *Ferroelectrics*, **49**, 61-70 (1983).

43. H. Vincent, C. Perrier, P. L'Heritier, M. Labeyrier, *Mater. Res. Bull.*, **28**, 951-58 (1993).

44. A. J. Jacobson, B. M. Collins and B. E. F. Fender, *Acta, Cryst*., **B32**, 1083-86(1993)

45. H. Ohuchi, M. Okajima and H. Ito, *Electroceramics-V*, Book 2, 1-4 (1996).

46. M. Thirumal, I. N. Jawahar, K.P. Surendiran, P. Mohanan and A. K. Ganguly, *Mater. Res. Bull.*, **37**, 2321-34 (2002).

47. T. Takahashi, *Jpn. J. Appl. Phys*., **39**, 5637-41 (2000).

48. S. Nomura, K. Toyama and K. Kaneta, *Jpn. J. Appl. Phys*., 21, L 624-26 (1982)

49. S. Kawashima, M. Nishida, I. Ueda, H. Ouchi and S. Hayakawa, *Proc. of the 1st meeting on Ferroelectric Materials and their Applications*, Keihin Printing Co. Ltd., Kyoto, p. 293-96 (1977).

50. F. S. Galasso, *Structure, Properties and Preparation of Perovskite type Compounds*, Pergamon Press, Oxford (1969).

51. H-J. Yoon, K-Y. Kim and H. Kim, *Jpn. J. Appl. Phys*., **35**, 3947-53 (1996).

52. A. J. Jacobson, B. M. Collins and B. E. F. Fender, *Acta Crystallogr.*, **B32,** 1083-87 (1986).

53. T. Shimada, *J. Eur. Ceram. Soc.*, **24**, 1799-1803 (2004).

CHAPTER 7

TAILORING THE MICROWAVE DIELECTRIC PROPERTIES OF $RETiAO_6$ [A=Ta, Nb] CERAMICS

This Chapter deals with $RETiNbO_6$ and $RETiTaO_6$ ceramics which have orthorhombic structure but have two different symmetries (aeschynites and euxenites) depending on RE ionic radius. The aeschynites have high dielectric constant and positive t_f and euxenites have low dielectric constant and negative t_f. This chapter discusses the tailoring of the microwave dielectric properties by making solid solution phases between aeschynites and euxenites in an effort to develope a possible zero t_f material. This has been successfully achieved in 5 different systems such as $Pr_{1-x}Gd_xTiNbO_6$, $Nd_{1-x}Dy_xTiNbO_6$, $Sm_{1-x}Y_xTiNbO_6$, $GdTiNb_{1-x}Ta_xO_6$ and $Sm_{1-x}Y_xTiTaO_6$ dielectric ceramics. The range of solid solution formation and the effect of morphotropic phase transition from aeschynite to euxenite on the density, phase evolution and microwave dielectric properties of the solid solution phases are described

7. 1 RE'RE"$TiNbO_6$ [RE'= Pr, Nd, Sm; RE"= Gd, Dy, Y] CERAMICS

7. 1. 1 Introduction

There has been an increasing demand for dielectric resonator materials in the microwave frequency region with the rapid progress in microwave communication satellite broadcasting (UHF and SHF) and microwave integrated circuit technology (MIC)[1]. Apart from complex perovskite ceramics like [2, 3] $Ba(B'_{1/3}B"_{2/3})O_3$ [B'=Mg, Zn ; B"= Ta, Zn] discussed in Chapters 3-6, there has been a good number of ceramics with promising microwave dielectric characteristics have been reported [4, 5, 6, 7, 8, 9, 10, 11, 12]. Still the search for new materials with improved dielectric properties for various applications is in progress.

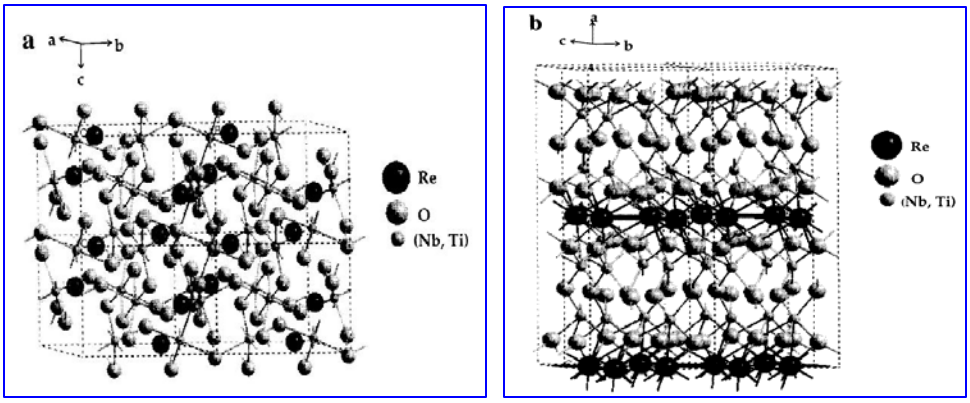

Fig. 7. 1 Crystal Structure of (a) Aeschynite and (b) Euxenite

Recently our research group reported [13, 14, 15] $RETiNbO_6$ (where RE: rare earth ion) as a useful material for dielectric resonator applications. The single crystals of these stoichiometric rare earth compounds are also used as ideal gain media for miniature solid-state lasers because of their exciting optical properties[16, 17] Seifert and Beck[18] synthesized $YTiNbO_6$ single crystals by hydrothermal synthesis in 1961. Pei-Shan Chang[19] then studied the chemical composition and physical properties of $CeTiNbO_6$-$YTiNbO_6$ ceramics. In 1963 Komkov[20] synthesized $RETiNbO_6$ compounds hydrothermally from the equivalent mixtures of RE_2O_3, TiO_2 and Nb_2O_5.

The compounds with atomic number of rare earth ion in the range 57 to 63 in the periodic table are reported to crystallize in the orthorhombic aeschynite structure with

four formula units per unit cell. They fall in the space group symmetry Pnma [16, 21]. Compounds with atomic number of the rare earth ions in the range of 64 to 71 have orthorhombic euxenite structure but are having a different symmetry Pbcn.[17, 19] The principal difference between RE^{3+} in these structures is that in aeschynites they lie in closely connected chains whereas in euxenites the RE^{3+} ions lie on densely packed parallel planes (see Fig. 7.1).[17]

The members of aeschynite group are reported [13, 14, 15] to have positive τ_f with high dielectric constant whereas euxenites have negative τ_f with relatively lower dielectric constant. Hence it may be possible to get a nearly zero τ_f material and to tune the microwave dielectric properties by preparing solid solution phase between aeschynites and euxenites. In the present work we report the preparation, characterization and properties of $Pr_{1-x}Gd_xTiNbO_6$, $Nd_{1-x}Dy_xTiNbO_6$ and $Sm_{1-x}Y_xTiNbO_6$ solid solution phases. The variation in the microwave dielectric properties, density and structure of these systems are investigated as a function of composition (x).

7. 1. 2 Experimental

The $RE_{1-x}RE'_xTiNbO_6$ {RE = Pr, Nd, Sm; RE' = Gd, Dy, Y} ceramics are prepared by the conventional solid-state ceramic route as discussed in Chapter 2, Sections 2. 1. 2. 1 to 2. 1. 2. 4. The thoroughly mixed reaction mixture powder is dried and calcined at 1200-1260^oC for 4 hours in air. The uniaxially pressed cylindrical compacts are sintered at 1360-1425^oC for 4 hours in air on platinum plates at a heating rate of 10^oC/min. After sintering the samples are allowed to cool down to room temperature at the rate of 5^oC/min. The well-polished ceramic pellets are used for microwave measurements. The powdered samples are used for analyzing the X-ray diffraction patterns using CuK_α radiation as described in Chapter 2, Section 2. 3. 1. The well-polished thin pellets are electroded by coating silver on both sides in the form of ceramic capacitors and are used for dielectric measurements at low frequencies (HP 4192 A - LF). The sintered samples are thermally etched for 30 minutes at a temperature about 50^oC below the sintering temperature and the surface morphology is studied using a scanning electron microscope (JEOL JSM 5600LV).

The dielectric properties ε_r, Q_u and τ_f of the materials were measured in the microwave frequency range using resonance technique[22,23] as described Chapter 2, Sections 2. 2. 2 to 2. 2. 4.

7. 1. 3 Results and Discussion

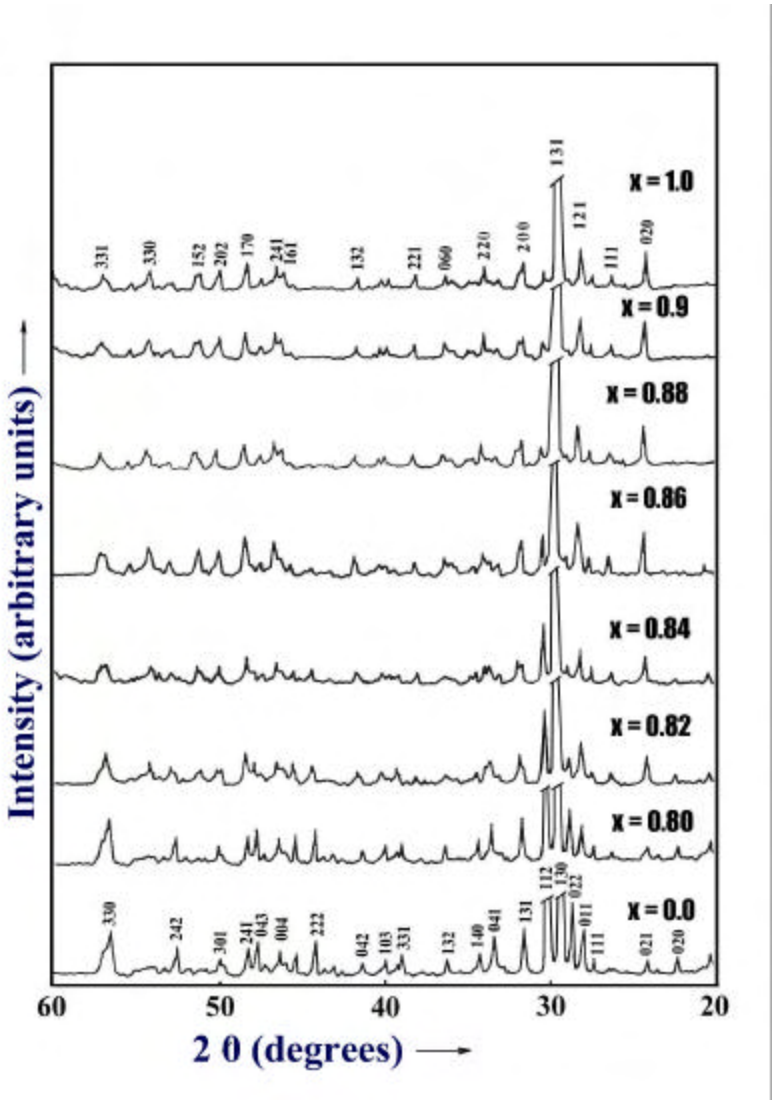

Fig. 7. 2 The XRD pattern of $Pr_{1-x}Gd_xTiNbO_6$ ceramics for x=0.0, 0.80, 0.82, 0.84, 0.86, 0.88 0.90 and 1.0.

The XRD patterns of $RETiNbO_6$ [RE = Pr, Nd, Sm] and $RE'TiNbO_6$ [RE'= Gd, Dy, Y] are in agreement with JCPDS file card numbers 20-1216, 20-1218, 20-1401, 20-1471, 15-864, 27-205 and 27-221. The $PrTiNbO_6$, $NdTiNbO_6$ and $SmTiNbO_6$ have similar XRD patterns and have orthorhombic $CaTa_2O_6$ type structure with Pnma space

group.[16, 17, 24] Similarly the XRD patterns of $GdTiNbO_6$, $DyTiNbO_6$ and $YTiNbO_6$ are similar and have orthorhombic coulombite structure with space group Pbcn as reported earlier[25, 26, 27]. Fig. 7.2 shows the XRD pattern of $Pr_{1-x}Gd_xTiNbO_6$ for x=0.0, 0.80, 0.82, 0.84, 0.86, 0.88, 0.90 and 1.0. In $Pr_{1-x}Gd_xTiNbO_6$ ceramics the XRD pattern is similar to that of aeschynite structure for x<0.8 and it is similar to that of euxenites when x>0.9. The structural phase transition from Pnma to Pbcn symmetry occurs between x= 0.8 and 0.9. Both euxenite and aeschynite phases coexist near the transition region. Similar XRD patterns are obtained in the other two solid solutions at their respective transition points. In $Nd_{1-x}Dy_xTiNbO_6$ system the crystal structure is comparable to aeschynites for x<0.4. The structural transformation occurs between x=0.4 and x=0.5. For x>0.5 the euxenite structure prevails. In $Sm_{1-x}Y_xTiNbO_6$ solid solution, similar structural transition occurs between x=0.2 and x=0.3. The crystal structure is similar to aeschynites for x<0.2 and the euxenite structure for x>0.3.

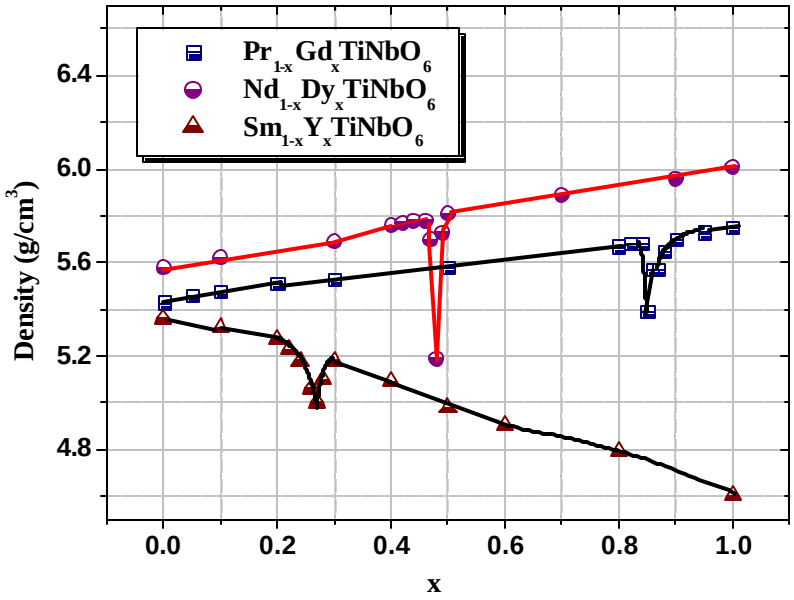

Fig. 7. 3 Variation of density with composition (x)

Fig. 7.3 shows the variation of density as a function of composition (x) in $Pr_{1-x}Gd_xTiNbO_6$, $Nd_{1-x}Dy_xTiNbO_6$ and $Sm_{1-x}Y_xTiNbO_6$. These materials are sintered up to 92 to 97 percent of their theoretical densities except at the transition region. The samples are difficult to sinter near the transition point which is a two phase region. Increasing the sintering temperature results in melting of the samples. In $Pr_{1-x}Gd_xTiNbO_6$ and Nd_{1-x}

Dy_xTiNbO_6 the density increases with x due to the substitution of heavier atom. But in $Sm_{1-x}Y_xTiNbO_6$ the density decreases with x due to the substitution of lighter Y^{3+} ions at Sm^{3+} site. The Fig. 7.3 shows a sharp change in

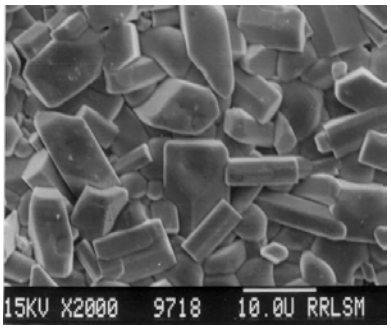

Fig. 7.4 (a)

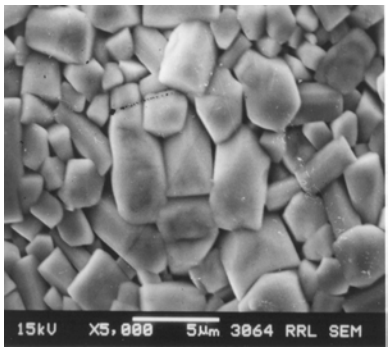

Fig. 7.4 (b)

Fig. 7.4 (c)

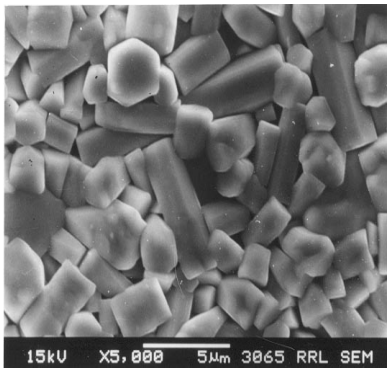

Fig. 7.4 (d)

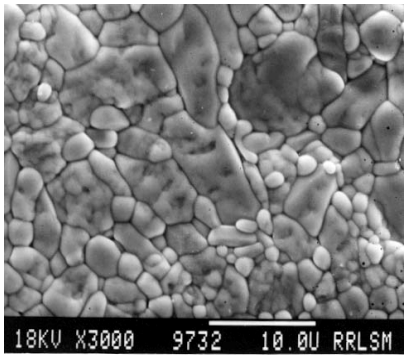

Fig. 7(e)

Fig. 7. 4 SEM micrographs of (a) $NdTiNbO_6$, (b) $Nd_{.53}Dy_{.47}TiNbO_6$ (c) $Nd_{.52}Dy_{.48}TiNbO_6$, (d)$Nd_{.51}Dy_{.49}TiNbO_6$ and (e) $DyTiNbO_6$

density at x=0.86 for $Pr_{1-x}Gd_xTiNbO_6$, x=0.48 for $Nd_{1-x}Dy_xTiNbO_6$ and x=0.27 for $Sm_{1-x}Y_xTiNbO_6$. The sharp change in density corresponds to the point of transition from aeschynite to euxenite as evidenced by the XRD pattern in Fig. 7.2 and dielectric properties in Figs. 7.5 and 7.6.

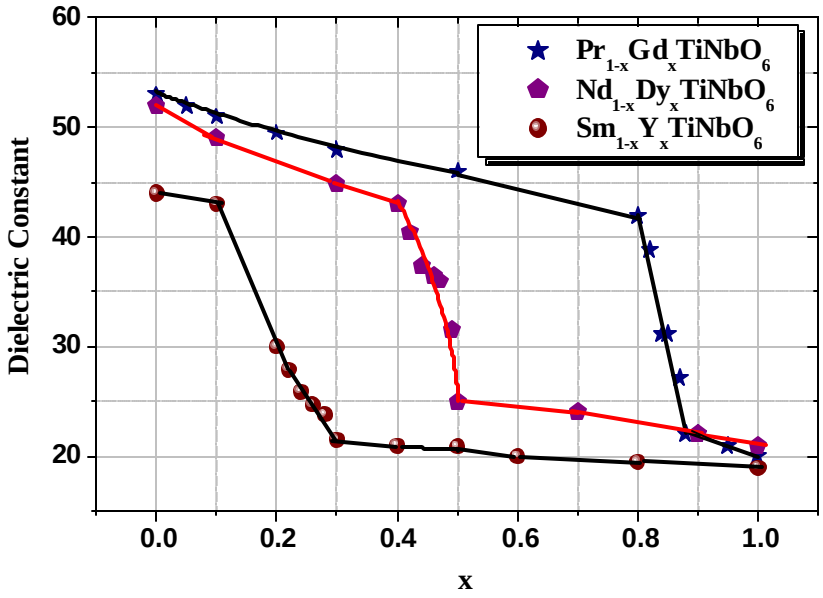

Fig. 7. 5 Variation of the dielectric constant with composition (x).

Figs. 7.4 shows the SEM picture recorded from $Nd_{1-x}Dy_xTiNbO_6$ ceramics for x=0.0, 0.46, 0.47, 0.48 and 1.0 respectively. Figure 7.4(a) represents the typical microstructure of $NdTiNbO_6$ (aeschynite). The other ceramics in the aeschynite group show microstructures similar to Fig. 7.4(a). The grains are elongated and are up to about 6 µm in size. Fig. 7.4(e) shows the microstructure of $DyTiNbO_6$ and other ceramics in the euxenite group show similar microstructure. In the solid solution phase close to the transition point i.e. the $Nd_{.53}Dy_{.47}TiNbO_6$ and $Nd_{.53}Dy_{.47}TiNbO_6$ shows the presence of two types grains belonging to aeschynite and euxenite [Figs. 7.4(b) & 7.4(d)]. At the transition point ($Nd_{.52}Dy_{.48}TiNbO_6$) the ceramic showed high porosity with very different microstructure (Fig. 7.4(c)). It may be noted that the samples are very difficult to sinter for compositions near the transition region. The $Nd_{.52}Dy_{.48}TiNbO_6$ ceramic was sintered at a relatively high temperature of 1425^oC for 4 hours. These samples melt on sintering at

temperatures above 1430°C. The bulk density of $Nd_{.52}Dy_{.48}TiNbO_6$ is less than 85 % of the theoretical density. It has been reported [29] that unloaded quality factor of a ceramic is strongly dependent on porosity which may be the reason for poor resonance in the two phase region.

The variation in dielectric constant in $Pr_{1-x}Gd_xTiNbO_6$, $Nd_{1-x}Dy_xTiNbO_6$ and Sm_{1-x} Y_xTiNbO_6 are shown in Fig. 7.5. In $Pr_{1-x}Gd_xTiNbO_6$ samples, the dielectric constant of $PrTiNbO_6$ is 53 and that of $GdTiNbO_6$ is 20. The solid solution phases of Pr_{1-x} Gd_xTiNbO_6 is expected to have dielectric constant in between 53 and 20 depending on the value of x. With the substitution of Gd^{3+} ion on the Pr^{3+} site the dielectric constant decreases steadily from 53 to 42 for $x < 0.8$ where the solid solution phases crystallize to the orthorhombic aeschynite symmetry. Again for $x > 0.9$, dielectric constant decreases linearly from 22 to 20 where the phase is euxenite. The dielectric constant decreases abruptly for values of x between 0.8 and 0.9 where the resonance is very weak (see Fig. 7.5). The ceramic sample for $x = 0.86$ does not resonate because of the very large dielectric loss factor. We could not measure the dielectric constant of this composition by the Hakki-Coleman post resonator method because of their poor resonance at microwave frequency range. Hence using an impedance analyzer the dielectric constant at this composition was measured as 29.68 at 13 MHz. The ϵ_r of the samples will be slightly higher at MHz range as the polarization mechanisms controlling the dielectric phenomena are different at different frequency ranges[28]. The extrinsic factors like poor densification and the resulting porosity and moisture may be the reason for high loss factor near the transition point. In addition, for x=0.86 the atoms are in a state of reorientation for transition from aeschynite to euxenite structure which may results in large dielectric loss. Thus the measurements made at low frequency using an impedance analyzer showed that the samples near the transition point have relatively large dielectric loss with intermediate dielectric constants. In $Nd_{1-x}Dy_xTiNbO_6$ system the dielectric constant of $NdTiNbO_6$ is 52 and that of $DyTiNbO_6$ is 21. As expected the dielectric constant decreases from 52 to 43 where Dy^{3+} substitutes Nd^{3+} upto 40 mole %. Between $x = 0.4$ and $x = 0.5$, the resonance is very poor and the composition does not resonate at $x = 0.48$ where dielectric loss is large. Again the dielectric constant varies smoothly from

25 to 21 when the molar concentration of $DyTiNbO_6$ in $NdTiNbO_6$ is increased from 50 to 100 % (Fig.7.5). In $Sm_{1-x}Y_xTiNbO_6$ solid solution the dielectric constant decrease linearly from 44 to 30 for $x < 0.2$ and then from 21.5 to 19 when $x>0.3$. The variation of the dielectric constant is abrupt between x=0.2 and x=0.3 as shown in Fig. 7.5. This may be the transition region for $Sm_{1-x}Y_xTiNbO_6$ where the samples show very weak resonance. The samples around $x = 0.27$ do not resonate where the dielectric loss factor is maximum.

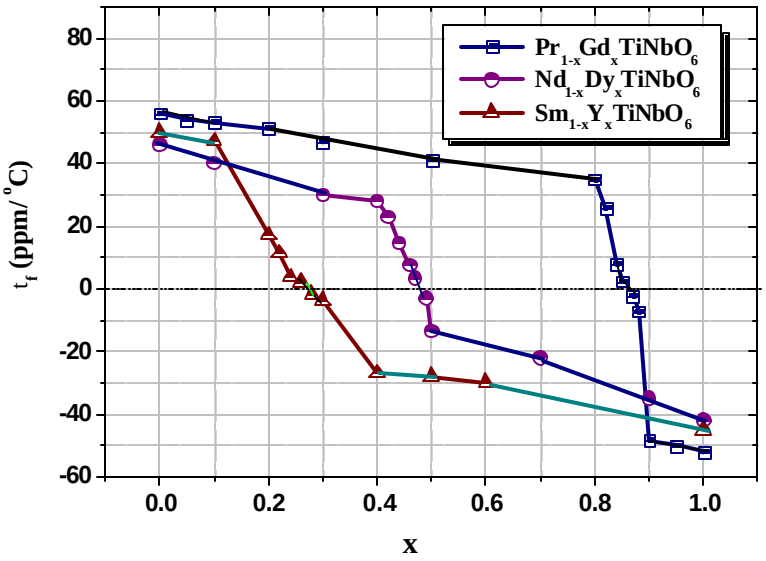

Fig. 7. 6 Variation of t_f with composition (x)

The variation of the temperature coefficient of resonant frequency (τ_f) for the three systems of solid solution is plotted in Fig. 7. 6. The variation of τ_f with composition (x) is similar to the variation of the dielectric constant with x (see Fig. 7. 5). In the case of $Pr_{1-x}Gd_xTiNbO_6$ the value of τ_f for x=0.85 is +2.4 ppm/^oC and that for x=0.87 is –2.1ppm/^oC. Since the system shows no resonance between $x = 0.85$ and 0.87, a simple interpolation of the τ_f curve between these two points shows that the particular composition for x=0.86 in $Pr_{1-x}Gd_xTiNbO_6$ has τ_f near to zero. Similarly in $Nd_{1-x}Dy_xTiNbO_6$ system the value of τ_f for x=0.47 and 0. 49 are +3.4 and –3.0. It is clear from Fig.7. 6 that $x = 0.48$ is the composition where τ_f approaches the zero value which does not resonate. In the case of

$Sm_{1-x}Y_xTiNbO_6$ ceramics, the composition for x = 0.27 may be the point of transition. Thus it is expected that the resonant frequency is invariant with temperature for compositions $Pr_{.14}Gd_{.86}TiNbO_6$, $Nd_{.52}Dy_{.48}TiNbO_6$ and $Sm_{.73}Y_{.27}TiNbO_6$. But it is not possible to measure their dielectric properties at microwave frequencies since they do not resonate due to the large loss factor.

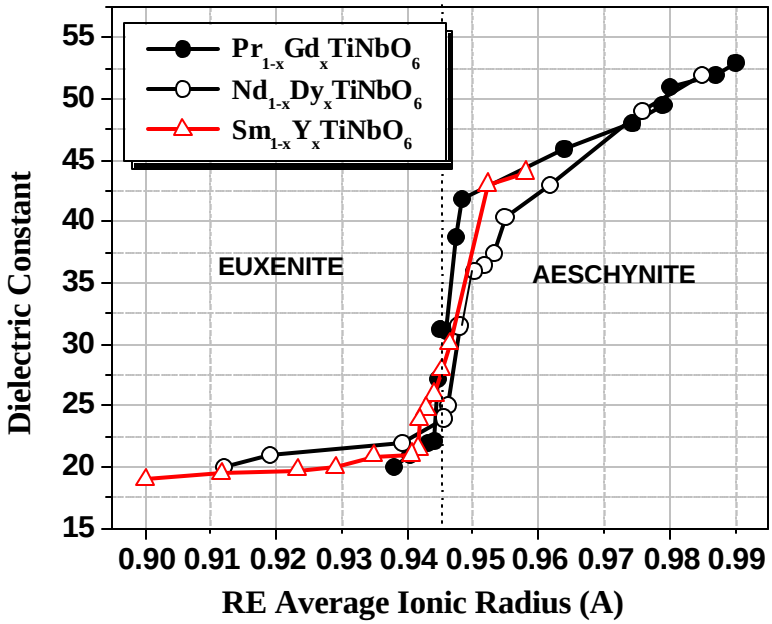

Fig. 7. 7 Variation of the dielectric constant with average ionic radius of the rare earth

The average ionic radius of rare earth ion in $RE_{1-x}RE'_xTiNbO_6$ [RE=Pr, Nd, Sm; RE'=Gd, Dy, Y] is calculated using the data reported by Shannon[29]. Fig. 7.7 and 7.8 show the variation of dielectric constant and τ_f with average ionic radius (IR) of the rare earth ions. The dielectric constant and τ_f values show a sharp and abrupt change when the average rare earth ionic radius is about 0.945 Å. This indicates that the aeschynite to euxenite transition occurs when the average ionic radius of the rare earth ions in $RE_{1-x}RE'_xTiNbO_6$ is about 0.945 Å (see Fig 7.7). The results show that $RETiNbO_6$ compounds crystallize in the euxenite form for IR<0.945 Å and in aeschynite form when IR>0.945 Å. Moreover it is found from Fig. 7.8 that the sign of τ_f strongly depends on the

average ionic radius of the rare earths. For IR< 0.945 Å the material will have positive τ_f and for IR>0.945 Å the τ_f will be negative. The results indicate that one can obtain a

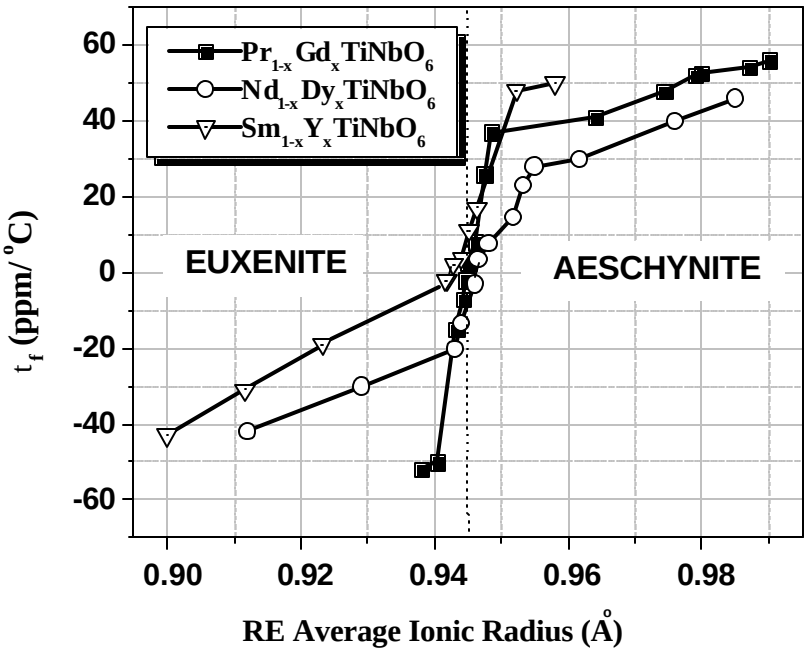

Fig.7. 8 Variation of the t_f with average ionic radius of the rare earth

nearly zero τ_f material by tuning the average rare earth ionic radius to be around 0.945 Å in the $RETiNbO_6$ compounds. This is in agreement with the fact that $EuTiNbO_6$ (Eu ionic radius = 0.947 Å) has a very low τ_f of +5 ppm/^oC [14].

7. 2 $GdTiNb_{1-x}Ta_xO_6$ and $Sm_{1-x}Y_xTiTaO_6$ CERAMICS

7. 2. 1 Introduction

The orthorhombic ternary oxides of the type $RE(AB)O_6$ [RE= Rare Earths ; A = Ti, Hf ; B = Ta, Nb] has been studied by several investigators [13-21] who were in search of stable high melting materials with low thermal expansivity. The single-phase occurrence of $A^{3+}B^{4+}Ta^{5+}O_6$ was first reported by Kazantsev et al. [30] in 1974. They established the optimum conditions for the formation of double tantalates of rare-earth elements with titanium based on the formula $LnTiTaO_6$ where Ln is a Lanthanide. They also reported

that rare-earth titanium tantalate compounds with rare-earth atomic number in the range 57-66 have orthorhombic aeschynite symmetry whereas compounds with rare-earth atomic number 67-71 have orthorhombic euxenite symmetry. Later Holcombe [31 32] studied the crystal structure of ternary oxides such as $AlTiTaO_6$ and $YTiTaO_6$ since these compounds possess unique low thermal expansion coefficient and high melting point. In 1987 Maeda et al.[33] suggested the possibility of using tantalates and niobates related to TiO_2 such as $MTi(Ta,Nb)O_6$ [M=Al, Y and Dy] for microwave frequency applications. He proposed that the possible high dielectric constant and high quality factor might be due to the contribution from the TiO_6 octahedron. The $RETiTaO_6$ ceramics with RE ions with atomic number between 58 and 66 exhibit an aeschynite orthorhombic Pnma (D_{2h}^{16}) structure, with four molecules per unit cell which showed high dielectric constant and positive τ_f. The compounds with Y and RE atomic number higher than 67, exhibit an euxenite orthorhombic Pbcn (D_{2h}^{14}) structure and these materials showed low dielectric constant and negative τ_f [40, 34]. A solid solution between aeschynites and euxenites by partially replacing one rare earth with another can tailor the τ_f to a minimum, which had been achieved successfully in $RETiNbO_6$ ceramics[35]. In this work, we report the preparation, characterization and microwave dielectric properties of $GdTiNb_{1-x}Ta_xO_6$ and $Sm_{1-x}Y_xTiTaO_6$ [x = 0.0-1.0] ceramics. The range of solid solution formation and the effect of morphotropic phase transition from aeschynite to euxenite on the density and microwave dielectric properties of the solid solution phases were discussed.

7. 2. 2 Experimental

The $GdTiNb_{1-x}Ta_xO_6$ and $Sm_{1-x}Y_xTiTaO_6$ ceramics were prepared by the conventional solid-state ceramic route as discussed in Chapter 2, Sections 2. 1. 2. 1 to 2. 1. 2. 4. The calcination was 1250°C for 8 hrs with intermediate grinding. The sintering temperature for $GdTiNb_{1-x}Ta_xO_6$ was in the range 1520-1540°C and that of $Sm_{1-x}Y_xTiTaO_6$ was 1550-1650 °C. The crystal structure was studied using XRD technique.

The dielectric properties ε_r, Q_u and τ_f of the materials were measured in the microwave frequency range using resonance technique as described Chapter 2, Sections

2. 2. 2 to 2. 2. 4. Thin ceramic samples were electroded and their dielectric properties were studied using impedance analyzer (HP 4192 LF).

7. 2. 3 Results and Discussion

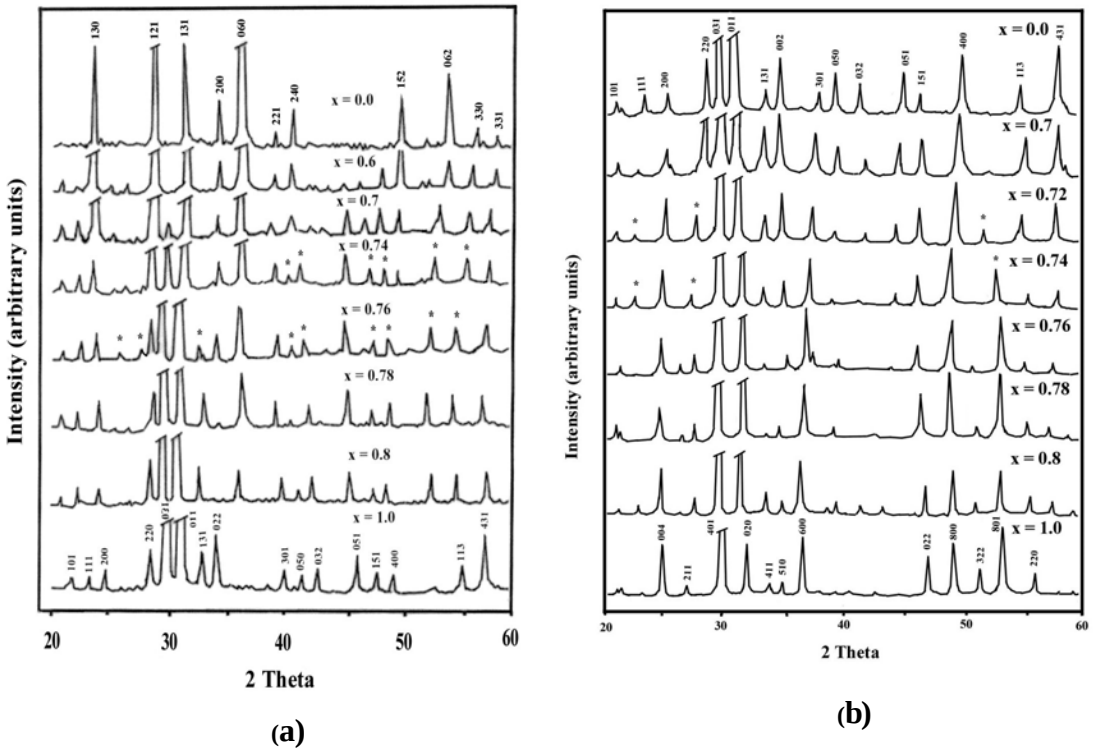

Fig. 7. 9 (a) Powder diffraction pattern of $GdTiNb_{1-x}Ta_xO_6$ for x = 0.0, 0.7, 0.74, 0.76, 0.78, 0.8 and 1.0.
Fig. 7. 9 (b) Powder diffraction pattern of $Sm_{1-x}Y_xTiTaO_6$ for x = 0.0, 0.7, 0.72, 0.74, 0.76, 0.78, 0.8 and 1.0. (* represents unknown peaks)

The powder diffraction patterns recorded from $GdTiNb_{1-x}Ta_xO_6$ for x = 0.0, 0.6, 0.7, 0.74, 0.76, 0.8 and 1.0 are given in Fig. 7.9 (a). The $GdTiNbO_6$ crystallizes in orthorhombic euxenite structure having Pbcn (D_{2h}^{14}) structure, with four formula units per unit cell. The XRD pattern of $GdTiNbO_6$ is comparable with JCPDS File Card No. 27-1449 for $TbTiNbO_6$ and that of $GdTiTaO_6$ is comparable to JCPDS File Card No. 28-1289 for $TbTiTaO_6$. It is evident from Fig. 7.9(a) that the XRD pattern of $GdTiNb_{1-x}Ta_xO_6$ ceramics deviates from aeschynites when x approaches 0.7 and is similar to that of aeschynites for x > 0.8. The structural phase transition occurs between x = 0.7 and x =

0.8. In this range of x in $GdTiNb_{1-x}Ta_xO_6$ some new phases appear which could not be indexed using the powder patterns of the end phases (see * marks in Figs. 7.9(a) & (b)). It is well established [36] that the presence of additional phases can impede densification process in microwave ceramics which in turn will result in the degradation of their unloaded quality factor. The XRD pattern of $SmTiTaO_6$ (Fig.7.9 (b)) is comparable to JCPDS File Card No. 28-1289 for $TbTiTaO_6$ with orthorhombic aeschynite structure and that of $YTiTaO_6$ is identical with JCPDS File Card No. 32-1452 with euxenite symmetry which is however different from the rest of the euxenite ceramics in $RETiTaO_6$. In $Sm_{1-x}Y_xTiTaO_6$ solid solution also the presence of additional phases is visible near the phase transition region between x = 0.7 and 0.8 (see Fig. 7. 9(b)). For x < 0.7, the crystal structure is aeschynite and for x > 0.8 euxenite structure prevails.

The variation of bulk density of $GdTiNb_{1-x}Ta_xO_6$ and $Sm_{1-x}Y_xTiTaO_6$ [x = 0.0-1.0] as a function of x is given in Fig. 7.10. The theoretical density[21] of $GdTiNbO_6$ is 6.26 g/cm^3 while that of $GdTiTaO_6$ is 7.47 g/cm^3. Hence in the solid solution $GdTiNb_{1-x}Ta_xO_6$ the bulk density increase with x as tantalum replaces niobium ion except near the phase transition region (x = 0.75) where they showed poor densification. Increasing the sintering temperature resulted in the melting of the samples. As the concentration of aeschynites in euxenites increases the structural disparity which can result in the

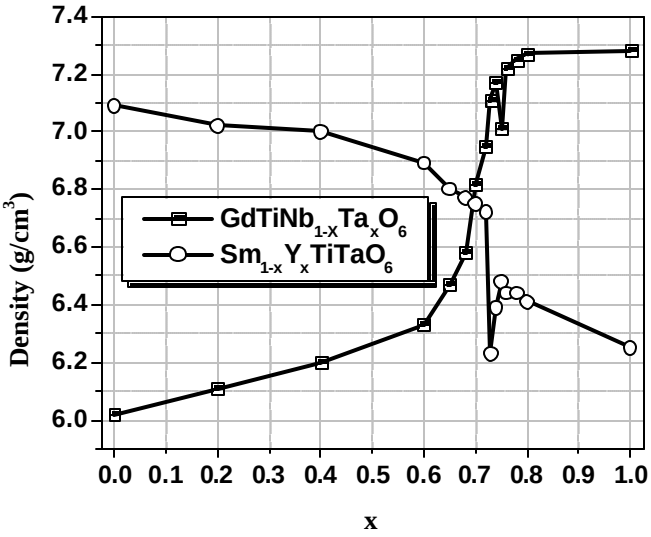

Fig. 7. 10 Variation of bulk density of the solid solution phases with composition x

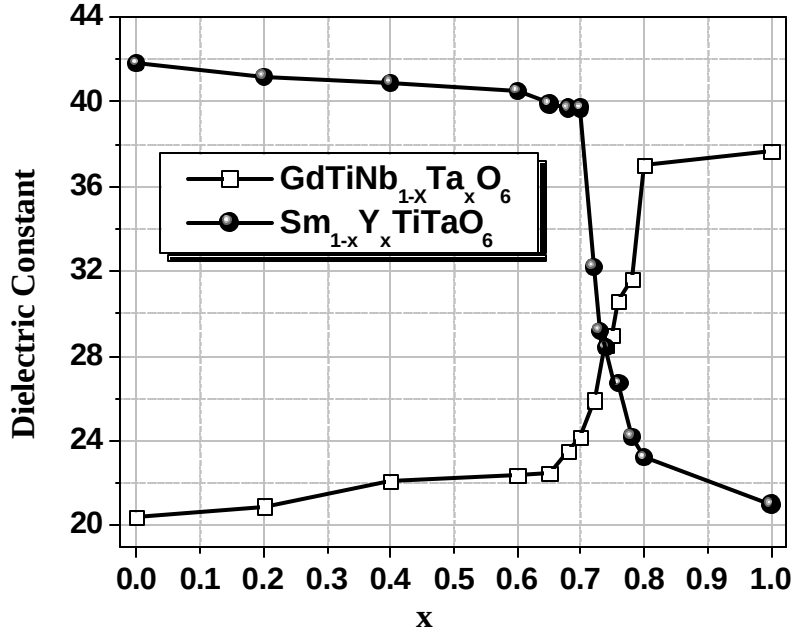

Fig. 7. 11 Variation of dielectric constant of the solid solution phases with composition x

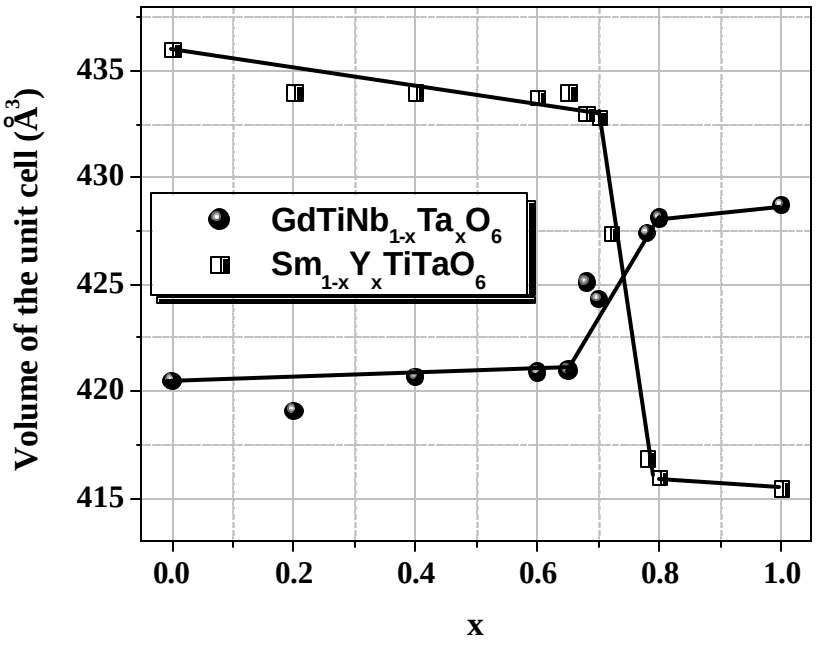

Fig. 7. 12 Variation of unit cell volume of the solid solution phases in $GdTiNb_{1-x}Ta_xO_6$ and $Sm_{1-x}Y_xTiTaO_6$ [x = 0.0 – 1. 0] ceramics

formation of additional phases which could not be indexed. The anomalous behaviour of density may be attributed to the presence of these new unidentified phases in these ceramics near the transition region as seen in Figs. 7. 9 (a) & (b). It is interesting to note that a similar trend of poor densification near the aeschynite to euxenite phase transition was observed in $[RE_{1-x}RE'_x]TiNbO_6$ [RE = Pr, Nd, Sm; RE' = Gd, Dy, Y] ceramics as described in 7. 1. 3. On the other hand the theoretical density[14] of $SmTiTaO_6$ is 7.29 g/cm^3 while that of $YTiTaO_6$ is 6.38 g/cm^3. In $Sm_{1-x}Y_xTiTaO_6$ the density decreases with x because of the substitution of the rare earth ion with a lighter ion. In $Sm_{1-x}Y_xTiTaO_6$ solid solution, the bulk density drops at x = 0.73 which is expected to be contributed by the presence of additional phases (see Fig. 7. 10).

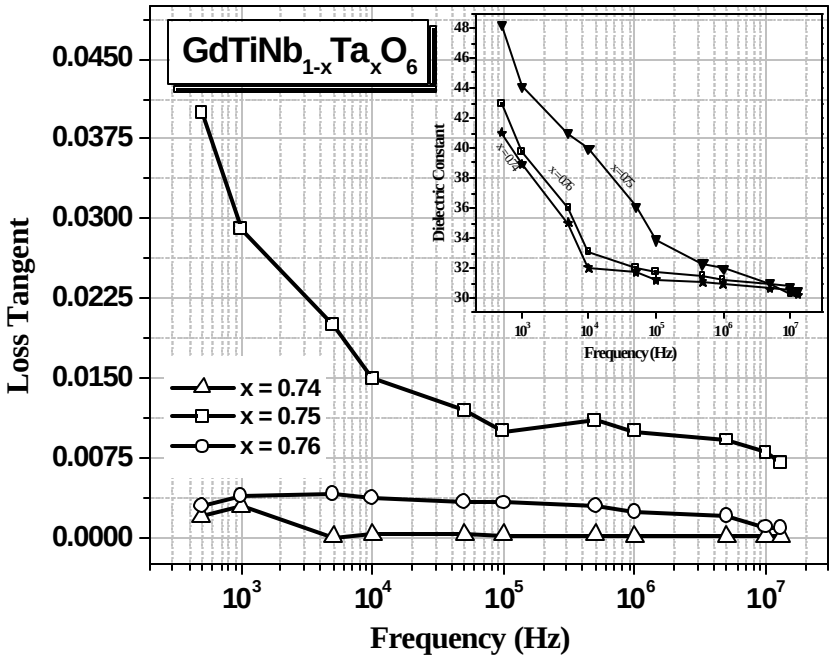

Fig.7. 13 Variation of the loss tangent and dielectric constant (inset) for x = 0.74, 0.75 and 0.76 in $GdTiNb_{1-x}Ta_xO_6$ in the radio frequency range (10^2 - 1.3 x 10^7 Hz)

The dielectric constant of $GdTiNbO_6$ is 20 (at 6.27 GHz) while that of $GdTiTaO_6$ is 38 (at 5.21 GHz). The variation of the dielectric constant of the solid solution phases with x is plotted in Fig. 7.11. The solid solution phases of $GdTiNb_{1-x}Ta_xO_6$ is expected to

have e_r in between 20 and 38. With the substitution of Ta^{5+} at the Nb^{5+} e_r increases from 20 to 24. This is expected since the ionic polarisability of Ta^{5+} ion (= 4.73) [37] is greater than that of Nb^{5+} (=3.97) and the intrinsic dielectric constant of a material depends on the total ionic polarisability and unit cell volume of the constituent ions according to Claussius-Massotti equation. Again for x > 0.8 the dielectric constant increases from 37 to 38. The dielectric constant varies abruptly for values of x between 0.7 and 0.8.

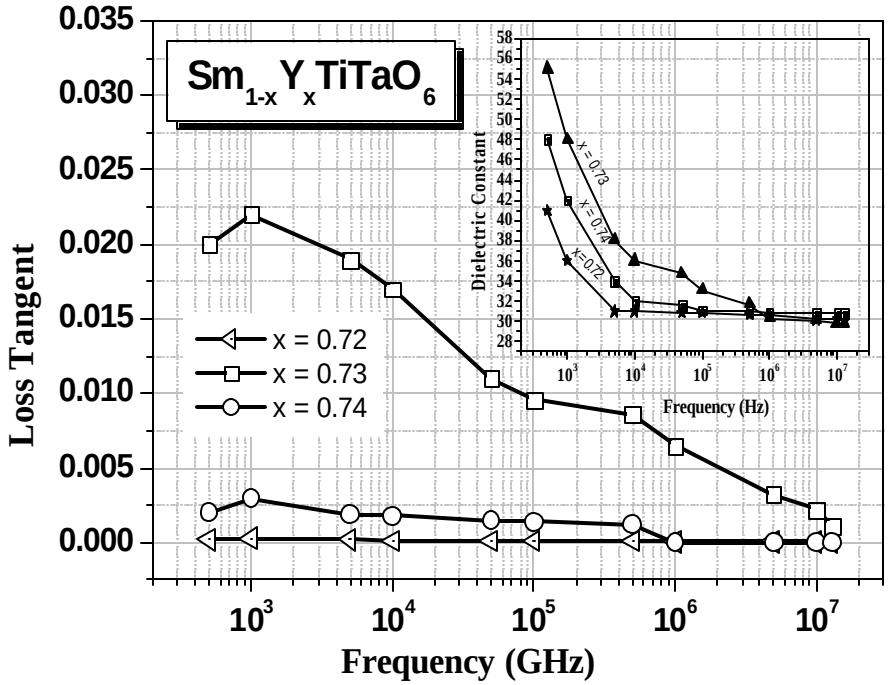

Fig. 7. 14 Variation of the loss tangent and dielectric constant (inset) for x = 0.72, 0.73 and 0.74 in $Sm_{1-x}Y_xTiTaO_6$ in the radio frequency range (10^2 - 1.3 x 10^7 Hz)

The volume of the unit cell calculated using the powder diffraction data recorded from $GdTiNb_{1-x}Ta_xO_6$ and $Sm_{1-x}Y_xTiTaO_6$ ceramics within the limits of experimental error is plotted against x in Fig. 7.12. The abrupt change in the volume of the orthorhombic unit cell in the phase transformation region supports the sudden change in dielectric constant between x = 0.7 and 0.8. The dielectric ceramic $GdTiNb_{.25}Ta_{.75}O_6$ could not be characterized by microwave method due to the very large dielectric loss factor (i.e.no resonance). Hence the solid solution compositions for x = 0.74, 0.75 and 0.76 in $GdTiNb_{1-x}Ta_xO_6$ were characterized in the low frequency region (50 Hz-13 MHz)

using an impedance analyzer. The dielectric constant of $GdTiNb_{0.25}Ta_{0.75}O_6$ ceramic was measured as 30.5 at 13 MHz (see Fig. 7.13). It is also evident that the dielectric loss factor for this ceramic is unusually high where the atoms are believed to be in a state of reorientation for a first order phase transformation from aeschynite to euxenite structure. This resulted in the formation of unidentified phases which resulted in high dielectric loss. The dielectric constant of $SmTiTaO_6$ is 42 (at 5.16 GHz) and that of $YTiTaO_6$ is 21 (at 6.23 GHz). The variation of dielectric constant of $Sm_{1-x}Y_xTiTaO_6$ as a function of x is given in Fig. 7.11. The dielectric constant varies linearly up to x = 0.7 and then again beyond x = 0.8. The resonance vanishes for x = 0.73 in $Sm_{1-x}Y_xTiTaO_6$ whose dielectric constant was measured as 29.9 at 13 MHz (see Fig. 7.14). The abnormal variation of the dielectric constant and dielectric loss factor for x = 0.75 in $GdTiNb_{1-x}Ta_xO_6$ and x = 0.73 in $Sm_{1-x}Y_xTiTaO_6$ with frequency are due to higher percentage of porosity, presence of secondary phases and the fact that atoms are in a state of reorientation to effect phase transition.

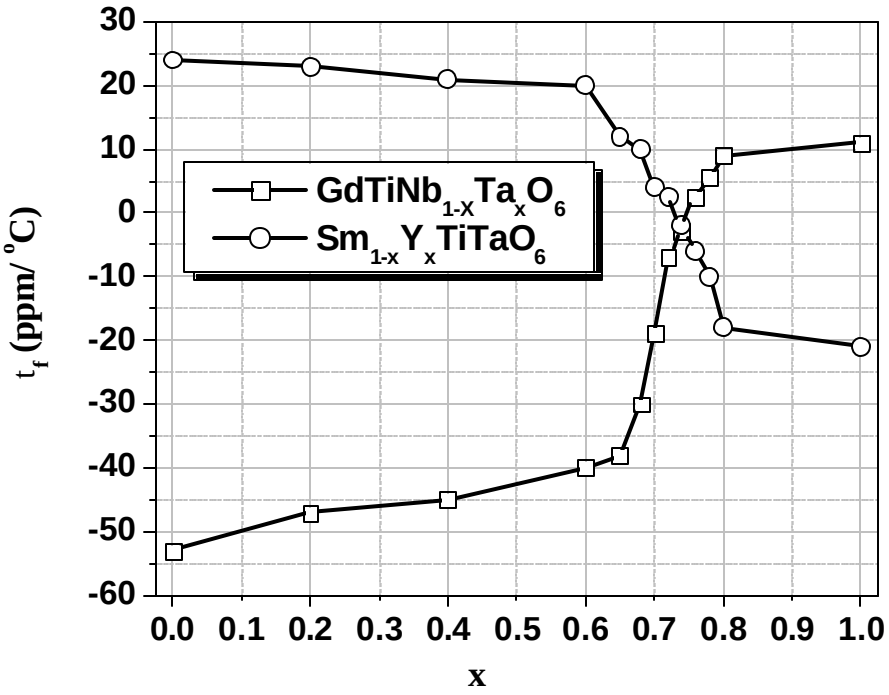

Fig. 7. 15 Variation of the temperature coefficient of resonant frequency (t_f) with composition x

The variation of the temperature coefficient of resonant frequency τ_f with composition x is given in Fig. 7.15. In $GdTiNb_{1-x}Ta_xO_6$ the value of τ_f is –3 ppm/^oC for x = 0.74 and τ_f is + 2.6 ppm/^oC for x = 0.76. A simple interpolation of the τ_f curve between x = 0.74 and 0.76 showed that τ_f is near to zero for composition x = 0.75. But it was not possible to measure it owing to the poor resonance in this region. Similarly in $Sm_{1-x}Y_xTiTaO_6$ ceramics it can be seen that τ_f is +2.6 ppm/^oC for x = 0.72 and –2 ppm/^oC for x = 0.74. The temperature coefficient approaches zero value for x = 0.73 (Fig. 7.15). Thus it is expected that the resonant frequency is invariant with temperature for solid solution compositions $GdTiNb_{0.25}Ta_{0.75}O_6$ and $Sm_{0.27}Y_{0.73}TiTaO_6$ but it was not possible to measure their dielectric properties due to the high loss factor for these compositions.

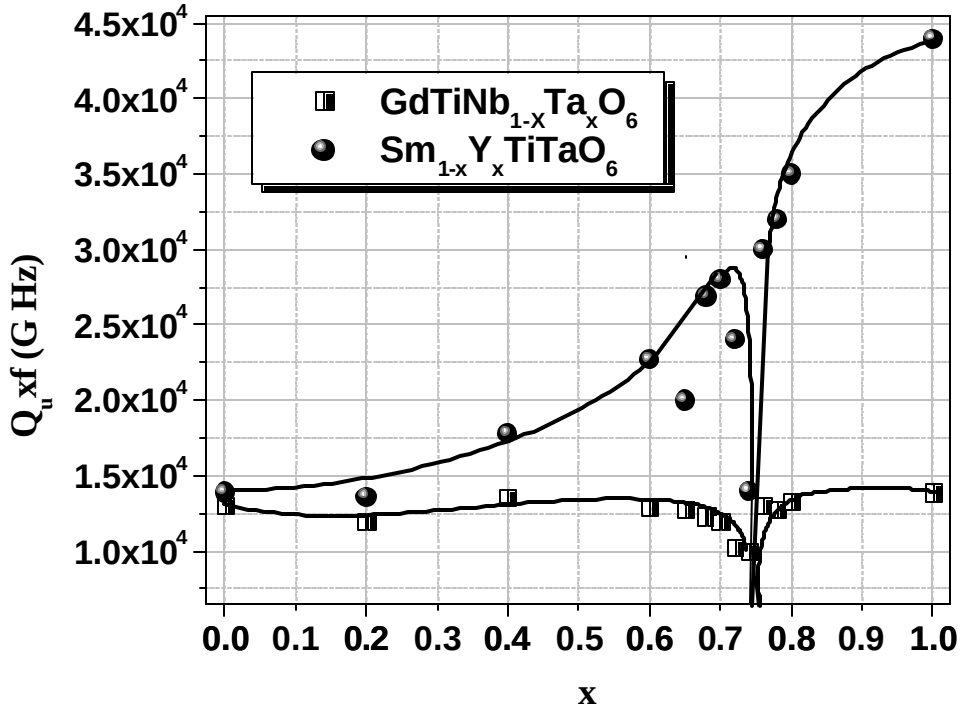

Fig. 7. 16 Variation of the unloaded quality factor (Q_u) with composition x

The unloaded quality factor of these ceramics is plotted in Fig. 7.16 as a function of x. In $GdTiNb_{1-x}Ta_xO_6$ solid solution the $Q_u$xf of the end members are around 13,000 GHz except near the transition region. On the other hand in $Sm_{1-x}Y_xTiTaO_6$ ceramics the

quality factor increases from a $Q_u$xf of 14,000 to 44,000 as Sm^{3+} are replaced with Y^{3+} ions. The ceramics are highly porous for $GdTiNb_{0.25}Ta_{0.75}O_6$ and $Sm_{0.27}Y_{0.73}TiTaO_6$ which resulted in the poor resonance of these ceramics.

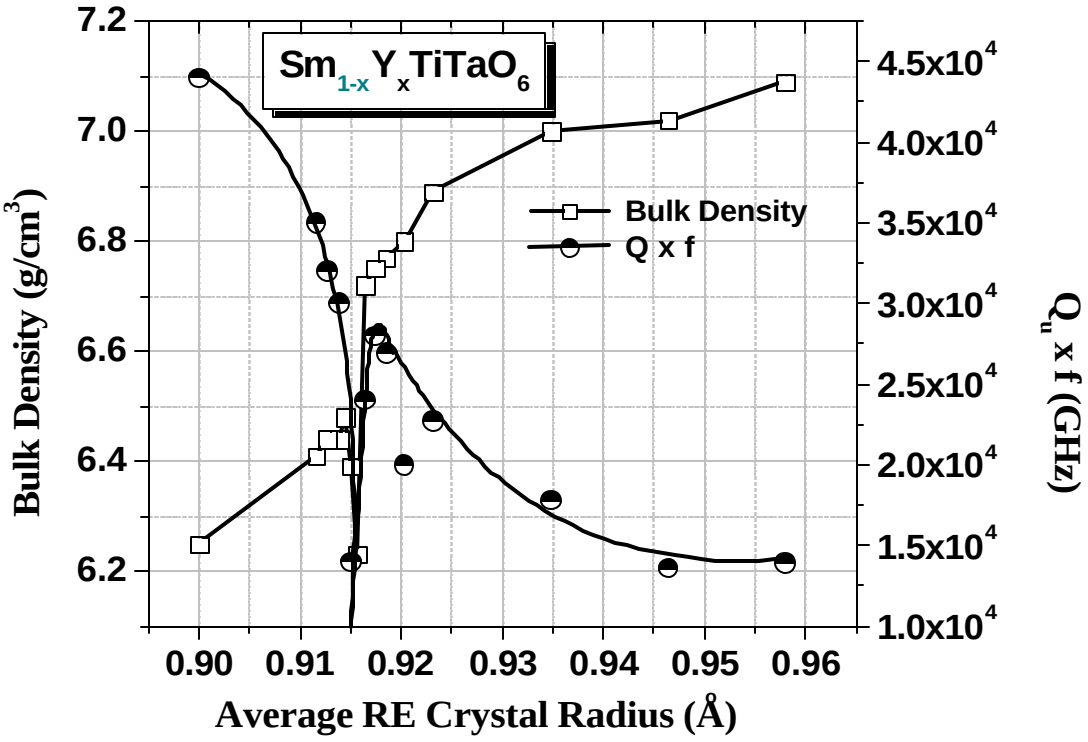

Fig. 7. 17 Variation of bulk density and unloaded quality factor with average ionic radius of rare earths in $Sm_{1-x}Y_xTiTaO_6$

It is interesting to note that the abrupt change in the microwave dielectric properties depend up on the average ionic radius of the rare earth ions in $Sm_{1-x}Y_xTiTaO_6$ ceramics. The average ionic radii [33] of the solid solution phases are plotted against bulk density and unloaded quality factor (see Fig. 7.17). It is evident that the bulk density and quality factor drop abruptly when average rare earth ionic radius (IR) is 0.915 Å. Moreover it is clear from Fig.7.18 that τ_f approaches zero value when the average rare earth ionic radius approaches 0.915 Å. Hence $Sm_{1-x}Y_xTiTaO_6$ ceramics will have aeschynite phase with positive τ_f when IR> 0.915 Å and vice versa. These results are in

good agreement with the detailed investigation on the microwave dielectric properties of $RETiTaO_6$ made before which predicted that τ_f is minimum [38] when ionic radius of the rare earth is between 0.91Å (for $DyTiTaO_6$) and 0.92 Å (for $HoTiTaO_6$) and the border line of the aeschynite-euxenite phase transition lies for 0.91 Å < IR < 0.92 Å. In other words the microwave dielectric properties of $RE_{1-x}RE'_xTiTaO_6$ ceramics can be tailored by suitably adjusting the average ionic radius of the rare earth ions which is similar to the observations made on $RE_{1-x}RE'_xTiNbO_6$ where the morphotropic phase transition occurs when IR = 0.945 Å.

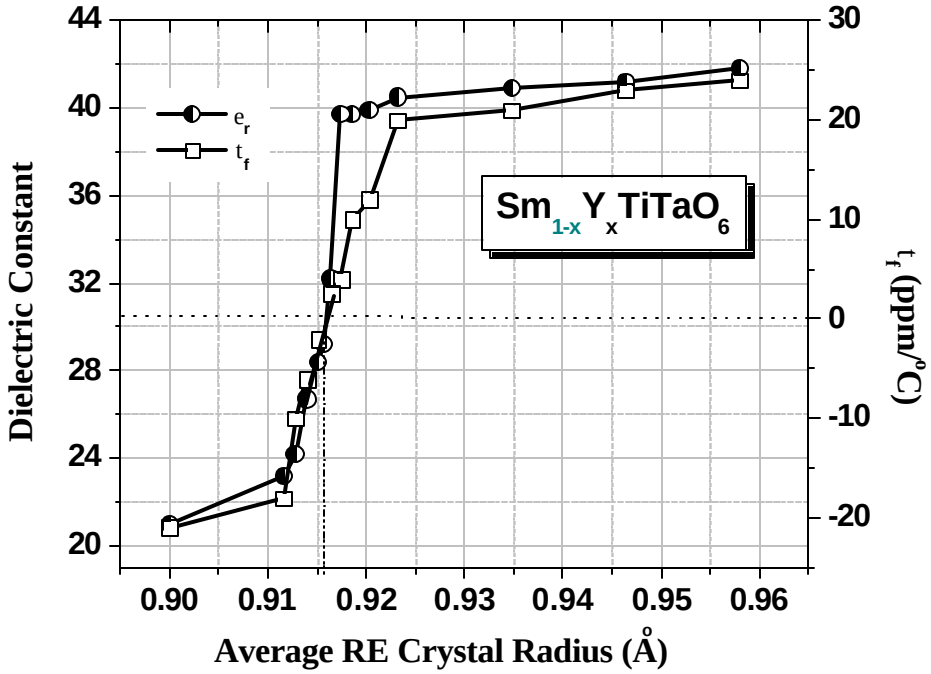

Fig. 7. 18 Variation of t_f and e_r with average ionic radius of rare earths in $Sm_{1-x}Y_xTiTaO_6$ $Sm_{1-x}Y_xTiTaO_6$

The fact that the solubility of $YTiTaO_6$ in $SmYTiTaO_6$ is very poor in the region between 60 and 70 mole % of the latter in the former was consolidated with the help of scanning electron microscopy. Fig. 7. 19 (a), (b) and (c) gives the typical surface morphology of $SmTiTaO_6$, $Sm_{0.28}Y_{0.72}TiTaO_6$ and $YTiTaO_6$ respectively. Two distinct types of grains are visible in Fig. 7. 21 (b) which is the scanning electron micrograph corresponding to transition region containing secondary phases. This fact has been well

confirmed by the XRD analysis as given in 7.11. The grain size of YTiTaO6 is greater than that of $SmTiTaO_6$ due to the former's higher sintering temperature.

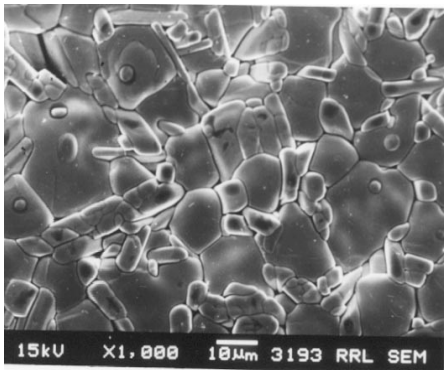

Fig. 7. 19 (a)

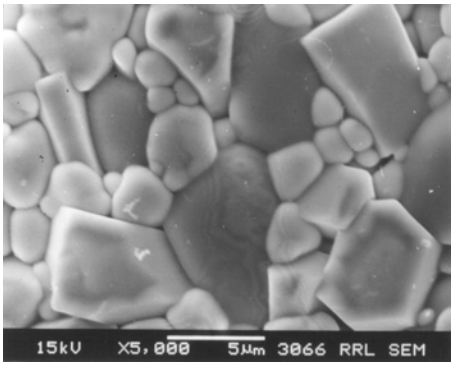

Fig. 7. 19 (b)

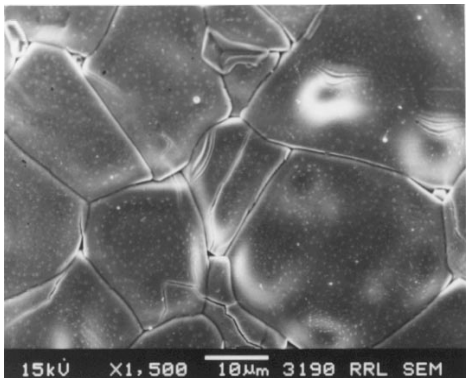

Fig. 7. 19 (c)

Fig. 7. 19 Scanning Electron Micrographs of (a) $SmTiTaO_6$, (b) $Sm_{0.28}Y_{0.72}TiTaO_6$ and (c) $YTiTaO_6$ sintered at 1550, 1570 and 1650^oC respectively.

7. 3 CONCLUSIONS

- Solid solution phases of $RE_{1-x}RE'_xTiNbO_6$ [RE=Pr, Nd, Sm; RE'=Gd, Dy, Y] are synthesized for different values of x by the conventional solid-state ceramic route and their dielectric properties are studied at microwave frequency range. The density decreases abruptly close to the point of phase transition because of the fact that the atoms are in a state of reorientation for transformation from

aeschynite to euxenite and due to the presence of secondary phases. The dielectric properties vary linearly as a function of x, until phase transition from aeschynite to euxenite occurs. Again the dielectric properties vary linearly as a function of x in the new phase. The crystal structure and sign of τ_f depends on the average crystal radius of the rare earths in $RE_{1-x}RE'_xTiNbO_6$ [RE = Pr, Nd, Sm; RE' = Gd, Dy, Y]. If the average crystal radius of the rare earths is less than 1.09 Å then the system crystallizes in orthorhombic euxenite form with negative τ_f and if it is greater than 1.09 Å then the system crystallizes in the orthorhombic aeschynite structure with positive τ_f. This indicates the possibility of developing a material with τ_f near to zero in the solid solution $RE_{1-x}RE'_xTiNbO_6$ by adjusting the average crystal radius of the rare earth to be 1.09 Å which is in agreement with results on $EuTiNbO_6$. However the quality factor is very much decreased close to the transition region due to porosity and secondary phases.

- In $GdTiNb_{1-x}Ta_xO_6$ and $Sm_{1-x}Y_xTiTaO_6$ [x = 0.0 -1.0] ceramics, the dielectric properties vary linearly as function of x until a phase transition from aeschynite to euxenite occurs. The microwave dielectric properties vary abruptly near the morphotropic phase transition, which is contributed by the relative proportions of the two coexisting phases in the two-phase region. The x-ray diffraction analysis reveals the coexistence of both aeschynite and euxenite phase between x = 0.7 and 0.8 in $GdTiNb_{1-x}Ta_xO_6$ and $Sm_{1-x}Y_xTiTaO_6$. Again the dielectric properties vary linearly as a function of x in the new phase region. The bulk density attains minimum value for x = 0.75 in $GdTiNb_{1-x}Ta_xO_6$ and x = 0.73 in $Sm_{1-x}Y_xTiTaO_6$ where the τ_f changes sign. The range of solid solubility of aeschynite in euxenite and vise versa depends on the average ionic radius of the rare earth ion in $RE_{1-x}RE'_xTiTaO_6$ ceramics. If the average ionic radius of the rare earths in $RE_{1-x}RE'_xTiTaO_6$ is less than 0.915 Å then the structure is euxenite with negative τ_f and when it is greater than 0.915 Å then τ_f is positive with aeschynite structure. The results indicate the possibility of developing a near zero τ_f material in the solid solution $RE_{1-x}RE'_xTiTaO_6$ by adjusting the average ionic radius of rare earth

to be about 0.915 Å. which provides vital contribution towards the structure-property relationship of microwave ceramics

7. 4 REFERENCES

1. D. Kajfez and P. Guillon, *Dielectric Resonators*, Artech House, Massachusetts, (1986).

2. S. Nomura, K. Toyama and K Kaneta, *Jpn. J. Appl. Phys*., **21**(10), L624-626 (1982).

3. S. B. Desu and H. M. O'Bryan, *J. Am. Ceram. Soc*., **68**, 546-51 (1985).

4. D. J. Masse, R. A. Purcel, D. W. Ready, E. A. Maguire, and C. P. Hartwig, *Proc. IEEE*, **59** (11), 1628-29 (1971).

5. H. M. O'Bryan Jr., J.Thomas Jr. and J. K. Plourde, *J. Amer. Cer. Soc*., **57**, 450-453 (1974).

6. J. K. Plourde, D. F. Linn, H. M. O'bryan Jr. and J. Thomas Jr., *J. Am. Ceram. Soc*., **58**, 418-420 (1975).

7. G. Wolfram and E. Gobel, *Mater, Res. Bull*., **16**, 1455-1463 (1981).

8. K. Wakino, K. Minai and H. Tamura, *J. Am. Ceram. Soc*., **67**, 278-281 (1984).

9. H. Sreemoolanathan, M. T. Sebastian and P. Mohanan, *Mater. Res. Bull*., **30**, 653-58 (1995).

10. M. T. Sebastian, *J. Mat. Sci. Mater. Electron*., **10**, 475-78 (1999).

11. P. V. Bijumon, P Mohanan and M. T. Sebastian, *Jpn. J. Appl. Phys*., Part I, **41**, 3384 – 85 (2002).

12. G. L. Roberts, R. J. Cava, W. F. Peck and J. J. Krajewski, *J. Mater. Res*., **12**, 526-30 (1997).

13. M. T. Sebastian, R. Ratheesh, H. Sreemoolanathan, S. Solomon and P. Mohanan, *Mater. Res. Bull.*, **32**, 1279-84 (1997).

14. M. T. Sebastian, S. Solomon, R. Ratheesh, J. George and P. Mohanan, *J. Am. Ceram. Soc.*, **84,** 1487-89 (2001)

15. S. Solomon. M. Kumar, K. P. Surendran, M. T. Sebastian and P. Mohanan, *Mat. Chem. Phys.*, **67**, 291-93 (2001).

16. X. Qi, T. P. J. Han, H. G. Gallagher, B. Henderson, R. Illingworth and I. S. Ruddock, *J. Phys. Condens. Mater*., **8**, 4837-45 (1996).

17. X. Qi, R. Illingworth, H. G. Gallagher, T. P. J. Han and B. Henderson, *J. Cryst. Growth,* **160**, 111-18 (1996).

18. H. Seifert and B. Beck, *Fortschr. Minerol.*, **39**, 36-39 (1961).

19. P-S. Chang, *Sci. Sinica*., **12**, 2337-43 (1963).

20. I. Komkov, *Dokl. Acad. Nauk*. *SSSR,* **148**, 1182-83 (1963).

21. V. B. Aleksandrov, *Dokl. Akad. Nauk*. *SSSR,* **142**, 181-84 (1963).

22. B. W. Hakki and P. D. Coleman, *IRE Trans. on Microwave Theory Tech*., **MTT-8**, 402-10 (1960).

23. W. E. Courtney, *IEEE Trans. on Microwave Theory Tech.*, **MTT-18**, 476-85 (1970).

24. A. A. Kominskii, *Laser Crystals,* 2nd Ed., Springer, Berlin, (1990).

25. G. Blasse, *J. Inorg. Nucl. Chem*., **28**, 1122-24 (1966).

26. L. Jahnberg, *Acta Chem. Scand*., **17**, 2548-51 (1963).

27. M. Maeda, T. Yamamura and T. Ikeda, *Jpn. J. Appl. Phys. Supl*., **26**, 76-79 (1987).

28. F. W. Peek Jr, *Dielectric Phenomena in High Voltage Engineering*, Wexford College Press, Wexford (1999).

29. R. D. Shannon, *Acta Cryst*., **A32**, 751-67 (1976).

30. V. V. Kazantsev, E. I. Krylov, A. K. Borisov and A. I. Chupin, *Russian. J. Inorg. Chem*., **19**, 506-07 (1974).

31. C. E. Holcombe M. K. Morrow, D.D. Smith and D. A. Carpenter, *Survey Study of Low Expending, High Melting, Mixed Oxides*, Y-1913, Union Carbide Corporation, Nuclear Division, Oak Ridge, Tennessee (1974).

32. C. E. Holcombe, J. Mater. Sci. Lett., **14,** 2255-58 (1974).

33. M. Maeda, T. Yamamura and T. Ikeda, *Proc. 5th Meeting on Ferroelectric*

Materials and Their Applications. Kyoto (1974). Jpn. J. Appl. Phys. **26**, 76 (1974).

34. S. Solomon, *Synthesis characterization and properties of some rare earth based ceramic dielectric resonators*. Ph. D Thesis, University of Kerala (1999).

35. K. P. Surendran, Manoj Raama Varma, P. Mohanan and M.T. Sebastian.. *J. Am. Ceram. Soc.*, **86**, 1695-99 (2003).

36. Fang, Y., Hu, A., Ouyang, S. and Oh, J. J., *J. Euro. Ceram. Soc*., **21**, 2745-50 (2001).

37. R. D. Shannon, *J. Appl. Phys*., **73**, 348-66 (1993).

38. K. P. Surendran, Manoj Raama Varma, P. Mohanan and M.T. Sebastian, *J. Mater. Res*., **17**, 2561-66 (2002).

CHAPTER 8

MAl_2O_4-TiO_2 [M=Mg, Zn] DIELECTRICS FOR SUBSTRATE APPLICATIONS

This Chapter probes the dielectric loss phenomena of $ZnAl_2O_4$ and $MgAl_2O_4$ spinels. The dielectric properties of these spinels were tailored by preparing isomolar mixtures with TiO_2 in an effort to tune their t_f close to zero. It was found that two low dielectric constant materials $0.83ZnAl_2O_4$-$0.17TiO_2$ and $0.75MgAl_2O_4$-$0.25TiO_2$ have excellent dielectric properties for possible applications in microelectronic packaging. The substrate characteristics of the new temperature stable low loss material $0.83ZnAl_2O_4$-$0.17TiO_2$ which is even advantageous over alumina, have been investigated.

8.1 (1-x)$ZnAl_2O_4$-xTiO_2 CERAMICS

8.1.1 Introduction

Ceramic substrates find wide range of applications in wireless access circuits that use millimeter waves for 3rd generation cell phones, blue-tooth equipped devices, wireless LAN, optical communications as well as peripheral electronic devices. Ideal ceramic substrates should have a low permittivity (to minimize cross-coupling with conductors and to shorten the time for the electronic signal transition) for the application of advanced substrate materials needed for microwave integrated circuits (MIC)[1]. The typical characteristics needed for a dielectric substrate are: (a) low dielectric constant, (b) bw dielectric loss and (c) matching coefficient of thermal expansion to that of the material attached to it. These substrate materials also ought to exhibit high Q factors in order to maintain overall high-Q circuits by lowering power dissipation. Typical dielectric properties of some commonly used low-permittivity ceramic substrates show less reliable properties for the MIC application[2]. Alumina[3] and Forsterite[4] are two good candidates for substrate applications but their high negative temperature coefficients of resonant frequencies (which means high positive temperature coefficient of dielectric constant, τ_ε) put constraints on their use as temperature stable microwave devices such as oscillators. Hence the search for new substrate materials with optimum balance of the dielectric properties is considered as a big challenge in the research of microwave materials.

A lot of investigation has been done [5, 6] on complex perovskites based on $Ln(Zn_{1/2}Ti_{1/2})O_3$ [Ln = Lanthanides, Y, Al, In]. Recently Santha et al. [7] suggested the possibility of using materials like $Al(Zn_{1/2}Ti_{1/2})O_3$, $In(Zn_{1/2}Ti_{1/2})O_3$ etc. as useful candidates for dielectric resonator applications. Later it has been revealed that the x-ray diffraction patterns of $Al(Zn_{1/2}Ti_{1/2})O_3$ is different from the rest of similar complex perovskites which raised serious doubts about the very existence of such a compound. A detailed powder diffraction investigation showed that the stoichiometric composition $Al(Zn_{1/2}Ti_{1/2})O_3$ is nothing but a poly phase mixture of two compounds, the spinel $ZnAl_2O_4$ and rutile (TiO_2). This draw our special attention to the spinel structured aluminate compounds which must be of low dielectric loss, as a necessary and sufficient condition for the mixture $ZnAl_2O_4$-TiO_2 to exhibit resonance in the microwave frequency range. The microwave dielectric properties of TiO_2 is well known [8] which is a material with high positive τ_f (~ 450 ppm/^oC)

and high dielectric constant (~100). The microwave dielectric properties of spinels have not been explored before.

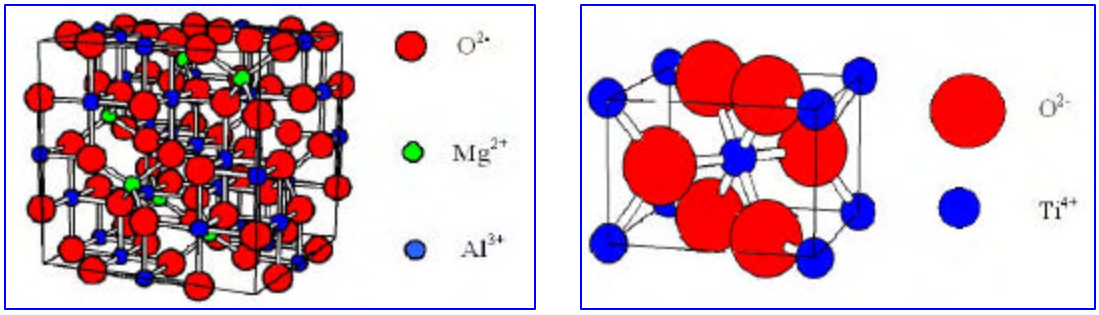

Fig. 8. 1 Crystal structure of spinel (left) and rutile (right)

The compounds with the general formula AM_2O_4 [A= Mg, Zn, Co, Ni, Cu ; M = Al, Ga, Fe] is referred as spinels [9] which belongs to the face centered cubic symmetry group $Fd\bar{3}m$. Their cubic cell contains a close packed array of 32 oxygen atoms with cations in the tetrahedral and octahedral interstices. In the normal spinel structure, tetrahedral sites are occupied by divalent cations whereas octahedral sites are occupied by trivalent cations [10] (see Fig. 8.1). The aluminate spinel materials are reported to be ideal candidates for serving as radiation resistant matrices in nuclear bombardment experiments and as a support for Pt and Pt-Sn catalysts because of its high thermal stability and low acidity. Furthermore, a recent survey revealed that zinc aluminate spinels were also finding versatile applications in industrial ceramics[11], as a second phase in glaze layers of white ceramic tiles to improve wear resistance and mechanical properties and to preserve whiteness, which has been supported by the increasing number of research papers in the literature. The mixture characteristics of $ZnAl_2O_4$-TiO_2 were also studied even though the emphasis was to explore the possibility of developing ultra filtration membranes with the goal of increasing the electrical interaction of $ZnAl_2O_4$ and TiO_2 layers towards the filtered ionic species[12, 13]. It has been reported [2] earlier that zinc aluminate has very low electrical conductance (5.4×10^{-6} ohm^{-1}) which is a unique characteristic of low loss dielectrics. In a very recent publication[14], a group of Dutch researchers attempted to measure its dielectric constant but their results throw no light into the dielectric loss behavior of these ceramics. The present

investigation revealed that $ZnAl_2O_4$ is a high Q dielectric with negative τ_f. In the following section we discuss the microwave dielectric properties of $ZnAl_2O_4$ spinels and tailoring its properties by making molar mixtures with TiO_2 to form $(1-x)ZnAl_2O_4$-$xTiO_2$ in an effort to develop an alternate substrate material composition for applications in mobile communication devices.

8. 1. 2 Experimental

The $(1-x)ZnAl_2O_4$-$xTiO_2$ ceramics were prepared by the conventional mixed oxide route as described in Chapter. 2, Sections 2.1.2.1 to 2.1.2.7. The reaction mixture was calcined at 1100 ^oC for 4 hours. It was then ball milled with Anatase TiO_2 (Aldrich 99.9 % pure) according to the formula $(1-x)ZnAl_2O_4$-$xTiO_2$ (x = 0.0, 0.1, 0.12, 0.14, 0.15, 0.15, 0.17, 0.18, 0.19, 0.20, 0.25, 0.3, 0.4, 0.5, 0.6, 0.7, 0.9 and 1.0) for 24 hours using deionized water as the mixing medium. The sintering is done in the temperature range 1375-1425 ^oC for 4 hours. In synthetic spinels, a disordered distribution of cations exists systematically[10] in such a way that a fraction of trivalent aluminium ions occupy tetrahedral sites for zinc. So the sintered samples were annealed at 1000 ^oC for 5 hours. The powdered samples were used for analyzing the X-ray diffraction patterns using Cu K_α radiation (Rigaku, Japan).

The dielectric properties ε_r and τ_f of the materials were measured in the microwave frequency range using resonance technique as described Chapter 2, Sections 2.2.2 to 2.2.5

8. 1. 3 Results and Discussion

The density of pure $ZnAl_2O_4$ was measured to be 4.38 g/cm^3 which is around 96 % of its theoretical density [9] (4.58 g/cm^3). To enhance densification we doped the spinel with 1 mole % of additives such as $CaCO_3$, SnO_2 and Eu_2O_3. It is evident that, on doping $ZnAl_2O_4$ with $CaCO_3$, Ca^{2+} is not indeed entered in the spinel lattice as this would have been resulted as a modification of the cell parameter (see Table 8.1), but may remain at the grain boundary. When SnO_2 is added to zinc aluminate the cell parameter is modified slightly. On the other hand doping $ZnAl_2O_4$ with Eu_2O_3 altered the unit cell parameter however it deteriorated the densification process. The theoretical density of TiO_2 (rutile) is 4.26 g/cm^3.

Table 8. 1 Properties of $ZnAl_2O_4$ and TiO_2 ceramics

Material	Den. (g/cm^3)	Sinter. Temp.	% Density	Cell Parameter a (Å)	Cell Parameter c (Å)	e_r	t_f	Q_u x f (GHz)
$ZnAl_2O_4$ Pure	4.38	1425	95.6	8.0899	--	8.5	-79	56300
$ZnAl_2O_4$+ I mole % $CaCO_3$	4.37	1400	95.4	8.0902	--	8.5	-81	58000
$ZnAl_2O_4$+ I mole % SnO_2	4.42	1400	96.5	8.0913	--	8.7	-85	52000
$ZnAl_2O_4$+ I mole % Eu_2O_3	4.35	1450	94.9	8.0841	--	8.2	-72	48500
TiO_2 (Rutile) Pure	4.00	1500	93.8	4.5911	2.9599	104.2	+411	17600
TiO_2 + 1 mole % Fe_2O_3	4.09	1500	96.0	4.5928	2.9588	105.1	+398	26900
TiO_2 (Rutile) Sol-Gel Route	3.69	1300	86.6	4.5824	2.9441	93.3	+423	12400

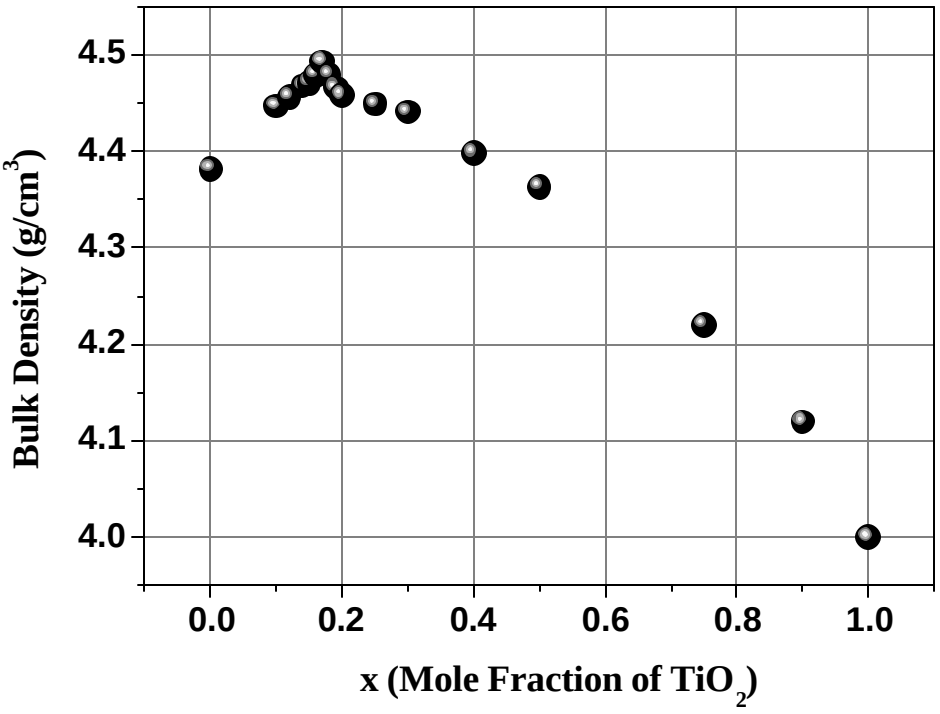

Fig. 8. 2 Variation of the bulk density of $(1-x)ZnAl_2O_4$-$xTiO_2$ with x

Fig. 8.1 represents the variation of bulk density of $ZnAl_2O_4$ as a function of TiO_2 concentration. From the figure it is evident that the density of $ZnAl_2O_4$ samples increase with TiO_2 addition reaches a maximum for x = 0.17 in (1-x) $ZnAl_2O_4$ - $xTiO_2$ and there

after it decreases. Incidentally this composition is considered as an ideal one for practical dielectric resonators and microwave substrate applications. It has been reported [15] that the densification behaviour of TiO_2 is hindered due to the anatase to rutile phase transition consequent to the reduction of Ti^{4+} to Ti^{3+} state. It is believed [16] that addition of dopants with valencies 2 and 3 improves its densification process, which can compensate its oxygen vacancy that could be developed at the time of sintering. We used anatase titania as the starting material in this investigation, and then it is doped with 1 mole % additive Fe_2O_3 which improved the densification process. The densification performance of TiO_2 sample prepared from alkoxide sol -gel route was very poor (see Table 8.1).

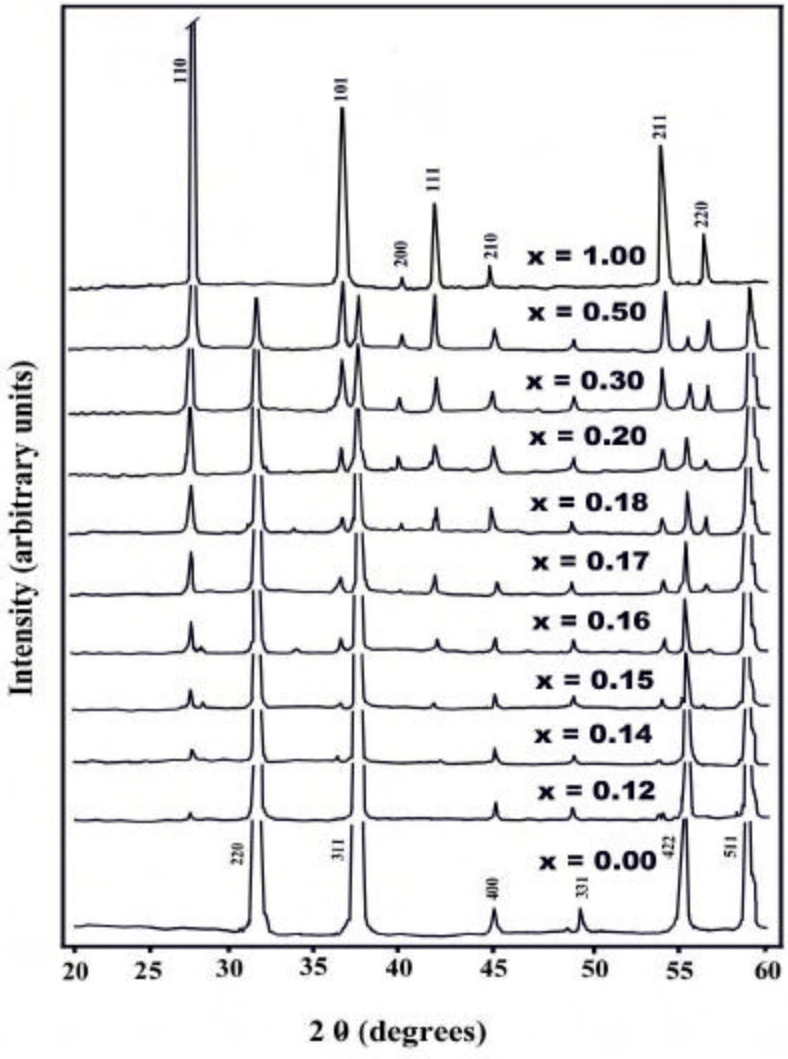

Fig. 8. 3 Powder diffraction patterns of $(1-x)ZnAl_2O_4$-$xTiO_2$ mixed phases for x =0.0, 0.12, 0.14, 0.15, 0.16, 0.17, 0.18, 0.2, 0.3, 0.5, 1.0

Fig. 8.3 represents the XRD patterns recorded from samples for x = 0.0, 0.12, 0.15, 0.16, 0.17, 0.18, 0.2, 0.3, 0.4, 0.5 and 1.0 in (1-x)$ZnAl_2O_4$-xTiO_2. The powder diffraction pattern of $ZnAl_2O_4$ is indexed as per JCPDS File Card Number 5-669. The crystal structure of TiO_2 (rutile) is tetragonal. The powder diffraction pattern of specimen for x=1.0 is identical with JCPDS File Card Number 21-1276 for TiO_2 (rutile). The powder diffraction pattern suggests that $ZnAl_2O_4$ will not form a solid solution with TiO_2 which has been one of the reasons behind selecting them for preparing ultrafiltration membranes[12, 13]. The variation of physical and dielectric properties of the mixture compositions were proportional to the variation of the molar concentration of the contributing phases.

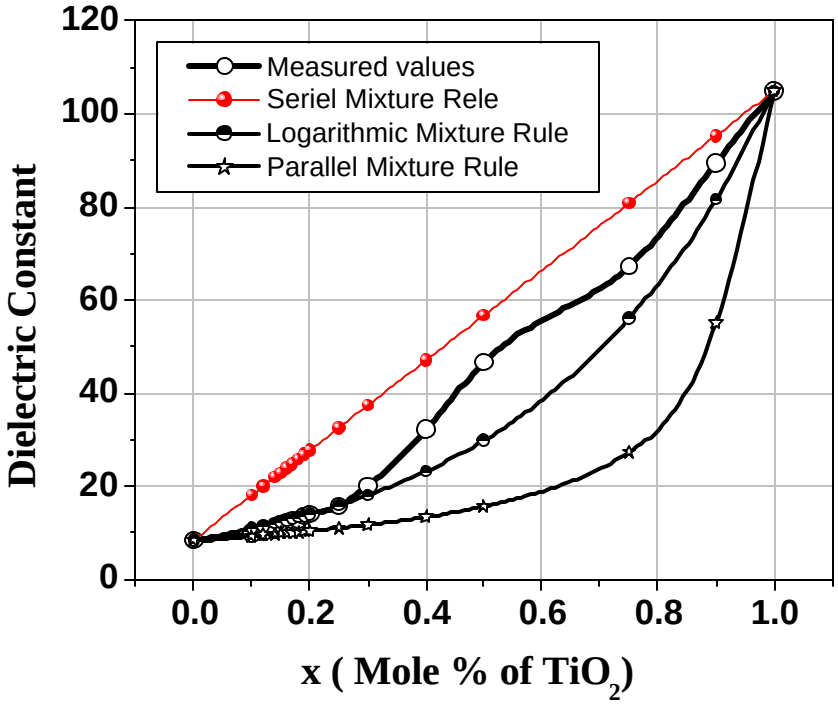

Fig. 8. 4 Variation of the e_r of (1-x)$ZnAl_2O_4$-xTiO_2 with x

The microwave dielectric properties of zinc aluminate spinel are found to be quite interesting since the dielectric loss factor of this ceramic is found to be low enough for microwave substrate applications. The measured dielectric constants are corrected for porosity[17]. The dielectric constant of pure zinc aluminate is 8.5 while that for Ca^{2+}, Sn^{4+} and Eu^{3+} doped spinels are 8.5, 8.7 and 8.2 respectively. The variation of the dielectric

constant of $ZnAl_2O_4$ with TiO_2 addition is plotted in Fig. 8.4. The dielectric constant of a mixture can be calculated using the general Maxwell- Wagner formula[18]

$$\varepsilon_r^{\alpha} = \Sigma V_i \varepsilon_{ri}^{\alpha} \qquad (8.1)$$

where V_i and ε_{ri} are the volume fraction and relative dielectric constant of the i^{th} material and α is a constant which assumes values depending on the type of the mixing rule. Putting $\alpha = -1$ (serial mixing model), $\alpha = 0$ (logarithmic mixing model) and $\alpha = 1$ (parallel mixing model) in Eqn. (8.1) we derive the following mixing formulae:

$$\varepsilon_r = v_1 \varepsilon_{r1} + v_2 \varepsilon_{r2} \qquad (8.2)$$

$$\ln \varepsilon_r = v_1 \ln\varepsilon_{r1} + v_2 \ln\varepsilon_{r2} \qquad (8.3)$$

$$1/\varepsilon_r = v_1/\varepsilon_{r1} + v_2/\varepsilon_{r2} \qquad (8.4)$$

where ε_{r1} and ε_{r2} are the dielectric constants of phases with volumes v_1 and v_2. The above empirical formulae (8.2) represent serial, (8.3) logarithmic and (8.4) parallel mixing models respectively. It must be remembered that this mixture rule does not have any physical implication but was introduced as a curve fitting construct. Furthermore, the behavior of the dielectric constant of $ZnAl_2O_4$-TiO_2 mixture does not follow any other mixture rules for random binary phase materials. The dielectric constant shows reasonably good agreement with the logarithmic mixing rule [23] (Eqn. (8.3) for smaller values of x while it shows noticeable deviation as the value of x increases. The dielectric constant of pure TiO_2 is 104 while that doped with Fe_2O_3 is 105.1 (Table 8.1). The dielectric constant of the TiO_2 sample made of chemically derived powder is 93.2 only. The lower dielectric constant of this sample made from powder obtained from chemical method is due to its poor densification. Very recently, Van der Laaga et al. [14] reported that ε_r of $ZnAl_2O_4$ was 9.46 at a frequency of 10 MHz, where the dielectric constant would be higher than what was measured at microwave frequency.

The temperature coefficient of resonant frequency (t_f) of pure $ZnAl_2O_4$ is –79 ppm/^oC while that for Ca^{2+}, Sn^{4+} and Eu^{3+} doped samples are -81, -85 and -72 ppm/^oC respectively. In one of our previous reports it has been shown that variation of t_f in a

random mixture is proportional to the molar variation of the constituent phases[16]. Hence the t_f of the mixture phases can be computed using a general mixture formula[19]

$$t_{f\,(eff)} = v_1\, t_{f1} + v_2\, t_{f2} \tag{8.5}$$

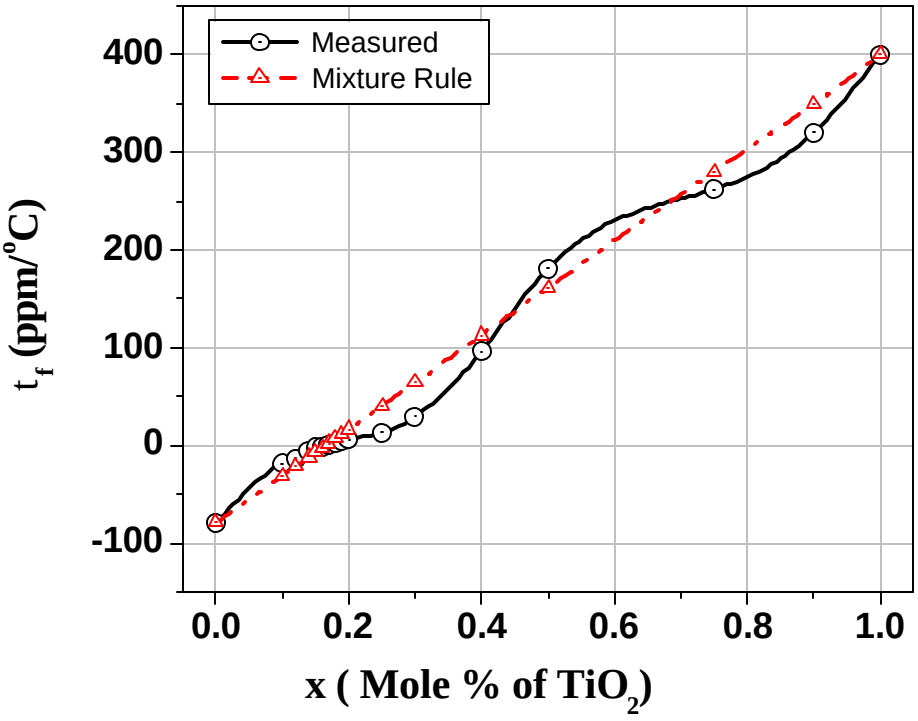

Fig. 8. 5 Variation of the temperature coefficient of resonant frequency of (1-x) $ZnAl_2O_4$-xTiO_2 with x

The variation of t_f of the mixed phases of $ZnAl_2O_4$-TiO_2 was plotted in Fig. 8.5 from which it is obvious that the variation of mixed phases swinged around the straight line corresponding to the rule of mixtures. The value of t_f for x = 0.16 is -1.9 ppm/°C while that for x=0.18 is +1.5 ppm/°C from which one can interpolate that the zero t_f composition will be around x=0.17 in (1-x)$ZnAl_2O_4$-xTiO_2 mixture. Hence we prepared the composition 0.83$ZnAl_2O_4$-0.17TiO_2 and measured the t_f as 0.74 ppm/°C which can be approximated as zero within the limits of experimental errors. However, the error of the experimental value from the zero t_f value predicted by the rule of mixtures (0.825 Al_2O_4-0.165 TiO_2) given by Eqn. 8.5 is marginal. Furthermore, there was no additional phase formation detected consequent to the chemical reaction between $ZnAl_2O_4$ and TiO_2 throughout the complete

range of mixtures. On the other hand, additional phase formation of $MgTi_2O_5$ was observed in a recent report [4] on substrate material when rutile was added to high Q forsterite which resulted in anomalous behavior of t_f in the mixture.

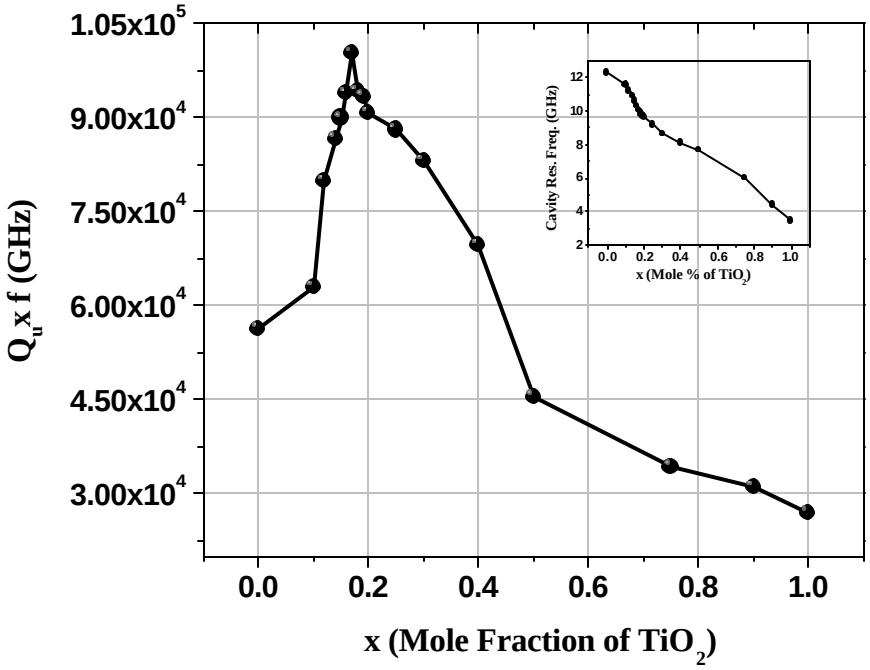

Fig. 8. 6 Variation of the unloaded quality factor and resonant frequency of $(1-x)ZnAl_2O_4$-$xTiO_2$ with x

The resonant frequency of the dielectrics in the mixed phase measured using a microwave cavity was plotted in Fig. 8.6 with respect to the molar addition of TiO_2 into the spinel. The resonant frequency of samples of same dimensions should decrease linearly from $ZnAl_2O_4$ to TiO_2 rich compositions which have larger dielectric constants. The nonlinear variation of the resonant frequency (see inset of Fig. 8. 6) is due to the slight variations of dimension of the ceramic samples, since the resonant frequency depends on the sample dielectric constant and dimensions. The unloaded quality factor of pure $ZnAl_2O_4$ is reasonably good (Q_u x f = 56,000 GHz) which is well above that of many of the conventional low dielectric constant materials. Doping with $CaCO_3$ improved the Q factor slightly but SnO_2 addition deteriorated it (Table 8.1). The addition of Eu_2O_3 also decreased the dielectric quality factor of the material. The variation of unloaded factor of the various mixture phases are plotted in Fig. 8.6 as a function of the increasing TiO_2 content. It must

be noted that the microwave quality factor, which depends greatly on the synthesizing conditions, porosity, grain morphology etc. do not show any specific relationship with the rule of mixtures. The product Q_u x f is maximum (~1,00,200 GHz) around x=0.17 in (1-x)$ZnAl_2O_4$-xTiO_2 where the t_f assumes a minimum value (zero). It is worthwhile to note that the intermediate phases shows better quality factors compared to the end phase components which is unusual in dielectric mixtures. From Fig. 8.5, it is clear that the drop in the quality factor is more for the TiO_2 rich compositions. It is well known that the anatase to rutile phase transition which occurs around 700 ^oC was a major source of concern in its dielectric loss quality since it involves collapse of the relatively open anatase structure. This collapse takes place by a distortion of the oxygen framework and shifting of the majority of Ti^{4+} ions by rupturing the two out of the six Ti-O bonds to form new bonds[20]. Shannon[20] suggested that doping with aliovalent additives or sintering in reduced atmosphere can accelerate oxygen vacancy formation and expedite the anatase to rutile transformation. In our experiment doping of TiO_2 with Fe_2O_3 yielded a better quality factor of Q_ux f = 28,900 GHz even though it is lower than the quality factor reported by Templeton[21] et al. The TiO_2 samples derived from sol-gel precursor also showed a poor microwave quality factor. In the case of this specimen the particle size was small. Hence the densification was poor due to the uniform size distribution of particles which is not favorable for material transport associated with densification. Moreover in a recent paper Radecka and Rekas [21] observed that titania samples containing smaller grains exhibit about twice as much electrical conductivity as those with larger grains, because materials with smaller grains have a higher concentration of intergrain contacts than those with larger grains. Thus it is possible that the lower Q factor of TiO_2 ceramic specimen made from chemically derived powder is due to its high electrical conductivity.

The above discussion revealed that the composition 0.83 $ZnAl_2O_4$-0.17 TiO_2 is an ideal temperature stable, high Q dielectric resonator, which can be comparable to many of the conventional low dielectric constant microwave dielectrics like Al_2O_3. In spite of the fact that that alumina has high quality factor at microwave frequency range[3], its τ_f is –60 ppm/^oC and being a well-known refractory, its processing temperature is high (>1700^oC). But the new 0.83$ZnAl_2O_4$-0.17TiO_2 rutile-spinel mixture composition is advantageous over Al_2O_3 in respect to temperature compensation which is a necessary requirement for

microwave dielectric substrate applications. In addition to these microwave dielectric properties, $0.83ZnAl_2O_4$-$0.17TiO_2$ possess a number of additional merits over conventional microwave substrates used in microelectronic applications, which is discussed in the following section.

8. 2 SUBSTRATE PROPERTIES OF $(1-x)ZnAl_2O_4$-$xTiO_2$ CERAMICS

8. 2. 1 Introduction

Modern electronics are based on the integrated circuit, which is an assembly of millions of interconnected components such as transistors and resistors that are built up on a tiny chip of silicon. In order to maintain their reliability, these circuits are kept on insulating materials that can serve as substrates and packages. These packaging structures seal a circuit from the environment and make it a single, compact unit[22]. The thermal expansion coefficient of the substrate should be minimum and comparable to that of silicon since the materials joined in an electronic package have a wide range of linear coefficients of thermal expansion[23]. In addition to that the thermal conductivity of the substrate should be sufficiently high to dissipate the generated heat away. These are additional prerequisites in addition to low dielectric constant and dielectric loss that have to be considered when a new microelectronic substrate is developed.

The insulating properties of ceramics are well known, and these properties have found application in advanced ceramic materials for substrates and packages. Among the ceramics employed as electronic substrates and packages, the dominant material is alumina. The advantages of alumina include high resistivity, good mechanical and dielectric strength, excellent thermal and corrosion stability, and the ability to provide hermetic seals. Its major disadvantages are associated with its delayed signal propagation tendencies due to their dielectric characteristics and low thermal conductivity which makes it inefficient in drawing away the heat. For these reasons ceramic materials with improved properties are under development[24]. Among the alternate materials developed in recent times are berylia (BeO) and aluminium nitride (AlN) which posses a lot of advantages like low dielectric constant and small thermal expansion characteristics. But berylia is a toxic material which constraints its wide commercial use as a packaging substrate. On the other hand the cofiring characteristics of AlN is very poor since it will oxidize and subsequently lose its

substrate properties. Glass-ceramic materials like corderite, forsterite etc. have low strengths and low thermal conductivities.

In this perspective the development of a new low loss ceramic substrate always catch attention as a substitute for the existing conventional ceramic insulators that are used in microelectronic packaging. As discussed in Section 8.1, we have successfully developed a new temperature compensated low dielectric constant, low loss and high thermal conducting substrate in the spinel-rutile system $0.83ZnAl_2O_4$-$0.17TiO_2$. In this study the substrate characteristics of the material $0.83ZnAl_2O_4$-$0.17TiO_2$ such as the thermal conductivity, thermal expansion coefficient, electrical resistivity, temperature coefficient of the dielectric constant, mechanical strength and reactivity of the material with metallic silicon etc. are investigated.

8. 2. 2 Experimental

The $0.83ZnAl_2O_4$-$0.17TiO_2$ specimens were prepared as described in 8. 1. 2. The surface morphology of thermally etched sintered samples is studied using a Scanning Electron Microscope (JEOL JSM 5600LV). The coefficient of thermal expansion of the ceramic composition $0.83ZnAl_2O_4$-$0.17TiO_2$ was determined using thermo mechanical analyzer (TMA-60 H) in the temperature range 30-1200 ^oC. The thermal conductivity of the ceramic substrate specimen was calculated using photopyroelectric technique in the temperature range 30-400^oC. The polished thin pellets (diameter 12 mm and thickness 2 mm) were electroded for dielectric measurements at low frequencies (50Hz-13MHz) using an impedance analyzer (HP 4102 A - LF) . The temperature variation of dielectric constant (τ_e) was calculated using the following relation

$$\tau_e = \frac{1}{\varepsilon} \times \frac{\Delta\varepsilon}{\Delta T} \qquad (8.6)$$

where e is the dielectric constant at 30^oC, Δe is the variation in dielectric constant in the temperature range 30 -210^oC and ΔT is the corresponding difference in temperature. The high temperature phase stability of the ceramic was determined using DTA/TGA Analysis

in the temperature range 30-1200 ^{o}C using Shimadzu Thermal Analyser, Japan (model 50H) in air at a heating rate of 10°C/min. The electrical resistivity of the sample was also determined using impedance analyzer at two frequencies 1MHz and 5MHz.

8. 2. 3 Results and Discussion

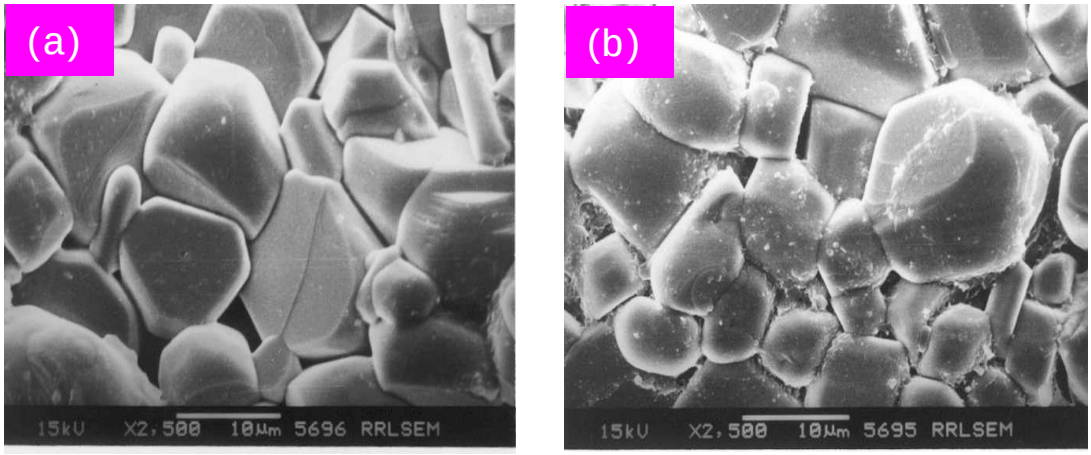

Fig. 8. 7 Scanning Electron Micrograph of two typical 0.83$ZnAl_2O_4$-0.17TiO_2 specimen sintered at 1425^{o}C for 4 hours

The surface morphology of the mixture composition 0.83$ZnAl_2O_4$-0.17TiO_2 recorded from two typical samples are given in Fig.8.7 (a) and 8.7 (b). The fact that the spinel-rutile mixture do not react each other to form any intermediate phase, is revealed from the scanning electron micrographs. The polygonal grain is believed to be of $ZnAl_2O_4$ with an approximate size of ~ 5-8 µm while TiO_2 presents an elongated grain structure.

The variation of the dielectric constant and dielectric loss factor (at 5MHz) as a function of temperature is given Fig. 8.8. The dielectric constant initially decreases from 13.107 to 13.07 when the temperature is increased from 30 to 210 ^{o}C. At low temperature the presence moisture in the sample give rise to slightly higher values of dielectric constant. This is because of the fact that the migrational polarization setting processes are comparatively slow and can take even minutes or hours. In the temperature range 80-220^{o}C the dielectric constant shows steady values but increases thereafter. As temperature is increased the ionic polarization takes over and the time for ionic polarization to set in is

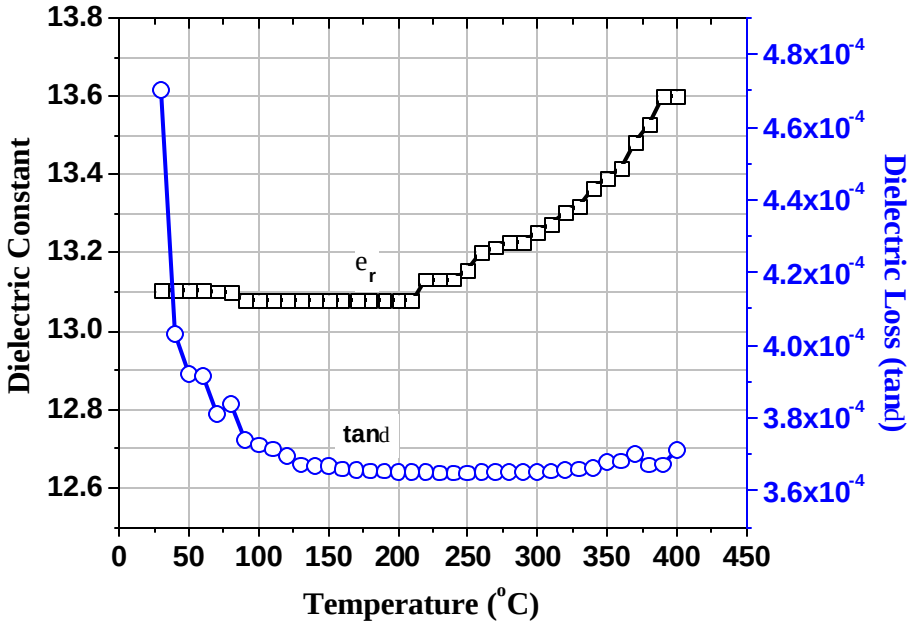

Fig. 8. 8 Variation of dielectric constant and loss tangent as a function of temperature for 0.83 $ZnAl_2O_4$-0.17 TiO_2 ceramics.

very small compared to the half period of alternating voltage. But the increase in dielectric constant at higher temperatures as seen from the Fig. 8.8 may be due to the increase in lattice vibrations with temperatures. From the variation of the dielectric constant with temperature, the temperature coefficient of relative permittivity is calculated using equation 8.5 as -15.6 ppm/^oC. In microelectronic circuits, materials with low temperature variation of the dielectric constant are sought to reduce inductive crosstalk and noise generation in the circuit. Also it is evident from Fig. 8.8 that the dielectric loss of the substrate material 0.83$ZnAl_2O_4$-0.17TiO_2 is very small (3-4 x10^{-4} at 5 MHz) which decreases with temperature. The higher values of loss tangent are expected to be due to the presence of moisture related interfacial polarization at low temperature[25]. The smaller values of tanδ and t_e is ideal for microwave substrate applications. For transfer loss of print substrates that form microwave integrated circuits, there is dielectric loss at the insulation layer, as well as loss in areas such as the copper foil in the conductive layer[29]. Generally, the bss at the dielectric is high. It is well understood that, lower the relative dielectric constant and dissipation factor, the lower the signal transfer loss.

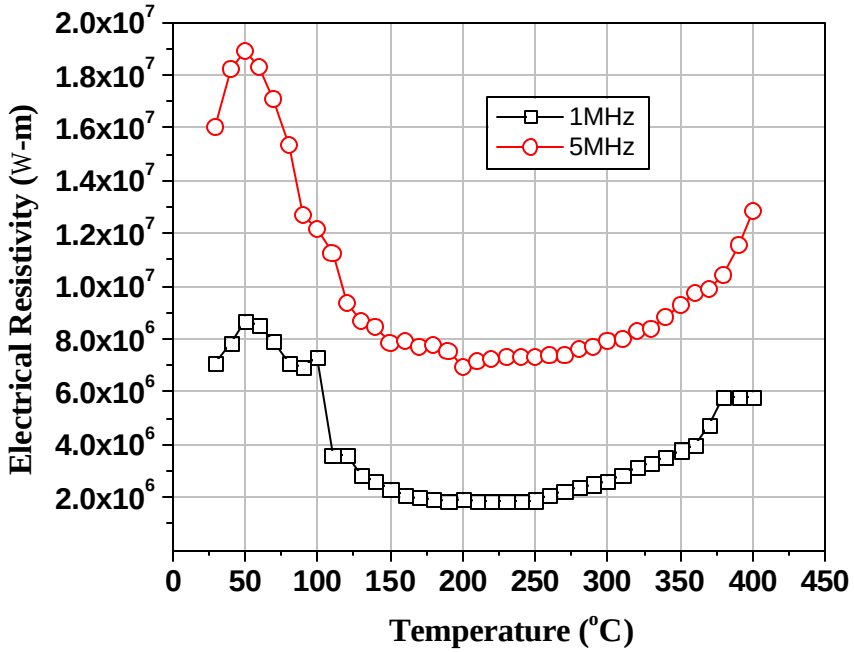

Fig. 8. 9 Variation of the ac electrical conductivity of $0.83ZnAl_2O_4$-$0.17TiO_2$ with respect to temperature

The plot of electrical resistivity of the substrate material $0.83ZnAl_2O_4$-$0.17TiO_2$ in the temperature range 30-400 ^oC is given in Fig. 8.9. The electrical insulating properties of this material is good (~20 MΩ-m) which provide better isolation between microelectronic components in Integrated Chip Circuitry. The non uniform variation of the ac conductivity with temperature may be attributed to moisture dependant surface conductivity[26] of the ceramic at room temperatures.

It is well known that a lot of compounds with poly phase structural compositions undergo a series of sequential decompositional reactions with increase of temperature which is accompanied by a compositional weight change. The differential thermal analysis (DTA)[27] coupled with thermogravimatric (TG) technique is used as a rapid means to study the possible thermo chemical reactions occurring during the heat treatment of the pre-sintered as well as post-sintered ceramics. The high temperature stability of the sintered $0.83ZnAl_2O_4$-$0.17TiO_2$ dielectric material was tested using DTA/TGA as given in Fig. 8.10. From the DTA plot, it is clear that no specific exothermic reactions like decomposition nor are there any endothermic reactions like melting, fusion etc. occurring

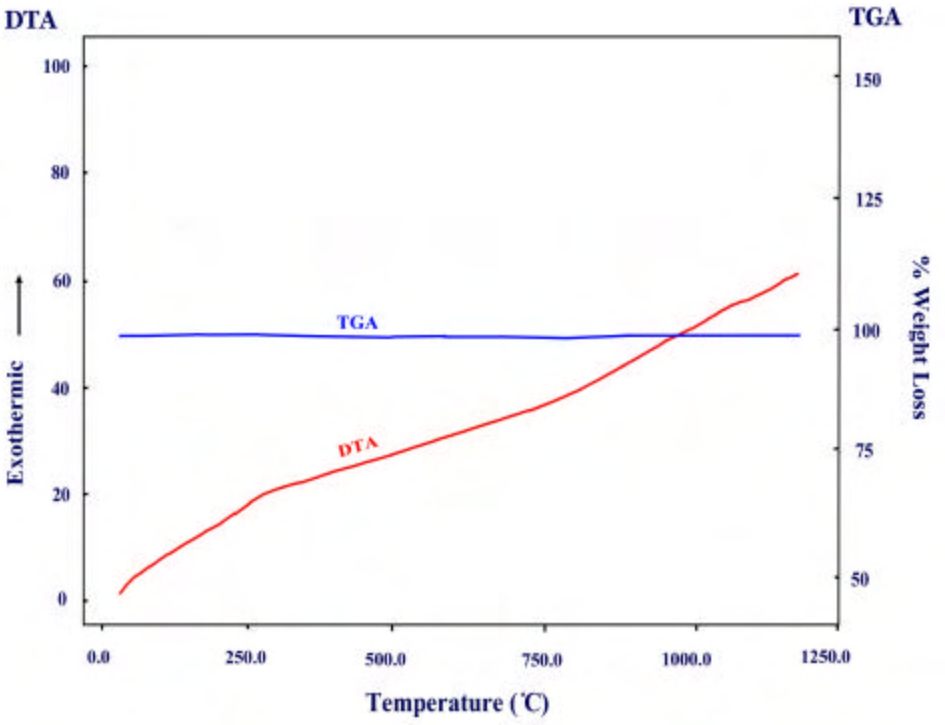

Fig. 8. 10 Differential thermal analysis and thermo gravimetric analysis plots of sintered $0.83ZnAl_2O_4$-$0.17TiO_2$ dielectrics.

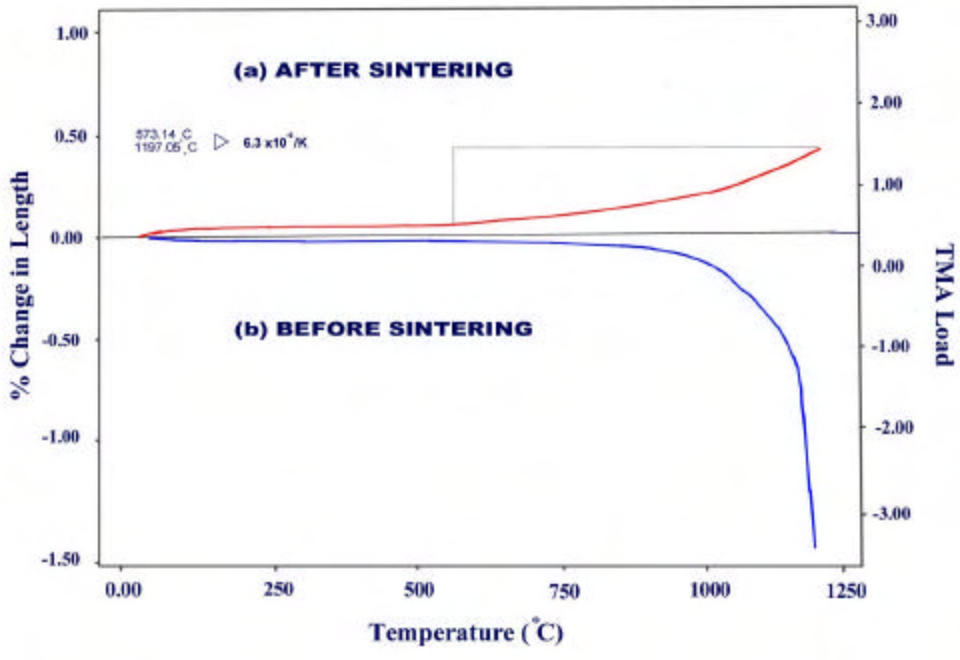

Fig. 8. 11 Plot of thermal expansion of $0.83ZnAl_2O_4$-$0.17TiO_2$ ceramics in the range 30-1200 ^oC.

during the heat treatment of the substrate in the temperature range 30-1250^{o}C. It is well known that thermogravimatric studies are advantageous over other dynamic techniques in evaluating the thermal stability of a mixture ceramic due to its versatility in getting output in a quantitative way and instrumental factors such as baseline drift are minimized[28]. Since there are no chemical changes observed at temperatures below 1250 ^{o}C, the thermo gravimetric analysis presents a near straight line plot (see Fig. 8.10).

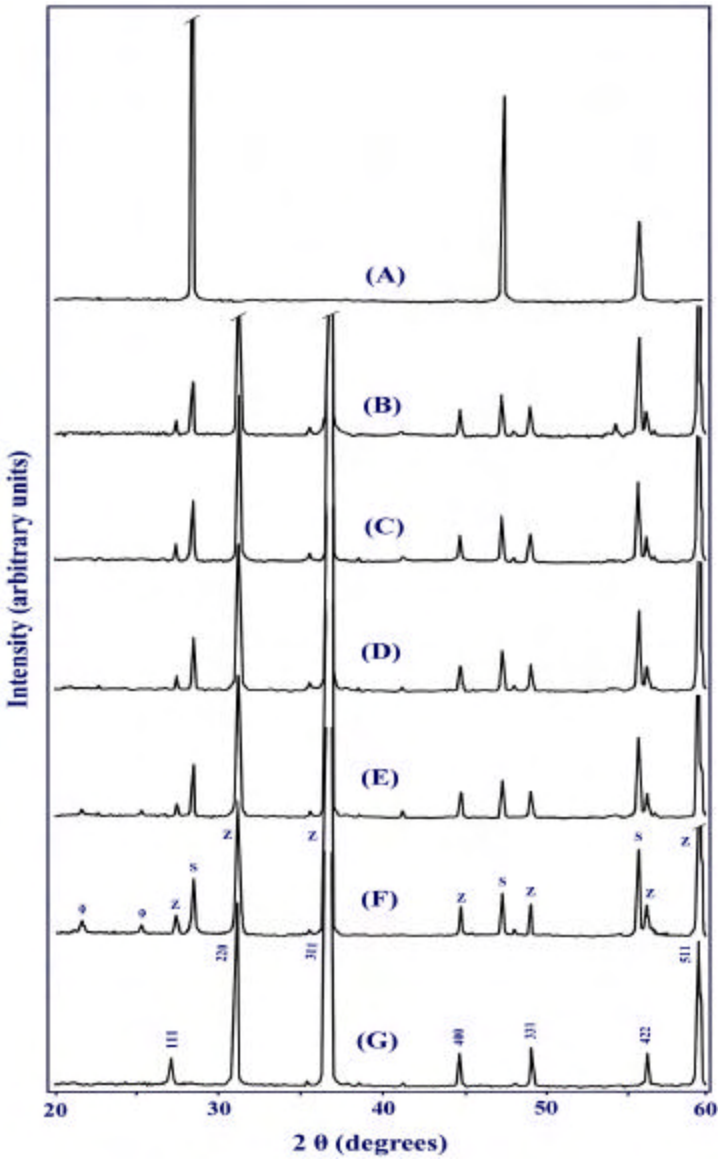

Fig. 8. 12 The XRD pattern of $0.83ZnAl_2O_4$-$0.17TiO_2$ (abbreviated as Z) mixed with Si metal(abbreviated as S). (A) Pure Si at room temperature, (B) S +Z (50:50) heated at 800 ^{o}C, (C) heated at 900 ^{o}C, (D) heated at 1000 ^{o}C, (E) heated at 1100 ^{o}C, (F) heated at 1200 ^{o}C, ✠ represent SiO_2, (G) Pure $ZnAl_2O_4$ sintered at 1425 ^{o}C.

The coefficient of thermal expansion of the substrate material $0.83ZnAl_2O_4$-$0.17TiO_2$ is studied in the temperature range 30-1250 ^oC before and after the sintering of the sample. Most of the conventional dielectric substrates currently in use like Al_2O_3, AlN and BeO have reported thermal expansion coefficients of 6.5, 7.6 and 6.05 ppm/^oC. The thermal expansion coefficient of the present sample was calculated (Fig. 8.11 (a)) in the temperature range 573 and 1197^oC as 6.3 ppm/^oC which is comparable to that of metallic silicon (4.2 ppm/^oC). The plot of linear shrinkage occurs during the sintering phenomena of the sample is also given in Fig. 8.11 (b). It must be remembered that the coefficient of thermal expansion of a material may be related to the strength of its atomic bonding. In order for the atoms to move from their equilibrium positions, energy in the form of heat must be introduced into the material. For materials with greater bond strength, the atoms separate to a lesser degree and hence low linear coefficient of expansion and greater melting point[29]. So the mixture composition $0.83ZnAl_2O_4$-$0.17TiO_2$ ceramic is likely to have comparably higher bond strength

As discussed in Chapter1, Section 1.3.3, the coefficient of thermal expansion (α) and the coefficient of thermal variation of the dielectric constant (τ_ε) are correlated to the temperature coefficient of resonant frequency of a dielectric resonator by the relation

$$\tau_f = -\alpha - \frac{\tau_\varepsilon}{2} \qquad (8.7)$$

On substituting the measured values of α and τ_ε as 6.3 ppm/^oC and 15.6 ppm/^oC respectively we obtain τ_f of the composition $0.83ZnAl_2O_4$-$0.17TiO_2$ as 1.5 ppm/^oC. It is to be remembered that this agrees well with measured value of temperature coefficient of resonant frequency at microwave frequency (0.74 ppm/^oC) as described in Section 8.1.3.

The thermal conductivity of a material is equivalent to the quantity of heat that passes in unit time through unit area of a plate, when its opposite faces are subject to unit temperature gradient[30] (e.g. one degree temperature difference across a thickness of one unit). In general thermal conductivity = heat flow rate ÷ (area × temperature gradient). The specific heat and thermal diffusivity of the composition $0.83ZnAl_2O_4$-$0.17TiO_2$ was determined as 0.36 J/g-K, and 0.37 cm^2/s respectively. Hence the thermal conductivity of

this new substrate material was computed as 59 W/m-K. This thermal conductivity is about twice the value of conductivity of commercial alumina substrate (see Table 8.2).

Electronic packages which are the housings for semiconductor devices, can be described as all of the materials around the semiconductor including, a printed wiring board. A package typically consists of the semiconductor mounted and wired to a dielectric substrate that is encapsulated to seal the device from the environment. The ideal electronic package[31] must serve four functions: (a) provide electrical contact to the chip; (b) act as an electrical space transformer to take electronic functionality from the dense surface of the chip to the coarser pitched outside world; (c) provide environmental isolation to the semiconductor (d) and provide an avenue for heat conduction away from the device. Usually the silicon based semiconductor materials are grown on the dielectric substrate which makes it imperative to study the reactivity of the semiconductor with metallic silicon. With this objective we prepared an equimolar mixture of $0.83ZnAl_2O_4$-$0.17TiO_2$ with metallic silicon and heated them at various temperatures 800, 900, 1000, 1100 and 1200 ^oC. It is observed (see Fig. 8.12) that this new dielectric substrate does not form any intermediate compounds with silicon powder (JCPDS File Card No. 5-565) apart from traces of silicon dioxide formed consequent to the oxidation of silicon at high temperature. Hence the inertness of the present substrate material with semiconductor chip material silicon is confirmed using XRD.

Table 8. 2 Comparison of properties of $0.83ZnAl_2O_4$-$0.17TiO_2$ with alumina and aluminium nitride substrates

Physical Property	Alumina (Al_2O_3)	Aluminium Nitride (AlN)	$0.83ZnAl_2O_4$-$0.17TiO_2$
Density	3.8	3.26	4.49
Dielectric loss	0.0001	0.001	0.0004
Dielectric Constant	9.8	8.9	12.6
Electrical Resistivity (ohm-m)	210	275	20
Thermal Conductivity (W/m-K)	24	290	59
Thermal Expansion (ppm/^oC)	6.5	7.6	6.3

From the above discussion it is evident that the substrate properties of 0.83Zn Al_2O_4-$0.17TiO_2$ is comparable to the conventional substrate materials available in the

market. Table 8.2 summarizes the general characteristics of $0.83ZnAl_2O_4$-$0.17TiO_2$ ceramics in comparison with two typical substrates like Alumina and Aluminium Nitride. It is worth while to note that the newly developed dielectric ceramic has got excellent dielectric and thermal properties but their mechanical strength is not appreciably high which can be enhanced using suitable additives.

8. 3 (1-x)$MgAl_2O_4$ -xTiO_2 DIELECTRICS FOR SUBSTRATE APPLICATIONS

8. 3. 1 Introduction

Magnesium aluminate ($MgAl_2O_4$) spinel is a potential refractory material with excellent high temperature mechanical, thermal and chemical properties. The development of magnesium aluminate spinel bodies and method of fabricating spinel refractories were available from about a century ago[32]. It has a high melting point (2130 ^oC) and low thermal expansivity (7.45 ppm/^oC). It should be noted that the phase diagram of $MgO–Al_2O_3$ system was established[33] as early as in 1916. A lot of efforts have been done to improve the densification and physical properties of these materials. Fluorine ion[34] (such as AlF_3 or CaF_2) and chlorine ions[35] (such as $AlCl_3$) are found to enhance the solid state reaction synthesis of magnesium aluminate spinel when it is incorporated in the lattice by replacing oxygen ions. Better sintered products of magnesium aluminate spinel were also reported through the addition of rare earth oxides [36] like Yb_2O_3, Y_2O_3 and Dy_2O_3.

The effect of addition of TiO_2 on the development of magnesium aluminate spinel is also available in literature. Y. H. Baik[37] worked on the sintering of magnesium aluminate in the presence of TiO_2 and MnO_2 and reported that TiO_2, is more beneficial in improving the densification than that of MnO_2. Yu and Hiragushi [38] worked on the sintering behaviour of spinel with 0.2 to 2 mass % of TiO_2. They found a continuous improvement in the sintered density with an increasing amount of TiO_2 up to a maximum of 1.5 mass%. Above 1.5% of TiO_2, the authors found no further improvement in density and concluded that exsolution of alumina and dissolution of TiO_2 in spinel was probably the reason for better densification. Recently Sarkar and Bannerjee [39] confirmed the improvement in the densification for smaller amount of TiO_2 additive in alumina rich and stoichiometric

spinels sintered at 1550°C and deteriorating effect at higher percentage of additive was due to grain growth. Photomicrographs marked the increase in the roundedness of the grains in presence of TiO_2 that affected the mechanical strength.

The dielectric properties of $MgAl_2O_4$ was studied by many [40,41, 42]. authors. In 1991, Shannon and Rossman[43] have measured the dielectric loss factor (0.0008 at 1 MHz) and dielectric constant (8.325) of single crystal $MgAl_2O_4$ using a two-terminal method. Nevertheless, the microwave dielectric properties of $MgAl_2O_4$ spinels has not been reported till now, which could have been useful to the investigators in search of new substrate materials. The present study revealed that similar to $ZnAl_2O_4$ as described in Section 8.1 of this chapter, $MgAl_2O_4$ is also a high Q dielectric with high negative τ_f. We carried out a detailed study on the mixture characteristics of $MgAl_2O_4$ with TiO_2 which has high positive τ_f and high dielectric constant, in an effort to tune the temperature coefficient of resonant frequency to zero. The present investigation reports the microwave dielectric properties of $MgAl_2O_4$ spinels and tailoring its properties by making molar mixtures with TiO_2 to form $(1-x)MgAl_2O_4$-$xTiO_2$ in an effort to develop an alternate temperature stable substrate material composition for applications in mobile communication devices.

8. 3. 2 Experimental

The $(1-x)MgAl_2O_4$-$xTiO_2$ ceramics were prepared by the conventional mixed oxide route as described in Chapter. 2, Sections 2.1.2.1 to 2.1.2.7. The reaction mixture was calcined at 1100 ^oC for 4 hours. It was then ball milled with Anatase TiO_2 (Aldrich 99.9 % pure) according to the formula $(1-x)MgAl_2O_4$-$xTiO_2$ (x = 0.0, 0.1, 0.12, 0.14, 0.16, 0.18, 0.20, 0.25, 0.3, 0.4, 0.5, 0.6, 0.7, 0.8, 0.9 and 1.0) for 24 hours using deionized water as the mixing medium. The cylindrical compacts were sintered in the temperature range 1400-1460 ^oC for 4 hours. The sintered samples were annealed at 1000 ^oC for 5 hours. The bulk density of the sintered samples were measured using Archimedes method. The powdered samples were used for analyzing the X-ray diffraction patterns using Cu K_α radiation (Rigaku, Japan) as described in Chapter 2, Section 2. 3. 1.

The dielectric properties ε_r and τ_f of the materials were measured in the microwave frequency range using resonance technique as described Chapter 2, Sections 2.2.2 to 2.2.5.

8. 3. 3 Results and Discussion

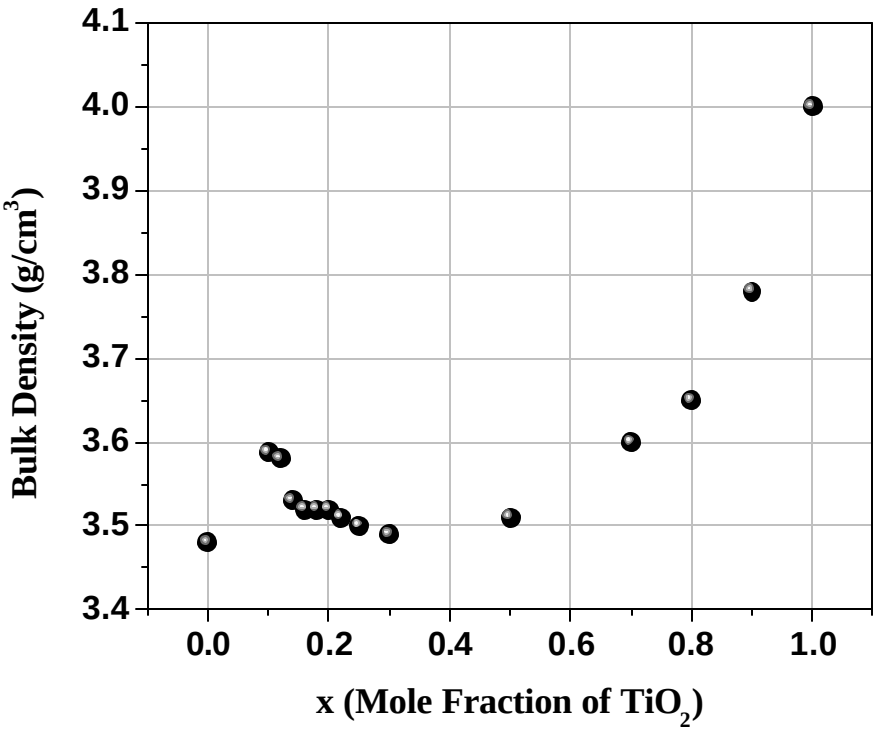

Fig. 8. 13 Variation of bulk density of $MgAl_2O_4$ with mole fraction of TiO_2 addition

The densification of $MgAl_2O_4$ has been studied by many investigators. The density of sintered pure $MgAl_2O_4$ was measured to be 3.48 g/cm^3 which is around 97 % of its theoretical density [9] (3.58 g/cm^3). The theoretical density of TiO_2 (rutile) is 4.26 g/cm^3. It has been reported [20] that the densification behaviour of TiO_2 is hindered due to the anatase to rutile phase transition consequent to the reduction of Ti^{4+} to Ti^{3+} state. Fig. 8.13 shows the variation of bulk density of $(1-x)MgAl_2O_4$-$xTiO_2$ phases as a function of x In our investigation on both the systems it is evident that the non linear densification trends in $MgAl_2O_4$-TiO_2 bears noticeable deviation from [44]$ZnAl_2O_4$-TiO_2 system where the densification. is maximum near the zero t_f region. It is understood that magnesium titanates such as $MgTiO_3$ and Mg_2TiO_4 were formed in the mixed phase region which can severely affect the microwave dielectric properties of spinel-rutile mixtures. It should be noted that

a slightly better densification is observed near x= 0.15 where the unloaded quality factor reaches a maximum.

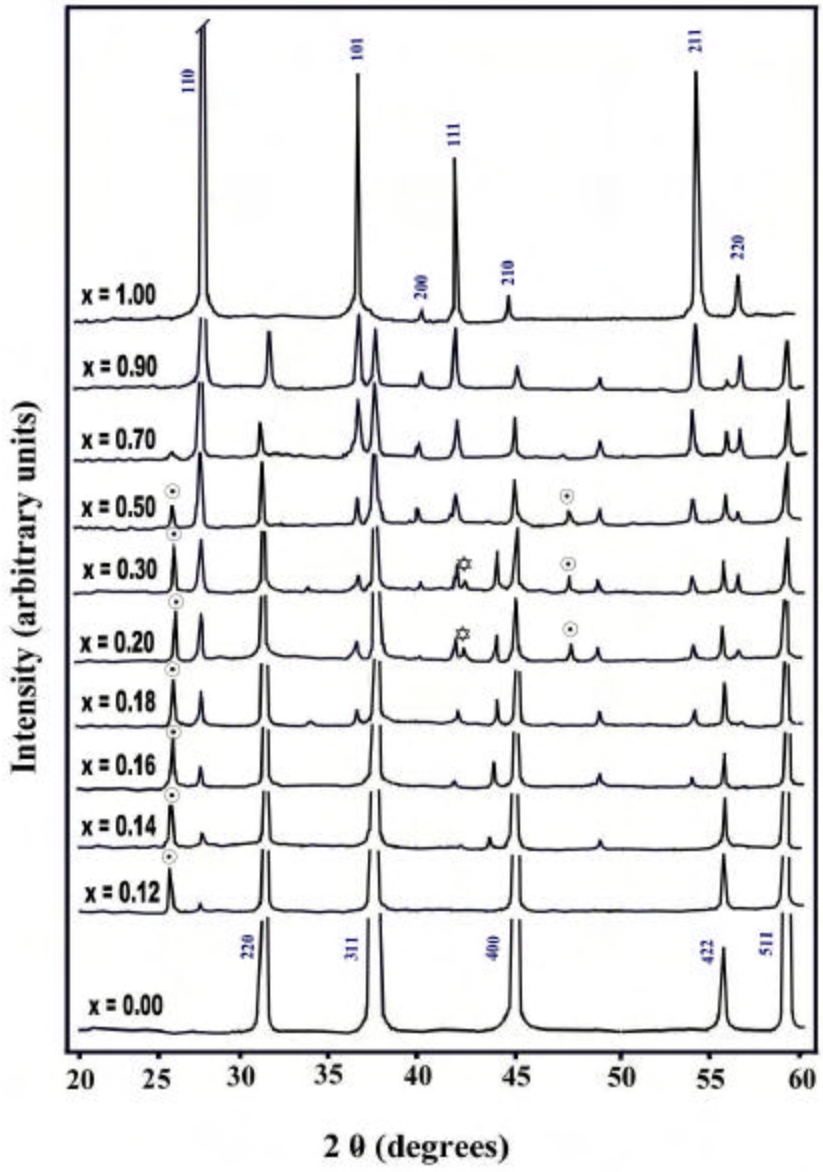

Fig. 8. 14 Powder diffraction pattern of (1-x)$MgAl_2O_4$-xTiO_2 system for x= 0.0, 0.12, 0.14, 0.16, 0.18, 0.20, 0.30, 0.50, 0.70, 0.90 and 1.0. ⊙ represents $MgTiO_3$ and ✡ represents Mg_2TiO_4 phases.

The X-ray diffractograms recorded from x = 0.0, 0.12, 0.14, 0.16, 0.18, 0.2, 0.3, 0.5, 0.7, 0.9 and 1.0 in (1-x)$MgAl_2O_4$-xTiO_2 is given in Fig. 8.14. The crystal structure of $MgAl_2O_4$ is fcc cubic which can be indexed using the JCPDS File Card No. 33-853. As the concentration of TiO_2 in $MgAl_2O_4$ increases an additional phase $MgTiO_3$ (JCPDS File Card

No. 6-494) is formed consequent to the reaction between spinel and rutile. For 20 and 30 mole % of TiO_2 additions the presence of another magnesium titanate, Mg_2TiO_4 (JCPDS File Card No. 25-1157) is also detected in the XRD- patterns. It is worthwhile to note that the formation of spinel structured Mg_2TiO_4 cannot be ruled out as a recent study[45] points out that a stable solid solution is possible between similar structured $MgAl_2O_4$ and Mg_2TiO_4. A previous investigation [46] revealed that presence of a low melting phase formed at the grain boundary during over doping of TiO_2 caused microcracks which could deteriorate the densification of spinel. The formation of low dielectric constant phases like $MgTiO_3$ and Mg_2TiO_4 on the addition of TiO_2 into $MgAl_2O_4$ was confirmed in another investigation by [45] Yu and Hiragushi. Anatase TiO_2 was used in this investigation, which coverts itself into rutile (JCPDS File Card No. 21-1276) at temperature 700°C which is given for x =1.0 in Fig. 8.14.

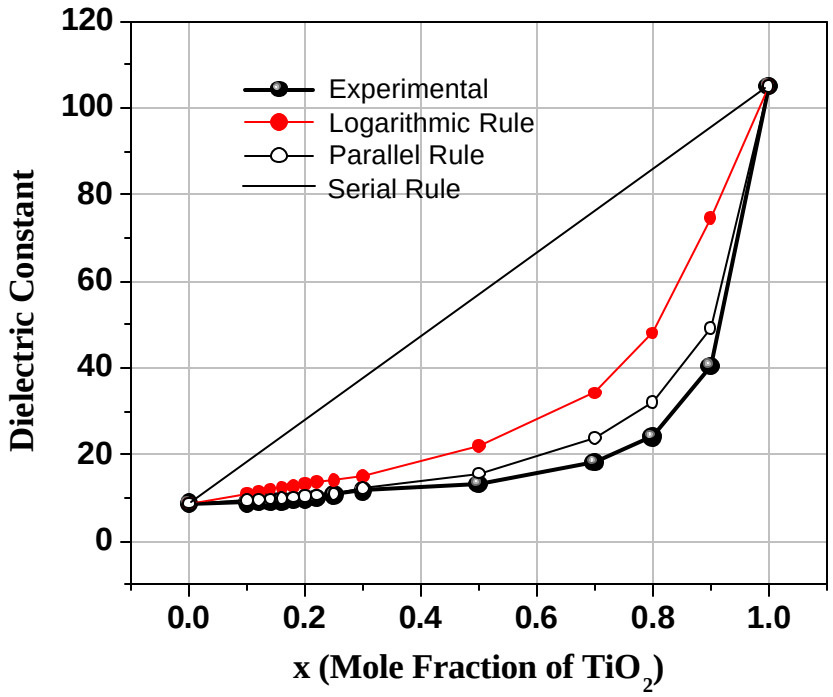

Fig. 8. 15 Variation of e_r of $MgAl_2O_4$ with mole fraction of TiO_2 addition

The dielectric constant of pure $MgAl_2O_4$ is measured to be 8.75. The zinc aluminate spinels doped with Cr_2O_3 has a dielectric constant of 8.34. The dielectric constant of pure TiO_2 is 93.8 and that doped with Fe_2O_3 is 105. Using the rule of mixtures

given by Eqns. 8.2 (serial mixture rule), 8.3 (logarithmic rule) and 8.4 (parallel mixture rule) the dielectric constant of the mixture has been calculated which is plotted as function of the mole fraction of TiO_2 addition as shown in Fig. 8.15. As explained before in Section 8.1.3, this curve fit doesn't bear any physical significance in the two phase region. The deviation from the ideal curve fitting plots are believed to be due to the presence of additional phases. Similar mixture rule treatment has been attempted in other dielectric mixtures too[15, 51]. It is interesting to note that the dielectric constant is ~ 20 for the mixture phases between 0.7 and 0.8 in (1-x)$MgAl_2O_4$-xTiO_2 ceramics where the t_f approaches zero value.

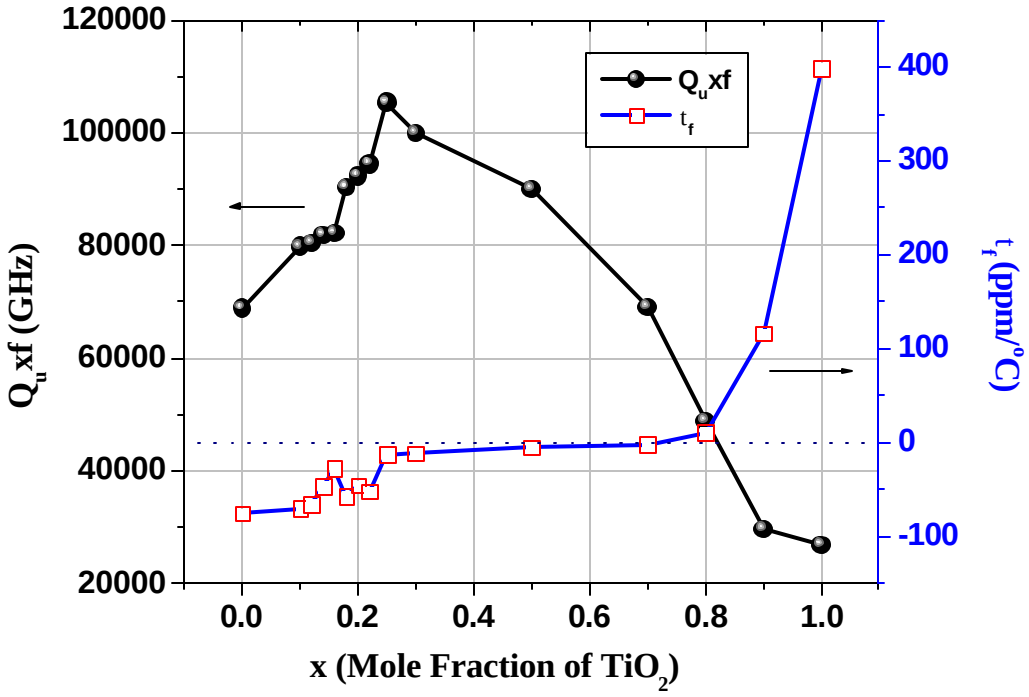

Fig. 8. 16 Variation of Q_u and t_f of $MgAl_2O_4$ with mole fraction of TiO_2 addition

The unloaded quality factor and t_f of $MgAl_2O_4$ are plotted in Fig. 8.16 with increasing concentration of TiO_2. Our literature survey revealed that though there has been a lot of investigations have been done on the physical aspects of $MgAl_2O_4$, no work was done on the microwave dielectric properties of this spinel. Our studies revealed that the $Q_u$xf of pure $MgAl_2O_4$ is 68,900 GHz which is well ahead that of many of the conventional

spinels with low dielectric constant. As the TiO_2 concentration in $MgAl_2O_4$ increases, the microwave quality factor also increases reaches a maximum value of $Q_u$xf =105,430 GHz for x=0.25 in (1-x)$MgAl_2O_4$-xTiO_2. For higher TiO_2 contents, the quality factor decreases as evident from Fig. 8.16. Compositions in the mixture region between x=0.7 and 0.8 in (1-x) $MgAl_2O_4$-xTiO_2 where the τ_f approaches minimum values, are having reasonably good quality factors ($Q_u$xf = 49000 to 69000 GHz). It must be remembered that the quality factor which depends considerably on the synthesizing conditions, purity of the chemicals and densification of the samples during sintering, does not follow any mixture rule in the entire range of spinel-rutile mixtures. Moreover, the quality factor of the intermediate phases is more than the end members which we have observed in another rutile-spinel [51] mixture too (see Section 8.1.3).

The temperature coefficient of resonant frequency (τ_f) of pure $MgAl_2O_4$ is -75 ppm/^oC and when it is doped with Cr_2O_3 the τ_f became more negative (-79 ppm/^oC). The TiO_2 was measured to have a high temperature coefficient of resonant frequency of 399 ppm/^oC. As the TiO_2 content in $MgAl_2O_4$ increases the τ_f must assume less negative values owing to a general mixture rule. But it can be seen from Fig. 8.16 that for x=0.16 τ_f is -27 but for x= 0.18 it again shifted to -57 ppm/^oC. The fluctuating nature of the temperature coefficient of TiO_2 added $MgAl_2O_4$ may be attributed to the formation of $MgTiO_3$ which is also a low loss dielectric. The zero region of the mixture is expected to be between 0.3$ZnAl_2O_4$-0.7TiO_2 and 0.2$ZnAl_2O_4$-0.8TiO_2 compositions. In (1-x) $ZnAl_2O_4$-xTiO_2 mixture, the zero t_f region is in the spinel rich region (see Section 8.1.3) where as in (1-x)$MgAl_2O_4$-xTiO_2, it occurs in the rutile rich region of the mixture.

The scanning electron micrographs recorded from the surfaces of two samples (0.3$MgAl_2O_4$-0.7TiO_2 and 0.2$MgAl_2O_4$-0.8TiO_2) which are believed to be lying on the boundary of temperature stable (zero t_f) composition are given in Fig. 8.17(a) and (b) respectively. The grain size is around 2-3 μm. It is evident that these samples are porous and exhibit poor densification which may be due to the formation of additional phases. This account for the comparatively lower values of microwave quality factor between 0.3$MgAl_2O_4$-0.7TiO_2 and 0.2$MgAl_2O_4$-0.8TiO_2 compositions where the t_f changes its sign from negative to positive.

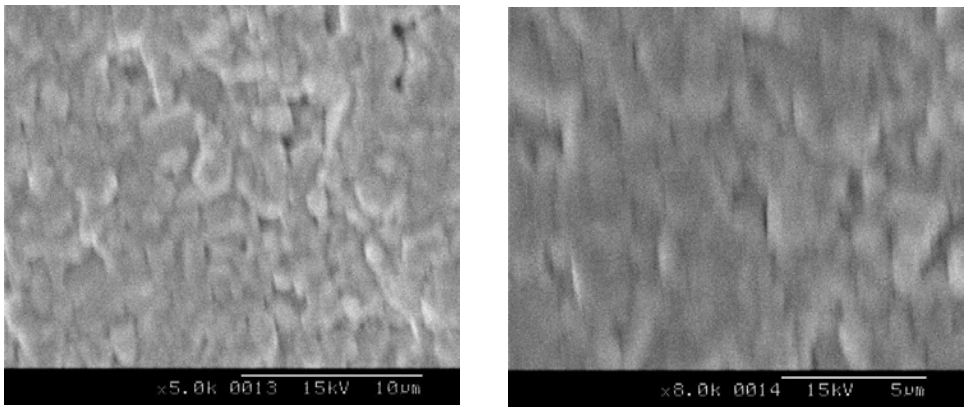

(a) **(b)**

Fig. 8. 17 Typical Microstructure of (a) 0.3$MgAl_2O_4$-0.7TiO_2 and (b) 0.2$MgAl_2O_4$-0.8TiO_2 sintered at 1450^oC for 4 hours.

From the above discussion it is revealed that unlike $ZnAl_2O_4$, $MgAl_2O_4$ spinels reacts with TiO_2 and hence formed intermediate phases restrict the unloaded quality factor of the mixed phases. In (1-x)$MgAl_2O_4$-xTiO_2 system, the temperature compensated low loss dielectrics could be developed only if the formation of additional phases such as $MgTiO_3$ and Mg_2TiO_4 could be controlled using suitable modification of the synthesizing conditions or using dopants.

8. 4 CONCLUSIONS

- Low dielectric constant, face centered cubic ceramics based on $ZnAl_2O_4$ were synthesized using mixed oxide route. The $ZnAl_2O_4$ spinels have ε_r = 8.5, Q_ux f = 56300, τ_f = -79 ppm/^oC in the microwave frequency range. The dielectric constant was increased with the molar addition of TiO_2 into the spinel to form mixtures based on (1-x)$ZnAl_2O_4$-xTiO_2 (x = 0.0-1.0). The densification was improved and the quality factor reached a maximum value of Q_ux f = 100,200 GHz for x = 0.17 in (1-x)$ZnAl_2O_4$-xTiO_2. The resonant frequency remained unchanged with temperature for the composition with x = 0.17 (i.e.τ_f = 0). There is no chemical reaction between spinel and rutile to form secondary low Q phases in the mixture. The 0.83$ZnAl_2O_4$-0.17TiO_2 with e_r=12.67, excellent quality factor and temperature stability is proposed as a suitable microwave substrate material. This composition is

advantageous over alumina due to its temperature stability and lower preparation temperature.

- The $0.83ZnAl_2O_4$-$0.17TiO_2$ substrate has a temperature coefficient of relative permittivity (τ_ε) of -15.6 ppm/^oC. The electrical insulating properties of this material is good (~20 MΩ-m) which provide better isolation between microelectronic components in Integrated Chip Circuitry. The DTA/TGA studies conducted in the range 30-1250^oC, established the thermo chemical stability of this material. The thermal expansion coefficient of the composition $0.83ZnAl_2O_4$-$0.17TiO_2$ was measured in the range 573-1197 ^oC as 6.3 ppm/^oC which is comparable to that of metallic silicon used in microelectronic circuitry. The thermal conductivity of this ceramic was measured as 59 W/m-K which is almost double the value of alumina substrate. A mixture of the newly developed substrate material with metallic silicon when heated at various temperatures did not form any additional phase with it apart form SiO_2 formed due to the oxidation of silicon. These results indicate that the mixture ceramic $0.83ZnAl_2O_4$-$0.17TiO_2$ posses most of the qualification to be projected as an ideal substitute for alumina substrate which is commoly used in microelectronic packaging.
- The $MgAl_2O_4$ spinels have ε_r = 8.75, Q_ux f = 68,900 GHz, τ_f = -75 ppm/^oC in the microwave frequency range. The dielectric constant was increased with the molar addition of TiO_2 into the spinel to form mixtures based on (1-x)$MgAl_2O_4$-xTiO_2 (x = 0.0-1.0). The formation of low dielectric constant phases like $MgTiO_3$ and Mg_2TiO_4 on the addition of TiO_2 into $MgAl_2O_4$ has affected the densification and dielectric properties of these ceramics. The microwave quality factor also increases reaching a maximum value of $Q_u$xf =105,430 GHz for x=0.25 in (1-x)$MgAl_2O_4$-xTiO_2 where ε_r and τ_f are 11.035 and -12 ppm/^oC respectively. For DRs in the mixture region between x=0.7 and 0.8 (1-x) $MgAl_2O_4$-xTiO_2 where the τ_f approaches minimum values, have high quality factors ($Q_u$xf = 49,000 to 69,000 GHz). In (1-x)$MgAl_2O_4$-xTiO_2 system, the temperature compensated low loss dielectrics could be developed only if the formation of additional phases such as $MgTiO_3$ and Mg_2TiO_4 could be controlled using suitable modification of the synthesizing conditions or using dopants.

8. 5 REFERENCES

1. A. Roosen, *Ceram. Trans*., **106**, 479-98 (2000).

2. R.C. Buchanan, *Ceramic Materials for Electronics*, Marcel Dekker, New York (1996).

3. N. M. Alford, S. J. Penn, A. Templeton, X. Wang and S. Webb, *Materials and Processing Developments in Microwave Ceramics*, Proc. 9th CIMTEC, World Ceramic Congress and Forum on New Materials, 14-19 June, Florence, Italy (1998).

4. T. Tsunooka, M. Andou, Y. Higashida, H. Sugiura and H. Ohsato, *J. Eur. Ceram. Soc.*, **23**, 2573-76 (2002).

5. N. V. Porotnikov, O.V. Godzhieva and L.N. Margolin, *Russian J. Inorg. Chem*., **32**, 793-94 (1987).

6. L.N. Margolin, O.V. Godzhieva and K. I. Petrov, *Russian J. Inorg. Chem*., **32**, 1676-77 (1987).

7. N. Santha, K. P. Surendran, M. T. Sebastian and P. Mohanan, *Proc. of National Symposium on Antennas & Propagation (APSYM-2000)*, CUSAT, Kochi - 682022., 6-8 Dec., (2000).

8. X. Wang, S. J. Penn, N. McN. Alford and A. Templeton, MRS Fall Meeting, Boston, USA, 1-5 December (1997).

9. H. M. Buschbaum, *J. All. Comp*., **349**, 49-104 (2003).

10. D. Someone, C. Dodane-Thiriet, D. Gosset, P. Daniel and M. Beauvy, *J. Nucl. Mater*., **30**, 151-60 (2002).

11. A. Escardino, J. L. Amoro´ s, A. Gozalbo, M. J. Orts and A. Moreno, *J. Am. Ceram. Soc*., **83**, 2938-44 (2000).

12. Y. Elamarraki, M. Cretin, M. Persin, J. Sarrazin and A. Larbott, *Mater. Res. Bull.,* **36,** 227-37 (2001).

13. Y. Elamarraki, M. Persin, J. Sarrazin, M. Cretin and A. Larbott, *Sep. Purif. Technol.,* **25**, 493-97 (2001).

14. N. J. van der Laaga, M. D. Snela, P. C. M. M. Magusinb, G. de With, *J. Eur.* Ceram. Soc., (2004) (in press)

15. R. D. Shannon and J. A. Pask, *J. Am. Ceram. Soc*., **48**, 391-98 (1965).

16. A. Templeton, X. Wang, S. J. Penn, S. J. Webb, L. F. Cohen and N. McN. Alford, *J. Am. Ceram. Soc*., **83**, 95-100 (2000).

17. S. J. Penn, N. M. Alford, A. Templeton, X. Wang, M. Xu, M. Reece and K. Schrapel, *J. Am. Ceram. Soc*., **80**, 1885-88 (1997).

18. W. D. Kingery, H. K. Bowen, D. R. Uhlmann, *Introduction to Ceramics*, 2nd Edn., John Wiley & Sons. Ltd., New Jersey (1976).

19. A. E. Paladino, *J. Am. Ceram. Soc*., **54**, 168-71 (1971).

20. D –W. Kim, K. H. Ko, D. K. Kwon and K. S. Hong, *J. Am. Ceram. Soc*., **85,** 1169-72 (2002).

21. M. Radecka and M. Rekas, *J. Am. Ceram. Soc.*, **85**, 346-54 (2002).

22. K.Otsuka, *Multilayer Ceramic Substrate-Technology for VLSI Package/Multichip Module*, Routledge, Hong Kong (1991).

23. D. S. Morgan, (Ed). *Electronic Materials Handbook*: Volume 1: Electronic Packaging, Materials Park, Ohio, USA, ASM (1989).

24. K. M. Nair (Ed), *Dielectric Materials and Devices*, American Ceramic Society, Ohio, USA (2002).

25. A. K. Jonscher, *Universal Relaxation Law*, Chelsea Dielectric, London (1996)

26. G. Garcia-Belmonte, V. Kytin, T. Dittrich, J. Bisquert, *J. Appl. Phys*., 94, 5261-64(2003)

27. P. J. Hains, M. Reading and F. W. Wilburn, *Differential Analysis and Differential Scanning Calorimetry in Handbook of Thermal Analysis and Calorimetry*, Ed. M. E. Brown. Elsevier, Amsterdam, Vol. 1, Chapter 5, (1998).

28. C. J. Keattch and D. Dollimore, *An Introduction to Thermogravimetry*, 2nd Edn., Heyden, London (1975).

29. D. R. Askeland and P. P. Phule, *The Science and Engineering of Materials*, Thomson Asia Pvt. Ltd. Singapore (2003)

30. K. Wataeri and S. L. Shinde, *High Thermal Conductivity Materials, MRS Bull.*, June 2001, 440-41 (2001)

31. D. R. Frear, *JOM*, 51, pp. 22-27 (1999).

32. A. D. Karisheff, *Refractory products and method of fabrication*. French Patent No. 350016, dated 24 August (1905).

33. G. A. Rankin and H.E. Merwin, *J. Am. Chem. Soc*. **38**, 568–88 (1916).

34. E. Kostic, S. Boskovic and S. Kis, Influence of fluorine ion on the spinel synthesis. *J. Mater. Sci. Lett.*, **1**, 507–510 (1982),.

35. I. Ganesh, S. Bhattacharjee, B. P. Saha, R. Johnson and Y. R. Mahajan, *Ceram. Inter.*, **27**, 773-79 (2001).

36. L. A. Skomorovskaya, *Glass & Ceramics*, **3–4**, 165–168 (1993).

37. Y. H. Baik, *Yoop Hikoech*, **22**, 29–36 (1985).

38. J. Yu and K. Hiragushi, *Taikabutsu Oversea*, **16**, 61-65 (1996).

39. R. Sarkar and G. Bannerjee, *J. Eur. Ceram. So*c., **20**, 2133-2141 (2000).

40. N. W. Grimes, J. *Phys.: Condens. Matter.*, **4,** L567-L570 (1992).

41. A. Ibarra, R. Vila and F. A. Garner, *J. Nucl. Mater.*, **233-237**, 1336-39 (1996).

42. C. Kennedy, J. Mollá, A. Ibarra, H. M. Frost, F. W. Clinard, M. Jiménez de Castro, *J. Nucl. Mater.*, **179-181**, 375-78 (1991).

43. R. D. Shannon and G. R. Rossman, *J. Phys. Chem. Solids*, **52**, 1055-59 (1991).

44. K. P. Surendran, N. Santha, P. Mohanan and M. T. Sebastian, *Eur. Phys. J. B* (in press) (2004).

45. M. A. Petrova, G. A. Mikirticheva, A. S. Novikova, and V. F. Popova, *J. Mater. Res*., 12, 2584-88 (1997).

CHAPTER 9

CONCLUSIONS AND SCOPE FOR FUTURE WORK

This Chapter outlines the useful results presented in various chapters and the scope for further extension of the work discussed in the thesis.

This thesis reports the synthesis, characterization and properties of three different groups of low loss ceramics (a) ordered complex perovskites $Ba(Mg_{1/3}Ta_{2/3})O_3$ [BMT], (b) orthorhombic ceramics $RETiAO_6$ [RE = Rare Earths, A = Ta, Nb] with aeschynite and euxenite mineral structure and (c) aluminate spinels based on MAl_2O_4 [M = Mg, Zn]. The microwave dielectric properties of BMT are improved with the introduction of a slight cation nonstoichiometry, fluxing with low melting glass additives and adding suitable dopants. The microwave dielectric properties of aeschynites having positive t_f were tailored by making solid solution with euxenites with negative t_f, in an effort to develop a temperature stable DR material. Furthermore, two spinel-rutile compositions with high thermal conductivity and temperature stability suitable for microwave substrate applications were also developed.

In Chapter 3, the scientific and technological importance of simple and complex perovskites are discussed with special emphasis to $A(B'_{1/3}B''_{2/3})O_3$ ceramics. The chronological evolution of $Ba(Mg_{1/3}Ta_{2/3})O_3$ [BMT] complex perovskites as the ideal dielectric resonator material, is reviewed. The microwave dielectric properties of the samples prepared through wet chemical methods like co-precipitation and citrate gel routes are very poor in spite of their small particle size. The influence of A and B-site cation non-stoichiometry on the sinterability and microwave dielectric properties of low loss barium magnesium tantalate ceramic is explored by deliberately altering the barium and magnesium ion concentration. Small deviation from stoichiometry is found to increase density and cation ordering parameter and also improve τ_f and Q factor. The improvement of the microwave dielectric properties is more for Ba deficient BMT as compared to Mg deficient ones. However large deviations from stoichiometry considerably deteriorate the microwave dielectric properties. The fully ordered $Ba_{0.9925}(Mg_{0.33}Ta_{0.67})O_3$ has e_r = 24.71, τ_f = 1.2 ppm/^oC, $Q_u$xf = 152,580 GHz, which is the best among the non-stoichiometric samples studied in this investigation. The cation ordering between Mg^{2+} and Ta^{5+} ions reaches a maximum for x = 0.015 in $Ba(Mg_{0.33-x}Ta_{0.67})O_3$ which also shows relatively better microwave dielectric properties [e_r = 25.12, τ_f = 3.3 ppm/^oC and $Q_u$xf = 120,500 GHz] as compared to stoichiometric BMT. Raman spectroscopy was employed to study the effects of nonstoichiometry and related lattice distortions in BMT ceramics on their vibrational modes.

The structural and microwave dielectric property modifications in BMT as a result of doping with inorganic oxides is discussed in Chapter 4. The microwave dielectric properties of pure BMT ceramic sintered at 1625 ^{o}C and annealed at 1450 ^{o}C for 40 hrs are e_r = 24.4, $Q_u$xf = 100,500 GHz and t_f= 8 ppm/^{o}C. With the addition of 0.1 mole % of the divalent impurity $MnCO_3$, the dielectric properties of BMT was improved to e_r = 26.72, $Q_u$xf = 162,800 GHz, and t_f = 6.3 ppm/^{o}C. The addition of trivalent impurities are found to be disastrous to the microwave dielectric properties of BMT whereas the addition of tetravalent impurities bring about noticeable influence on the cation ordering of BMT ceramics. The cation ordering is poor (0.597) for BMT added with 0.5 mole % of ZrO_2 but the dielectric properties are appreciably higher (e_r = 25.29, $Q_u$xf = 162,500 GHz, and t_f= 4.5 ppm/^{o}C). The densification and dielectric properties of BMT is excellent when doped with Sb_2O_3. Doping BMT with 0.1 mole of Sb_2O_3 gives e_r = 24.78, $Q_u$xf = 172,500 GHz, and t_f = 3.1 ppm/^{o}C. The addition of hexavalent impurities imparts better ordering in BMT due to the greater charge difference between B-site cation. The BMT when doped with 0.5 mole % of WO_3 has e_r = 24.9, $Q_u$xf = 144,500 GHz, and t_f = 4.1 ppm/^{o}C. The average ionic radius of B-site cation of BMT (*i.e.* $Mg_{1/3}Ta_{2/3}$) is calculated as 0.653 Å. It is observed that when the ionic radius of the dopants are between 0.6 and 0.7 Å (*i.e.* close to the average ionic radii of the B-site ion in BMT) the quality factor reaches maximum values. The quality factor of as sintered pure BMT decreases as temperature of the specimen is decreased below zero. On the other hand when BMT sample is doped with $MnCO_3$ and annealed, the unloaded quality factor increases with as we go down to cryogenic temperatures.

In Chapter 5, the liquid phase sintering aspects of complex perovskite $Ba(Mg_{1/3}Ta_{2/3})O_3$ is investigated. Different weight percentage of glasses such as B_2O_3, SiO_2, B_2O_3-SiO_2, ZnO-B_2O_3, 5ZnO-2B_2O_3, Al_2O_3-SiO_2, Na_2O-2B_2O_3.10H_2O, BaO-B_2O_3-SiO_2, MgO-B_2O_3-SiO_2, PbO-B_2O_3-SiO_2, ZnO-B_2O_3-SiO_2 and 2MgO-Al_2O_3-5SiO_2 were added to calcined $Ba(Mg_{1/3}Ta_{2/3})O_3$ precursor. The sintering temperature of BMT ceramics was reduced to about 1300^{o}C from 1650^{o}C by the addition of glass. Best densification of above 97 % of the theoretical density was observed for BMT added with small amount of B_2O_3, 5ZnO-2B_2O_3 and ZnO-B_2O_3-SiO_2 glass additives. Glass addition suppressed the formation secondary phases such as $Ba_5Ta_4O_{15}$ and $Ba_7Ta_6O_{22}$. The

microwave quality factor is found to be directly related to the ordering parameter. The microwave dielectric properties of pure unannealed $Ba(Mg_{1/3}Ta_{2/3})O_3$ (e_r = 24.8, t_f = 8 ppm/^oC and $Q_u xf$ = 80, 000 GHz) was improved when it is doped with 1.0 wt. % of B_2O_3 ($Q_u xf$ = 124,700 GHz, e_r = 24.25, and t_f = -1.3 ppm/^oC). The unloaded Q factor of 0.2 wt. % ZnO-B_2O_3 doped BMT is 136,500 GHz while that of 1.0 wt. % of 5ZnO-2B_2O_3 added ceramic is $Q_u xf$ = 141,800 GHz. The best microwave quality factor is observed for ZnO-B_2O_3-SiO_2 glass added ceramics which can act as a perfect liquid phase medium for the sintering of BMT. The microwave dielectric properties of 0.2 wt. % ZnO-B_2O_3-SiO_2 added BMT dielectric is $Q_u xf$ = 152,800 GHz, e_r = 25.54, and t_f = -1.5 ppm/^oC. The sintering temperature is brought down to about 1300 from 1650^oC by the addition of a small amount of glass. The results indicate that possibility of lowering the sintering temperature further down for LTCC applications by adding large amounts of glasses. Addition of such glasses in larger quantities not only lowers the sintering temperature but also decreases the dielectric constant and quality factor considerably.

The effect of substitution on the B-site of BMT is described in Chapter 6 where two typical solid solutions $Ba(Mg_{1/3}Ta_{(2-2x)/3}W_{x/3}Ti_{x/3})O_3$ and $Ba(Mg_{1/3}Ta_{2/3})_{1x}Ti_xO_3$ [x = 0.0 – 1.0] were investigated. The densification and dielectric constant decreases, while t_f approaches negative values with increase of x in $Ba(Mg_{1/3}Ta_{(2-x)/3}W_{x/3}Ti_{x/3})O_3$. The temperature coefficient of resonant frequency is approaching zero between x = 0.1 and 0.15 in $Ba(Mg_{1/3}Ta_{(2-2x)/3}W_{x/3}Ti_{x/3})O_3$. The microwave dielectric properties of $Ba(Mg_{1/3}W_{1/3}\ Ti_{1/3})O_3$ are e_r =15.4, t_f -25.1 ppm/^oC, $Q_u xf$= 35,400 GHz. The zero t_f compositions in the solid solution ($0.1 < x < 0.15$ in $Ba(Mg_{1/3}Ta_{(2-2x)/3}W_{x/3}Ti_{x/3})O_3$) have reasonably high quality factor ($Q_u xf$ = 80,000 - 90,000 GHz). In $Ba(Mg_{1/3}Ta_{2/3})_{1x}Ti_xO_3$ solid solutions, the density decreases with increase of substitution of Ti at the B-site of BMT. The dielectric constant of the solid solution phases increases with increasing concentration of $BaTiO_3$. The resonance vanishes in the compositions for $0.5 < x < 1.0$ in $Ba(Mg_{1/3}Ta_{2/3})_{1-x}Ti_xO_3$ due to greater dielectric loss introduced by the presence of lossy $BaTiO_3$ dielectric. The quality factor of the specimen decreases as the value of x in $Ba(Mg_{1/3}Ta_{2/3})_{1-x}Ti_xO_3$ increases, while t_f increases. A correlation was established between the quality factor of the solid solution phases to their tolerance factor. The upper

limit of tolerence factor for a partial substitution of tetravalent Ti^{4+} ion at the B-site of BMT is 1.045.

Seventh Chapter deals with the tailoring of microwave dielectric properties by making solid solution phases between positive (aeschynites) and negative (euxenites) t_f materials to develop a possible zero t_f material. Solid solution phases of $RE'_{1-x}RE"_xTiNbO_6$ [RE' = Pr, Nd, Sm; RE"= Gd, Dy, Y], $GdTiNb_{1-x}Ta_xO_6$ and $Sm_{1-x}Y_xTiTaO_6$ are investigated. In $RE'_{1-x}RE"_xTiNbO_6$ ceramics, the dielectric properties vary linearly as a function of x, until phase transition from aeschynite to euxenite occurs. Again the dielectric properties vary linearly as a function of x in the new phase. The t_f approaches zero for compositions $Pr_{0.14}Gd_{0.86}TiNbO_6$, $Nd_{0.52}Dy_{0.48}TiNbO_6$ and $Sm_{0.73}Y_{0.27}TiNbO_6$ which have high dielectric loss. The crystal structure and sign of τ_f depend on the average crystal radius of the rare earths in $RE_{1-x}RE'_xTiNbO_6$. If the average crystal radius of the rare earths is less than 1.09 Å, the system crystallizes in orthorhombic euxenite form with negative τ_f and if it is greater than 1.09 Å then the system crystallizes in the orthorhombic aeschynite structure with positive τ_f. The bulk density attains minimum value for x = 0.75 in $GdTiNb_{1-x}Ta_xO_6$ and x = 0.73 in $Sm_{1-x}Y_xTiTaO_6$ with a change in the sign of τ_f and has very high dielectric loss. If the average ionic radius of the rare earths in $RE_{1-x}RE'_xTiTaO_6$ is less than 0.915 Å then the structure is euxenite with negative τ_f and when it is greater than 0.915 Å then τ_f is positive with aeschynite structure. The results indicate the possibility of developing a near zero τ_f material in the solid solutions $RE'_{1-x}RE"_xTiNbO_6$ and $RE'_{1-x}RE"_xTiTaO_6$ by adjusting the average ionic radius of rare earth to be 1.09 Å and 0.915 Å respectively.

The development of ideal microwave substrate materials in aluminate spinel-rutile mixture is discussed in Chapter 8. The microwave dielectric properties of $ZnAl_2O_4$ spinels are ε_r = 8.5, $Q_u$xf = 56,300, τ_f = -79 ppm/^oC. The dielectric constant was increased with the molar addition of TiO_2 into the spinel to form mixtures based on $(1-x)ZnAl_2O_4$-$xTiO_2$ (x = 0.0-1.0). The densification and quality factor reached a maximum value of $Q_u$xf = 1,00,200 GHz for x = 0.17 in $(1-x)ZnAl_2O_4$-$xTiO_2$ where τ_f = 0. The $0.83ZnAl_2O_4$-$0.17TiO_2$ ceramic with ε_r = 12.67, is proposed as a suitable microwave substrate material which is advantageous over alumina due to its temperature stability and lower preparation temperature. The temperature coefficient of relative permittivity (τ_ε)

of this dielectric was determined as -15.6 ppm/^{o}C. The thermal expansion coefficient 6.3 ppm/^{o}C which is comparable to that of metallic silicon used in microelectronic circuitry. The thermal conductivity of this ceramic was measured as 59 W/m-K which is almost double the value of alumina substrate. These results indicate that the mixture ceramic $0.83ZnAl_2O_4$-$0.17TiO_2$ is a possible substitute for alumina substrate which is commonly used in microelectronic packaging. The microwave dielectric properties of $MgAl_2O_4$ spinels are ε_r = 8.75, Q_ux f = 68,900 GHz, τ_f = -75 ppm/^{o}C. The dielectric constant was increased with the molar addition of TiO_2 into the spinel to form mixtures based on (1-x)$MgAl_2O_4$-xTiO_2. The formation of low dielectric constant phases like $MgTiO_3$ and Mg_2TiO_4 by the addition of TiO_2 into $MgAl_2O_4$ has affected the densification and dielectric properties of these ceramics. The microwave quality factor also increases reaching a maximum value of $Q_u$xf =105,430 GHz for x = 0.25 in (1-x)$MgAl_2O_4$-xTiO_2 where ε_r and τ_f are 11.03 and -12 ppm/^{o}C respectively. DRs in the mixture region between x = 0.7 and 0.8 in (1-x)$MgAl_2O_4$-xTiO_2 where τ_f approaches minimum values, have high quality factors ($Q_u$xf = 49,000 to 69,000 GHz).

The future directing of this thesis work is mainly aimed at developing a Low Temperature Co-fired Ceramic (LTCC) composition using low loss BMT through the addition of excess amount of wetting glasses like B_2O_3, $5ZnO$-$2B_2O_3$ and ZnO-B_2O_3-SiO_2. For LTCC applications, the sintering temperature has to be reduced to 960^{o}C without compromising too much on the microwave dielectric properties. Even though the preliminary studies revealed that wet chemical synthesis of BMT through co-precipitation and citrate-gel route is expensive and could give only poor dielectric properties, alternate methods like hydrothermal, sol-gel etc. will be attempted to synthesize $Ba(Mg_{1/3}Ta_{2/3})O_3$ and substrates MAl_2O_4-TiO_2 [M=Zn, Mg]. The dielectric properties of single crystals are superior to their polycrystalline counterparts. Hence another future directing in dielectric resonator research is to grow single crystals of BMT large enough for microwave applications.

PICTURES OF TYPICAL DIELECTRIC RESONATORS

$Ba(Mg_{1/3}Ta_{2/3})O_3$ CERAMICS

$Ba(Mg_{1/3}Ta_{2/3})O_3$ DOPED WITH $MnCO_3$

$Ba(Mg_{1/3}Ta_{2/3})O_3$ DOPED WITH GLASS

$ZnAl_2O_3$-TiO_2 SUBSTRATES

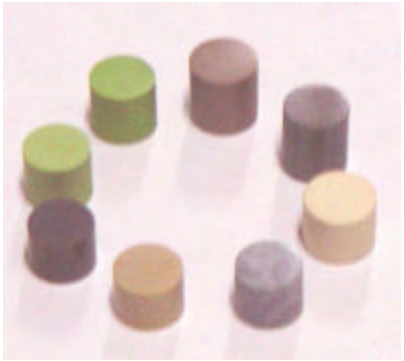

RE'RE"$TiNbO_6$

LIST OF PUBLICATIONS

SCI Journals

1. **K. P. Surendran**, P. Mohanan, M.T. Sebastian, The effect of glass additives on the microwave dielectric properties of $Ba(Mg_{1/3}Ta_{2/3})O_3$ ceramics, *J. of Solid State Chem*., in press (2004) [Elsevier Science Ltd., USA]

2. **K. P. Surendran**, N. Santha, P. Mohanan and M. T. Sebastian, Temperature stable low loss ceramic dielectrics in $(1-x)ZnAl_2O_4$-$xTiO_2$ system for microwave substrate applications, *Eur. Phys. J. B*, in press [Institute of Physics, U.K] (2004).

3. **K. P. Surendran**, M. T. Sebastian, P. Mohanan, R. L. Moreira, and A. Dias, The Effect of Nonstoichiometry on the Structure and Microwave Dielectric Properties of $Ba(Mg_{0.33}Ta_{0.67})O_3$, *Chem. Mater*., in press (2004) [American Chemical Society, USA].

4. **K. P. Surendran**, P. Mohanan and M.T. Sebastian, The effect of dopants on the microwave dielectric properties of $Ba(Mg_{1/3}Ta_{2/3})O_3$ ceramics, *J. Eur. Ceram. Soc.*, communicated (2004) [European Ceramic Society, United Kingdom].

5. **K. P. Surendran**, P. Mohanan, M.V. Manjusha, J. Philip and M. T. Sebastian, Microwave substrate applications of $0.83ZnAl_2O_4$-$0.17TiO_2$ dielectrics, *Appl. Phys. Lett*., communicated (2004) [Institute of Physics, London].

6. **K. P. Surendran,** P.V. Bijumon, P. Mohanan and M. T. Sebastian Microwave dielectric properties of $(1-x)MgAl_2O_4$-$xTiO_2$ ceramics, *Mater. Sci. Engg. B*, communicated (2004)

7. **K. P. Surendran**, Manoj R. Varma, M. T. Sebastian and P. Mohanan, Microwave dielectric properties of $[RE'_{1-x}RE"_x]TiNbO_6$ (RE'= Pr, Nd, Sm; RE" = Gd, Dy, Y) dielectric ceramics, *J. Am. Ceram. Soc*., 86(10) 1695-99 (2003) [American Ceramic Society, USA]

8. **K. P. Surendran**, P. Mohanan and M. T. Sebastian, Tailoring the Microwave Dielectric Properties of $GdTiNb_{1-x}Ta_xO_6$ and $Sm_{1-x}Y_xTiTaO_6$ [x=0.0-1.0] Ceramics, *J. Eur. Ceram. Soc.*, 23, 2489-2495 (2003) [European Ceramic Society, United Kingdom]

9. **K. P. Surendran**, Manoj R. Varma, M. T. Sebastian and P. Mohanan, Microwave Dielectric Properties of $RETiTaO_6$ [RE= La, Ce, Pr, Nd, Sm, Eu, Gd, Tb, Dy, Ho, Y, Er, Yb, Al and In] Ceramics, *J. Mater. Res.*, 17, 2561-2566 (2002) [Materials Research Society, U. S. A]

10. C. W. A. Paschoal, R. L. Moreira, C. Fantini, M. A. Pimenta**, K. P. Surendran** and M. T. Sebastian, Raman Scattering study of $RETiTaO_6$ Dielectric Ceramics, *J. Eur. Ceram. Soc*., 23, 2661-2666 (2003) 2003 [European Ceramic Society, United Kingdom]

11. M. Thirumal, I. N. Jawahar, **K. P. Surendran**, P. Mohanan and A. K. Ganguli, $Ba_3ZnTa_{2-x}Nb_xO_9$ and $Ba_3MgTa_{2-x}Nb_xO_9$ ($0<x<1$): Synthesis, Structure and Dielectric Properties, *Mater. Res. Bull.*, 37, 2321-2334 (2002) [Pergamon-Elsevier Science Ltd.] United Kingdom

12. M. Thirumal, I. N. Jawahar, **K. P. Surendran**, P. Mohanan and A. K. Ganguli, Synthesis and Microwave Dielectric Properties of $Sr_3Zn_{1-x}Mg_xNb_2O_9$ Phases, *Mater. Res. Bull.*, 37, 185-191 (2002) [Pergamon-Elsevier Science Ltd.] United Kingdom

13. S. Solomon. M. Kumar, **K. P. Surendran**, M. T. Sebastian and P. Mohanan, Synthesis, characterization and properties of $[RE_{1-x}RE'_x]TiNbO_6$ dielectric ceramics, *Mater. Chem. Phys.*, 67, 291-93 (2001). [2001 Elsevier Science Ltd.] Switzerland

14. M.T. Sebastian, Manoj Raama Varma, N. Santha, I. N. Jawahar, **K. P. Surendran** and P. V. Bijumon, Ceramic Dielectric Resonators for Microwave Telecommunication Systems, *Metals, Materials and Processes* 13, No. 2-4, (2001) 327-338.

Papers under preparation

15. **K. P. Surendran**, P. Mohanan and M. T. Sebastian Microwave dielectric properties of $Ba(Mg_{1-x}Zn_x)_{1/3}Ta_{2/3})O_3$ (x=0-1) ceramics, (to be communicated to *J. European Ceram. Soc*.) (2004).

16. **K. P. Surendran,** P. Mohanan and M. T. Sebastian Microwave loss quality of $Ba[Mg_{1/3}Ta_{(1-x)2/3}Ti_{x/3}W_{x/3}]O_3$ ceramics, (to be communicated to *Mater. Sci. Engg. B*) (2004).

17. Microwave dielectric properties of $Ba(Mg_{1/3}Ta_{2/3})_{1-x}Ti_{2x}O_3$, (x= 0.0-1.0) ceramics, **K. P. Surendran** and M. T. Sebastian. (to be communicated to *J. Electroceramics*) (2004).

18. Manoj Raama Varma, Resmi Raghunandan, **K. P. Surendran** and M. T. Sebastian Synthesizing $Ba(Mg_{1/3}Ta_{2/3})O_3$ Ceramics through Solid State and Chemical Routes : A comparative Study, (to be communicated to *J. Am. Ceram. Soc*) (2004).

International Conference Proceedings

19. **K. P. Surendran,** P. Mohanan and M. T. Sebastian Towards LTCC application of $Ba(Mg_{1/3}Ta_{2/3})O_3$ through glass addition, Accepted for presentation at Asia Pacific Microwave Conference (APMC-2004), Dec. 15-18, New Delhi (2004).

20. **K. P. Surendran**, P. Mohanan and M. T. Sebastian " Tailoring the microwave dielectric properties of $Sm_{1-x}Y_xTiTaO_6$ and $GdTiNb_{1-x}Ta_xO_6$ ceramics" presented at the *Microwave Materials and Their Applications (2002)[MMA-2002]* held in York, UK from 1-3 September 2002.

21. C. W. A. Paschoal, R. L. Moreira, C. Fantini, M. A. Pimenta**, K. P. Surendran** and M. T. Sebastian, "Raman Scattering study of $RETiTaO_6$ Dielectric Ceramics" presented at the *Microwave Materials and Their Applications (2002)[MMA-2002]* held in York, UK from 1-3 September 2002.

22. Manoj Kumar, Sam Solomon, **K. P. Surendran**, M. T. Sebastian & P.Mohanan "Synthesis Characterization and Properties of $[RE_{1-x}RE'_x]TiNbO_6$ Ceramics for Dielectric Resonator Applications in Microwave Circuits" Presented *in the 7th International Conference on Sintering*, *(Sintering Science and Technology beyond 2000 AD*), Organized by The International Institute for the Science of Sintering, February22-25, 2000, New Delhi